THE INFLUENCE OF BERMS, ROUGHNESS AND OBLIQUE WAVES ON WAVE OVERTOPPING AT DIKES

Crest

Upper slope

Berm

Down slope

Weiqiu Chen

THE INFLUENCE OF BERMS, ROUGHNESS AND OBLIQUE WAVES ON WAVE OVERTOPPING AT DIKES

Weiqiu Chen

THE INFLUENCE OF BERMS, ROUGHNESS AND OBLIQUE WAVES ON WAVE OVERTOPPING AT DIKES

DISSERTATION

to obtain
the degree of doctor at the University of Twente,
on the authority of the rector magnificus,
prof. dr. ir. A. Veldkamp,
on account of the decision of the Doctorate Board,
to be publicly defended
on Thursday 16 of December 2021 at 14.45 hours

by

Weiqiu Chen

born on the 6th July 1991
in Jiangsu, China.

This dissertation has been approved by:

supervisor	:	Prof. dr. S. J. M. H. Hulscher	University of Twente
co-supervisors	:	Dr. J. J. Warmink	University of Twente
		Prof. dr. ir. M. R. A. van Gent	Deltares & Delft University of Technology

Graduation Committee

Chairman/secretary	prof.dr.ir. H. F. J. M. Koopman
Supervisors	prof. dr. S. J. M. H. Hulscher
Co-supervisor	dr. J. J. Warmink
	prof. dr. ir. M. R. A. van Gent
Additional committee members	prof. dr. R. W. M. R. J. B. Ranasinghe
	prof.dr. D. van der Wal
	prof. dr. ir. P. Troch
	prof. dr. ir. W. S. J. Uijttewaal
	dr. ir. A. Antonini

I will mount a long wind some day and break the heavy waves,
And set my cloudy sail straight and bridge the deep, deep sea.
长风破浪会有时，直挂云帆济沧海。

Bai Li, 744

CONTENTS

PREFACE

Standing at the tail of my PhD study and looking back the road that I spent four years walking through, I think of a phrase, "What's past is prologue". I am more confident to embrace the future equipped with the knowledge that I obtained during the past four years. Doing a PhD in Europe is a valuable and unforgettable experience in my whole life. In the journey of pursuing PhD degree, I am not alone with a number of brilliant people around me. It would be impossible for me to achieve this PhD without the support of these people. The following words are dedicated to them.

First of all, I am extremely grateful to my promotor Prof. Suzanne Hulscher for accepting me as a PhD candidate in the group of Marine and Fluvial Systems. You gave me a lot of encouragement during my PhD study which made me feel very warm and more confident to complete good scientific work. I also appreciate your invaluable advice, continuous support and patience towards me, which lays a solid foundation for the success of the PhD project.

I would also like to thank my daily supervisor Dr. Jord Warmink for the enormous guidance and support. You were always there for questions and willing to help me. Thank you for your encouragement after each of my presentations in the conferences, which gave me a lot of confidence with my research and the motivation to learn more. My research skills have been improved significantly compared to the beginning of my PhD study under your guidance and endless patience. You were also like a friend who inspired me with your positiveness and sense of humor when I felt stressful with the PhD research. This PhD project would not be possible without your help and support.

My gratitude extends to my another daily supervisor Prof. Marcel van Gent for offering me the precious opportunity to do my PhD study at Deltares. Every time I encountered any problems related to my research, you always provided me very professional and constructive suggestions on the solutions. Your expertise, ability to simplify difficult problems and thoughtful guidance helped me keep on the right track and shape my way of thinking critically. Your rigorous attitude towards the academic research had a positive influence on me, which benefited my PhD work in the past and will also benefit my future career.

I would like to give my thanks to my colleagues at MFS group and at Deltares. Special thanks to my office mates Vera and Daan. We have shared the office for almost four years and had many nice and interesting memories, such as the Christmas decorations, discussions on the research and cultural differences between China and Netherlands, different feelings of the same room temperature and hilarious chats. I would especially like to thank

SUMMARY

Dikes are important coastal structures to protect infrastructures, land and people in coastal areas from wave attack and flooding. Dike breaching can cause extensive damage and loss of lives. Wave overtopping is one of the failure mechanisms of dikes, which must be taken into account when designing a dike. The average overtopping discharge and flow parameters like flow velocity and layer thickness are often used to describe the wave overtopping. The average overtopping discharge is a key parameter to determine the crest level of coastal structures by ensuring the average overtopping discharge is below the permissible rate. The flow parameters related to individual overtopping events play an important role in eroding dike cover layers, possibly initiating dike breaching in a later stage. Thus, a reliable prediction of wave overtopping is essential for dike design and safety assessment of existing dikes. In practice, berms and roughness elements at the waterside slope are widely applied to reduce the wave overtopping. Additionally, the direction of incident waves is often oblique relative to the coastal structures. Existing guidelines have shown that roughness, berms and oblique waves can have significant influence on the wave overtopping at dikes. However, these effects have not been fully understood. Better estimates of these influence factors will help improve the prediction of wave overtopping and lead to more suitable estimates of the risk of coastal flooding events. Therefore, the aim of this thesis is to determine the effects of roughness, a berm and oblique waves on wave overtopping processes. To achieve this aim, both physical model tests and numerical simulations were performed for the research presented in this thesis.

In Chapter 2, we studied the effects of a berm and roughness on the average overtopping discharge by conducting small-scale physical model tests. Different configurations including both straight slopes and slopes with a berm were tested. Three types of slope surface were used, i.e. a smooth slope, slopes covered by protruding blocks and slopes covered by open blocks. The research showed that the value of the roughness factor for one certain type of roughness element was variable and depended on the wave properties and crest freeboard. A new empirical equation for the roughness influence factor was developed by taking these relevant parameters into account. The new roughness equation showed better performance in estimating the average wave overtopping discharge than using a constant value as suggested by existing guidelines (e.g. TAW, 2002 and EurOtop, 2018). Experimental results showed that the wave steepness also affected the berm influence factor in addition to the berm width and the berm level. Moreover, a permeable berm showed less reductive

influence on the average overtopping discharge than an impermeable berm. The new empirical formulas for estimating the influence of impermeable and permeable berms were proposed based on the modification of the existing berm equation provided by TAW (2002). It was found that the roughness elements applied on the upper slope led to the most reductive influence on the average overtopping discharge. Thus, an empirical formula was also developed to estimate the varying roughness along the waterside slopes with a berm by including the location-weighting coefficients to account for the location effects. These newly derived empirical formulas significantly improved the estimates of the average overtopping discharge compared to the existing empirical formulas within the experimental ranges.

In Chapter 3, the reductive influence of a berm and roughness of rock armour on the average overtopping discharge was analysed. Physical model tests in addition to those presented in Chapter 2 were performed. The new empirical equations for estimating the effect of a rock berm and the effect of rock armour were obtained by recalibrating the empirical coefficients introduced in the equations developed in Chapter 2. The analysis showed that the values of the location-weighting coefficients proposed in Chapter 2 were also valid for rock amour. Overall, the empirical equations with the calibrated values of empirical coefficients for rock amour led to more accurate estimates of the average overtopping discharge at rock-armoured dikes. The results presented in Chapter 3 demonstrated that it is feasible to extend the empirical formulas developed in Chapter 2 for other types of roughness elements and berms.

In Chapter 4, a 2DV OpenFOAM® model based on the Reynolds-Averaged Navier-Stokes (RANS) equations was described. This numerical model was validated by using the experiments presented in Chapter 2. The roughness of protruding blocks was explicitly modelled by refining the mesh around protrusions. The validation results showed that the 2DV OpenFOAM ® model was capable of reproducing the incident waves as applied in the experiments and predicting the average overtopping discharge with a good accuracy. Then, the berm width, berm level and roughness were varied in the numerical model in a wider range than that of the experiments to further investigate the roughness and berm influence on the average overtopping discharge. The influence of the coverage length of roughness at the top half of the upper slope on the overall roughness factor was studied. It was found that the roughness on the top half upper slope resulted in almost the same reductive influence on the average overtopping discharge as that of roughness applied on the entire upper slope. The numerical model results indicated that the berm equation might require improvement for very wide berms with $B/H_{m0} > 3.7$.

Finally, in Chapter 5, the 2DV numerical model developed in Chapter 4 was extended to simulate the flow velocity and layer thickness at the waterside edge of the dike crest using the experimental data from previous research. Also, the influence of oblique waves and a berm on the average overtopping discharge was investigated using a 3D OpenFOAM®

model. There is a good agreement between the numerically modelled and physically measured flow parameters. The applicability of existing empirical formulas of the flow velocity and layer thickness at smooth straight slope for the rough slopes or slopes with a berm was evaluated using the numerical results. It was found that the existing empirical formulas can also be applicable for rough slopes and smooth slopes with a berm. The distribution functions of flow velocities and layer thicknesses were also derived based on the modelled results. The extreme flow velocities follow a Rayleigh distribution function and the layer thickness follows a Weibull distribution function. A 3D OpenFOAM® model was developed based on the 2DV OpenFOAM® model to simulate the average overtopping discharge at the dike with a berm under oblique waves. The 3D numerical model results confirmed that the influence of oblique waves on the average overtopping discharge depends on the berm width. This dependency should be taken into account to accurately predict the average overtopping when the oblique waves and a berm play a role at the same time.

Overall, the performed research has provided new insights into the effects of roughness, berms and oblique waves on wave overtopping. New expressions to account for these effects have been developed based on physical and numerical modelling, which contributes to more accurate predictions of wave overtopping. The design and safety assessment of dikes can be improved based on the outcome of this research.

SAMENVATTING

Waterkeringen zoals dijken zijn belangrijk om infrastructuur, land en mensen in kustgebieden te beschermen tegen golven en overstromingen. Dijkdoorbraken kunnen grote schade en het verlies van levens veroorzaken. Golfoverslag is een van de belangrijkste faalmechanismen van dijken waarmee rekening moet worden gehouden bij het ontwerp van een dijk. Het gemiddeld overslagdebiet en stromingseigenschappen zoals de snelheid en de laagdikte worden vaak gebruikt om golfoverslag te beschrijven. Het gemiddeld overslagdebiet is een belangrijke parameter om de kruinhoogte van dijken te bepalen door te zorgen dat het gemiddeld overslagdebiet onder de toegestane hoeveelheid blijft. De stromingseigenschappen gerelateerd aan individuele golven spelen een belangrijke rol in de erosie van de dijkbekleding, en mogelijk in het initiëren van een dijkdoorbraak in een later stadium. Een betrouwbare voorspelling van overslag is dus essentieel voor het ontwerp van dijken en de veiligheidsbeoordeling van bestaande dijken. Bermen en ruwheidselementen aan de waterzijde worden in de praktijk veelvuldig toegepast om de hoeveelheid golfoverslag te reduceren. Bovendien bereiken de invallende golven de dijk meestal onder een hoek. Uit bestaande richtlijnen blijkt dat ruwheid, bermen en schuine golven een significante invloed kunnen hebben op de golfoverslag bij dijken. Deze effecten zijn echter nog niet volledig begrepen. Betere inschattingen van deze invloedsfactoren kunnen helpen om de voorspelling van golfoverslag te verbeteren en daarmee het risico op overstromingen beter in te schatten. Het doel van dit proefschrift is daarom om de effecten van ruwheid, bermen en schuin-invallende golven op golfoverslag te bepalen. Om dit doel te bereiken zijn zowel fysieke modeltesten als numerieke simulaties uitgevoerd voor het onderzoek dat in dit proefschrift wordt gepresenteerd.

In Hoofdstuk 2 is het effect van een berm en ruwheid op het gemiddeld overslagdebiet onderzocht door middel van kleinschalige fysieke modeltesten. Verschillende configuraties met zowel uniforme taluds als taluds met een berm zijn getest. Drie verschillende soorten taluds zijn getest: een glad talud, een talud bekleed met uitstekende blokken en een talud bekleed met een open steenzetting. Het onderzoek liet zien dat de waarde van de ruwheidsfactor voor één specifiek type ruwheidselement variabel is en afhangt van de golfkarakteristieken en de vrije kruinhoogte. Een nieuwe empirische formule voor de ruwheidsfactor is ontwikkeld waarbij deze relevante parameters zijn meegenomen. Deze nieuwe vergelijking voor de ruwheid leidde tot betere voorspellingen van het gemiddeld overslagdebiet ten opzichte van een constante waarde zoals geadviseerd in de bestaande richtlijnen (bv. TAW,

2002 en EurOtop, 2018). Daarnaast lieten de experimenten zien dat de golfsteilheid naast de bermbreedte en de bermhoogte ook invloed heeft op de bermfactor. Daarbij had een berm met een doorlatende onderlaagminder invloed op het gemiddeld overslagdebiet vergeleken met een berm met een ondoorlatende onderlaag. Nieuwe empirische formules voor de invloed van ondoorlatende en doorlatende bermen zijn voorgesteld gebaseerd op een aanpassing van de bestaande berm vergelijking in TAW (2002). Bovendien bleek dat ruwheidselementen geplaatst op het boventalud leidden tot de meeste afname van het overslag debiet. Daarom is er een empirische formule ontwikkeld om het effect van variërende ruwheid langs het buitentalud met een berm te schatten door een locatiewegingscoëfficiënt te introduceren om het effect van locatie van ruwheidelementen op het talud mee te nemen. De nieuw afgeleide empirische formules resulteren in een significante verbetering van het geschatte overslagdebiet in vergelijking tot bestaande empirische formules binnen het experimentele bereik.

In Hoofdstuk 3 is de afname van het gemiddeld overslagdebiet door een berm en ruwheid van breuksteen geanalyseerd. Extra experimenten zijn uitgevoerd aanvullend op de testen die in Hoofdstuk 2 zijn beschreven. Nieuwe empirische vergelijkingen voor het effect van een berm bestaande uit breuksteen en het effect van een volledige breuksteen bekleding zijn verkregen door het opnieuw kalibreren van de empirische coëfficiënten die zijn geïntroduceerd in de vergelijkingen ontwikkeld in Hoofdstuk 2. Deze analyse toonde aan dat de waarden van voorgestelde locatiewegingscoëfficiënten in Hoofdstuk 2 ook geldig zijn voor een breuksteenbekleding. In het algemeen leidden de empirische vergelijkingen met de gekalibreerde empirische coëfficiënten voor breuksteen tot nauwkeurigere schattingen van het gemiddelde overslagdebiet over dijken met breuksteenbekleding. De resultaten gepresenteerd in Hoofdstuk 3 laten zien dat het haalbaar is om de empirische formules ontwikkeld in Hoofdstuk 2 uit te breiden voor andere soorten ruwheidselementen en bermen.

In Hoofdstuk 4 werd een 2DV OpenFOAM® model beschreven, gebaseerd op de Reynolds-gemiddelde Navier-Stokes (RANS)-vergelijkingen. Dit numerieke model is gevalideerd door gebruik te maken van de experimenten gepresenteerd in Hoofdstuk 2. De ruwheid van de uitstekende blokken werd expliciet gemodelleerd door het model raster rond de uitsteeksels te verfijnen. De validatieresultaten lieten zien dat het 2DV OpenFOAM®-model in staat was om de invallende golven van de experimenten te reproduceren en het gemiddelde overslagdebiet met een goede nauwkeurigheid te voorspellen. Vervolgens zijn de bermbreedte, de bermhoogte en de ruwheid in het numerieke model gevarieerd over een groter bereik dan dat van de experimenten om de ruwheid en de invloed van de berm op het gemiddelde overslagdebiet nader te onderzoeken. De invloed van de lengte van de ruwheidselementen op het boven talud op de algehele ruwheidsfactor is bestudeerd. Het bleek dat ruwheid op alleen de bovenste helft van het boventalud bijna dezelfde reducerende invloed op het gemiddelde overslagdebiet veroorzaakte als die van de ruwheid op het gehele boventalud.

De resultaten van het numerieke model gaven aan dat de bermvergelijking mogelijk moet worden verbeterd voor zeer brede bermen met $B/H_{m0} > 3.7$.

Tot slot, in Hoofdstuk 5 is het 2DV numerieke model dat ontwikkeld is in Hoofdstuk 4 uitgebreid om de snelheid en de laagdikte aan de waterkant van de kruin te simuleren met behulp van de experimentele data uit eerder onderzoek. Ook is de invloed van schuine golven en een berm op het gemiddelde overslagdebiet onderzocht met behulp van een 3D OpenFOAM® model. De resultaten lieten een goede overeenkomst tussen de numeriek gemodelleerde en fysiek gemeten stromingsparameters zien. De toepasbaarheid van bestaande empirische formules voor de snelheid en de laagdikte voor een glad talud zonder berm zijn geëvalueerd voor ruwe taluds of taluds met een berm met behulp van de numerieke resultaten. Gebleken is dat de bestaande empirische formules ook toepasbaar kunnen zijn voor ruwe taluds en gladde taluds met een berm. Op basis van de gemodelleerde resultaten zijn ook de verdelingsfuncties van snelheden en laagdiktes afgeleid. De extreme snelheden volgen een Rayleigh-verdelingsfunctie en de laagdikte volgt een Weibull-verdelingsfunctie. Op basis van het 2DV OpenFOAM® model is een 3D OpenFOAM® model ontwikkeld om het gemiddeld overslag debiet op een dijk met een berm onder schuin-invallende golven te simuleren. De resultaten van het 3D-numerieke model bevestigden dat de invloed van schuin-invallende golven op het gemiddelde overslagdebiet afhankelijk is van de bermbreedte. Met deze afhankelijkheid moet rekening worden gehouden om het gemiddelde overslagdebiet nauwkeurig te voorspellen wanneer schuine-invallende golven en een berm tegelijkertijd een rol spelen.

Al met al heeft het uitgevoerde onderzoek nieuwe inzichten opgeleverd in de effecten van ruwheid, bermen en schuine-invallende golven op golfoverslag. Nieuwe formules om deze effecten mee te nemen zijn ontwikkeld op basis van fysieke en numerieke modellen, wat bijdraagt aan nauwkeurigere voorspellingen van golfoverslag. Op basis van de uitkomsten van dit onderzoek kan het ontwerp en de veiligheidsbeoordeling van dijken worden verbeterd.

1

INTRODUCTION

1

D UE to global climate change, sea-level rise, land subsidence and sediment supply, coastal flood risks are increasing for many countries (Figure 1.1) (Knutson et al., 2010; Lin et al., 2012; Temmerman et al., 2013; Hirabayashi et al., 2013), especially in low-lying countries such as The Netherlands and densely populated countries like China. Dikes are important coastal structures in the flood defence system protecting infrastructure and people in the coastal areas from storm attack (Besley, 1998; Dawson et al., 2005; Jonkman et al., 2008). Damages to dikes can lead to major casualties and property losses (Schmocker and Hager, 2009; Kellens et al., 2012). Research has been conducted on the statistical analysis of the historical dike failure (Fukunari, 2008; Van Baars and Van Kempen, 2009; Nagy, 2012; Danka and Zhang, 2015) and statistics revealed that overtopping was one of the most important causes of dike breaching. The amount of wave overtopping is a critical parameter for determining the dike crest level and flooding potential is estimated from the quantity of overtopping water and storm duration (Hughes et al., 2012). Knowledge of wave overtopping processes at dikes is therefore useful for reducing coastal flood risks.

Figure 1.1: Distribution of cities with more than 200,000 people exposed to coastal flood risks by 2070 worldwide (from Temmerman et al., 2013).

1.1. WAVE OVERTOPPING

1.1.1. WAVE RUN-UP

W AVE overtopping occurs when the wave run-up goes beyond the crest of dikes (Figure 1.2), which means that overtopping is closely related to wave run-up. The wave run-up height is defined as a vertical distance between the highest point of wave run-up and the

still water level (SWL) (Saville, 1956). Each wave will give a different run-up height due to the stochastic nature of waves in reality. To properly describe the wave run-up height, the $R_{u2\%}$ run-up height is often used, which refers to the wave run-up height that is exceeded by 2% of the number of incoming waves at the toe of dikes.
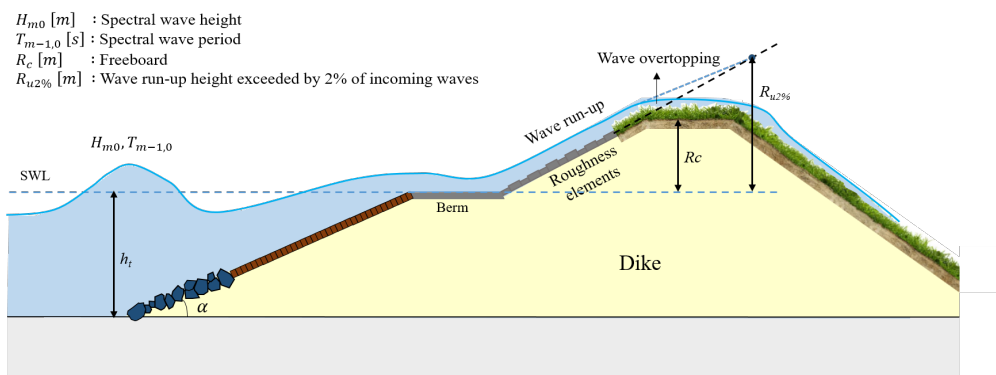
Figure 1.2: Sketch of wave run-up and wave overtopping at a dike.

It is hardly possible to describe the wave run-up height and wave overtopping processes at dikes using an exact mathematical way because of the stochastic nature of wave run-up and wave breaking (EurOtop, 2018). Empirical models (empirical formulae or neural network prediction methods) (Ahrens, 1981; Tautenhain et al., 1982; Van Gent, 2001; TAW, 2002; Burcharth and Hughes, 2002, Bonakdar and Etemad-Shahidi, 2011; EurOtop, 2018; Pillai, Etemad-Shahidi, et al., 2019; Huang et al., 2020) have been developed to predict the wave run-up height. Previous research has shown that the wave run-up height mainly depends on wave properties, wave obliqueness (β), dike geometries and roughness of revetments at the waterside of dikes. Run-up equations provided by EurOtop (2018) take the influence of roughness, berms and oblique waves into account by using influence factors (i.e., γ_f, γ_b and γ_β). These influence factors will be introduced in more detail in Section 1.2.

1.1.2. AVERAGE OVERTOPPING DISCHARGES

WAVE overtopping is stochastic, varying in both space and time. The average overtopping discharge is one of the parameters that are widely used to describe the wave overtopping at coastal structures. It is defined as the volume of overtopped water per unit of time, per meter of width expressed in $m^3/s/m$ or $l/s/m$ (EurOtop, 2018).The crest level and the geometry of coastal structures are usually determined by limiting the average overtopping discharge below permissible discharges (Franco et al., 1995; Van der Meer and Bruce, 2014; Altomare et al., 2020; Koosheh et al., 2021). Therefore, reliable prediction of the average overtopping discharge is required for the efficient design and safety assessment of

1

dikes.

Empirical formulas, including the influence of the most important parameters, have been used as the main tool to predict the average overtopping discharge. Most of the existing empirical formulas (e.g., Goda et al., 1975; Owen, 1980, Ward and Ahrens, 1992; Hebsgaard et al., 1998; Van Gent, 1999; Mase et al., 2013) were derived based on physical experiments. Selected overtopping empirical formulas are given in Table 1.1. Goda et al. (1975) proposed design diagrams for estimating the average overtopping discharge, which is one of the earliest empirical methods. This method employed the equivalent deepwater wave height H_0' as the key parameter in predictions of overtopping. This is different from most of overtopping formulas in Europe in which the spectral significant wave height H_{m0} at the toe of the structure is used. Goda (2009) developed an overtopping formula (see Table 1.1) for vertical walls and inclined seawalls taking the effect of foreshore into account. However, this empirical formula is only applicable for seawalls with smooth and impermeable surfaces. TAW (2002) provided overtopping formulas (later adopted in EurOtop, 2007) as listed in Table 1.1 applicable for a wider range of conditions. Influence factors were introduced to account for the effects of roughness, a berm, vertical walls and oblique waves on the average overtopping discharge. EurOtop (2018) slightly adapted the TAW overtopping formulas by applying a different power of 1.3 (see Table 1.1) in order to take the very low freeboards R_c including zero freeboard into account. In both TAW (2002) and EurOtop (2018), different formulas are provided for breaking and non-breaking wave conditions, which can be roughly distinguished by the Iribarren number $\xi_{m-1,0} \approx 1.8$. The estimates of the average overtopping discharge are bounded by a maximum of overtopping discharge which corresponds to non-breaking waves with $\xi_{m-1,0}$ larger than about 1.8. The average overtopping discharge of non-breaking waves is independent on the Iribarren number. Capel (2015) proposed an overtopping equation in order to better take the effect of waterside slope gradients into account and this overtopping equation is applicable for both breaking and non-breaking wave conditions.

The empirical formulas given in Table 1.1 indicate that the average overtopping discharge depends on many parameters that characterise the waves and the dike geometry. Pillai et al. (2017b) conducted a sensitivity analysis to study the effects of input variables on the average overtopping discharge at coastal structures with a berm. This study presented that the average overtopping discharge is the most sensitive to the dimensionless crest freeboard (R_c/H_{m0}); if the dimensionless berm width (B/H_{m0}) is larger than 2, the berm width has a significant reductive influence on the average overtopping discharge. According to the literature, apart from the berm, roughness elements at the waterside slope and oblique waves can also significantly reduce the overtopping discharge. These effects will be reviewed in Section 1.2.

Table 1.1: Summary of selected empirical formulas* for the average overtopping discharge

Authors	Equations	Application conditions
TAW (2002)	$\frac{q}{\sqrt{gH_{m0}^3}} = \frac{0.067}{\sqrt{\tan\alpha}}\gamma_b\xi_{m-1,0}\exp\left[-4.75\frac{R_c}{\xi_{m-1,0}H_{m0}\gamma_b\gamma_f\gamma_\beta\gamma_v}\right]$ with a maximum of $\frac{q}{\sqrt{gH_{m0}^3}} = 0.2\exp\left[-2.6\frac{R_c}{H_{m0}\gamma_f\gamma_\beta}\right]$	$\frac{R_c}{H_{m0}} \geq 0.5, 0 < \xi_{m-1,0} < 5$
Goda (2009)	$\frac{q}{\sqrt{gH_{m0}^3}} = \exp\left[-\left(A+B\frac{R_c}{H_{m0}}\right)\right]$ $A = A_0[(0.956+4.4\tan\theta)*(h_t/H_{m0}+1.242-2.032(\tan\theta)^{0.25})]$ $B = B_0[(0.822+2.22\tan\theta)*(h_t/H_{m0}+0.578+2.22\tan\theta)]$ $A_0 = 3.4-0.734\cot\alpha+0.239\cot^3\alpha-0.0162\cot^3\alpha$ $B_0 = 2.3-0.5\cot\alpha+0.15\cot^2\alpha-0.011\cot\alpha^3$	Smooth impermeable slopes; $0 < \cot\alpha < 7$
Capel (2015)	$\frac{q}{\sqrt{gH_{m0}^3}} = \frac{0.027}{\sqrt{\tan\alpha}}\xi_{m-1,0}\exp\left[-6.5\frac{R_c}{3.45\tanh(0.65\xi_{m-1,0})H_{m0}\gamma_f}\right]$	Impermeable slopes
EurOtop (2018)	$\frac{q}{\sqrt{gH_{m0}^3}} = \frac{0.023}{\sqrt{\tan\alpha}}\gamma_b\xi_{m-1,0}\exp\left[-\left(2.7\frac{R_c}{\xi_{m-1,0}H_{m0}\gamma_b\gamma_f\gamma_\beta\gamma_v}\right)^{1.3}\right]$ with a maximum $\frac{q}{\sqrt{gH_{m0}^3}} = 0.09\exp\left[-\left(1.5\frac{R_c}{H_{m0}\gamma_f\gamma_\beta\gamma^*}\right)^{1.3}\right]$	$\frac{R_c}{H_{m0}} \geq 0, s_{m-1,0} > 0.01, \xi_{m-1,0} < 5$

* $\xi_{m-1,0}$ is the Iribarren number that is defined as $\xi_{m-1,0} = \tan\alpha/\sqrt{2\pi H_{m0}/(gT_{m-1,0}^2)}$; h_t is the water depth at the toe of coastal structures; θ is the angle of the foreshore in front of coastal structures; α is the angle of the waterside slope; γ_b is the influence factor for a berm; γ_f is the influence factor for roughness of slopes; γ_β is the influence factor for oblique waves and γ_v is the influence factor for vertical crest elements.

1.1.3. OVERTOPPING FLOW PARAMETERS

THE average overtopping discharge described in the previous section is normally used as a design parameter for dikes. However, the average overtopping discharge does not describe the extreme individual overtopping events. During extreme events like a storm, dike failures are often initiated by the overtopping flow velocity and layer thickness related to individual overtopping events (Schüttrumpf, 2001; Bomers et al., 2018). The flow characteristics, overtopping flow velocity and layer thickness, are closely related to the stability

1

of coastal structures (Van Gent, 2002b; Argente et al., 2018; Mares-Nasarre et al., 2021). For example, the overtopping flow velocity and layer thickness are used as input in some erosion models (Dean et al., 2010; Hoffmans, 2012; Van Bergeijk et al., 2021) to estimate the cover erosion and stability of earthen dikes. Pedestrian safety during wave overtopping was also assessed using the flow velocity and layer thickness (Endoh and Takahashi, 1995; Bae et al., 2016; Mares-Nasarre et al., 2019; Suzuki et al., 2020). Therefore, flow parameters including the flow velocity and layer thickness are also important for the design and reliability assessment of coastal structures.

The flow velocity and layer thickness with a low probability of exceedance (2%) during a storm event are usually used to describe the overtopping flow since these extreme values are more relevant for predictions of the cover erosion or dike failures on the landward slopes. Several formulas are available for predicting the extreme flow velocity and layer thickness at the waterside slope, the crest and the landward slope. The flow characteristics at the waterside edge of the dike crest are especially important since they provide boundary conditions for estimates of flow characteristics along the crest and the landward slope. The first formulas for estimating the overtopping flow velocity and layer thickness were proposed by Schüttrumpf (2001) based on the physical model tests and theoretical analysis. According to the formulas, the calculation of the flow velocity and layer thickness at the waterside edge of the dike crest depends on the wave run-up height ($R_{u2\%}$) and the crest freeboard (R_c). Van Gent (2002b) developed formulas that have similar form with those by Schüttrumpf (2001) but have different values of the empirical coefficients. The results were later combined in Schüttrumpf and Van Gent (2003). Bosman et al. (2009) modified the formulas of Schüttrumpf and Van Gent (2003) by including the effect of seaward slope angle on the flow parameters. EurOtop (2018) also provided formulas for estimating the flow velocity and layer thickness at the waterside of the dike crest which are similar with those proposed by Schüttrumpf and Van Gent (2003). Formentin et al. (2019) performed numerical computations based on which they refitted the formulas by Schüttrumpf and Van Gent (2003) and proposed new forms of formulas of flow parameters. These mentioned formulas are summarised in Table 1.2 and plotted in Figure 1.3.

Figure 1.3a shows the comparison of estimated flow velocity using different empirical formulas listed in 1.2 for different waterside slopes. Bosman et al. (2009) stated that the waterside slope was of great importance in the flow velocities and layer thicknesses based on mathematical analysis. The estimated flow velocities given by the equation proposed by Formentin et al. (2019) are also different for different outer slopes. The Formentin et al. (2019) equation tends to give smaller flow velocities than other empirical equations. The equations were calibrated against the values of $u_{2\%}$ obtained based on the depth-averaged values of the velocities on the dike crest while the other empirical equations were derived based on the measurements of velocities from micro-propellers installed at a fixed height

above the crest. The EurOtop equations indicate that the waterside slope has minor influence on the flow velocity. The calculated flow velocities using the Schüttrumpf (2001) equations, Van Gent (2002b) equations and EurOtop (2018) equations are very close.

Table 1.2: Summary of empirical formulas* for estimating the flow velocity and layer thickness at the waterside edge of the dike crest

Authors	Formula	Coefficients
Schüttrumpf (2001)		$c_{u2\%} = 1.37; c_{h2\%} = 0.33;$ slope $= 1/6; a = 0$
Van Gent (2002b)	$u_{2\%} = c_{u2\%}\sqrt{g(R_{u2\%} - R_c)/\gamma_f{}^a}$ $h_{2\%} = c_{h2\%}\left[(R_{u2\%} - R_c)/\gamma_f{}^a\right]$	$c_{u2\%} = 1.30; c_{h2\%} = 0.15;$ slope $= 1/4; a = 1$
Bosman et al. (2009)		$c_{u2\%} = \frac{0.30}{\sin\alpha}; c_{h2\%} = \frac{0.009}{\sin^2\alpha}; a = 0$
EurOtop (2018)		$c_{u2\%} = 1.4\text{-}1.5$ for slopes of $1/3$ to $1/5; a = 0$ $c_{h2\%} = 0.2$ for slopes of $1/3$ and $1/4; c_{h2\%} = 0.25$ for a slope of $1/5; 0.3$ for a slope of $1/6$
Formentin et al. (2019)	$u_{2\%} = c_{u2\%}\left[(g(R_{u2\%} - R_c))^{0.5}\right]^{1.35}$ $h_{2\%} = c_{h2\%}(R_{u2\%} - R_c)^{1.35}$	$c_{u2\%} = 0.085\cot\alpha$ $c_{h2\%} = 0.12\cot\alpha + 0.41$

* $u_{2\%}$ and $h_{2\%}$ are the flow velocity and layer thickness exceeded by 2% of the incoming waves; α is the angle of the waterside slope; γ_f is the influence factor for roughness of slopes; $R_{u2\%}$ is the wave run-up height exceeded by 2% of the incoming waves.

The comparison of estimated flow layer thicknesses is shown in Figure 1.3b. It is worth noting that the layer thicknesses calculated using the Bosman et al. (2009) equation with a slope of 1/4 and 1/6 coincide with that using the Van Gent (2002b) equation and that using the Schüttrumpf (2001) formula, respectively. The Schüttrumpf (2001) formula predicts the layer thickness which is almost twice that given by Van Gent (2002b) formula. Note that the 2% values of velocity and layer thickness in Schüttrumpf (2001) were obtained based on only about 50 waves while $u_{2\%}$ and $h_{2\%}$ in Van Gent (2002b) were calculated based on 1000 waves, which could explain the difference. The Formentin et al. (2019) equation overall overestimates the layer thickness compared to other formulas, which could be caused by the overestimation of layer thicknesses produced by the numerical model based on which the formula was derived. It is worth mentioning that all of these empirical formulas were mainly derived based on the physical or numerical experiments in which only smooth straight waterside slopes were considered. It still remains unclear if these formulas are valid for slopes with a berm or roughness elements.

1
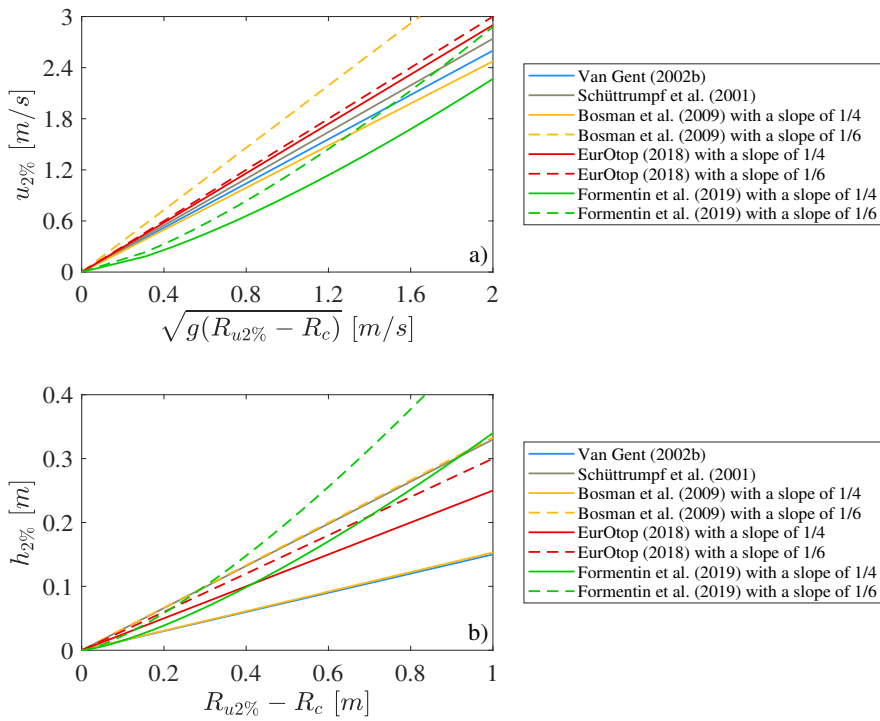
Figure 1.3: Comparison of existing empirical equations for a) overtopping flow velocity and b) layer thickness at smooth slopes.

1.2. INFLUENCE FACTORS ON WAVE OVERTOPPING

As mentioned in Section 1.1, predictions of wave overtopping depend on many factors. In addition to wave properties and crest freeboard, a berm, roughness of waterside slope surface, oblique waves, objects on the dike crest (see e.g. Kortenhaus et al., 2004; Pearson et al., 2005; Tuan, 2013; Van Doorslaer et al., 2015; Van Gent and Van der Werf, 2019), wind (e.g. De Waal et al., 1996; González-Escrivá, 2007; Lorke et al., 2012; Wolters and Van Gent, 2007) and water depth (e.g. Pillai, Lemckert, et al., 2019; Van Steeg et al., 2021) also have an influence on wave overtopping. In TAW (2002) and EurOtop (2018), the effects of a berm, roughness, oblique waves and vertical walls on the dike crest were accounted for by introducing influence factors in the overtopping or run-up formulas. In practice, berms and roughness elements at the waterside slope are widely used worldwide to reduce the wave overtopping at dikes. Additionally, the dikes are often subject to oblique wave attack. These factors can significantly affect the wave overtopping (Juhl and Sloth, 1995; Steendam et al., 2005; Moghim et al., 2015; Eldrup and Lykke Andersen, 2018; Dan et al.,

2020; Schoonees et al., 2021). Hence, the effects of roughness, a berm and oblique waves are subjects of this thesis, the literature on these effects are reviewed in more detail as follows.

1.2.1. EFFECT OF ROUGHNESS

WATERSIDE slopes of most existing dikes are protected by grass, asphalt, concrete or natural block revetments (Van Loon-Steensma and Schelfhout, 2017; Siegel, 2020). There is a great variety of studies (Shankar and Jayaratne, 2003; Andre et al., 2004; Molines et al., 2012; Van Gent and Luis, 2013; Deilami-Tarifi et al., 2015; Jiménez Moreno, 2017; Kerpen et al., 2019; Esteban et al., 2020; Vieira et al., 2021) that give values or estimation methods for the roughness influence factor (γ_f) for many different types of dike revetment elements.

The conventional approach to account for the roughness influence is to use constant values of the roughness factor. For example, TAW (2002) and EurOtop (2007, 2018) provide default values of roughness influence factors for different types of roughness elements in breaking wave conditions. For non-breaking waves, roughness factors are slightly affected by the Iribarren number ($\xi_{m-1,0}$). Bruce et al. (2009) investigated the roughness influence factors of different types of armor units by conducting small-scale physical model tests and determined the values of roughness factor for various kinds of roughness elements. These static roughness values were then used in the neural network prediction of overtopping (e.g., Van Gent et al., 2007; Verhaeghe et al., 2008). However, more recent research (Capel, 2015; Van Steeg et al., 2016; Schoonees et al., 2021) show that the roughness factors are not constant for breaking waves but that they are affected by wave conditions, dike configurations and characteristics of roughness elements. Capel (2015) studied the effect of special roughness patterns in placed-block revetments with protrusions on wave overtopping and wave run-up height. The results showed that the effect of roughness decreased with the average overtopping discharge increasing. This is because the flow depth of the overtopping water is larger in case of larger overtopping discharges and the roughness is therefore less experienced by the run-up flow. The roughness influence factor is also related to the wave steepness and the characteristics of the roughness pattern, such as the coverage area of the blocks and the protrusion height. A new empirical formula was proposed by Capel (2015) to assess the roughness influence factor of protruding blocks. This equation requires iteration to calculate the roughness factors and is therefore somewhat complicated when applying to practical engineering. Van Steeg et al. (2016) studied the roughness of three new types of blocks, i.e. Hillblock®, RONA®Taille and Verkalit®GOR, by conducting large-scale tests in the Delta Flume at Deltares. An empirical formula was developed to estimate the roughness influence of these three types of roughness elements. According to the empirical formula, the roughness factor was dependent on the significant wave height, the open volume per

square meter protection and the type of blocks.

In practice, various types of roughness elements are often combined in the slope protection of dikes (TAW, 2002). For the varying roughness along the slopes and berms, the various influence factors are weighted in TAW (2002) and EurOtop (2018) by including the lengths of the relevant sections of the slope. The roughness elements have little effect if they are positioned at a height of $0.25R_{u2\%,smooth}$ below the still water level or $0.5R_{u2\%,smooth}$ above the still water level, where $R_{u2\%,smooth}$ is the wave run-up height at smooth slopes. The combined roughness influence factor is then calculated by weighting the various influence factors $\gamma_{f,i}$ and including corresponding lengths L_i located between SWL-$0.25R_{u2\%,smooth}$ and SWL+$0.5R_{u2\%,smooth}$ using the following equation:

$$\gamma_f = \frac{\sum_{i=1}^{n} \gamma_{f,i} L_i}{\sum_{i=1}^{n} L_i} \tag{1.1}$$

However, the equation has not been systematically validated and therefore the accuracy of this formula remains unclear.

1.2.2. EFFECT OF BERMS

A berm is often applied at the waterside slope to reduce wave run-up and wave overtopping if the wave height is large, which is often the case at sea dikes or lake dikes. A berm is defined by the width of the berm B, the berm level d_h relative to the still water level, and the characteristic berm length L_{Berm}, which is shown in Figure 1.4a (EurOtop, 2018). In practice, impermeable and permeable berms are applied. Both types of berm can dissipate energy in a different way thereby resulting in different overtopping discharges.

(a) Definition of a berm given by EurOtop (2018)

(b) Equivalent slope considering the berm
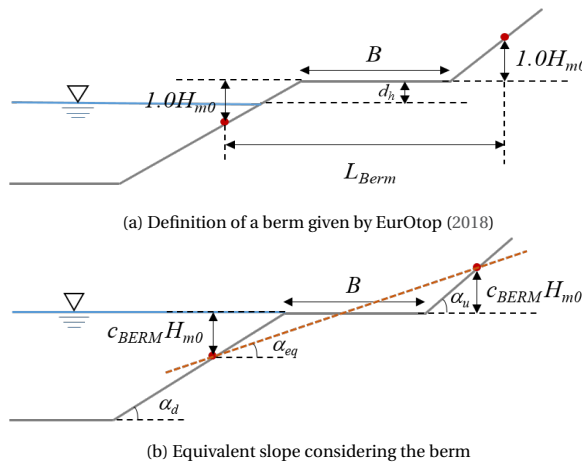
Figure 1.4: Schematic of a berm at the waterside slope.

A lot of research (e.g., De waal and Van der Meer, 1992; Van Doorslaer et al., 2010) has been conducted on the reductive influence of an impermeable berm on wave overtopping or wave run-up height. De waal and Van der Meer (1992) investigated the overtopping rate at impermeable bermed dikes and proposed empirical equations for berm influence factor γ_b. Van der Meer (2004) and Regeling et al. (2005) investigated the influence of a rock berm on overtopping discharge with a smooth upper slope. They proposed a predictive method for overtopping discharge on a smooth structure with a rough berm around the still water level. TAW (2002) and EurOtop (2018) also provide the methods to estimate the impermeable berm influence. The influence factor γ_b consists of two parts given by r_B and r_{dh}:

$$\gamma_b = 1 - r_B(1 - r_{dh}) \qquad 0.6 \leq \gamma_b \leq 1.0 \tag{1.2}$$

with the expressions for r_B and r_{dh}:

$$r_B = \frac{B}{L_{Berm}}$$

$$r_{dh} = 0.5 - 0.5\cos\left(\pi \frac{d_h}{R_{u2\%}}\right) \qquad \text{for a berm above the still water level}$$

$$r_{dh} = 0.5 - 0.5\cos\left(\pi \frac{d_h}{2H_{m0}}\right) \qquad \text{for a berm below the still water level}$$

According to the Eq. (1.2), the berm lying on the still water level is the most effective since the reduction of wave overtopping or wave run-up is the maximum for a berm on the still water level. A berm lying below $2H_{m0}$ or above $R_{u2\%}$ has no influence on wave run-up and wave overtopping. The applicability of Eq. (1.2) for permeable berms still remains unclear.

The other way to take the berm influence into account is to replace the slope by the characteristic slope considering the berm. The characteristic slope is determined between two levels, SWL$+c_{BERM}H_{m0}$ and SWL$-c_{BERM}H_{m0}$ as shown in Figure 1.4b where in Van Gent (1999) $c_{BERM} = 2$ was used and in Pillai et al. (2017a) $c_{BERM} = 1.5$ was used. This method does not make use of the berm influence factor and assumes that the berm position relative to the SWL has no effect on the overtopping discharge when the berm is located between $2H_{m0}$ above and $-2H_{m0}$ below the SWL. Even though there is extensive literature on the berm influence, research on the influence of a permeable berm of dikes is still limited.

1.2.3. EFFECT OF OBLIQUE WAVES

M OST of the existing experimental data on the average overtopping discharge are from physical model tests subject to perpendicular wave attack. In reality waves do not always propagate perpendicular to coastal structures. Oblique waves also have an influence on wave overtopping discharge. Previous research (De Waal and Van der Meer, 1992; Gal-

land, 1995; Lykke Andersen and Burcharth, 2009; Van Gent and Van der Werf, 2019) showed that oblique waves lead to less overtopping discharge and less severe overtopping events compared to perpendicular wave attack. Several empirical equations are available for estimating the influence factor (γ_β) of oblique waves that is included in the overtopping formulas from TAW (2002) and EurOtop (2018) to account for the influence of oblique waves on the average overtopping discharge. The existing formulas are summarised in Table 1.3 in which long-crested waves have no directional distribution and wave crests are parallel with infinite width, and the direction of individual short-crested waves is scattered around the main direction and the wave crests have a finite width.

Table 1.3: Existing empirical formulas for estimating the influence factor of oblique waves (γ_β).

	Short-crested waves		Long-crested waves	
	Impermeable strcutures	Permeable structures	Impermeable structures	Permeable structures
De Waal and Van der Meer (1992)	$\gamma_\beta = 1 - 0.0033\beta$ $\beta \le 80°$		$\gamma_\beta = 1$　$0° \le \beta \le 10°$ $\gamma_\beta = \cos^2(\beta - 10°)$　$10° \le \beta \le 50°$ $\gamma_\beta = 0.6$　$\beta \ge 50°$	
Galland (1995)				$\gamma_\beta = \cos^{\frac{1}{3}}\beta$ $0° \le \beta \le 75°$
Lykke Andersen and Burcharth (2009)		$\gamma_\beta = 1 - 0.0058\beta$ $\beta \le 60°$		$\gamma_\beta = 1 - 0.0077\beta$ $\beta \le 60°$
Van Gent and Van der Werf (2019)		$\gamma_\beta = (1 - c_\beta)\cos^2\beta + c_\beta$ $c_{beta} = 0.35$		$\gamma_\beta = (1 - c_\beta)\cos^2\beta + c_\beta$ $c_{beta} = 0.35$

More recently, Van Gent (2020) studied the oblique waves effect in combination with the effects of a berm and roughness elements and assumed that the influence of oblique waves on the average overtopping discharge is affected by the berm width. However, this assumption was not verified based on a variation of berm width.

1.3. Prediction tools of wave overtopping

Various tools are available to predict wave overtopping. Existing prediction tools mainly consist of empirical formulas derived based on physical model tests, machine learning method and numerical modelling. In this section, literature about these prediction tools is briefly reviewed.

1.3.1. Physical modelling and empirical formulas

Empirical formulations such as those listed in Table 1.1-1.4 have been used as a main tool during the last decades for the design of coastal structures (Losada et al., 2008). These formulas consider and parameterize the most relevant variables in the overtopping processes. Most of the empirical formulas are derived based on flume or wave basin experiments.

Physical model tests are a reliable method to determine the wave overtopping at coastal

structures with arbitrary geometries (EurOtop, 2018). Small-scale physical model tests are commonly conducted to determine the average overtopping discharge and wave run-up height. However, scale effects are likely to become relevant for small overtopping discharges e.g. smaller than $q^* = 10^{-6}$. In this case, results from small-scale physical model tests would be less reliable. In the experiments, the average overtopping discharge is often measured by using one wave gauge installed in a box where the overtopped water is guided into using a chute or by using a weighing scale. Micro-propellers and small wave gauges can be used to measure flow velocities and flow depths (Van Gent, 2002b). Wave run-up may be detected by a capacitance wire or a run-up stepgauge with pins along the slope (Capel, 2015). These conventional measurement techniques can also be combined with video imagery which could provide more details about the interactions between waves and coastal structures (Fairley et al., 2009; Sandoval and Bruce, 2018; Raby et al., 2019; Den Bieman et al., 2020). More information about physical model tests on wave overtopping can be found in Frostick et al. (2011).

For cases where empirical formulas are not applicable or the consequences of overtopping are very important, physical modelling may be the only reliable approach to predict overtopping (EurOtop, 2018).

1.3.2. MACHINE LEARNING METHOD

IN addition to empirical formulas and physical modelling, the collection of massive amounts of overtopping data has made it possible to apply machine learning method in the prediction of wave overtopping. A method based on neural networks (NN) has been developed by Van Gent et al. (2007) to predict the average overtopping discharge for many types of coastal structures, including dikes, rubble-mound breakwater, vertical breakwaters and other non-standard structures. The CLASH database has been used as training data for the machine learning models (see for instance Van Gent et al., 2007; Zanuttigh et al., 2016 and Den Bieman et al., 2020). CLASH is the abbreviation of 'Crest Level Assessment of Coastal Structures by full scale monitoring neural network prediction and Hazard analysis on permissible wave overtopping'. A database on wave overtopping was set up within the CLASH project and 10532 tests from 163 independent test series were included in this database (Steendam et al.,2005). Each overtopping test was described by means of 31 parameters which can be classified in three types: general parameters, hydraulic parameters and structural parameters. The database was updated later and the updated database consists of nearly 18000 model-scale tests performed at several institutes. A similar neural network approach was proposed by Zanuttigh et al. (2016) while training the NN also on very low values of the overtopping discharge. More recently, Den Bieman et al. (2020) applied the machine learning method XGBoost (Chen and Guestrin, 2016) to the prediction of the over-

1

topping discharge. This newer model reduces the prediction errors compared to the NN by Van Gent et al. (2007). Later, Den Bieman et al. (2021) further improved the XGBoost model by enlarging the training database and carefully substantiating the selection of features for model training.

However, many machine learning methods require large amounts of data before they are capable of giving reliable results. There are still many white spots of the overtopping database (Den Bieman et al., 2021), which can to some extent limit the application of the machine learning methods for predicting the wave overtopping discharge.

1.3.3. NUMERICAL MODELLING

EMPIRICAL formulas and machine learning method developed based on the physical model tests have limitations in applicability due to the limited ranges of available test results. The validity of these approaches is not always certain for the conditions and configurations that are outside the ranges of experiments. With the development of numerical methods and computational power, numerical modelling is becoming an important complementary tool to predict wave overtopping.

Various types of numerical models are available for simulating the interaction of waves with coastal structures. The performance of the numerical models depends on the governing equations and solving techniques. A computationally efficient approach to model wave interaction with coastal structures is based on the non-linear shallow water equations (NSWE) (see for instance Kobayashi and Wurjanto, 1989; Van Gent, 1995; 2000). However, this type of model has some limitations associated with the parameterized introduction of wave breaking and with the difficulty of dealing with complex geometries of coastal structures. For example, Martínez Pés (2013) performed a validation of the NSWE model SWASH for wave overtopping. The results showed that the SWASH model cannot deal with the wave breaking very well especially when abrupt changes are present in the bottom geometry or steep slopes and the model underestimated the overtopping discharge. A more recent approach is the Smooth Particle Hydrodynamic (SPH) method in its different versions. Several studies have been conducted on this method (see for instance, Li et al., 2004, Didier and Neves, 2009). SPH is a meshfree Lagrangian method which provides excellent capability to track large deformations of the free surface, while it has a clear disadvantage of low computational efficiency as it requires a lot of particles and small time steps to obtain sufficient accuracy. A third type of numerical model is based on the Navier-Stokes equations. The free surface is tracked using the volume of fluid (VOF) method and wave breaking is accounted for by incorporating a turbulence model in the Reynolds-Averaged Navier-Stokes (RANS) equations. This type of model overcomes the limitations associated with wave breaking and is overall computationally more efficient than the SPH models. Many numerical mod-

els for waves and coastal structures interaction have been developed based on the RANS-VOF equations, such as those by Van Gent (1995), Losada et al. (2008), Fang et al. (2010), Lan and Guo (2013), Higuera et al. (2013), Jacobsen et al. (2015) and PILECHI et al. (2018).

Among these models, the OpenFOAM models appear to become increasingly popular for coastal engineering. OpenFOAM® is an open-source computational fluid dynamics framework. Users have the freedom to modify and redistribute this software. The open-source nature contributes to many useful libraries and toolboxes that are freely shared in the public domain (Davidson et al., 2015), increasing the popularity of OpenFOAM across most areas of engineering and science. There has been some research focusing on simulating wave overtopping at coastal structures using OpenFOAM®. Jacobsen et al. (2012) developed the waves2Foam which is a toolbox based on OpenFOAM® that applies a relaxation zone technique to generate and absorb free surface water waves. Later, Jensen et al. (2014) applied this toolbox to simulate overtopping processes at impermeable and permeable structures that have a straight waterside slope. The numerical model of Jensen et al. (2014) gave a good estimate of the average overtopping discharge. However, no turbulence closure was introduced in the numerical model due to the fact that no or only little wave breaking occurred in the test cases. Therefore, it remains unknown whether this model is applicable for cases where wave breaking is important. Patil (2019) modelled the average overtopping discharge at a smooth straight slope and results showed that the OpenFOAM® model slightly underestimated the overtopping discharge. Higuera et al. (2013; 2014b) developed a three-dimensional (3D) Navier-Stokes solver called IHFOAM in the framework of OpenFOAM® to model the interaction between waves and a high mound breakwater. Since the 3D simulation was extremely time-consuming, only 40 s (about 4 waves) was simulated for wave overtopping, which could lead to many uncertainties of estimates of overtopping discharges. Thus, longer simulations were recommended by Higuera et al. (2014b) to obtain more reliable results of wave overtopping. Previous research mainly focused on the simulation of wave overtopping at structures with simple configurations, such as structures that have straight and/or smooth waterside slopes. An extensive validation of the capability of OpenFOAM® in predicting overtopping discharges at dikes that have a berm and roughness elements has not been studied.

1.4. KNOWLEDGE GAPS

BERMS and roughness on waterside slopes can significantly influence the average overtopping discharge at dikes (EurOtop, 2018). Existing methods to estimate the roughness influence usually use a constant influence factor for one certain type of roughness elements. Research like Capel (2015) and Van Steeg et al. (2016) indicated that the roughness influence factor might vary with wave conditions and dike configurations. Additionally, var-

ious types of roughness elements are often combined along the waterside slopes in practice. The only available empirical formula (Eq. (1.1)) for combined roughness influence has not been systematically validated against physical model tests. As for the berm influence, existing empirical equations, like Eq. (1.2) given by EurOtop (2018) and TAW (2002), mainly considered impermeable berms. Knowledge on the effect of permeable berms on the wave overtopping discharge at dikes is still limited. Also, little research can be found for the combined influence of a berm and roughness elements on the average overtopping discharge. The effects of roughness and a berm are not fully understood. Therefore, it is necessary to improve existing empirical equations for predicting the influence of a berm and roughness, thereby improving predictions of wave overtopping.

Empirical formulas are easy to use and straightforward in predicting wave overtopping at dikes. However, they are usually derived based on physical model tests in which only limited wave conditions and dike configurations are considered. Thus, empirical formulas have their limitations in applicability. As a complementary approach with empirical formulas, numerical modelling can be more flexible with wave conditions and structure configurations (Losada et al., 2008). OpenFOAM® is adopted in this PhD study considering it is open-source and it is becoming increasingly popular in coastal engineering. However, the capability of OpenFOAM® in simulating the overtopping discharge at dikes that have a berm and roughness elements has not been systematically studied. A validated OpenFOAM® model will be useful for a better understanding of the effects of a berm and roughness on the average overtopping discharge at dikes. In addition to the average overtopping discharge, overtopping flow velocities and layer thicknesses are also important for flooding events initiated by dike breaching due to wave overtopping (Van Gent, 2020). Empirical formulas listed in Table 1.2 for estimating the flow parameters are derived based on experiments in which only smooth straight waterside slopes were considered. It still remains unknown whether these empirical formulas are also applicable for slopes that have a berm or roughness.

Finally, in addition to a berm and roughness, oblique waves also affect the wave overtopping (De Waal and Van der Meer, 1992). Van Gent (2020) developed an empirical formula for the influence factor of oblique waves assuming this influence factor is dependent on the berm width. This assumption has not been verified based on variations of the berm width. A verification of this assumption is important for accurately predicting the influence of oblique waves on the overtopping discharge when a berm is present at the same time.

1.5. Research aim and questions

Research aim:

To determine the influence of roughness, a berm and oblique waves on wave overtopping processes at dikes by performing physical model tests and numerical simulations.

Research questions:

Q1   What are the effects of berms and roughness of block revetments on the average overtopping discharge at dikes?

Q2   How do the newly derived empirical equations in Q1 perform for predicting the influence factors of a berm and roughness at a rock-armoured dike?

Q3   What is the influence of berms and roughness varied outside of the tested ranges in Q1 on the average overtopping discharge by using numerical modelling?

Q4   By using numerical models, to what extent do roughness, berms and oblique waves affect the average overtopping discharge and the overtopping flow parameters including flow velocity and layer thickness?

1.6. Methodology

T HE overview of the methodologies of four research questions is shown in Figure 1.5. To study the effects of berms and roughness on the average overtopping discharge, physical model tests have been performed first. Part of the experimental data are used to develop empirical equations for the influence factors of roughness and berms (Q1). The remaining data are used to evaluate the performance of the newly derived empirical equations for a rock-armoured dike (Q2). In order to extend the applicability of the empirical equations, a 2DV numerical model is set up based on the OpenFOAM® framework and is validated for predicting average overtopping discharges using the experimental data in Q1 (Q3). Finally, the 2DV numerical model is applied to study the influence of roughness and a berm on overtopping flow velocities and layer thicknesses and the 2DV model is then extended into a 3D numerical model to take oblique waves into account (Q4). The methodology of each research question is further detailed as below.

M1   Small-scale physical model tests have been performed in the Pacific Basin at Deltares. In the experiments, two types of roughness elements including blocks with protrusions in chessboard pattern and open blocks are adopted to study the roughness influence. Herein, open blocks refer to the concrete cubes installed with open space in between. Also, various types of roughness elements are combined along waterside slopes, based on which we can analyze the combined roughness influence on the average overtopping discharge. Both smooth straight waterside slopes and slopes with a berm are tested to investigate the berm effect. Empirical equations for the roughness and berm influence factors are derived based
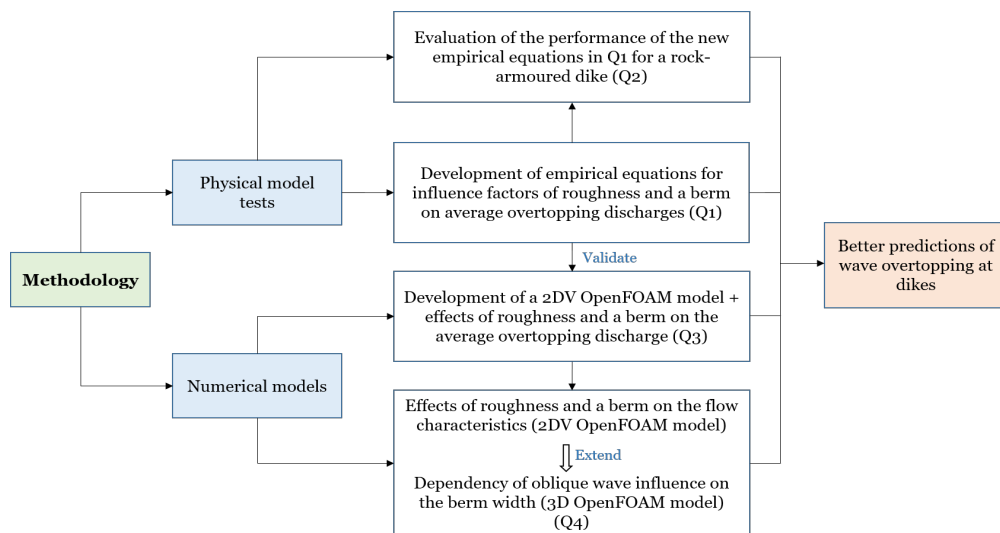
Figure 1.5: Overview of methodology of four research questions.

on the experimental data using the least square method.

M2   Rocks, as an economical and accessible material in nature, are often applied in the cover layer of coastal structures. To validate the developed empirical equations, we perform physical model tests on the overtopping discharge at a rock-armoured dike. The rock armour is applied at different locations along the waterside slope. A wider range of wave conditions and berm widths than the tested range in Q1 is applied here. The estimated values of average overtopping discharges using the empirical equations in Q1 are compared to the measured ones, to evaluate the validity of the new empirical equations for a different type of roughness elements and different structure configurations than those in Q1.

M3   We develop a 2DV numerical model using OpenFOAM® for predicting the average overtopping discharge at dikes. The toolbox waves2Foam developed by Jacobsen et al. (2012) is applied to generate irregular waves. The steering files for wave generation used in the experiments in Q1 are used as input for the numerical model such that the time series of free surface elevation in the experiments and in the numerical model are consistent. The wave breaking is accounted for by using a stabilized $k - \omega$ turbulence model proposed by Larsen and Fuhrman (2018). The roughness of protruding blocks is modelled explicitly by refining the mesh near the protrusions. The 2DV OpenFOAM® model is validated by comparing the modelled average overtopping discharges to the measured discharges from the experiments in Q1. The validated numerical model is then applied to study the effects of a berm and roughness on the average overtopping discharges by changing the berm width, berm level and coverage length of roughness at the waterside slope outside the tested ranges

in Q1 and Q2.

M4 To answer Q4, the developed 2DV numerical model in Q3 is further validated for the overtopping flow velocity and layer thickness using the experimental data from Van Gent (2002b). The influence of roughness on the overtopping flow characteristics is studied by creating protrusions along the waterside slope of a dike in the validated numerical model. We also change the berm width and berm level to analyze the berm influence on the flow velocity and layer thickness. The oblique waves are taken into account by extending the 2DV model into the 3D domain. This 3D numerical model aims to verify the assumption made by Van Gent (2020) that the influence of oblique waves on the average overtopping discharge is dependent on the berm width. For that purpose, the berm width is varied with a fixed direction of oblique waves in the 3D numerical model.

1.7. THESIS OUTLINE

THE thesis is structured as follows: Chapter 2 addresses the research question Q1 focusing on the effects of a berm and roughness on the average overtopping discharge by performing physical model tests. In Chapter 3, the research question Q2 is answered by comparing the estimated average overtopping discharges using empirical equations to the experimental results. Q3 is addressed in Chapter 4 by developing a 2DV OpenFOAM® model. Chapter 5 investigates the effects of roughness, a berm and oblique waves on overtopping flow characteristics and overtopping discharges by using a 2DV OpenFOAM® model and a 3D OpenFOAM® model. The overall discussion is provided in Chapter 6. Finally, Chapter 7 presents conclusions and recommendations for future research.

2

THE INFUENCE OF A BERM AND ROUGHNESS ON WAVE OVERTOPPING AT DIKES

2

ABSTRACT A reliable estimation of average overtopping discharge is important for dike design and safety assessment. Berms and roughness elements are widely applied to reduce the overtopping discharge over dikes. In this study, the effects of a berm and roughness on the wave discharge are investigated by means of physical model tests. New empirical formulae are derived from the analysis of the experimental data in order to provide more accurate estimations of reductive influence of berms and roughness on the wave overtopping discharge. Additionally, a new formula is developed to estimate the reductive influence of varying roughness along the waterside slopes with a berm. The new equations show a significantly better performance within the tested range when compared with existing formulae for the average overtopping discharge.

2.1. INTRODUCTION

$\mathbf{M}$ ANY coastal societies face increasing risks of coastal flood disasters as a result of climate change, sea level-rise and land subsidence (Borsje et al., 2011; Temmerman et al., 2013). Dikes are important coastal structures to protect infrastructure and people in coastal areas from storms (see for instance Goda, 2009). The average wave overtopping is often used to determine the required crest level and cross-section geometry of dikes by ensuring that the average overtopping discharge is below acceptable limits under specified design conditions. Therefore, a reliable prediction of the average overtopping discharge is essential for dike design and reliability (see also Jafari and Etemad-Shahidi, 2011).

Empirical formulations of average overtopping discharge have been a key tool used in the design of the crest level of coastal structures. TAW (2002) provides overtopping equations for breaking and non-breaking waves at dikes that are adopted in EurOtop (2007) to calculate the average overtopping discharge taking several influence factors (i.e. roughness, berms, oblique waves, vertical wall) into account (Appendix 2.A). In these formulae, all influence factors affect the overtopping discharge of the breaking waves while the overtopping discharge of the non-breaking conditions is only affected by the revetment roughness and oblique waves. EurOtop (2018) adapted the TAW (2002) overtopping expression especially for low freeboards, including the zero freeboard. The formulae provided by EurOtop (2018) are similar to those by TAW (2002) but have a power function in the exponent and different values for the empirical coefficients.The same influence factors are adopted in EurOtop (2018) as those in TAW (2002) but to a different power (1.3) (See Table 2.A.1 in Appendix 2.A). Gallach-Sánchez et al. (2018) calibrated the power coefficient for relative free board $R_c/H_m0 \geq 0$ based on more extensive tests and the calibrated value of the power coefficient is 1.1 instead of 1.3. Hence, there is still some dispute over the optimal value for the power coefficient. Capel (2015) derived an overtopping equation on the basis of the wave run-up on dikes. This equation is applicable to both breaking and non-breaking waves. The above mentioned empirical overtopping estimators are summarized in Appendix Table 2.A.1.

In practical engineering, berms and roughness elements are often applied to reduce the average overtopping discharge. In these empirical overtopping formulae, the amount of wave overtopping is affected by berms and by the roughness of the slope covers that are parameterized as influence factors.

There have been some methods available to estimate the berm influence. TAW (2002) and EurOtop (2007, 2018) recommend a method to calculate the berm influence factors as a function of the berm width and berm level relative to the still water level (Eq. (2.A.3)). Instead of introducing a berm factor, Van Gent (1999) includes the berm influence through a characteristic slope which refers to the mean slope of the waterside slopes taking the berms into account. This method assumes that the berm position relative to the SWL has no effect

on the overtopping discharge when the berm is located between $2H_{m0}$ above and $-2H_{m0}$ below the still water line. However, these research are limited to impermeable berms. Thus, a suitable method to take the influence of permeable berms of dikes into account is not available.

According to the literature, most of the research on roughness elements used constant values of the roughness factor to account for the roughness influence on the wave overtopping discharge. TAW (2002) and EurOtop (2007, 2018) provide default values of roughness influence factors for a large variety of roughness elements in breaking wave conditions. For non-breaking waves, roughness factors are slightly affected by the breaker parameter (Eq. (2.A.6)). Bruce et al. (2009) measured the relative difference in mean overtopping discharge for various types of armour units and presented the roughness factor values for various types of roughness elements. Those static roughness values were then used in the neural network prediction of overtopping (e.g., Van Gent, 2007; Verhaeghe et al., 2008). Nevertheless, Capel (2015) and Van Steeg et al. (2018) have shown that the roughness factors are not constant for breaking waves but that they depend on other parameters such as wave conditions and dike configurations. Capel (2015) studied the effect of the roughness of blocks with protrusion on wave overtopping and wave run-up and proposed a new equation to assess the roughness influence coefficient of protruding blocks (Eq. (2.A.7)). The results showed that the effect of roughness decreased with the increasing mean overtopping discharges. Capel (2015) also showed that the wave steepness at the toe of the structure also has an influence on the roughness factor that is not influenced by the slope. A new parameter, roughness density is introduced to describe the characteristics of the roughness pattern. The Capel (2015) formula improves overtopping discharge predictions for straight slopes covered by protruding blocks. However, this equation needs iteration to calculate the roughness factors and is therefore somewhat complicated when applying to practical engineering. Moreover, various types of roughness elements are often combined in the slope protection of dikes. For the varying roughness along the slopes and berms, the various influence factors are weighted in TAW (2002) by including the lengths of the relevant sections of the slope. If three types of roughness elements with lengths of $L1$, $L2$ and $L3$ and influence factors of $\gamma_{f,1}$, $\gamma_{f,2}$ and $\gamma_{f,3}$ respectively are applied along the slopes and berms, then the weighted average as proposed by TAW (2002) is:

$$\gamma_f = \frac{\gamma_{f,1}L_1 + \gamma_{f,2}L_2 + \gamma_{f,3}L_3}{L_1 + L_2 + L_3} \qquad (2.1)$$

This equation is the only available method to estimate the influence of a combination of various types of roughness elements along the slopes. However, Eq. (2.1) has not been validated systematically and therefore the accuracy of this formula remains unknown.

To summarise, existing methods to take the influence of berms and roughness into ac-

count still need improvement. Also, the combined influence of a berm and roughness on the wave overtopping discharge is poorly studied and the only currently available method has not been validated systematically against experimental data. Therefore, the goal of this study is to gain insight into the effects of berms and roughness on wave overtopping at dikes and to increase the prediction accuracy of the average overtopping discharge by improving the methods for estimating roughness and berm influence.

In the present study, physical model tests have been conducted to investigate the influence of a berm and roughness on the average overtopping discharge. Effects of the wave height and wave steepness, the dike configurations and the permeability are analysed to assess the influence of roughness and berms. After the influence factors of roughness and berms have been analysed, the combined influence of varying roughness along the slopes and berms are studied.

The physical model tests have been presented in Section 2.2. In Section 2.3, the analysis of the test results is described, including the introduction of new empirical formulae. In Section 2.4, a further discussion of the results is provided. In Section 2.5, the main conclusions of the presented research are summarised.

2.2. PHYSICAL MODEL TESTS

2.2.1. EXPERIMENTAL FACILITIES

PHYSICAL model tests were performed in the Pacific Basin at Deltares in The Netherlands. This basin is 18.6 m long, 14 m wide and 1.25 m deep (Figure 2.1a). To minimize the influence of reflected waves by the test section with a width of 3 m, a passive permeable wave damping slope has been applied over the full width of the wave basin. A second-order wave control was used to reduce the generation of spurious waves. In the present physical model tests, irregular waves based on the JONSWAP spectrum that has a peak enhancement factor of 3.3 were generated with different combinations of significant wave heights and periods. Three wave gauges were placed near the toe of the structure to measure the wave conditions. Incident and reflected waves were separated by using the method proposed by Mansard and Funke (1980). The wave conditions, including the spectral significant wave height H_{m0} and the mean energy wave period $T_{m-1,0}$, were obtained from the analysis of the measured incident waves at the toe of the structure.

2.2.2. MODEL SET-UP

THE wave basin is wide enough to allow three model sections to be tested simultaneously. The width of each section was 1.0 m. The core of the structures were all impermeable and is made of concrete. Plywood is detachable to be freely placed on the imperme-

able core as a smooth slope or to be removed to install blocks. Wooden boards were installed between the tested models to avoid the influence of adjacent sections. The overtopped water was led into the overtopping tanks by using chutes placed at the rear edge of the crest. One wave gauge was installed in each tank to detect the variations of the water level, which enables the measurement of the overtopped water volume. Both straight slopes without a berm and slopes with a berm were tested in this test programme. Three types of slope protection were considered in the tests: (1) protruding blocks (closed without open space); (2) open blocks without protrusion; (3) smooth slopes representing asphalt or grass. Applying the hypothetical geometrical model scale of 1:15, cubes of 50mm represented about the size of 0.75 m × 0.75 m at the prototype scale. The chessboard pattern of protruding blocks was created by placing a concrete tile of 10 mm thick underneath the blocks such that the protrusion equals the thickness of the concrete tile (Figure 2.1b - ①). Open blocks were placed on the filter layer with a thickness of 2.5 cm leaving small gaps between the blocks (Figure 2.1b - ②). The filter layer was placed directly on the smooth impermeable core. Previous research (Van Gent, 1999) showed that open space should be 25-30% (percentage of the volume of spaces between blocks divided by the total control volume) of the armour layer to obtain a reasonably stable revetment. Hence, 30% open space was used in the tests, which represents a suitable compromise between stability and the amount of blocks needed, resulting in the gap $d = 2$ cm. A slope of 1:3 which is a typical dike slope was used for the straight slopes as well as for the upper slope and for the down slope of sections that have a berm (Figure 2.2a). The structures were constructed such that the external boundaries of the slopes, excluding potential protruding parts, determine the slope parameters. Note that the highest points of the protruding blocks in the upper row may be slightly higher than the crest level. In Figure 2.2a, L_1, L_2 and L_3 represent the effective coverage length of roughness elements on the upper slope, berm and down slope respectively, which is further explained later. A berm width of 0.20m was applied (i.e. the total width of four blocks).

Various types of roughness elements and different configurations including straight slopes (S) and composite slopes with a berm (B) were combined resulting in four sets of sections (Figure 2b). The applied locations of the blocks along the slopes were varied. Numbers in the codes of these sections represent (1) upper slope, (2) upper slope and the berm and (3) entire surface. OB2-d represent the section with open blocks applied on the berm and down slope. COM denotes the combination of protruding blocks (PB) and open blocks (OB) applied on the surface simultaneously. Blocks on the down slope are installed along the entire down slope from the toe to the berm.
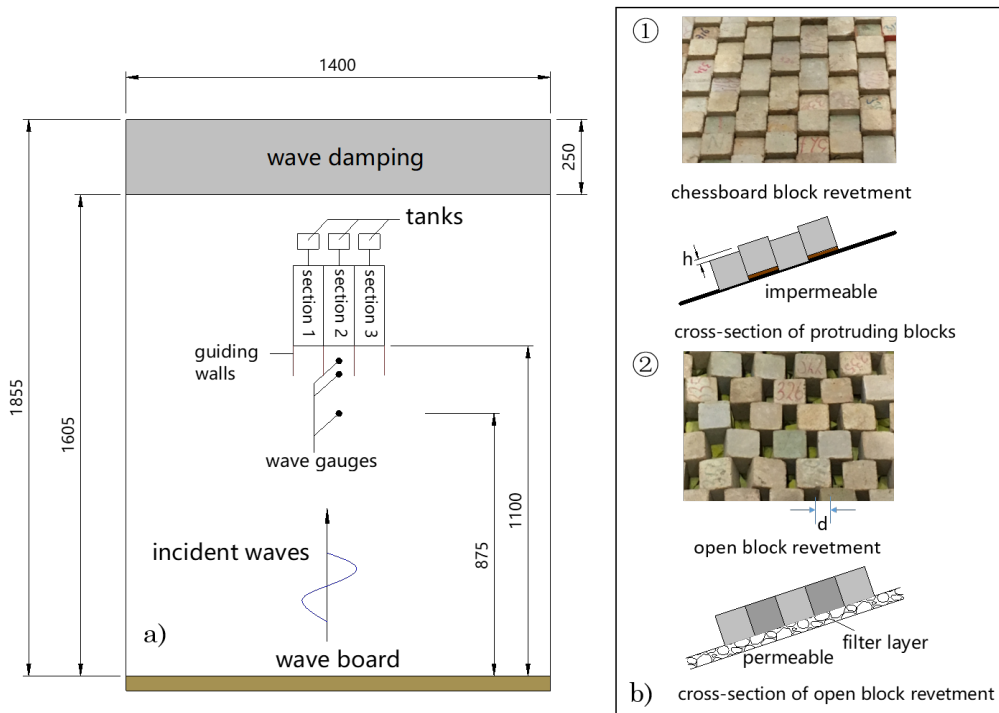
Figure 2.1: Overview layout of tested models with a) top view layout of test conditions (unit: cm); and b) roughness elements with ① the protrusion height $h = 1$ cm and ② $d = 2$ cm and thickness of the filter layer is 2.5 cm with $D_{n50} = 2.5$ cm.

2.2.3. TEST PROGRAMME

FOR each tested section, the berm position as shown in Figure 2.2a was fixed during the tests. Therefore, the berm level relative to the still water level only varies with changes in the water depth. Five freeboards were investigated by changing the water depth by 0.015 m for each test run. For each freeboard, the wave height H_{m0} and spectral wave period $T_{m-1,0}$ were varied resulting in the variation of the wave steepness $s_{m-1,0}$. The ranges of those parameters that were varied in this test programme are listed in Table 2.1, where R_c (0.12 m, 0.135 m, 0.15 m, 0.165 m and 0.18 m) is the relative freeboard, d_h (-0.03 m, -0.015 m, 0 m, 0.015 m, 0.03 m) is the water depth above the berm, $\xi_{m-1,0}$ is the breaker parameter (Iribarren parameter) and q^* ($=q/\sqrt{g H_{m0}{}^3}$) is the non-dimensional average overtopping discharge. Wave overtopping for each test was measured for at least 1000 waves. This time duration is considered sufficient for generating the full wave height and period distribution over the frequency domain of interest and for stabilizing statistical properties of wave overtopping. In total, 429 tests were conducted.

2

(a)

(b)
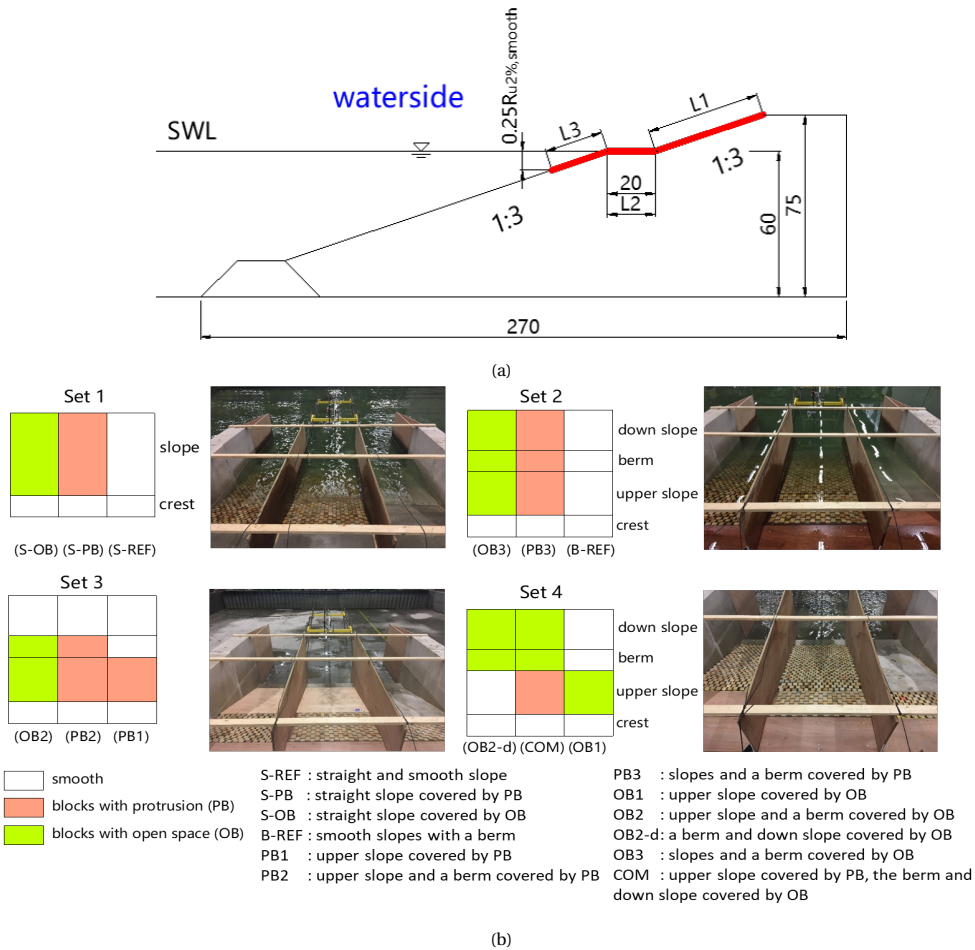
Figure 2.2: Schematic diagram of a) cross-section of tested slopes with a berm (unit: cm) and b) tested configurations with different types of roughness elements.

2.3. Analysis of experimental results

Since the TAW (2002) overtopping equations are still the most used methods for predicting the average overtopping discharge (Capel, 2015), the TAW equations are estimated and recalibrated using the data from the reference tests (Dataset S-REF) performed on smooth straight slopes. Once the structure profile is defined and wave conditions and overtopping discharge are known, the recalibrated TAW (2002) overtopping equations can serve as reference equations to calculate the effective roughness factors in case of no berm (γ_b=1) and berm factors with no roughness (γ_f=1) based on the experimental data. Regression analysis is conducted for effective berm and roughness coefficients, showing that the

Table 2.1: Summary of parameters of the datasets.

	Dataset	R_c [m]	d_h [m]	H_{m0} [m]	$s_{m-1,0}$ [-]	$\xi_{m-1,0}$ [-]	q^*	Number
Set1	S-REF	(0.12, 0.18)	—	(0.09, 0.123)	(0.027, 0.049)	(1.50, 2.03)	(0.001, 0.016)	62
	S-PB	(0.12, 0.18)	—	(0.09, 0.123)	(0.027, 0.049)	(1.50, 2.03)	(1e-4, 0.0076)	62
	S-OB	(0.12, 0.18)	—	(0.09, 0.123)	(0.027, 0.049)	(1.50, 2.03)	(1e-4, 0.006)	62
Set2	B-REF	(0.12, 0.18)	(-0.03, 0.03)	(0.09, 0.133)	(0.027, 0.040)	(1.67, 2.03)	(3e-4, 0.009)	47
	PB3	(0.12, 0.18)	(-0.03, 0.03)	(0.09, 0.133)	(0.027, 0.040)	(1.67, 2.03)	(1e-4, 0.003)	20
	OB3	(0.12, 0.18)	(-0.03, 0.03)	(0.09, 0.133)	(0.027, 0.040)	(1.67, 2.03)	(1e-4, 0.0023)	20
Set3	PB1	(0.12, 0.18)	(-0.03, 0.03)	(0.1, 0.133)	(0.027, 0.042)	(1.63, 2.03)	(1e-4, 0.003)	25
	PB2	(0.12, 0.18)	(-0.03, 0.03)	(0.1, 0.133)	(0.027, 0.042)	(1.63, 2.03)	(7e-5, 0.003)	25
	OB2	(0.12, 0.18)	(-0.03, 0.03)	(0.1, 0.133)	(0.027, 0.042)	(1.63, 2.03)	(6e-5, 0.002)	25
Set4	OB1	(0.12, 0.18)	(-0.03, 0.03)	(0.09, 0.12)	(0.027, 0.042)	(1.63, 2.03)	(4e-5, 0.002)	27
	OB2-d	(0.12, 0.18)	(-0.03, 0.03)	(0.09, 0.12)	(0.027, 0.042)	(1.63, 2.03)	(4e-4, 0.008)	27
	COM	(0.12, 0.18)	(-0.03, 0.03)	(0.09, 0.12)	(0.027, 0.042)	(1.63, 2.03)	(5e-5, 0.0034)	27

roughness factor varies with wave conditions and berm factor is also affected by wave steepness apart from berm geometry and location. The efficiency of the new formulae for berm and roughness coefficients obtained by regression are then compared with TAW (2002) formulae. The case in which a berm and roughness are combined is then analysed and different solution methods are proposed for impermeable and permeable berms. Finally, the varying roughness along the surface is analysed and weights are derived to combine roughness coefficients of different types of roughness elements on upper slope, berm and down slope.

2.3.1. RECALIBRATION OF TAW (2002) OVERTOPPING FORMULAE

MEASURED overtopping discharges for smooth straight slopes were compared against calculated discharges using the TAW overtopping formulae (Eqs. (2.A.1, 2.A.2)) (Figure 2.3a). The results show that the equation (Eq. (2.A.1)) for non-breaking waves predicts the overtopping discharges of smooth straight slopes quite well. However, the equation (2.A.2) for breaking waves slightly overestimates the overtopping discharges. Hence, for the analysis, this equation is recalibrated based on the present dataset. This was achieved by recalibrating the coefficient -4.75 in the equation for breaking waves to -4.90 through fitting the experimental data (Dataset S-REF) by applying the least squares method. To check the performance of the recalibrated equation for breaking waves (Eq. (2.2)), the calculated and measured overtopping discharges were compared and a good agreement was found as shown in Figure 2.3b. The recalibrated new equation (i.e. Eq. (2.2)) has a mean relative error (MRE) of 9.7%, which is smaller than the MRE of 15.6% for the TAW equation for breaking waves:

$$q^* = \frac{0.067}{\sqrt{\tan\alpha}} \gamma_b \xi_{m-1,0} \exp\left(-4.90 \frac{R_c}{H_{m0}\xi_{m-1,0}\gamma_b\gamma_f\gamma_\beta\gamma_v}\right) \tag{2.2}$$

where $\gamma_\beta = \gamma_v = 1$ in this study, and $q^* = \frac{q}{\sqrt{gH_{m0}^3}}$.

(a) TAW equations

(b) Recalibrated TAW equation
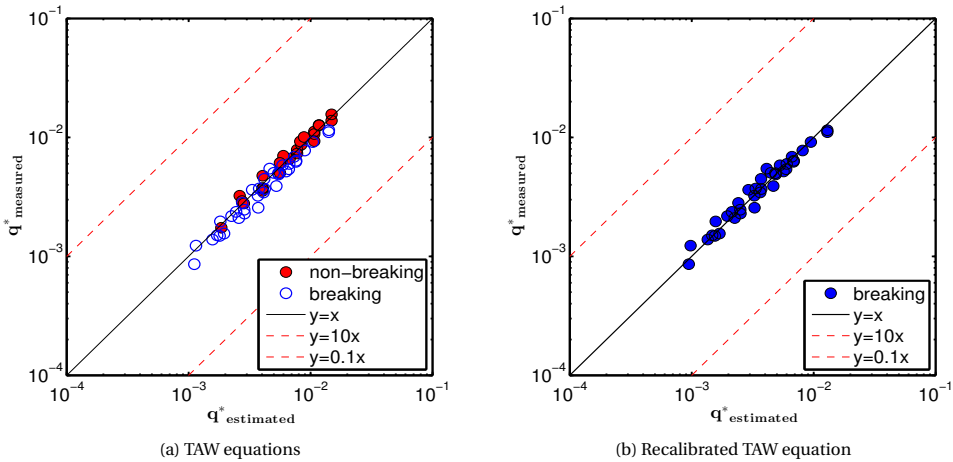
Figure 2.3: Measured dimensionless overtopping discharges versus estimated ones using a) TAW equations; and b) recalibrated TAW equation for breaking waves (Dataset S-REF).

The wave overtopping data of the tests for all sections, the TAW equations and the recalibrated TAW equations for breaking waves are plotted in Figure 2.4.This was done for both the breaking wave conditions and non-breaking wave conditions. TAW method (Eq. (2.A.3)) is adopted to calculate the berm factors. Roughness coefficient γ_f of 0.73 for protruding blocks is given by EurOtop (2018) and the value 0.49 or single layer of open blocks is given by Bruce et al. (2009) and also EurOtop (2018). The comparisons of roughness revetments applied in the tests with those from previous literature (Bruce et al., 2009; EurOtop, 2018) are present in Figure 2.5. Even though the recalibrated equation (2.2) predicts the overtopping discharge of smooth straight slopes rather good, Figure 2.4 shows large and systematic differences for the various dike geometries. These differences are caused by the TAW equations (2.A.3) and (2.A.6) failing to accurately estimate the berm influence and roughness influence factors.

The points from the Dataset S-OB show that the roughness influence is considerably overestimated by the TAW method. This might be, because the γ_f of 0.49 for open block roughness is obtained based on the tests on breakwaters with a permeable core. Thus, this value, which is recalibrated later using Dataset S-OB, may not be reasonable for dikes with an impermeable core. The influence of protruding blocks is estimated reasonably for non-breaking conditions while it is somewhat underestimated for conditions with breaking waves (see Dataset S-PB points). Additionally, the data for section B-REF (green circles in Figure 2.4a) lie below the TAW equation line, which indicates that the berm influence is underestimated. The roughness factors were calculated by using Eq. (2.1) for the sections that had various types of roughness elements applied. The differences between the measured
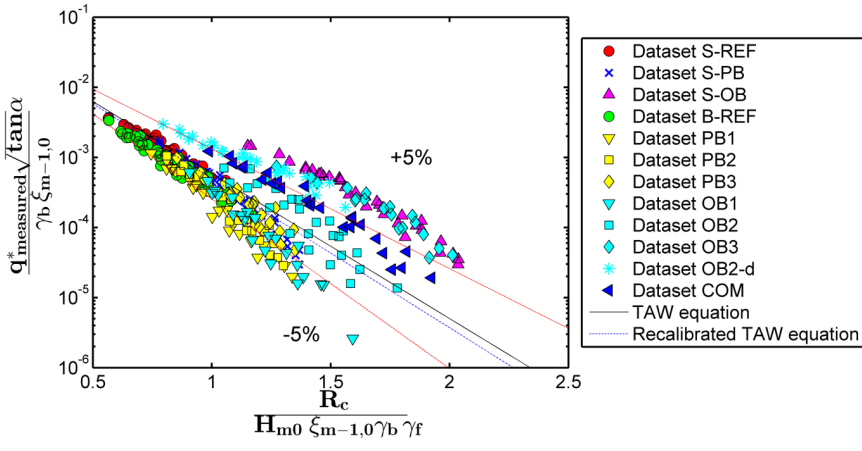
(a) Breaking wave conditions
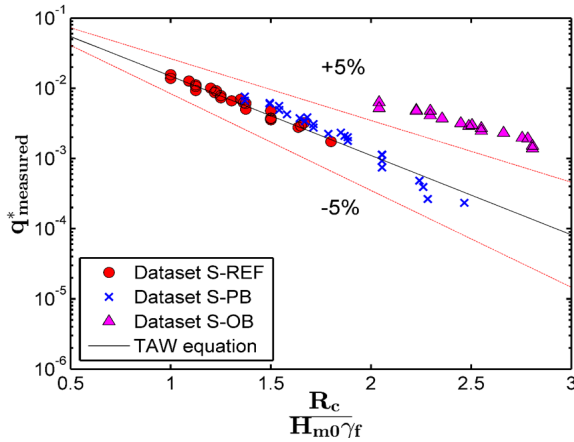
(b) Non-breaking wave conditions

Figure 2.4: Wave overtopping data for a) Breaking wave conditions; and b) Non-breaking wave conditions with the 5% exceedance lines (red dash lines) indicating the 90% confidence band of the TAW equations.

and calculated overtopping discharges demonstrate that Eq. (2.1) cannot accurately predict the reductive influence of varying roughness along the slopes with a berm. Therefore, it is necessary to improve the TAW equations for estimating the influence of a berm and roughness distribution on the average overtopping discharge.

2.3.2. RESULTS FOR PROTRUDING BLOCKS

I N subsection 2.3.2.1, the effective roughness factors of protruding blocks on the straight slope are obtained by directly solving the overtopping formulae with the overtopping discharge (q) substituted by the measured overtopping discharge (Dataset S-PB). Both equa-

Protruding block revetment in tests   Open block revetment in tests

Picture from EurOtop (2018)   Picture from Bruce et al. (2009)

a)   b)
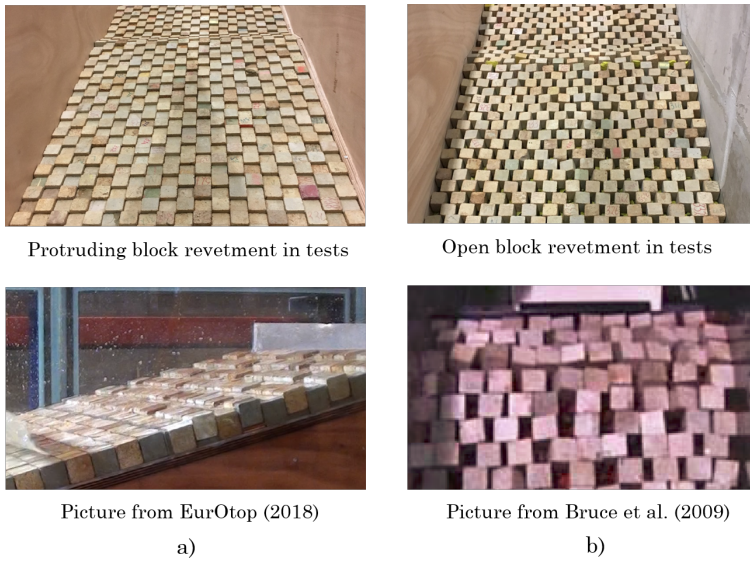
Figure 2.5: Comparison of rough slopes with those provided in previous literature with a) protruding block revetment and b) open block revetment.

tions for breaking waves and non-breaking waves include the roughness coefficient. Therefore, Eq. (2.2) is used to calculate the effective roughness factors for $\xi_{m-1,0} < 1.8$ and the TAW equation for non-breaking waves (Eq. (2.A.2) in the Appendix 2.A) is used for $\xi_{m-1,0} > 1.8$. Similarly, the breaking equation (Eq. (2.2)) was used as the basis of calculation of effective impermeable berm factors (Dataset B-REF) as presented in subsection 2.3.2.2. With the effective influence factors available, it is feasible to fit the experimental data and to derive new equations for roughness and berm effect factors. The newly derived equations are validated by comparing the estimated values with the effective influence factors obtained from the measured overtopping discharges. Subsection 2.3.2.3 deals with the roughness influence of protruding blocks applied on parts of the dike surface.

2.3.2.1. ROUGHNESS INFLUENCE OF PROTRUDING BLOCKS ON THE STRAIGHT SLOPE

THE effective roughness factors $\gamma_{f-effective}$ and dimensionless parameters R_c/H_{m0} and $\xi_{m-1,0}$ are plotted in Figure 2.6a with on the vertical axis the, for breaker parameter corrected, roughness factor '$(1-\gamma_{f-effective})/(1/\xi_{m-1,0})$' and on the horizontal axis the relative freeboard 'R_c/H_{m0}'. We use R_c/H_{m0} because the overtopping discharge is most sensitive to the relative freeboard when $R_c/H_{m0} > 1$ (Pillai et al., 2017a) and the roughness factor is affected by overtopping discharge (Capel, 2015). The data show a linear relation between these two terms. As the relative freeboard increases, the roughness influence increases (i.e. a lower reduction factor due to roughness). This can be explained as follows: the roughness

has more effect for conditions with a thinner layer thickness, which is the case for larger relative freeboards with less overtopping. In addition to the influence of the relative freeboard, conditions with a smaller breaker parameter also show an increase of the influence of the roughness (i.e. a lower reduction factor due to roughness). The linear relation in Figure 2.6a results in a new equation for roughness factors of protruding blocks by using the linear regression method:

$$\gamma_f = 1 - \frac{c_0 R_c}{H_{m0}\xi_{m-1,0}} \tag{2.3}$$

where $c_0 = 0.36$. It is feasible to calibrate the coefficient c_0 for other types of roughness elements on straight slopes. Note that the slope is not varied in the tests and therefore the breaker parameter $\xi_{m-1,0}$ is strictly related to wave steepness.
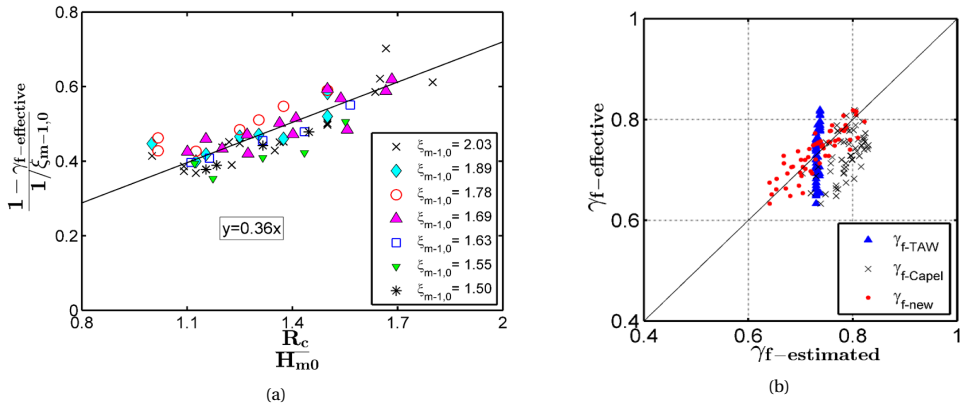
Figure 2.6: Analysis of factors of protruding blocks on the straight slope (Dataset S-PB) with: a) Influence of relative free board and breaker parameter on roughness influence factors; and b) Comparison of effective roughness factors and calculated roughness factors using TAW method, the Capel (2015) method and the new equation (Eq. (2.3)).

The estimated roughness factors ($\gamma_{f-estimated}$) by using TAW method (Eq. (2.A.6)), Capel equation (2.A.7) and the new equation (2.3) were compared with the effective roughness factors (Figure 2.6b) to validate the performance of the new equation that estimates the roughness influence of protruding blocks. The Nash–Sutcliffe model efficiency coefficient (NSE) is used to assess the predictive power of the empirical formulae and is defined as:

$$NSE = 1 - \frac{\sum_{i=1}^{N}(x_i - y_i)^2}{\sum_{i=1}^{N}(x_i - \bar{x})^2} \tag{2.4}$$

where N is the number of observations; x_i is the observed value; $\bar{x}$ is the mean value of the observed data; y_i is the predicted value. NSE can range from $-\infty$ to 1. $NSE = 1$ corresponds to a perfect match of predicted data to the measured data. $NSE = 0$ indicates that

the predicted values are as accurate as the mean of the measured data. $NSE < 0$ indicates that the observed mean is a better predictor than the empirical formula. The closer the NSE is to 1, the more accurate the empirical formula is.

The results show that the developed equation can estimate the roughness influence much better than the TAW (2002) and Capel (2015) equations with NSE improving from 0.07 for the TAW (2002) equation and -1.13 for the Capel equation to 0.71 for the new equation (2.3).

2.3.2.2. Influence factor of an impermeable berm

Dataset B-REF is used to investigate the reductive influence of an impermeable berm on the average overtopping discharge. Since the data on non-breaking waves are close to the transition from breaking waves to non-breaking waves and adding a berm would cause that the waves are more breaking than surging (Van Gent, 2013), the breaking equation (2.2) was used as the basis of calculation of effective berm factors by applying $\gamma_f = \gamma_\beta = \gamma_v = 1$ (i.e. the influence factors for roughness, oblique waves and vertical walls, respectively, all set at no influence). Plotting the inverse of the root square of the wave steepness $'1/\sqrt{s_{m-1,0}}'$ on the horizontal axis and the changed berm factors $'(1-\gamma_{b-effective})'/(r_B(1-r_{dh}))$ on the vertical axis (where r_B is a parameter taking the width of the berm into account and r_{dh} is a parameter to take the level of the berm into account) shows that wave steepness has an effect on the berm factors (Figure 2.7a). The berm influence increases as the wave steepness decreases. A modified equation (2.5) for impermeable berm factors was developed by fitting the experimental data:

$$\gamma_b = 1 - b_0 \frac{r_B(1 - r_{dh})}{\sqrt{s_{m-1,0}}} \qquad 0.6 \leq \gamma_b \leq 1.0 \tag{2.5}$$

with the expressions for r_B and r_{dh} from TAW (2002):

$$r_B = \frac{B}{L_{Berm}}$$

$$r_{dh} = 0.5 - 0.5\cos\left(\pi \frac{d_h}{R_{u2\%}}\right) \qquad \text{for a berm above the still water level}$$

$$r_{dh} = 0.5 - 0.5\cos\left(\pi \frac{d_h}{2H_{m0}}\right) \qquad \text{for a berm below the still water level}$$

where the empirically derived coefficient b_0 is 0.21. r_B [-] represents the influence of the berm width B [m] and r_{dh} [-] stands for the effect of the d_h [m] which refers to position of the berm relative to SWL; $R_{u2\%}$ is the wave run-up height that is exceeded by 2% of the number of incoming waves at the toe of the structure, which can be calculated using Eqs. (2.A.4, 2.A.5). The maximum influence is limited to $\gamma_b = 0.6$ (EurOtop,2018), which is also adopted in the new Eq. (2.5).

Figure 2.7b shows that the estimated berm factors by using Eq. (2.5) increases the *NSE* from -1.91 for TAW (2002) Eq. (2.A.4) to 0.60 for the new equation. It must be mentioned that Eq. (2.5) is developed for impermeable berms only, which are the smooth berms (B-REF) and berms covered with protruding blocks. The influence factors for a permeable berm covered by open blocks will be discussed later.

2

(a)

(b)
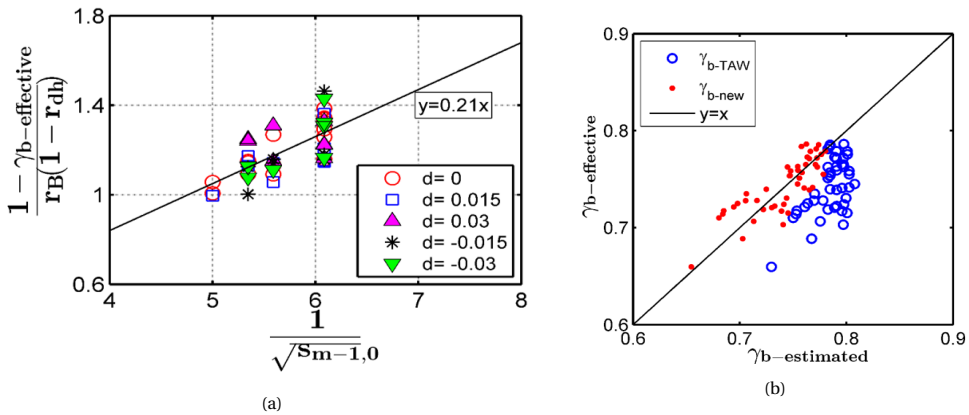
Figure 2.7: Analysis of impermeable berm factors using Dataset B-REF with: a) Influence of wave steepness on influence factors of an impermeable berm; and b) Comparison of effective berm factors with estimated factors using TAW (2002) equation and new equation (Eq. (2.5))

2.3.2.3. COMBINED INFLUENCE OF A BERM AND ROUGHNESS FOR PROTRUDING BLOCKS

Eq. (2.5) is assumed to be applicable for a berm covered by protruding blocks since the protruding block revetment is impermeable. Eq. (2.3) for roughness influence factors and Eq. (2.5) for berm factors are used in combination to calculate the combined influence $\gamma_b \gamma_f$ for Dataset PB3. With this combined influence known, the average overtopping discharges are calculated using Eq. (2.2), and are then compared with the measured ones from Dataset PB3 (Figure 2.8). The results show that there is good agreement between estimated and measured overtopping discharges, which suggests that Eq. (2.3) for the roughness influence is also valid for the slopes with a berm.

Datasets PB1, PB2 and PB3 are selected to investigate the reductive influence of varying roughness along the slopes that have a berm. Effective roughness factors of section PB1, PB2 and PB3 are calculated on the basis of Eq. (2.2) with berm factors being obtained using Eq. (2.5) and $\gamma_\beta = \gamma_v = 1$. Figure 2.9 shows the effective roughness factor data for protruding blocks on parts of the slopes that have a berm under various test conditions in terms of total coverage length of protruding blocks l (m) on the horizontal axis and effective roughness factor γ_f on the vertical axis.

The four points from left to right in each scatter diagram in Figure 2.9 represent the ef-
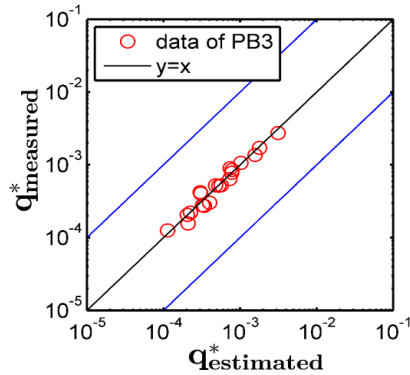
Figure 2.8: Measured versus estimated overtopping discharges over section PB3 that has protruding blocks applied on the slopes and the berm. The berm and the roughness influence factors are calculated by using Eq. (2.5) and by using Eq. (2.3) respectively.
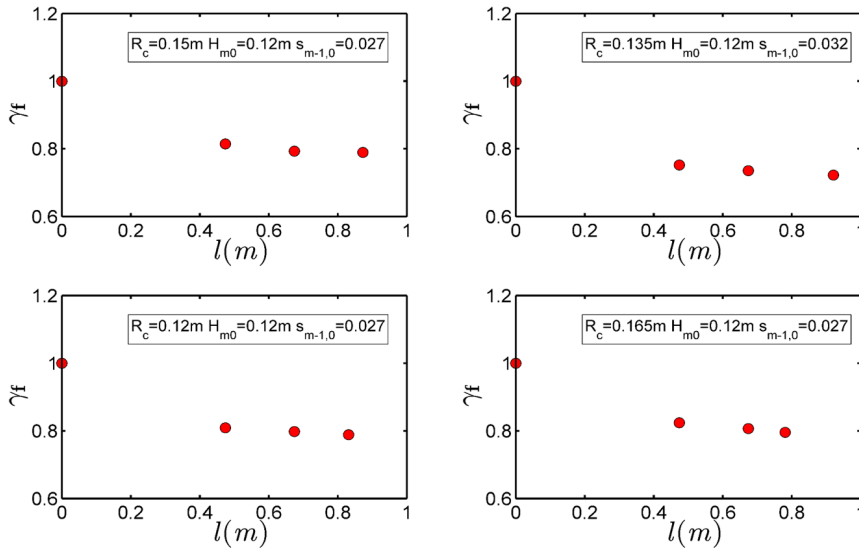
Figure 2.9: Comparison of roughness factors of the slopes for four test conditions selected from Datasets PB1, PB2 and PB3.

fective roughness factors of sections B-REF, PB1, PB2 and PB3 respectively. The values of the roughness factor significantly decrease from smooth slopes (B-REF) where $\gamma_f = 1$ for $l = 0$ m to slopes that have blocks on the upper slope (PB1) where $\gamma_f \approx 0.8$. However, the decrease of the roughness factor is small if the blocks are also applied to the berm and down slope. Therefore, blocks on the upper slope are effective while the blocks on the berm and down slope have only a limited effect on the total roughness influence. This can be explained as follows: the water layer thickness becomes much smaller on the upper slope than on the

berm and on the down slope, and therefore the roughness influence becomes more pro-
nounced for the upper slope. Blocks on various parts of the slopes contribute differently to
the total roughness factor, which demonstrates that the TAW (2002) equation for calculat-
ing varying roughness along the slopes is not accurate since the calculated roughness factor
using Eq. (2.1) decreases linearly as the coverage length increases. To describe the contribu-
tions of blocks on various parts of the surface (Figure 2.2a) (between $0.25R_{u2\%,smooth}$ under
the still water line and the crest in this study) to the total roughness factor, location weight-
ing coefficients are introduced for various parts of the waterside surface. The roughness
elements placed below $0.25R_{u2\%,smooth}$ under the still water level have little or no effect
on the total roughness factor (TAW, 2002). Therefore, only the roughness elements lying
between $0.25R_{u2\%,smooth}$ under the still water level and the crest are taken into account to
calculate the roughness influence factor. Accordingly, L_3 in Figure 2.2a is the effective cover-
age length above the $0.25R_{u2\%,smooth}$ under the still water level. $0.25R_{u2\%,smooth}$ is the wave
run-up on a smooth surface which can be calculated by using the Eq. (2.A.4, 2.A.5) (Ap-
pendix 2.A), with $\gamma_f = 1$. Consequently, the effective coverage length L_3 varies with wave
conditions, because the location of wave impact on the slope changes with hydrodynamic
conditions. Eq. (2.1) is modified to:

$$\gamma_f = \frac{\alpha_1\gamma_{f,1}L_1 + \alpha_2\gamma_{f,2}L_2 + \alpha_3\gamma_{f,3}L_3}{\alpha_1L_1 + \alpha_2L_2 + \alpha_3L_3} \tag{2.6}$$

where α_1, α_2 and α_3 are the location-weighting coefficients for roughness elements on the
upper slope, berm and down slope respectively and $\alpha_1 + \alpha_2 + \alpha_3 = 1$. $\gamma_{f,1}$, $\gamma_{f,2}$ and $\gamma_{f,3}$ are
the roughness factors of roughness elements applied over the entire surface. L_1, L_2 and L_3
are the effective coverage lengths of roughness elements as shown in Figure 2.2a.

For each test condition, the values of α_1, α_2 and α_3 can be obtained by solving Eq.
(2.6). Applying this procedure yields the mean values of α_1, α_2 and α_3 of 0.65 (±0.116),
0.22 (±0.062) and 0.13 (±0.071) for upper slope, berm and down slope respectively. The
standard deviations show that the location-weighting coefficients vary slightly for different
test conditions. This might be caused by the variation of the still water level. When the wa-
ter level is above the berm, the contribution of the roughness elements on the upper slope
to the roughness influence might slightly decreases.

Since the location weighting coefficients are known, it is feasible to calculate the reduc-
tive influence of varying roughness. For example, the roughness factors for the waterside
surface that have blocks applied on the upper slope in combination with a smooth berm
and a smooth down slope can be calculated by using Eq. (2.7):

$$\gamma_f = \frac{0.65\gamma_{f-PB3}L_1 + 0.22 * 1 * L_2 + 0.13 * 1 * L_3}{0.65L_1 + 0.22L_2 + 0.13L_3} \tag{2.7}$$

where γ_{f-PB3} can be calculated by using Eq. (2.3). The effective roughness factors and calculated values by using Eq. (2.1) in which γ_{f-PB3} was calculated using Eq. (2.3) and by using the new equation (2.6) are compared in Figure 2.10. Eq. (2.1) overestimates the combined roughness factors for PB1 and PB2. The new Eq. (2.6) performs much better in estimating the influence of varying roughness along the slopes with a berm with the NSE improving from -3.09 for Eq. (2.1) to 0.46 for the new equation.

(a) a) TAW equation (Eq. (2.1))   (b) b) New equation (Eq. (2.6))
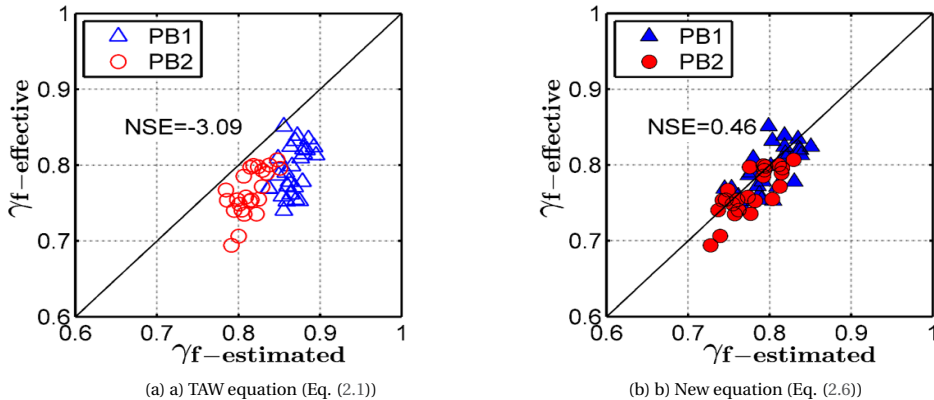
Figure 2.10: Comparisons of effective roughness factors with estimated roughness factors of PB1 and PB2.

2.3.3. RESULTS FOR PROTRUDING BLOCKS

THE effective roughness factors of open blocks applied on the straight slope (Dataset S-OB) are calculated using the same method as applied in the calculation of the effective roughness factors of protruding blocks. The coefficient c_0 in Eq. (2.3) was recalibrated for open blocks by fitting the Dataset S-OB, which yields $c_{0,OB} = 0.38$. The roughness of open blocks is slightly larger than that of the protruding blocks with $c_{0,OB} = 0.36$.

Since 0.49 is not a reasonable value for open blocks on an impermeable core, it is recalibrated using the Dataset S-OB as 0.7 and is then used in comparison with the newly derived Eq. (2.3). Validation of the new equation for roughness of open blocks is performed by comparing the estimated roughness factors ($\gamma_{f-estimated}$) against the effective values ($\gamma_{f-effective}$), and an evident improvement over the TAW (2002) equation for the roughness influence is shown in Figure 2.11 with NSE improving from 0.028 for the TAW (2002) equation to 0.39 for Eq. (2.3) with $c_{0,OB} = 0.38$.

The berm covered by open blocks with a 2.5 cm filter layer below the blocks is permeable. The observed overtopping discharges over section OB-2d with open blocks applied to the berm and down slope are larger than discharges of the smooth slopes that have a berm (B-REF) (see Figure 2.12). This is counterintuitive since OB2-d is expected to be rougher.
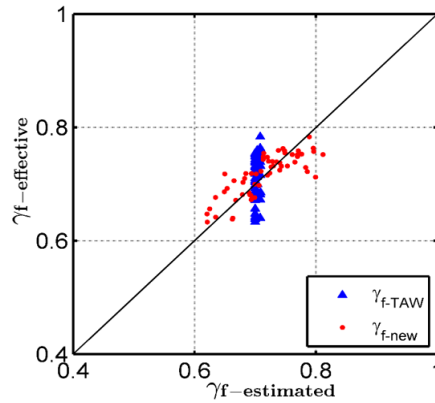
Figure 2.11: Effective roughness factors vs estimated values using TAW (2002) method and the new equation for the roughness of open blocks on the straight slope.
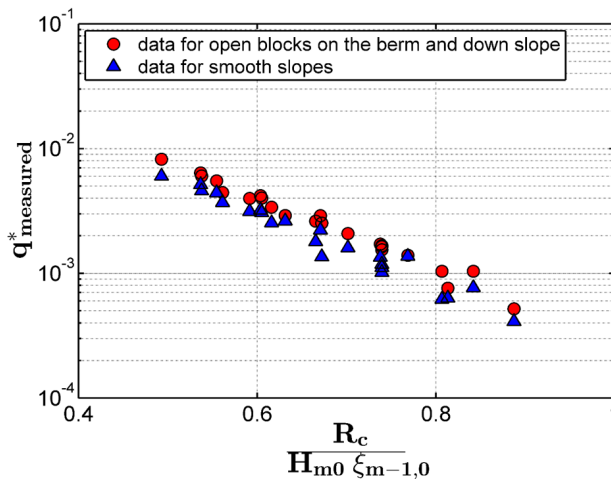
Figure 2.12: Comparison of average overtopping discharges of section that has open blocks on the berm and down slope (OB2-d) and the section of smooth slopes that includes a berm (B-REF).

Possibly, also the permeability plays a role, which is in accordance with the results of a rock berm described in Krom (2012): who suggested that waves can to some extent propagate through a permeable berm leading to less energy reflection and less concentration of wave energy over the available water depth. Therefore, the permeable berms can be expected to result in less wave breaking than an impermeable berm. This could then lead to less wave dissipation due to wave breaking, and therefore a larger overtopping.

If the form of Eq. (2.5) for an impermeable berm is adopted for a permeable berm, then the γ_b should be larger for a permeable berm and consequently the empirical coef-

ficient b_0 should be smaller than 0.21. Applying the equation for the roughness influence of open blocks on the straight slope to calculate the roughness factors of open blocks on the slopes that have a berm, results in a calibrated, b_0 of 0.22 using Dataset OB3. This is in contradiction with the observation that for permeable berms the influence of the berm is smaller than for an impermeable berm (since $b_0 = 0.22$ and not $b_0 < 0.21$). Therefore, the roughness influence equation for open blocks on the straight slope is not used for those composite slopes that have a berm (section OB3). To derive the equations for the permeable berm influence and for the roughness influence of open blocks, the forms of Eq. (2.3, 2.5) are applied with the coefficients b_0 and c_0 unknown. An important assumption made here is that the location weighting factors γ_1, γ_2 and γ_3 proposed for protruding blocks are also applicable for open blocks on parts of the slopes that have a berm. Based on this assumption, Datasets OB1, OB2-d, OB3 are selected to calibrate coefficients b_0 and c_0 by using the method of least squares such that the sum of squares of the errors is at a minimum. The error is defined as:

$$\epsilon_i = \log q^*_{i\_calculated} - \log q^*_{i\_measured} \tag{2.8}$$

Applying this procedure, we determine b_0 and c_0 as 0.13 and 0.55 respectively (Figure 2.13). The standard errors of b_0 and c_0 are 6.74×10^{-3} and 4.70×10^{-3} respectively.

Datasets OB2 and COM are used to validate the assumption that we made and the new equations for open blocks. Figure 2.14 shows that the measured and calculated overtopping discharges generally match well, which demonstrates the validity of the assumption and of the new derived equations for open blocks.
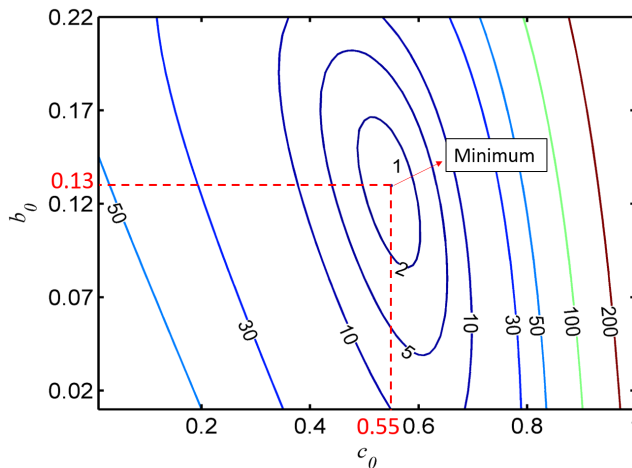
Figure 2.13: Sum of the squares of the errors ϵ_i of overtopping data.
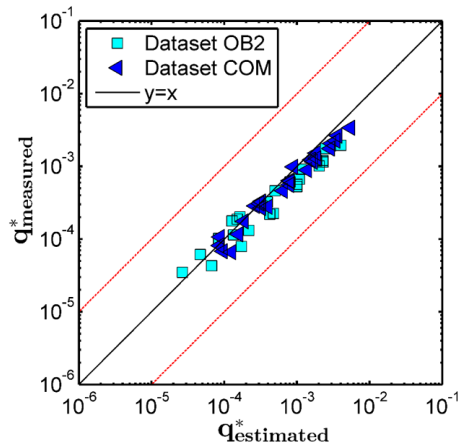
Figure 2.14: Measured versus calculated dimensionless average overtopping discharges for: (1) section OB2 with open blocks applied on the upper slope and berm; and (2) section COM with protruding blocks on the upper slope and open blocks on the berm and down slope.

2.4. DISCUSSION

2.4.1. NEW FORMULAE FOR ROUGHNESS AND BERM INFLUENCE AT DIKES

THE reductive effects of a berm and roughness on the average overtopping discharges at dikes were investigated by performing the proposed physical model tests for different slope configurations and wave conditions. Three new equations for berm and roughness influence factors (given in Box 2.1) are derived based on the analysis of the experimental results.

From the analysis of the roughness influence of protruding blocks and open blocks, we found that the roughness factors are not static values but are influenced by relative free-board and breaker parameter. The empirical coefficient c_0 in Eq. (2.3) is related to the properties of roughness elements and dike configuration. For the open blocks, the value of c_0 for straight slopes is smaller than that for the slopes with a berm. This could be because the overtopping discharge is smaller due to the berm influence and therefore the open block revetment is rougher. In contrast, the values of c_0 for protruding blocks on the straight slopes and slopes with a berm are the same, which might be a coincidence. Hence, the coefficient c_0 is not necessarily the same for the straight slopes and for slopes with a berm. Figure 2.6b and Figure 2.10b show that Eq. (2.3) performs better than the TAW (2002) method. Moreover, Eq. (2.3) is straightforward and does not require an iterative calculation compared to the Capel (2015) roughness equation. It is feasible to adapt Eq. (2.3) to other types of roughness elements by calibrating the coefficient c_0.

The TAW equation for estimating the berm influence was modified by taking into ac-

2

count the wave steepness. The results showed that the berm influence decreases as the wave steepness increases. The permeable berm shows smaller reductions on the overtopping discharge than the impermeable berm. This is found by the experimental results showing that the overtopping discharges over section OB2-d are larger than B-REF under the identical wave conditions. Similarly, smaller overtopping discharges were also observed at section OB1 than at section OB3. A new equation was derived to calculate the berm influence factors with different values of the coefficient b_0 for impermeable and permeable berms. The coefficient b_0 should be a function of berm permeability and possibly other properties of the berm material. In this study, only three types of materials were considered. Therefore, we recommend to further investigate the berm influence by including larger variations of the permeability of the berm. A new equation was developed to calculate the reductive influence of varying roughness along the slopes that have a berm. Roughness elements applied on the upper slope were more effective than those on the berm or down slope in reducing the overtopping discharges (Figure 2.9). This phenomenon was also reported in Hunt-Raby et al. (2010). Location-weighting coefficients α_1, α_2 and α_3 are introduced to describe the effect of applied locations of roughness elements on the overall roughness influence factors. In this study, coefficients α_1, α_2 and α_3 are determined to be 0.65, 0.22 and 0.13 for the upper slope, berm and down slope respectively, which clearly shows that the upper part has the largest weight. It should be noted that the still water levels in the tests were varied around the berm position within a narrow range of -0.03~0.03m. The determined values of location weight factors are only valid within the tested ranges. Therefore, further investigation of the location weighting coefficients outside the tested ranges in this study are recommended.

2.4.2. Comparison with existing overtopping equations

THE performance of the newly derived equations presented in this study is compared with three other overtopping formulae applicable for dikes among the full test data set (Figure 2.15). The Capel (2015) method is only applicable for protruding blocks. Moreover, the Capel (2015) overtopping equation does not incorporate the berm influence factor γ_b. Therefore, the recalibrated value of 0.70 is applied to calculate the roughness factors of the open blocks in the extended Capel (2015) overtopping equation by the reductive factor for berms γ_b.

Figure 2.15 shows a much better agreement between $q^*_{measured}$ and calculated q^* for the newly derived formulae compared with existing overtopping equations. The calculated statistical indicator NSE estimates are 0.82 (TAW, 2002), 0.81 (EurOtop, 2018), 0.84 (Capel, 2015) and 0.97 (new formulae), which shows that the newly derived formulae for berms and roughness perform better than the existing methods within the tested ranges. The Capel
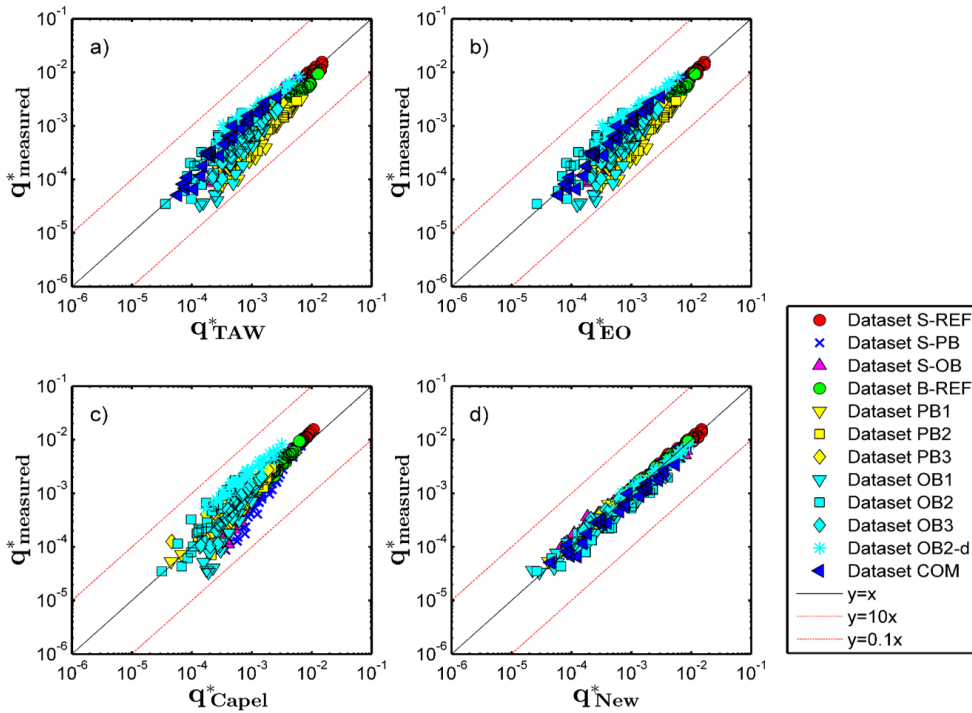
Figure 2.15: Comparison between measured dimensionless overtopping discharges and calculated values by using a) TAW (2002), b) EurOtop (2018) (EO), c) Capel (2015) and d) modified methods (New)

(2015) method gives a better estimation of the overtopping discharges than other existing equations since the method takes into account the variation of roughness factors of protruding blocks with wave conditions and blocks applied on parts of the slope surface. However, Capel (2015) equation cannot deal with the roughness of the combination of protruding blocks and other types of armour units. EurOtop (2018) performs similarly with the TAW (2002) within the calibration set.

2.4.3. VALIDATION OF NEW BERM INFLUENCE EQUATION

THE equation to account for the influence of berms on the wave overtopping discharges has been based on the present data-set. To show its validity beyond the tested ranges, Eq. (2.5) has been compared to existing data for smooth impermeable slopes. Two datasets A and B (Van der Meer and De Waal, 1990; 1993) were used for this purpose; the ranges of parameters in these two datasets are listed in Table 2.2. Measured and calculated dimensionless overtopping discharges are plotted in Figure 2.16. The new equation performs similarly with $NSE = 0.53$ for Dataset A and $NSE = 0.57$ for Dataset B compared with the TAW (2002) method with $NSE = 0.58$ for Dataset A and $NSE = 0.52$ for Dataset B. One rea-

son for the similar performance of both methods is that the minimum value of berm factor is 0.6. This implies that, if the calculated value is less than 0.6, the value 0.6 is used. The new method also adopts this specification. Most of Datasets A and B resulted in berm influence factors smaller than 0.6 due to a large berm width and therefore both the new and TAW methods give the same values for the berm factor. The relatively low NSE values for both the TAW (2002) formulas and the new formula indicate that additional research is needed to determine the berm factors for very wide berms.

Table 2.2: Parameters of the selected datasets (Dataset A and B).

Parameters	Ranges
B [m]	0.4-1.0
H_{m0} [m]	0.1-0.2
d_h [m]	-0.08-0.13
R_c [m]	0.1-0.35
$\tan \alpha$ [-]	1:3-1:4
$s_{m-1,0}$ [-]	0.024-0.05
$\xi_{m-1,0}$ [-]	1.10-1.55
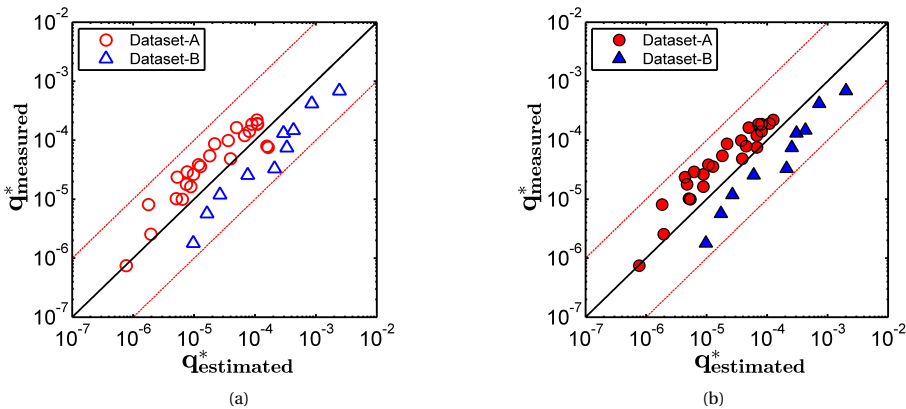
Figure 2.16: $q^*_{measured}$ versus $q^*_{calculated}$ using a) TAW (2002) method and b) new equation of impermeable berm influence using selected data recordings from Van der Meer and De Waal (1990, 1993).

2.4.4. SCALE EFFECTS

SCALE effects cannot be avoided when performing scaled model tests (EurOtop, 2018). This is because it is impossible to fulfil Froude's law and Reynold's law at the same time to obtain completely reliable results from scaled models. Froude scaling is important for a scale reproduction of waves since the inertia and gravity are the dominant forces in flows

related to waves. The consequence of Froude modelling is that viscous forces are high in the model if identical fluids are used in both the prototype and the model. Previous research (Schüttrumpf, 2001) has shown that the influence of kinematic viscosity on wave overtopping increases as the overtopping discharges decrease. Small-scale model tests tend to give smaller values of overtopping rates compared to those of large-scale model tests (Kajima and Sakakiyama, 1994). There is a tendency of rougher behaviour of revetments for small overtopping quantities below 0.4 l/s/m in prototype scale compared with the real cases (Capel, 2015). De Rouck et al. (2005) showed that results of model and prototype are in relatively good agreement for relatively larger overtopping discharges. The vast majority of the data in the present study corresponds to larger overtopping discharges (> 0.4 l/s/m). Therefore, viscous forces have not caused significant scale effects on wave overtopping discharge in this study.

2.5. Conclusions

I n this study 429 tests were performed to determine the influence of a berm and roughness on the wave overtopping over dikes. Based on the analysis of the model tests, new formulae have been derived to estimate the reduction of wave overtopping at dikes due to the roughness, due to a berm, and a combination of both.

We found that roughness influence factors appear not to be constant as assumed by TAW (2002) and EurOtop (2007, 2018) but vary in response to the wave conditions and dike configurations. The wave steepness is included in the new equation in addition to the relative berm width and the berm level to improve the accuracy of predicting the berm influence. This new formula to take the influence of berms into account has been validated against existing data and was found to perform similarly with the TAW (2002) method. Experimental results suggest that a permeable berm has a slightly smaller reductive influence than an impermeable berm. Location-weighting coefficients are applied to account for the different contributions of roughness elements on different parts of the waterside slopes to the overall roughness influence factor. This method can be used to estimate the reduction influence of varying roughness along the slopes and the berm.

The new formulae derived as listed in Box 2.1 in this study fit well with the experimental data with NSE of 0.97 and perform better than existing formulae to predict average overtopping discharges within the calibration set. This improvement is obtained by using variable roughness coefficients and by taking wave steepness into account when calculating berm coefficients. Also, the location-weighting coefficients for roughness elements contribute to the improvement of overtopping estimation. The restricted calibration dataset is probably the reason of the poor result of validation with two datasets (A and B) which are not used in the calibration. It is recommended to further validate these new formulae with more exten-

sive data being available.

Box 2.1: Summary of derived formulae in this study.

Berm influence factor

$\gamma_b = 1 - (b_0/\sqrt{s_{m-1,0}})r_B(1 - r_{dh})$

with $b_0 = 0.21$ for an impermeable berm and $b_0 = 0.13$ for a permeable berm covered by open blocks.

Roughness influence factor

$\gamma_f = 1 - c_0 R_c/(H_{m0}\xi_{m-1,0})$

with $c_0 = 0.36$ for protruding blocks on the straight slopes and composite slope slopes with a berm; $c_0 = 0.38$ for open blocks on the straight slope and $c_0 = 0.55$ for open blocks on the slopes with a berm.

Varying roughness along the slopes and berms

$\gamma_f = (\alpha_1\gamma_{f,1}L_1 + \alpha_2\gamma_{f,2}L_2 + \alpha_3\gamma_{f,3}L_3)/(\alpha_1 L_1 + \alpha_2 L_2 + \alpha_3 L_3)$

with $\alpha_1 = 0.65$ for the upper slope, $\alpha_2 = 0.22$ for the berm and $\alpha_3 = 0.13$ for the down slope.

ACKNOWLEDGEMENT

2.A. AN APPENDIX TO CHAPTER 2

2.A.1. EMPIRICAL OVERTOPPING FORMULAE

TAW (2002) provides the overtopping formulae for breaking and non-breaking waves as given below:

$$\frac{q}{\sqrt{gH_{m0}^3}} = \frac{0.067}{\sqrt{\tan\alpha}}\gamma_b\xi_{m-1,0}\exp\left[-4.75\frac{R_c}{H_{m0}\xi_{m-1,0}\gamma_b\gamma_f\gamma_\beta\gamma_v}\right] \tag{2.A.1}$$

with a maximum of

$$\frac{q}{\sqrt{gH_{m0}^3}} = 0.2\exp\left[-2.6\frac{R_c}{H_{m0}\gamma_f\gamma_\beta}\right] \tag{2.A.2}$$

where q $[m^3/s/m]$ is the average overtopping discharge, R_c [m] is the freeboard which is the vertical distance of the dike crest relative to the Still Water Level (SWL), $\xi_{m-1,0}$ ($=\tan\alpha/\sqrt{s_{m-1,0}}$) is the breaker parameter, γ_b [-] is the influence factor for berms, γ_f [-] is the roughness factor, γ_β [-] is the influence factor for oblique waves, γ_v [-] is the influence factor for vertical walls. The other empirical overtopping formulae are shown in Table 2.A.1, where G_c is the width of armour crest [m].

Table 2.A.1: Summary of the empirical overtopping formulae.

Reference	Formula
TAW (2002)	$\dfrac{q}{\sqrt{gH_{m0}^3}} = \dfrac{0.067}{\sqrt{\tan\alpha}}\gamma_b\xi_{m-1,0}\exp\left[-4.75\dfrac{R_c}{H_{m0}\xi_{m-1,0}\gamma_b\gamma_f\gamma_\beta\gamma_v}\right]$
	with a maximum of
	$\dfrac{q}{\sqrt{gH_{m0}^3}} = 0.2\exp\left[-2.6\dfrac{R_c}{H_{m0}\gamma_f\gamma_\beta}\right]$
EurOtop (2018)	$\dfrac{q}{\sqrt{gH_{m0}^3}} = \dfrac{0.023}{\sqrt{\tan\alpha}}\gamma_b\xi_{m-1,0}\exp\left[-\left(2.7\dfrac{R_c}{H_{m0}\xi_{m-1,0}\gamma_b\gamma_f\gamma_\beta\gamma_v}\right)^{1.3}\right]$
	with a maximum of
	$\dfrac{q}{\sqrt{gH_{m0}^3}} = 0.09\exp\left[-\left(1.5\dfrac{R_c}{H_{m0}\gamma_f\gamma_\beta}\right)^{1.3}\right]$
Capel (2015)	$\dfrac{q}{\sqrt{gH_{m0}^3}} = \dfrac{0.027}{\sqrt{\tan\alpha}}\xi_{m-1,0}\exp\left[-6.5\dfrac{R_c}{3.45\tanh(0.65\xi_{m-1,0})H_{m0}\gamma_f}\right]$

2.A.2. BERM INFLUENCE EQUATION

TAW (2002) and EurOtop (2007, 2018) recommend a method to calculate the berm influence factors.

$$
\begin{aligned}
\gamma_b &= 1 - r_B(1 - r_{dh}) \qquad \text{if} \quad 0.6 \le \gamma_b \le 1.0 \\
r_B &= \frac{B}{L_{berm}} \\
r_{dh} &= 0.5 - 0.5\cos\left(\pi\frac{d_h}{R_{u2\%}}\right) \quad \text{for a berm above still water line} \\
r_{dh} &= 0.5 - 0.5\cos\left(\pi\frac{d_h}{2H_{m0}}\right) \quad \text{for a berm below still water line}
\end{aligned}
\tag{2.A.3}
$$

In which $R_{u2\%}$ is the wave run-up height exceeded by 2% of the incident waves and it can be calculated by using the following equations (TAW, 2002):

$$\frac{R_{u2\%}}{H_{m0}} = 1.65\gamma_b\gamma_f\gamma_\beta\xi_{m-1,0} \qquad \text{with} \quad \xi_{m-1,0} = \tan\alpha/\sqrt{s_{m-1,0}} \qquad (2.A.4)$$

with a maximum of

$$\frac{R_{u2\%}}{H_{m0}} = \gamma_f\gamma_\beta\left(4 - \frac{1.5}{\sqrt{\xi_{m-1,0}}}\right) \qquad (2.A.5)$$

where r_B [-] represents the influence of the width B [m] and r_{dh} [-] stands for the effect of the d_h [m] which refers to position of the berm relative to SWL, L_{Berm} [m] is the characteristic berm length (Figure 2.A.1).
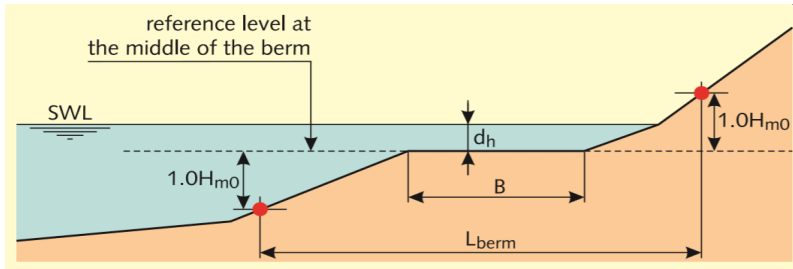
Figure 2.A.1: Definition of the berm of a dike (from TAW, 2002).

2.A.3. Roughness influence equation

The method given by TAW (2002) and EurOtop (2007, 2018) to account for roughness can be described as below:

$$\gamma_f = \begin{cases} \gamma_{f-rec} & \text{if } \gamma_b\xi_{m-1,0} < 1.8 \\ \gamma_{f-rec} + (\gamma_b\xi_{m-1,0} - 1.8)\frac{1-\gamma_{f-rec}}{8.2} & \text{if } 1.8 < \gamma_b\xi_{m-1,0} < 10 \\ 1.0 & \text{if } \gamma_b\xi_{m-1,0} > 1.8 \end{cases} \qquad (2.A.6)$$

in which γ_{f-rec} [-] refer to the recommended values of the roughness factor by TAW (2002) and EurOtop (2007, 2018).

A new equation to assess the roughness influence coefficient of protruding blocks was proposed by Capel (2015).

$$\gamma_f = 1 - \left\{0.585\sqrt{0.075 - s'_{m-1,0}}\sqrt{\rho_{\gamma_f}}\left[-\ln\left(\frac{q}{\sqrt{gH_s^3}}\right)\right]\right\} \qquad (2.A.7)$$

where $s'_{m-1,0}$ [-] is the local wave steepness; ρ_{γ_f} [-] is the roughness density parameter; H_s [m] is the significant wave height; $\gamma_{f,w}$ [-] is the dimensionless roughness width, which refers to the total width of the exposed elements per meter dike; h_{prot} [m] is the protrusion height.

2

3

EXPERIMENTAL STUDY ON THE INFLUENCE OF BERMS AND ROUGHNESS ON WAVE OVERTOPPING AT ROCK-ARMOURED DIKES

3

ABSTRACT The average overtopping discharge is an important parameter for the design and reinforcement of dikes. Rock armour on the waterside slopes and berms of dikes is widely used to reduce the wave overtopping discharge by introducing slope roughness and dissipation of energy in the permeable armour layer. However, methods for estimating the influence of a rock berm and roughness of rock armour at dikes on the average overtopping discharge still need to be developed and/or validated. Therefore, this study aims to develop empirical equations to quantify the reductive influence of rock armour on wave overtopping at dikes. Empirical equations for estimating the effects of rock berms and roughness are derived based on the analysis of experimental data from new physical model tests. The influence of roughness of the rock armour applied on parts of waterside slopes is estimated by introducing the location weighting coefficients. Results show that the newly derived equations to predict the average overtopping discharge at dikes lead to a significantly better performance within the tested ranges compared to existing empirical equations.

3.1. INTRODUCTION

D IKES protect property and people living in the hinterland from flooding (Schmocker and Hager, 2009). Low-lying countries especially rely heavily on good and strong dikes (Van der Meer, 2017). Nowadays, climate change and sea level rise might result in extreme events occurring more frequently, which increases the probability of wave overtopping at dikes. Wave overtopping over dikes may cause dangerous situations, like grass erosion at the inner slope (e.g. Bomers, 2015 and Van Bergeijk et al., 2019) or even breaching of dikes (Van Gent, 2002a). Wave overtopping can be characterised by average overtopping discharge ($m^3/s/m$ or $l/s/m$), which acts as a key parameter in the design and reinforcement of dikes. Many studies have been conducted in the last decades on wave overtopping (see for instance TAW, 2002; EurOtop, 2007, Goda, 2009; Van Doorslaer et al., 2015; EurOtop, 2018 and Williams et al., 2019) and empirical formulas are available for estimating the average overtopping discharge at dikes (see Appendix 3.A).

With the background of climate change and sea level rise, some existing dikes may not satisfy the safety standard and therefore require reinforcement. Berms and roughness elements are widely applied to dikes, which effectively reduce the average overtopping. Herein, rock armour is often combined with other types of roughness elements (for instance Figure 3.1). Empirical equations from previous research including TAW (2002) and EurOtop (2018) take the effects of berms and roughness on the wave overtopping discharge into account by introducing a berm influence factor γ_b and a roughness influence factor γ_f. When the influence factors are 1.0, no influence of berms or the roughness is present, where smaller values of the influence factors indicate a larger reduction of wave overtopping due to a berm or slope roughness.

Figure 3.1: Rock armour on the low part of the seaward slope (from Van der Meer, 2004)

Several approaches have been proposed to account for the effects of roughness and berms. For the roughness influence factor, TAW (2002) and EurOtop (2018) provide reference values for various types of roughness elements in breaking wave conditions. Roughness factors are slightly influenced by the breaker parameter $\xi_{m-1,0}$ (Eq. 3.A.5) in non-breaking wave conditions. For combinations of different types of roughness elements on the waterside slopes of a dike, Eq. (3.A.6) is proposed by TAW (2002) and EurOtop (2018) to estimate the overall roughness of the slopes. The roughness influence factor for two layers of rock armour on an impermeable core is recommended as 0.55 in TAW (2002). Bruce et al. (2009) determined roughness factors for 13 types of armour by conducting small-scale physical model tests and recommended that the roughness influence factor corresponds to a constant for one specific type of roughness element. Those influence factors suggested by Bruce et al. (2009) have been applied to the neural network prediction of overtopping (see for instance Van Gent et al., 2007). However, some research (e.g., Capel, 2015; Van Steeg et al., 2018; Kerpen et al., 2019; Chen, Van Gent, et al., 2020) showed that the roughness influence factors are not constant but change with wave conditions and structure configurations. Until now, there is no validated method available to evaluate the roughness influence factor of rock armour taking the effects of wave conditions and dike configurations into account.

For the estimation of the berm influence factor, TAW (2002) and EurOtop (2018) provide equations for calculating the influence factor of impermeable berms for breaking wave condition. Recently, Liu et al. (2018) developed empirical equations with different forms from those given by TAW (2002) and EurOtop (2018) for impermeable berms that distinguish between breaking and non-breaking wave conditions. Nevertheless, these studies are limited to impermeable berms while validated equations for estimating the influence of a permeable rock berm on the average overtopping discharge at dikes are not available to the knowledge of the authors.

Chen, Van Gent, et al. (2020) developed empirical equations for the roughness and berm influence factors based on the analysis of experimental results. The equation for the berm influence factor was derived based on tests on both permeable and impermeable berms, but has until now not been validated for rock-armoured dikes.

$$\gamma_b = 1 - \frac{b_0}{\sqrt{s_{m-1,0}}} r_B (1 - r_{dh}) \tag{3.1}$$

in which b_0 is an empirical coefficient and the value of this coefficient is affected by the type of armour layer on the berm. An increasing value of b_0 means an increasing reductive influence of a berm on the average overtopping discharge; $s_{m-1,0}$ is the wave steepness ($s_{m-1,0} = \frac{2\pi H_{m0}}{g T_{m-1,0}^2}$), in which H_{m0} is the significant wave height and $T_{m-1,0}$ is the mean energy wave period; r_B is a parameter representing the effect of berm width and can be cal-

culated using Eq. (3.A.7); r_{dh} represents the influence of the berm level. The equation for roughness influence developed by Chen, Van Gent, et al. (2020) is given below:

$$\gamma_f = 1 - c_0 \frac{R_c}{H_{m0}\xi_{m-1,0}} \tag{3.2}$$

in which c_0 is an empirical coefficient which can vary with the type of revetment and the permeability of the structure. A larger value of c_0 means a larger reductive influence of the revetment on the average overtopping discharge. For combinations of various types of armour applied along the waterside slopes of dikes, Chen, Van Gent, et al. (2020) introduced location weighting coefficients to account for different contributions of roughness elements installed on the upper slope, berm and down slope to the overall roughness influence factor.

$$\gamma_f = \frac{\alpha_1 \gamma_{f1} L_1 + \alpha_2 \gamma_{f2} L_2 + \alpha_3 \gamma_{f3} L_3}{\alpha_1 L_1 + \alpha_2 L_2 + \alpha_3 L_3} \tag{3.3}$$

where L_1, L_2 and L_3 represent effective coverage lengths of roughness elements located between SWL - $0.25Ru_{2\%\,smooth}$ and SWL + $0.5Ru_{2\%\,smooth}$ as shown in Figure 3.2. According to TAW (2002) and EurOtop (2018), roughness elements outside of the range of SWL - $0.25Ru_{2\%\,smooth}$ and SWL + $0.5Ru_{2\%\,smooth}$ have little influence on the overall roughness factor. γ_{f1}, γ_{f2} and γ_{f3} are roughness influence factors of roughness elements applied on the upper slope, on the berm and on the down slope respectively; α_1, α_2 and α_3 are location weighting coefficients with $\alpha_1 = 0.65$ for upper slope, $\alpha_2 = 0.22$ for a berm and $\alpha_3 = 0.13$ for down slope. The values of the location weighting coefficients indicate the contributions of roughness elements applied on different locations along the waterside slope to the overall roughness influence factor. Therefore, the roughness elements applied on the upper slope with $\alpha_1 = 0.65$ are the most effective in reducing the average overtopping discharges while roughness elements on the berm ($\alpha_2 = 0.22$) and on the down slope ($\alpha_3 = 0.13$) have a relatively small reductive influence on the overtopping discharge. It is worth mentioning that the berm equation (3.1), the roughness equation (3.2) and the combined roughness equation (3.3), were derived based on the physical model tests on smooth slopes, slopes covered by protruding blocks and open blocks. It remains unknown if these location weighting coefficients are still valid for rock armour combined with other types of roughness elements. Model tests on rock armour have not been reported in Chen, Van Gent, et al. (2020). Therefore, the applicability of Eqs. (3.1, 3.2 & 3.3) for rock armour is still unclear.

This study aims to develop empirical equations for the berm and roughness influence factors of rock armour thereby improving the predictive accuracy of average overtopping at rock-armoured dikes. Chen, Van Gent, et al. (2020) forms the basis of this research. In the present study, small-scale physical model tests were conducted on the wave overtopping at rock-armoured dikes. The berm equation (3.1) and the roughness equation (3.2) will be

3
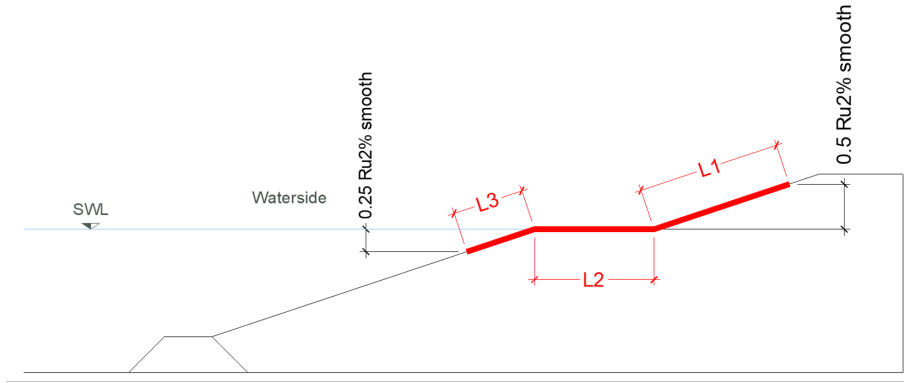
L1: Effective coverage length of roughness elements on the upper slope
L2: Effective coverage length of roughness elements on the berm
L3: Effective coverage length of roughness elements on the down slope
$R_{u2\% \text{ smooth}}$: Wave run-up height exceeded by 2% of the incident waves on smooth slopes

Figure 3.2: Coverage lengths of roughness elements applied along the waterside slopes

evaluated for rock armour based on the analysis of experimental data. Additionally, the
validity of the location weighting coefficients that are included in the combined roughness
equation (3.3) is evaluated for rock armour.

This paper is structured as follows: Section 3.2 describes test set-up, including the experimental facility and test procedure; In Section 3.3, the results from the physical model
tests are presented; Section 3.4 follows with the detailed analysis of the berm and roughness
influence of rock armour. The influence of the location weighting coefficients on estimated
overtopping discharges is also discussed. The performances of the newly derived equations
for berm and roughness influence factors of rock armour are discussed in section 3.5. Section 3.6 summarises the main conclusions of the presented research.

3.2. TEST SET-UP

3.2.1. EXPERIMENTAL FACILITY

PHYSICAL model tests on wave overtopping at rock-armoured dikes were performed in
the Pacific Basin at Deltares in the Netherlands, as shown in Figure 3.3. This is the same
experimental facility as applied in Chen, Van Gent, et al. (2020). In the following, a review
of the experimental facility which was also used in the present investigation is given. The
Pacific Basin has a length of 18.6 m, a width of 14 m and a depth of 1.25m. The basin is
equipped with a cradle type wave board which is capable of generating both regular and
irregular long-crested waves. This wave board makes use of a second order wave control

to compensate for spurious waves. An irregular wave condition was applied in all of the physical model tests based on the JONSWAP spectrum with an enhancement factor of $\gamma =$ 3.3. Wave conditions were measured by using three wave gauges installed near the toe of the modelled structures as shown in Figure 3.4a. The incident and reflected waves were separated by using the method given by Mansard and Funke (1980). The analysis was based on the time series of incident waves. The spectral significant wave height ($H_{m0} = 4\sqrt{m_0}$) and the wave period ($T_{m-1,0} = m_{-1}/m_0$) were obtained from the measured wave energy spectra. In Van Gent (1999) and Van Gent (2002a) the wave period $T_{m-1,0}$ was found to appropriately describe the influence of wave energy spectra on wave run-up and wave overtopping. A wooden tank was placed behind each model to collect the overtopped water led by a chute connecting with the inner edge of the crest (see Figure 3.4b). One wave gauge was installed in each overtopping tank to measure the variations of water level, in which way the volume of overtopping water can be determined.
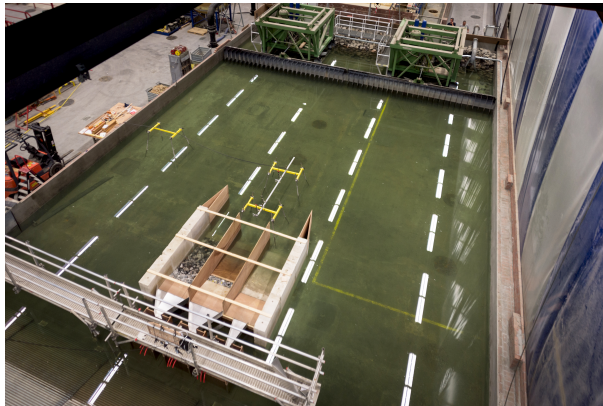
Figure 3.3: Pacific Basin with models.
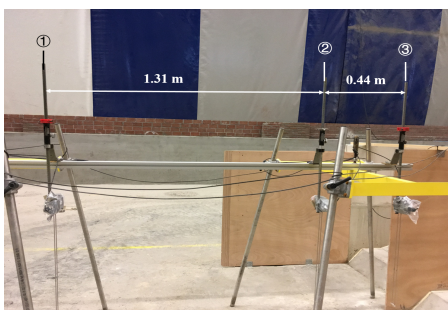
Figure 3.4: Experimental instruments for measurement with (a) wave gauges in front of models (side view) and (b) overtopping chute and overtopping tank with wave gauge (top view).

3

3.2.2. TESTED STRUCTURES AND TEST PROCEDURE

THE width of each model was 1.0 m. The core of each tested structure was imperme-
able and was made of concrete. The basic configurations consisted of slopes with a
horizontal berm with a 1:3 slope above and below the berm. The position of the dike crest
was fixed during the tests. The variations in the physical model tests included the applied
location of rock armour, the berm width, the water level and the wave conditions (H_{m0} and
$T_{m-1,0}$), resulting in six series of tests of which the configurations are listed below:

- R1: Rock-armoured upper slope and a smooth berm (0.2 m) and lower slope (Figure
  3.5);

- R2: Rock-armoured upper slope and berm (0.2 m), and a smooth lower slope (Figure
  3.6);

- R3: Rock-armoured structure over the entire structure with a berm (0.2 m) (Figure
  3.7);

- RB: Rock-armoured berm (0.2 m) with a smooth upper and lower slope (Figure 3.8);

- R1N: Rock-armoured upper slope and a smooth berm (0.2 m) and down slope with
  wider ranges of test conditions including water levels and wave conditions than Model
  R1 (Figure 3.9);

- R3WB: Rock-armoured structure over the entire structure with a wider berm (0.5 m)
  than Model R3 (0.2 m) (Figure 3.10).
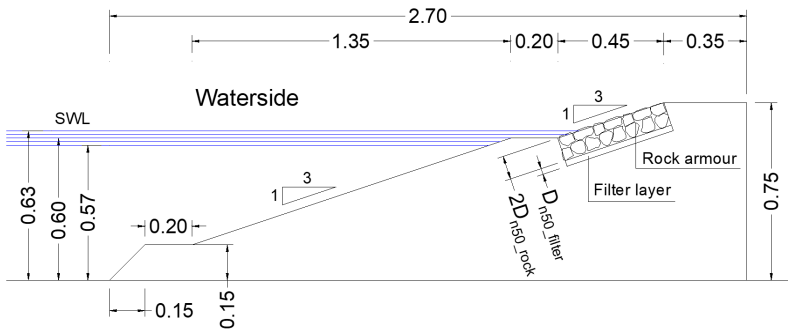
Figure 3.5: Test configuration (unit: m) of the R1 tests, with a rock-armoured upper slope, a smooth berm and a
smooth lower slope and with D_{n50_rock} = 5 cm and D_{n50_filter} = 2.5 cm.

Rock armour consisted of two layers of rocks (D_{n50_rock} = 5 cm, total thickness d_{rock} =
10 cm) with a filter layer underneath (thickness d_{filter} = 2.5 cm with D_{n50_filter} = 2.5 cm).
The filter layer was placed on the smooth impermeable core. Smooth parts of structures

Figure 3.6: Test configuration (unit: m) of the R2 tests, with a rock-armoured upper slope, a rock-armoured berm and a smooth lower slope and with D_{n50_rock} = 5 cm and D_{n50_filter} = 2.5 cm.

Figure 3.7: Test configuration (unit: m) of the R3 tests, with the entire slopes and a berm covered by rock armour and with D_{n50_rock} = 5 cm and D_{n50_filter} = 2.5 cm.

Figure 3.8: Test configuration (unit: m) of the RB tests, with a smooth upper slope, a rock-armoured berm and a smooth lower slope and with D_{n50_rock} = 5 cm and D_{n50_filter} = 2.5 cm.

were made of detachable plywood which could be easily installed or removed to install rock armour. Rock armour was applied to different parts of the waterside slope surface to study

Figure 3.9: Test configuration (unit: m) of the R1N tests, with a rock-armoured upper slope, a smooth berm and a smooth lower slope with wider test conditions (including water levels and wave conditions) than R1. D_{n50_rock} = 5 cm and D_{n50_filter} = 2.5 cm.
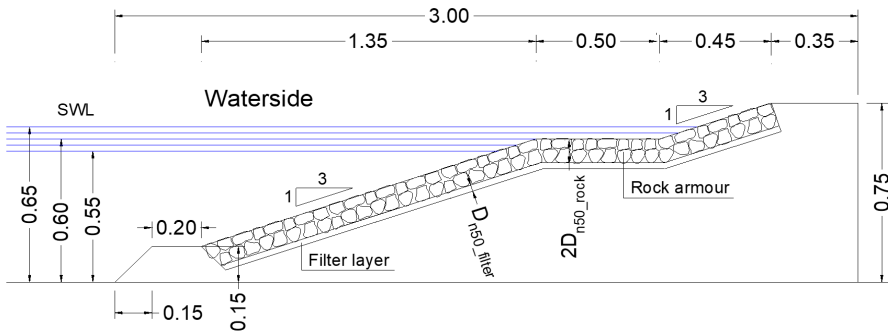
Figure 3.10: Test configuration (unit: m) of the R3WB tests, with rock armour on the entire slopes with a wider berm (0.5 m) than Model R3 (0.2 m) and the same test conditions as R1N. D_{n50_rock} = 5 cm and D_{n50_filter} = 2.5 cm.

the roughness influence including the varying roughness along the slope surface. A berm (impermeable made of concrete or permeable made of rock armour) was applied to all of the tested models in order to investigate the berm influence.

For each configuration, a series of tests were performed with various still water levels (SWL) and different wave conditions (H_{m0} and $T_{m-1,0}$). The overtopping volume was measured for approximately 1000 waves for each test condition. The berm position as shown in Figures 3.5-3.10 remained unchanged in the tests. Thus, the berm level relative to the still water level varied with the variation of the water depth. Datasets R1, R2, R3 and RB were analyzed to derive new equations for the berm and roughness influence factors of rock armour. Datasets R1N and R3WB were used to evaluate the performance of the newly derived equations based on the analysis of Datasets R1, R2, R3 and RB. In the four Datasets R1, R2, R3 and RB, the water depth increased from 0.57 m to 0.63 m in a step of 0.015 m for each series of tests resulting in five freeboards R_c (0.18 m, 0.165 m, 0.15 m, 0.135 m, 0.12 m) where

R_c refers to the distance between the crest level and SWL and five berm levels d_h with respect to SWL (-0.03 m, -0.015 m, 0 m, 0.015 m, 0.03 m). For each water level, different wave heights (H_{m0}) were combined with different wave periods ($T_{m-1,0}$). The wave steepness ($s_{m-1,0} = \frac{2\pi H_{m0}}{g T_{m-1,0}^2}$) covered the range of (0.026, 0.036). Dataset R1N, which was an extension of Dataset R1, had the same configuration as that in R1 but with a wider range of test conditions. The water level varied between 0.55 m and 0.65m in steps of 0.025 m and the corresponding five freeboards R_c were (0.2 m, 0.175 m, 0.15 m, 0.125 m, 0.1 m). The wave steepness $s_{m-1,0}$ varied between 0.013 and 0.042. Note that a fixed berm width B of 0.2 m was applied in Datasets R1, R2, R3, RB and R1N. Dataset R3WB was similar to the configuration of R3, but had a wide berm, with the width of 0.5 m. Wave conditions in Dataset R3WB were in nearly the same ranges as those in Dataset R1N. A summary of the parameter ranges in the tests is given in Table 3.1, in which $\xi_{m-1,0}$ is the breaker parameter ($\xi_{m-1,0} = \frac{\tan\alpha}{\sqrt{s_{m-1,0}}}$). In total, 139 tests were performed in this study.

Table 3.1: Summary of parameter ranges of all tests

Data set	R_c [m]	d_h [m]	H_{m0} [m]	$s_{m-1,0}$ [-]	$\xi_{m-1,0}$ [-]	B [m]	Number
R1	(0.12, 0.18)	(-0.03, 0.03)	(0.119, 0.141)	(0.026, 0.036)	(1.76, 2.05)	0.2	21
R2	(0.12, 0.18)	(-0.03, 0.03)	(0.119, 0.14)	(0.026, 0.036)	(1.76, 2.05)	0.2	21
R3	(0.12, 0.18)	(-0.03, 0.03)	(0.119, 0.14)	(0.026, 0.036)	(1.76, 2.05)	0.2	21
RB	(0.12, 0.18)	(-0.05, 0.05)	(0.127, 0.141)	(0.027, 0.036)	(1.74, 2.03)	0.2	16
R1N	(0.1, 0.2)	(-0.05, 0.05)	(0.1, 0.134)	(0.013, 0.042)	(1.63, 2.86)	0.2	38
R3WB	(0.1, 0.2)	(-0.03, 0.03)	(0.1, 0.134)	(0.014, 0.045)	(1.71, 2.83)	0.5	22
Total number							**139**

3.3. TEST RESULTS OF THE AVERAGE OVERTOPPING DISCHARGES

T HIS section presents the results of measured average overtopping discharges from the physical model tests. All the experimental data are plotted in Figure 3.11a with the relative freeboard $\frac{R_c}{H_{m0}\xi_{m-1,0}}$ on the horizontal axis and dimensionless average overtopping discharge ($q^*_{measured} = \frac{q_{measured}}{\sqrt{g H_{m0}^3}}$) on the logarithmic vertical axis. Figure 3.11a shows that the measured dimensionless mean overtopping discharges cover a wide range between 10^{-6} and 10^{-2}. Note that there also are some data points that have low values of $q^*_{measured} < 10^{-6}$. However, these small values mostly result in overtopping rates less than 0.5 l/s/m in prototype in reality (which is outside the relevant range) while these very small measured discharges can be affected by scale effects in the model (see for instance, Capel, 2015 and Sigurdarson and Van Der Meer, 2012). Therefore, those data points inside the shaded area in Figure 3.11a are discarded in the data analysis in this study. For completeness, four discarded data points are depicted in Figure 3.11a and in the figures related to the following analysis.

3

(a)

(b)
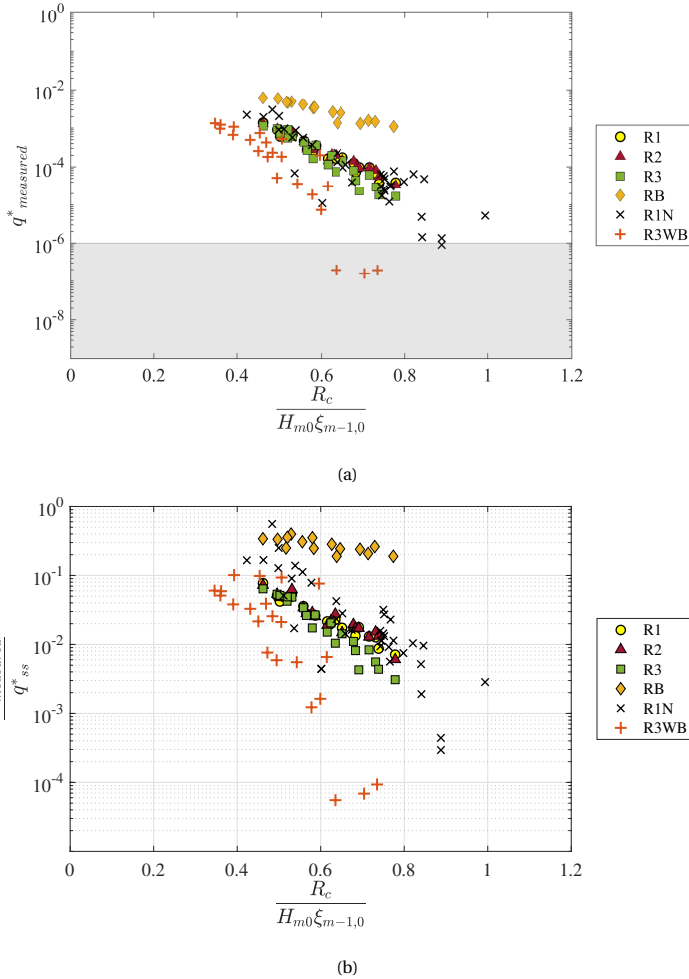
Figure 3.11: Experimental results of average overtopping discharge with (a) Overtopping data for all physical model tests and (b) Overtopping ratio of measured average overtopping discharge ($q^*_{measured}$) at rough bermed slopes and overtopping discharge (q^*_{ss}) at smooth straight slopes calculated by using overtopping equations (3.A.1 & 3.A.2).

In order to have an intuitive understanding of the effectiveness of a berm and roughness in reducing the average overtopping discharge, we plotted the ratio of measured dimensionless mean overtopping discharge ($q^*_{measured}$) at rough bermed structures and the corresponding discharges (q^*_{ss}) over smooth and straight slopes as shown in Figure 3.11b. q^*_{ss} was calculated using TAW (2002) overtopping equations (3.A.1) and (3.A.2) since Chen, Van Gent, et al. (2020) showed that Eqs. (3.A.1) & (3.A.2) can provide accurate estimations of mean overtopping discharge at smooth straight slopes. It can be observed from Figure 3.11b that the application of a berm and rock armour at dikes could reduce the average

overtopping discharge by up to 1000 times, demonstrating that berms and roughness can dramatically influence the average overtopping discharge. Nevertheless, this overtopping reduction ratio varies over quite a wide range between 0.5 and 0.001. Therefore, the predictive accuracy of berm and roughness influence is essential for estimating the mean average overtopping discharge at dikes.

3.4. ANALYSIS

3.4.1. EVALUATION OF EXISTING OVERTOPPING EQUATIONS

TAW and EurOtop equations provided by TAW (2002) and EurOtop (2018) respectively are widely used for predicting average overtopping discharge. The performances of these two sets of overtopping equations are first evaluated. Figure 3.12 shows all the measured overtopping data and the empirical equations. Note that for rock armour applied over the entire seaward side, the value of the roughness influence factor γ_f, present in $\frac{R_c}{H_{m0}\xi_{m-1,0}\gamma_b\gamma_f}$ on the horizontal axis, is 0.55 for two layers of rock with an impermeable core as suggested by TAW (2002) and EurOtop (2018). For a combination of various types of roughness elements applied along the waterside slope surface (e.g. Model R1), Eq. (3.A.6) is used to calculate the overall roughness influence factor γ_f. The berm influence factor γ_b is obtained by using Eq. (3.A.7).

From Figure 3.12, we can see that the existing TAW and EurOtop equations can give reasonable estimates of discharges for the models R3 and R3WB in which the rock armour was applied over the whole waterside slopes. However, both TAW and EurOtop equations significantly overestimate the average overtopping discharge for cases in which rock is only applied on parts of the seaward side (R1, R2 and R1N). This means that they underestimate the reductive influence of berms and roughness on the overtopping discharge, especially for rock armour on the upper slope only (R1 and R1N). Thus, it is necessary to improve the predictive methods for the berm and roughness influence of rock armour on mean overtopping discharge at dikes.

3.4.2. DEVELOPMENT OF EQUATIONS FOR ROCK BERM AND ROCK ROUGHNESS INFLUENCE

As mentioned in Section 3.1, Chen, Van Gent, et al. (2020) developed empirical equations for the berm and the roughness influence and introduced the location weighting coefficients to deal with the varying roughness along the waterside slopes that have a berm. Here, the equations developed by Chen, Van Gent, et al. (2020) are used as a basis for the derivation of new equations for the berm and roughness influence factors of rock armour. First, it is assumed that the location weighting factors (0.65 for the upper slope, 0.22 for the

3

(a)

(b)
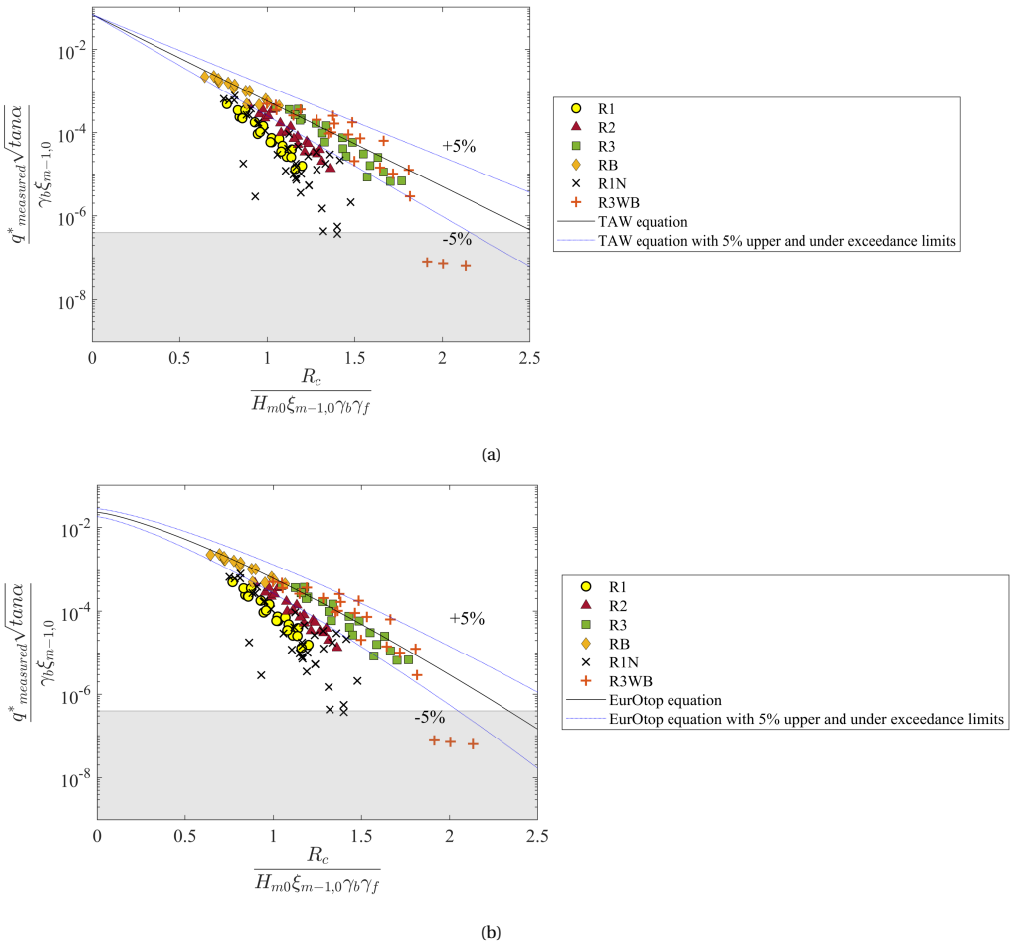
Figure 3.12: Comparisons between measured overtopping data and empirical equations from (a) TAW (2002) and (b) EurOtop (2018).

berm and 0.13 for the down slope) as derived by Chen, Van Gent, et al. (2020) are also valid for rock armour. Thereafter, the equations (3.1 & 3.2) for the berm and roughness influence factors are applied to rock armour where the two empirical coefficients b_0 and c_0 in Eqs. (3.1) & (3.2) require recalibration. Data sets R1, R2, R3 and RB are used for the recalibration. The berm factor γ_b for R1 is calculated by using Eq. (3.1) with $b_0 = 0.21$ for impermeable berms as suggested in Chen, Van Gent, et al. (2020) since rock armour was only applied on the upper slope while the berm and down slope were smooth and impermeable in model R1. Chen, Van Gent, et al. (2020) recalibrated the TAW (2002) overtopping equation (3.A.6) for breaking wave conditions based on the overtopping data on smooth straight slopes. The recalibrated overtopping equation (3.4) was then used as the reference formula when in-

vestigating the influence of berms and roughness elements in Chen, Van Gent, et al. (2020). This study is an extension of Chen, Van Gent, et al. (2020), and the same experimental facilities were used in this study as those in Chen, Van Gent, et al. (2020). Thus, the recalibrated overtopping equation (3.4) is also applied here as a reference equation in the analysis.

$$\frac{q}{\sqrt{gH_{m0}^{3}}} = \frac{0.067}{\sqrt{\tan\alpha}}\gamma_b\xi_{m-1,0}\exp(-4.9\frac{R_c}{H_{m0}\xi_{m-1,0}\gamma_b\gamma_f}) \tag{3.4}$$

The least square method is used to calibrate the values of b_0 and c_0 for rock armour such that the sum of the errors is at a minimum, and the error is defined as:

$$\epsilon_i = \log(q^*_{i\_estimated}) - \log(q^*_{i\_measured}) \tag{3.5}$$

The sum of squared estimates of errors (SSE) is defined as follows:

$$SSE = \sum_{i=1}^{N} \epsilon_i^{2} \tag{3.6}$$

where N is the total number of measurements; $q^*_{i\_estimated}$ is the estimated dimensionless average overtopping discharge using empirical equations; $q^*_{i\_measured}$ is the measured dimensionless average overtopping discharge from one test. Applying this procedure, we determine b_0 and c_0 as 0.19 and 0.7 respectively for rock armour. Chen, Van Gent, et al. (2020) suggested that the permeable berm may have less reductive influence on the average overtopping compared with the impermeable berm with $b_0 = 0.21$. It is worth noting that $b_0 = 0.19$ for rock armour is also smaller than 0.21, showing that the permeable rock berm also has a slightly smaller reductive effect than an impermeable berm, which is in consistency with the result in Chen, Van Gent, et al. (2020). Chen, Van Gent, et al. (2020) derived $c_0 = 0.36$ for protruding blocks. Here, c_0 is calibrated for rock armour as 0.7 using Eq. (3.2). With the same freeboard (R_c) and wave condition (H_{m0} and $T_{m-1,0}$), $c_0 = 0.7$ for rock armour results in larger reductive influence than that for protruding blocks. This is in line with earlier found results, as for instance described in EurOtop (2018), that the roughness of rock armour is larger than a protruding block revetment. Thus, the application of the weighting location coefficients as suggested by Chen, Van Gent, et al. (2020) leads to reasonable values of b_0 and c_0 for rock armour. The new equations for berm and roughness influence factors of rock armour are given below:

$$\gamma_b = 1 - \frac{0.19}{\sqrt{s_{m-1,0}}}r_B(1 - r_{dh}) \tag{3.7}$$

$$\gamma_f = 1 - \frac{0.7R_c}{H_{m0}\xi_{m-1,0}} \tag{3.8}$$

where r_B and r_{dh} can be calculated using Eq. (3.A.7).

The wave overtopping data and empirical equations are shown in Figure 3.13, in which γ_f is calculated using the Eq. (3.8) and the overall roughness factor for rock armour installed on parts of slope surface is calculated by applying Eq. (3.3). Eq. (3.7) is used to calculate the berm influence factor γ_b for the rock berm. There is only a slight difference between TAW equation and the recalibrated TAW equation (3.4), which means that the application of Eq. (3.4) leads to a limited improvement of the predictions of average overtopping discharge. In contrast, Figure 3.13 shows that the new berm and roughness equations for rock armour contribute to much less scatter than TAW and EurOtop methods presented in Figure 3.12. The data points calculated by using the new equations are more concentrated around the empirical equation lines compared to existing equations (3.A.5, 3.A.6 & 3.A.7) for the roughness and berm influence.
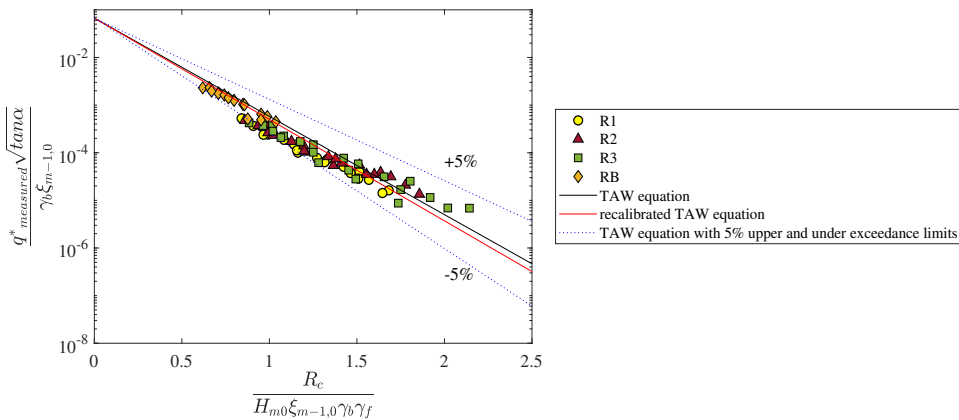
Figure 3.13: Wave overtopping data calculated using the new berm and roughness equations for rock armour.

The performances of the new equations (3.7 & 3.8) and the existing prediction methods are also quantitatively evaluated and compared using the accuracy metrics of $Bias$, Root Mean Square Error ($RMSE$) and Nash–Sutcliffe model efficiency coefficient (NSE) defined as follows:

$$Bias = \frac{1}{N} \sum_{i=1}^{N} [\log(q^*{}_{estimated}) - \log(q^*{}_{measured})] \qquad (3.9)$$

$$RMSE = \sqrt{\frac{1}{N} \sum_{i=1}^{N} [\log(q^*{}_{estimated}) - \log(q^*{}_{measured})]^2} \qquad (3.10)$$

$$NSE = 1 - \frac{\sum_{i=1}^{N} [\log(q^*_{measured}) - \log(q^*_{estimated})]^2}{\sum_{i=1}^{N} [\log(q^*_{measured}) - \overline{\log(q^*_{measured})}]^2} \tag{3.11}$$

where N is the total number of measurements; $\overline{\log(q^*_{measured})}$ represents the mean value of $\log(q^*_{measured})$. $Bias$ indicates the tendency of the prediction method to overestimate or underestimate the average overtopping discharge. $RMSE$ reflects the difference between the predicted and measured average overtopping discharge, where a small $RMSE$ indicates a tight fit of prediction models to the measured data. NSE is a measure of correlation between the measured and the predicted overtopping rates and it can vary between $-\infty$ and 1. $NSE = 1$ corresponds to a perfect match of predicted data to the measured data. $NSE = 0$ indicates that the predicted values are as accurate as the mean of the measured data and $NSE < 0$ means that the measured mean is a better predictor than the empirical formula. The closer the NSE is to 1, the more accurate the prediction model is. Table 3.2 presents the accuracy measures of different prediction equations and shows that the $Bias$ and $RMSE$ of the new equations (3.7 & 3.8) are better than those given by TAW and EurOtop equations. Both TAW and EurOtop equations give the same value of $Bias$ (0.42) and the same value of $RMSE$ (0.56), which indicates that these two methods provide comparable estimates of average overtopping discharges within the tested ranges. The $Bias$ value of 0.42 shows that TAW and EurOtop overall overestimate the average overtopping discharge, which is in accordance with the observations from the scatter diagram (Figure 3.12). The new equations have a much smaller positive value (0.09) of $Bias$, showing a significantly smaller overestimation of the average overtopping discharge. The $RMSE$ of new equations has a value of 0.21 which is smaller than 0.56 produced by TAW and EurOtop. The NSE for Eqs. (3.7 & 3.8) is 0.89, which is also significantly better than the NSE values given by TAW and EurOtop equations, further demonstrating that the new equations significantly improved the estimates of the overtopping rates compared to the existing prediction methods.

Table 3.2: Accuracy measures of estimates given by new equations and existing methods for data sets R1, R2, R3 and RB

Accuracy indicator	TAW	EurOtop	New equations
BIAS	0.42	0.42	0.09
RMSE	0.56	0.56	0.21
NSE	0.25	0.24	0.89

3.4.3. INFLUENCE OF LOCATION WEIGHTING FACTORS ON ESTIMATED AVERAGE OVERTOPPING DISCHARGES

IN the derivation of new equations for berm and roughness factors of rock armour, it was assumed that the location weighting factors (0.65, 0.22 and 0.13) are still valid for rock-

armoured structures. The location weighting coefficients were first introduced by Chen,
Van Gent, et al. (2020) to deal with combinations of different types of roughness elements
installed along the slopes with a berm and are therefore expected to not be affected by types
of armour units. According to Chen, Van Gent, et al. (2020), these weighting factors (0.65,
0.22 and 0.13) work well for protruding blocks or open blocks applied on parts of the sea-
ward side as well as combinations of protruding blocks and open blocks applied along the
slope surface (e.g., protruding blocks on the upper slope and open blocks on the berm and
down slope). Here, it is analyzed whether these values also work well for estimating the
overall roughness factor for rock armour applied on parts of the waterside slopes that have
a berm. The analysis was performed following the procedure as listed below:

1. Vary the location weighting coefficients, i.e. α_1, α_2 and α_3 in the range of (0, 1) with
   $\alpha_1 + \alpha_2 + \alpha_3 = 1$. For each set of values of α_1, α_2 and α_3, the least square method is
   applied to calibrate the values of empirical coefficients b_0 and c_0 using all data sets
   such that the sum of squares of the errors ϵ_i (Eq. (3.6)) is at the minimum. Here, we
   introduce the least of sum of squared estimates of errors (*LSSE*) to represent the min-
   imum value of SSE. Thus, each set of location weighting factors produces one *LSSE*
   value. Smaller *LSSE* indicates better estimates of average overtopping discharge.

2. In Section 3.4.2, we already argue that b_0 should be smaller than 0.21 (for imperme-
   able berms) and c_0 is expected to be larger than 0.36. Therefore, all the resulting data
   that have $b_0 > 0.21$ or $c_0 < 0.36$ were regarded as invalid and therefore be discarded.

3. The contour of the effective data of *LSSE* varying with the variations of α_1 and α_2
   ($\alpha_3 = 1 - \alpha_1 - \alpha_2$) is plotted in Figure 3.14.

Figure 3.14 shows that *LSSE* is the most sensitive to the value of α_1 for upper slope. If
the value of α_1 is fixed, the variations of the values of α_2 and α_3 do not change the values of
LSSE significantly. As seen from Figure 3.14, the minimum of *LSSE* is 19.4 corresponding
to $\alpha_1 = 0.56$, $\alpha_2 = 0.33$ and $\alpha_3 = 0.11$. However, we do not aim at searching for the optimal
values of location weighting factors. Instead, the focus is to check whether the assumed
values (0.65, 0.22 and 0.13) lead to good estimates of the average overtopping discharge at
slopes partly covered by rock armour. If the assumed weighting factors produce a *LSSE*
that is much larger than the minimum 19.4, they cannot be regarded as being valid for rock
armour. Figure 3.14 shows that the assumed values of the location weighting factors result
in a *LSSE* of 20.4 which is quite close to the minimum 19.4. Therefore, even though the as-
sumed weighting factors are not the optimal values, they can still provide accurate estimates
of the average overtopping discharges with a relatively small value of *LSSE*. We therefore
conclude that the location weighting coefficients (0.65, 0.23 and 0.13) are also valid for rock
armour applied on parts of the waterside slopes with a berm.
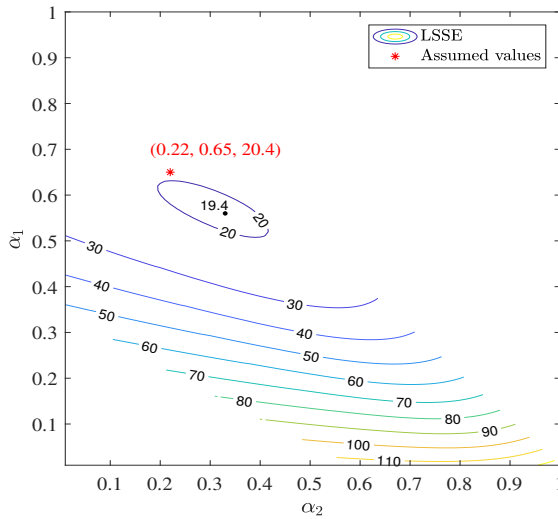
Figure 3.14: Effect of variations of location weighting factors with $b_0 < 0.21$ and $c_0 > 0.36$ on LSSE of overtopping data from all data sets R1, R2, R3, RB, R1N and R3W

3.5. Discussion

NEW empirical equations for berm and roughness influence factors of rock armour are derived by recalibrating the empirical coefficients in the berm and roughness equations developed by Chen, Van Gent, et al. (2020), making use of Datasets R1, R2, R3 and RB. In this section, the newly derived empirical equations are first validated by using Datasets R1N and R3WB. Following that, comparisons of the measured and the predicted average overtopping discharges given by the new equations and existing prediction methods for all data sets are provided.

3.5.1. Validation of new equations

IN order to check the performance of the new equations for estimating the average overtopping discharge at rock-armoured dikes, Datasets R1N with a wider range of test conditions and R3WB with a wider berm, i.e. 0.5 m are analysed.

Figure 3.15 shows the comparisons between the measured and the predicted dimensionless average overtopping discharges using TAW (2002), EurOtop (2018) and the new equations. There is less scatter present in Figure 3.15c than in Figures 3.15a & 3.15b. The performance of the new equations is significantly better for the structure R1N tested for a wider range of test conditions (wider ranges of wave steepness and berm levels, etc) but for the structure with a very wide berm, there is no improvement using the new equations

compared to TAW and EurOtop equations.
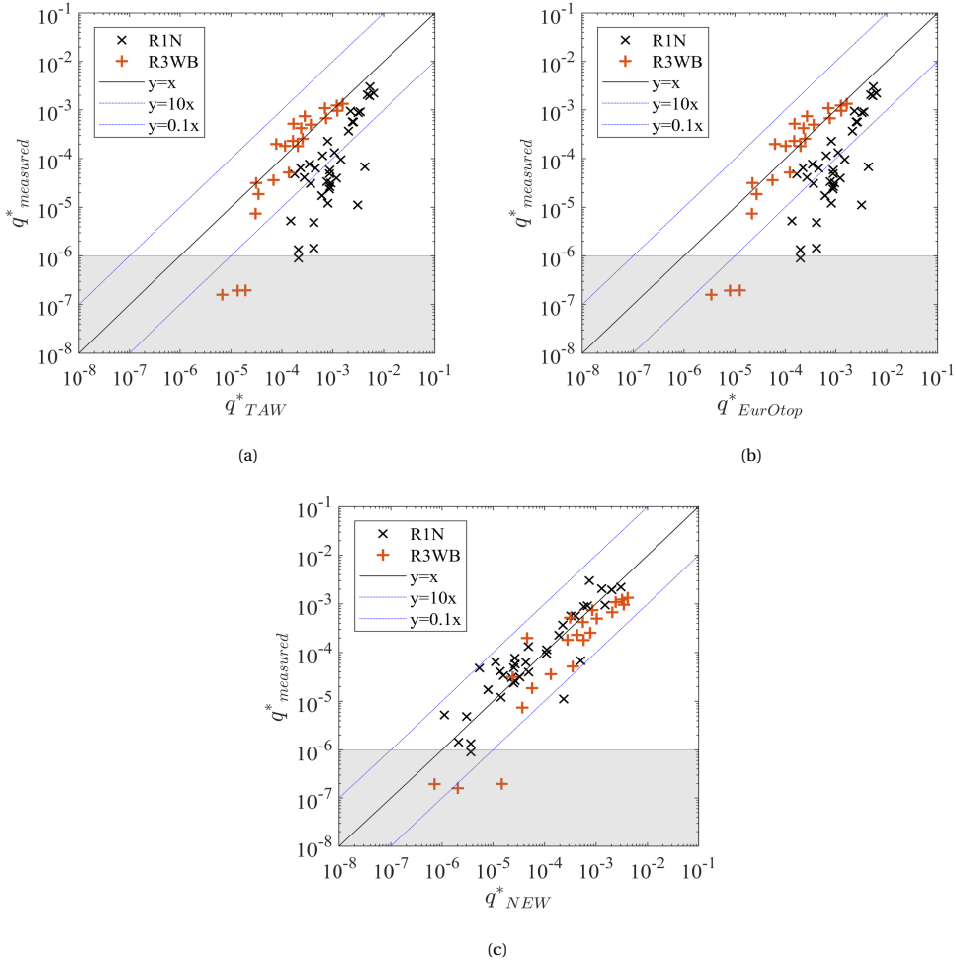
Figure 3.15: Comparisons of dimensionless average overtopping discharges between the measured and the predicted values for the Datasets R1N and R3WB using (a) the TAW equations given by TAW (2002), (b) the EurOtop equations given by EurOtop (2018) and (c) the new equations.

The *NSE* factors are -0.70 for TAW equations, -0.71 for EurOtop equations and 0.68 for the new equations, which demonstrates that the new equations on average improve the estimations of the average overtopping discharge. For the Dataset R1N (a wider range of test conditions), the new equations lead to a significantly better performance than the other equations: -1.32 for TAW, -1.33 for EurOtop and 0.7 for the new equations. For the Dataset R3WB (very wide berm, $\frac{B}{H_{m0}} > 3.7$), the NSE factor is 0.81 for TAW, 0.82 for EurOtop and 0.5 for the new equations.
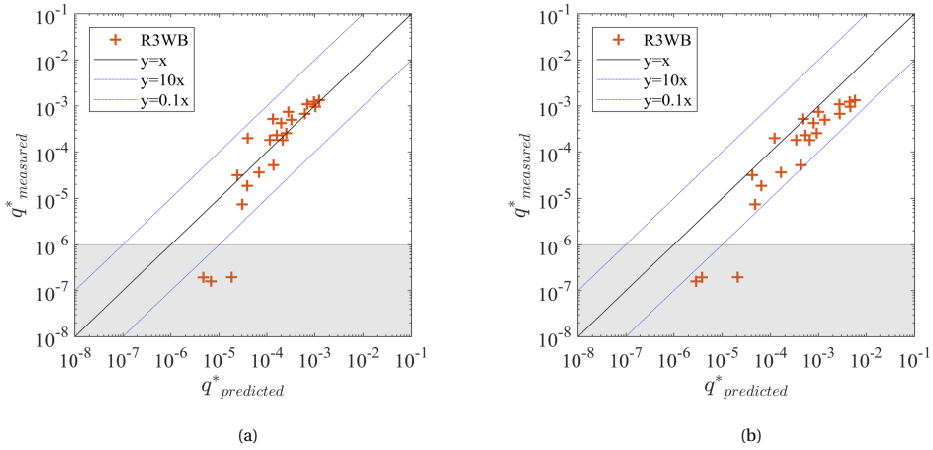
Figure 3.16: Comparisons between measured and estimated average overtopping discharge for Dataset R3WB by using (a) New berm equation (3.7) with roughness factor of 0.55 and (b) New roughness equation (3.8) with TAW berm equation (3.A.7).
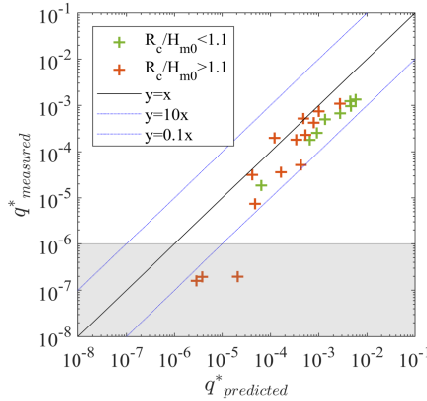
Figure 3.17: Measured vs estimated average overtopping discharge with different ranges of relative freeboard for Dataset R3WB.

To explain possible causes for the reduced performance of the new equations for the structure with a very wide berm, further analysis is performed by analysing whether the expression for the berm (Eq.(3.7)) or the expression for the roughness (Eq. (3.8)) contributes the most to the reduced performance for a very wide berm. Therefore, the data for the wide berm (Dataset R3WB) is compared to the new berm equation (Eq. (3.7)) in combination with the TAW roughness value, and to the new roughness equation (Eq. (3.8)) in combination with the TAW berm equation. Figure 3.16 shows the results by using the new equation for the berm influence (Eq. (3.7)) combined with the roughness factor of 0.55 recommended

by TAW (2002). By comparing Figure 3.16a with Figure 3.15a, we can see that the results are similar to those given by TAW. The NSE factors for the data in Figure 3.16a and Figure 3.15a are 0.75 and 0.81 respectively, which means that the new berm equation performs with similar accuracy as the TAW berm equation for this very wide berm (0.5 m). Figure 3.16b shows the results using the new equation for the roughness (Eq. (3.8)) combined with the TAW berm equation (Eq.(3.A.7)), indicating the new roughness equation results in an overestimation of average overtopping discharge. The NSE factor decreases from 0.81 for TAW to 0.36. Thus, it is the new roughness equation (Eq. (3.8)) that mainly reduces the accuracy of the new set of equations for a very wide berm. The possible cause of the overestimation given by the new roughness equation is that this equation (Eq. (3.7)) overestimates the overtopping for small relative freeboard $\frac{R_c}{H_{m0}} < 1.1$ as shown in Figure 3.17. Similar results are also found in Figure 6 in Chen, Van Gent, et al. (2020) in which some data with $\frac{R_c}{H_{m0}} < 1.1$ deviate from the fitting curve, resulting in an underestimation of roughness influence on average overtopping discharge. This underestimation of the roughness influence is limited in Dataset R1N as the rock armour is only applied on the upper slope. Thus, further research on roughness influence for smaller relative freeboard ($\frac{R_c}{H_{m0}} < 1.1$), is needed to further improve the predictions of the overtopping discharge, especially for cases with combined wide berms and roughness elements applied on the most of or the entire waterside slope surface.

3.5.2. Comparison with existing equations

The performance of the new equations for berm and roughness influence of rock armour derived in this study is compared with TAW (2002) and EurOtop (2018) equations using all data sets. The comparisons of the measured and the predicted average overtopping discharges using the new equations and the existing equations in Figure 3.18 show that the new equations lead to much less scatter than the mentioned existing equations. Additionally, the number of outliers larger than a factor of 10 difference between the measured and predicted values, are reduced using the new equations. The new equations fit well with the experimental data with a $Bias$ of 0.073, an $RMSE$ of 0.34 and a NSE of 0.8. TAW equations with an $RMSE$ of 0.81 and a NSE of -0.13 performs similarly as, although slightly better than, EurOtop equations with an $RMSE$ of 0.82 and a NSE of -0.14 and both of them overestimate the average overtopping discharges with the same $Bias$ of 0.56, especially for rock armour applied on parts of the waterside slope surface. The new equations for the berm and the roughness influence factors of rock armour significantly improved the predictions of the average overtopping discharge within the tested ranges.
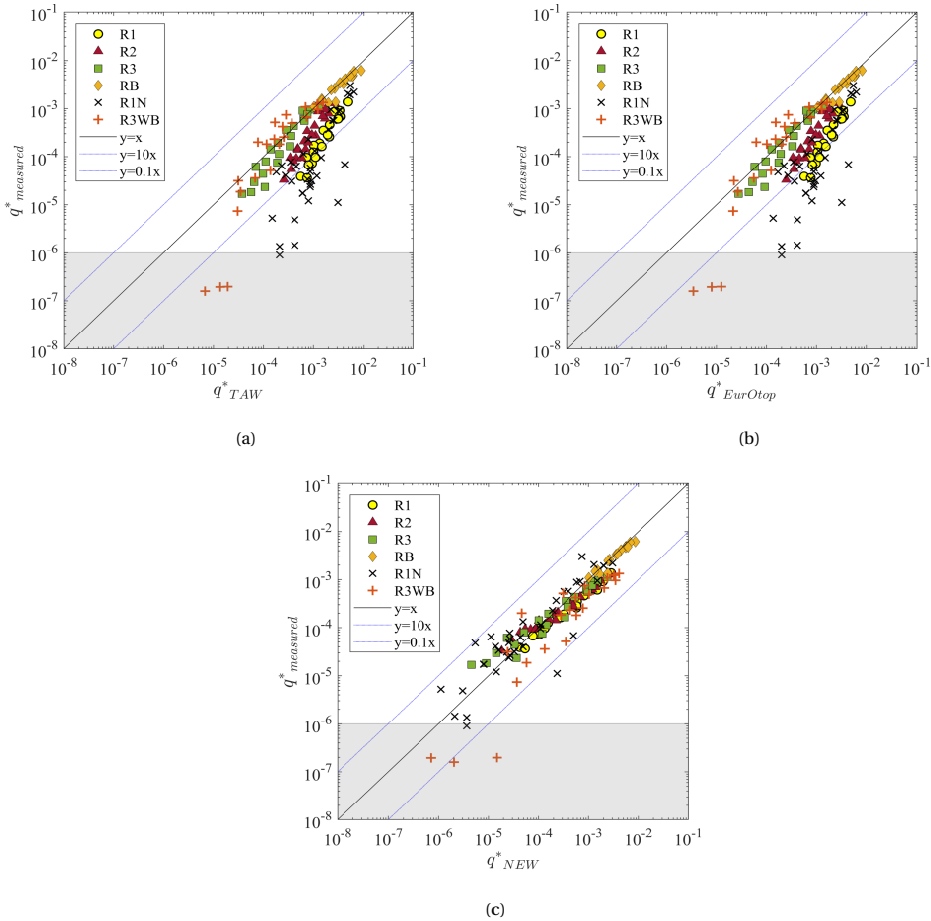
Figure 3.18: Comparisons of measured and predicted dimensionless average overtopping discharges calculating using (a) TAW equations given by TAW (2002), (b) EurOtop equations given by EurOtop (2018) and (c) New equations for all data sets.

3.6. CONCLUSIONS

THIS study is an extension of Chen, Van Gent, et al. (2020). The effects of a berm and roughness of rock armour on the average overtopping discharge are investigated through small-scale physical model tests. 139 tests were performed in total by varying wave conditions and structure configurations.

Test results show that the application of a berm and rock armour can significantly reduce the average overtopping discharge compared to that at smooth straight slopes. New equations for estimating the berm and roughness factors of rock armour are derived based on most of the experimental data by recalibrating the empirical coefficients in the equations

(3.1) & (3.2) as suggested by Chen, Van Gent, et al. (2020) for structures with other protections. The location weighting factors proposed by Chen, Van Gent, et al. (2020) are used to estimate the overall roughness of slope partly covered by rock armour. The influence of the values of the location weighting factors on predictions of average overtopping discharges is also investigated. It is found that the values of location weighting factors as proposed by Chen, Van Gent, et al. (2020) for structures with other slope protections, appear to be valid for rock-armoured slopes as well.

The performance of the new equations is validated by using the experimental data with a wider range of test conditions compared with the calibration set. The new equations contribute to an obvious improvement with a NSE of 0.7 on estimates of average overtopping discharge over the structure with rock armour applied on the upper slope, even though the wave conditions are outside the calibration ranges. For the structure with a wider berm ($\frac{B}{H_{m0}} > 3.7$), the new berm equation performs comparably with the TAW berm equation. The range of validity of the new expression for roughness is limited to rock-armoured structures that have a larger relative freeboard ($\frac{R_c}{H_{m0}} > 1.1$). Thus, the new equation for the influence of roughness on rock-armoured slopes needs further investigation for smaller relative freeboards ($\frac{R_c}{H_{m0}} < 1.1$) in combination with very wide berms ($\frac{B}{H_{m0}} > 3.7$). Overall, the new equations to account for the influence of a rock berm and the influence of roughness of rock armour significantly improve the predictions of the average overtopping discharges at rock-armoured dikes with $NSE = 0.8$ within the tested ranges.

The present study is performed with relatively deep-water at the toe of the dike ($\frac{h_{toe}}{H_{m0-toe}} > 4$). It is recommended to verify the findings from the present study also for conditions with shallow foreshores, including conditions with severe wave breaking on the foreshore.

The berm and roughness equations developed in this study can be applied to estimate the effectiveness of a rock berm or rock armour in reducing the average overtopping discharge when designing or reinforcing a dike. An accurate estimation of berm and roughness influence on the average overtopping discharge would help with the cost-effective design or reinforcement and safety assessment of a dike.

ACKNOWLEDGEMENT

3.A. AN APPENDIX TO CHAPTER 3

3.A.1. OVERTOPPING EQUATIONS

Overtopping equations for breaking and non-breaking waves are given by TAW (2002) as below:

$$\frac{q}{\sqrt{gH_{m0}{}^3}} = \frac{0.067}{\sqrt{\tan\alpha}}\gamma_b\xi_{m-1,0}\exp\left(-4.75\frac{R_c}{H_{m0}\xi_{m-1,0}\gamma_b\gamma_f\gamma_\beta\gamma_v}\right) \tag{3.A.1}$$

with a maximum of

$$\frac{q}{\sqrt{gH_{m0}{}^3}} = 0.2\exp\left(-2.6\frac{R_c}{H_{m0}\gamma_f\gamma_\beta}\right) \tag{3.A.2}$$

EurOtop (2018) adapted the TAW (2002) overtopping equations especially for low freeboards, including a zero freeboard. The EurOtop (2018) overtopping equations are listed as follows

$$\frac{q}{\sqrt{gH_{m0}{}^3}} = \frac{0.023}{\sqrt{\tan\alpha}}\gamma_b\xi_{m-1,0}\exp\left[-\left(2.7\frac{R_c}{H_{m0}\xi_{m-1,0}\gamma_b\gamma_f\gamma_\beta\gamma_v}\right)^{1.3}\right] \tag{3.A.3}$$

with a maximum of

$$\frac{q}{\sqrt{gH_{m0}{}^3}} = 0.09\exp\left[-\left(1.5\frac{R_c}{H_{m0}\gamma_f\gamma_\beta\gamma^*}\right)^{1.3}\right] \tag{3.A.4}$$

where q [m^3/s/m] is the average overtopping discharge; α is the angle of waterside slope; R_c [m] is the freeboard which is the vertical distance between the dike crest and the still water level; $\xi_{m-1,0}$ is the breaker parameter; γ_b [-] is the influence factor for berms; γ_f [-] is the influence factor for roughness; γ_β [-] is the influence factor for oblique waves; γ_v is the influence factor for vertical walls; γ^* [-] is a combined factor of all kind of geometrical influences.

3.A.2. EQUATIONS FOR ROUGHNESS AND BERM INFLUENCE FACTORS

The method given by TAW (2002) and EurOtop (2018) to deal with the roughness is described as:

$$\gamma_f = \begin{cases} \gamma_{f-rec}, & \gamma_b\xi_{m-1,0} < 1.8 \\ \gamma_{f-rec} + (\gamma_b\xi_{m-1,0} - 1.8)\frac{1-\gamma_{f-rec}}{8.2}, & 1.8 \le \gamma_b\xi_{m-1,0} \le 10 \\ 1.0, & \gamma_b\xi_{m-1,0} > 10 \end{cases} \tag{3.A.5}$$

in which γ_{f-rec} refers to the recommended values of the roughness factors by TAW (2002) and EurOtop (2018). For varying roughness along the slopes and berms, the various influ-

ence factors are weighted in TAW (2002) and EurOtop (2018) by using the lengths of the relevant sections of the slope. For example, if three types of roughness elements with applied lengths of L_1, L_2 and L_3 and influence factors of γ_{f1}, γ_{f2} and γ_{f3} respectively are applied along the slopes with a berm, then the weighted average as proposed by TAW (2002) and EurOtop (2018) is:

$$\gamma_f = \frac{\gamma_{f1}L_1 + \gamma_{f2}L_2 + \gamma_{f3}L_3}{L_1 + L_2 + L_3} \tag{3.A.6}$$

TAW (2002) and EurOtop (2018) provide a method to calculate the influence factor for berms.

$$\gamma_b = 1 - r_B(1 - r_{dh}) \qquad \text{if} \quad 0.6 \leq \gamma_b \leq 1.0$$
$$r_B = \frac{B}{L_{berm}}$$
$$r_{dh} = 0.5 - 0.5\cos\left(\pi\frac{d_h}{R_{u2\%}}\right) \quad \text{for a berm above still water line} \tag{3.A.7}$$
$$r_{dh} = 0.5 - 0.5\cos\left(\pi\frac{d_h}{2H_{m0}}\right) \quad \text{for a berm below still water line}$$

where r_B [-] represents the influence of the berm width B [m] and r_{dh} represents the effect of d_h [m] which refers to the water depth above the berm; L_{berm} is the characteristic berm length (see Figure 3.A.1); $R_{u2\%}$ is the wave run-up height that is exceeded by 2% of the number of incoming waves at the toe of the structure and can be calculated by using the equations below (TAW, 2002):

$$\frac{R_{u2\%}}{H_{m0}} = 1.65\gamma_b\gamma_f\gamma_\beta\xi_{m-1,0} \tag{3.A.8}$$

with a maximum of

$$\frac{R_{u2\%}}{H_{m0}} = \gamma_f\gamma_\beta\left(4 - \frac{1.5}{\sqrt{\xi_{m-1,0}}}\right) \tag{3.A.9}$$
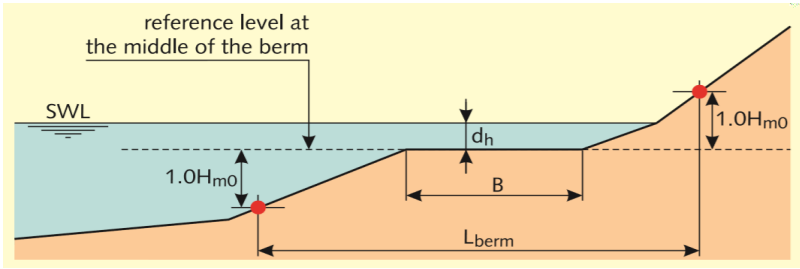
Figure 3.A.1: Definition of a berm of a dike (TAW, 2002).

3

4

NUMERICAL MODELLING OF WAVE OVERTOPPING AT DIKES USING OPENFOAM ®

ABSTRACT Accurate calculation of wave overtopping is important for determining the required crest height and geometry of a dike. Berms and roughness elements are widely used to reduce the average overtopping discharge at dikes while the reductive effects of berm and roughness are still not fully understood. Several empirical formulae are available to predict the overtopping rate at coastal structures. However, the extrapolation of these empirical formulae is not always applicable for complex structures (e.g. a dike that has a berm and/or roughness elements on the waterside slopes) or wave conditions that are outside the applicability of the empirical predictors. A 2D numerical model based on OpenFOAM® is set up in this study for predicting wave over-topping at dikes that have complex configurations with berms and roughness elements. The validation results show that this OpenFOAM® model is capable of reproducing the incident waves accurately and predicting the wave overtopping discharge with good accuracy. Subsequently, the numerical model is applied to study the reductive influence of a berm and protruding blocks on the mean overtopping discharge at dikes. The roughness of protruding blocks is incorporated by explicitly modelling the protrusions using refined mesh. The model shows reasonable behaviour of the reduction of wave overtopping influenced by a berm and roughness. This indicates the capabilities of the numerical model in the design and safety assessment of dikes.

4.1. INTRODUCTION

$\mathbb{A}$N accurate prediction of wave overtopping discharge is an important for the design and safety assessment of dikes. The average overtopping discharge at coastal structures should be below acceptable limits under specified wave conditions and water levels in the design of dikes to ensure the stability of coastal structures thereby protecting infrastructure and people in the hinterland (CIRIA et al., 2007). In order to satisfy these criteria, berms and roughness elements are often applied at the seaward side of dikes in areas where it is not feasible, undesirable or uneconomic to raise the crest level of dikes. However, the effects on the average overtopping discharge are still not fully understood. Several empirical formulae are available to estimate the reductive influence on wave overtopping at dikes. The TAW (2002) and EurOtop (2018) manuals provide empirical methods for calculating the influence factors of berms and roughness. Nevertheless, Chen, Van Gent, et al. (2020) and Chen, Marconi, et al. (2020) made clear that both the TAW (2002) and EurOtop (2018) equations showed weak performance for estimating these two influence factors by comparing them to experimental data. Therefore, Chen, Van Gent, et al. (2020) developed empirical equations for berm and roughness influence factors, based on the analysis of experiments. However, the validity of empirical methods that are mainly based on physical model tests within a limited range of conditions and configurations is not always certain for other conditions and configurations. For example, the validity of the empirical equations developed by Chen, Van Gent, et al. (2020) is uncertain for dike configurations or wave conditions outside the tested ranges. Additionally, new detailed physical model tests can be costly and it can be time consuming to prepare a new physical model setup.

With the development of numerical methods and computational resources, numerical modelling has become an important complementary tool with experiments for modelling interaction of waves with coastal structures. There are different types of numerical models depending on the governing equations and solving technique. A computationally efficient approach to model wave interaction with coastal structures is based on the nonlinear shallow water equations (NSWE) (see for instance Kobayashi and Wurjanto, 1989; Van Gent, 1995, 2000; Ma et al., 2012), such as the SWASH model (e.g. Zijlema et al., 2011; Suzuki et al., 2017). Models based on NSWE can be very efficient, providing the possibility of simulating wave trains of 1000 waves rapidly (Losada et al., 2008). However, one restriction of the use of NSWE is associated with the difficulty of dealing with complex geometries of coastal structures (Suzuki et al., 2017). There exist many numerical models based on the Reynolds-Averaged Navier-Stokes (RANS) equations. In the numerical models based on RANS equations, there exist two main free surface tracking techniques, i.e. volume of fluid (VOF) and particle methods like Smooth Particle Hydrodynamic (SPH). SPH is capable of tracking large deformations of the free surface accurately and has been applied to simulate

wave overtopping on impermeable coastal structures (Didier and Neves, 2009 and Akbari, 2017). Nevertheless, the SPH method is expensive in terms of computational time since it requires a large number of particles and small time steps ($O(10^{-5}$ s)) to obtain enough accuracy (Klapp et al., 2016). Models based on the VOF method are capable of dealing with large free surface deformation and are less computationally expensive than the models based on SPH, such as the models by Van Gent (1995), Losada et al. (2008), Fang et al. (2010) and Higuera et al. (2013).

OpenFOAM® is an open-source computational fluid dynamics framework that allows users to run tasks in parallel on multiple processors. The open-source nature often leads to useful libraries and toolboxes that are freely shared in the public domain (Davidson et al., 2015). Additionally, OpenFOAM® has recently been developed with the capability of modelling interaction of waves and structures and it appears to become increasingly popular for coastal engineering (Jacobsen et al., 2015). Therefore, OpenFOAM® is adopted in this study to model wave overtopping at dikes that have complex configurations.

Several studies have been conducted on numerical modelling of wave overtopping at coastal structures making use of OpenFOAM®. Higuera et al. (2013) applied a three dimensional Navier-Stokes (NS) solver called IHFOAM built on OpenFOAM® to investigate the interaction between waves and a high mound breakwater. A 3D model is computationally expensive and therefore only a total of 40 s is simulated for wave overtopping with irregular waves, which is insufficient for estimations of average overtopping discharge. Higuera et al. (2013) also mentioned that long simulations should be carried out to obtain reliable results of wave overtopping. Jensen et al. (2014) simulated wave overtopping over a smooth straight impermeable structure and a porous breakwater that has a straight waterside slope. In their 2D numerical model, waves were generated and absorbed using waves2Foam package (Jacobsen et al., 2012) which is a toolbox based on OpenFOAM® that applies the relaxation zone technique to generate and absorb free surface water waves. The numerical model in Jensen et al. (2014) was found to give a good agreement between the simulated and measured average overtopping discharges. Since not too much wave breaking was observed during the physical model tests that were used to validate the numerical model in Jensen et al. (2014), no detailed turbulence model was applied in the model. Patil (2019) also used OpenFOAM® with waves2Foam to model wave overtopping over a smooth straight slope and there was a reasonable agreement between the modelled and experimental results while the overtopping discharge was slightly underestimated by the numerical model. Previous research mainly focused on the simulation of the overtopping process at structures that have simple configurations, such as structures with straight and/or smooth seaward slopes. Validation of the capability of OpenFOAM® in modelling overtopping discharge with long time series of irregular waves at dikes that have complex configurations with a berm and roughness elements is to the authors' knowledge still not available.

The objectives of this study are to explore the capability of the OpenFOAM® model for accurately estimating wave overtopping discharges at impermeable dikes that have a berm and roughness elements at the seaward side as well as to explore the applicability of the numerical model to investigate the influence of several configurations of berms and roughness on average overtopping discharge at dikes. The OpenFOAM® version 1812 is used in this study. The existing waves2Foam package is applied to generate waves and the solver waveIsoFoam is applied to solve the numerical model. Physical model tests from Chen, Van Gent, et al. (2020) are used to validate the OpenFOAM® model for different configurations including a smooth straight slope (SS), a smooth slope with a berm (SB), a straight slope covered by protruding blocks (PbS), a bermed slope covered by protruding blocks (PbB) and a bermed slope with only the upper slope covered by protruding blocks (PbB_up). Following the validation, the berm width and berm level relative to the still water line (SWL) are varied in the numerical model to study the reductive influence of a berm on the average overtopping discharge at dikes for conditions and configurations outside the tested ranges. Additionally, the coverage length of protruding blocks on the upper slope is varied to investigate how the coverage length of roughness elements affects the total roughness factor.

This paper is organised as follows: A description of the methodology is given in Section 4.2. In Section 4.3, the validation of the OpenFOAM® model is presented. Section 4.4 focuses on the application of the validated model to investigate the berm influence on the overtopping discharge. Model results of roughness influence are presented in Section 4.5. Applicability, limitations and efficiency of the numerical model are further discussed in Section 4.6. Section 4.7 summarises the main conclusions of this study.

4.2. METHODOLOGY

IN this section, the physical model tests that are used later to validate the numerical model are introduced first. Following that, a detailed description of the numerical model setup is given.

4.2.1. DESCRIPTION OF PHYSICAL MODEL TESTS

EXPERIMENTS in Chen, Van Gent, et al. (2020) on the influence of a berm and roughness on average overtopping discharge at dikes were performed in the Pacific Basin at Deltares in The Netherlands. The basin is 18.6 m long, 14 m wide and 1.25 m deep. An irregular wave condition was applied in all of the physical model tests based on the JONSWAP spectrum with an enhancement factor of $\gamma_f = 3.3$. Various types of roughness elements and different configurations including straight slopes and composite slopes with a berm were tested.

28 physical model tests selected from Chen, Van Gent, et al. (2020) were used to validate the performance of the OpenFOAM® model for predicting the wave overtopping discharge at dikes. The selected physical model tests include five campaigns over five dike configurations (Figures 4.1 & 4.2): a smooth straight slope (SS), a smooth slope with a berm (SB), a straight slope covered by protruding blocks (PbS), a bermed slope covered by protruding blocks (PbB) and a bermed slope with only the upper slope covered by protruding blocks (PbB_up). The protruding block revetment is considered as impermeable. A slope of 1:3 was used for the straight slope and for the down and upper slopes of structures that have a berm. The core of all the structures was impermeable and was made of concrete. The berm position and berm width (0.2 m), see Figure 4.2b, remained unchanged in the physical model tests. In Figure 4.2, the size of the cubes was 5 cm×5 cm×5 cm. The chessboard of protruding block revetment was made by installing a concrete tile of 1 cm thick underneath the cubes. Thus, the protrusion height was 1 cm. In practice, installation of these artificial blocks is conducted mechanically. About 16 to 18 units forming a 1 by 1 m panel are installed at once (Capel, 2015) and Figure 4.3 shows the chessboard pattern block revetment. The modelled structures were placed at a distance of 11m from the wave board. Three wave gauges were placed near the toe of the tested structure to measure wave conditions including the significant wave height H_{m0} and the wave period $T_{m-1,0}$. Incident and reflected waves were separated making use of the method developed by Mansard and Funke (1980). The wave height H_{m0}, wave steepness $s_{m-1,0}$ ($s_{m-1,0}=2\pi H_{m0}/(gT_{m-1,0}^2)$), freeboard R_c (which refers to the distance between the crest and the still water level, SWL), and berm level (d_h) relative to SWL were varied in the physical model tests. Note that the freeboard R_c and berm level d_h were varied in the ranges of (0.12 m, 0.18m) and (-0.03 m, 0.03m) respectively by varying the water depth between 0.57 m and 0.63 m with the positions of crest and berm fixed. The overtopped water was collected using an overtopping box in which a wave gauge was installed to detect the water surface variation. The average overtopping discharge was measured for about 1000 waves for each test run.

4.2.2. NUMERICAL SETUP

T HE numerical method in OpenFOAM® is based on a finite volume discretisation with a collocated variable arrangement on grids. In this study, the Navier-Stokes equations are solved for the two-phase flow (air and water). The interface of water and air is captured using the isoAdvector developed by Roenby et al. (2016) as suggested by Larsen et al. (2019). The isoAdvector algorithm is a VOF based interface advection method. It is applicable for arbitrary meshes aiming to keep the accuracy of geometric schemes and obtain acceptable calculation time making the geometric operations at a minimum.

The 2DV numerical wave flume was set up to mimic the experimental layout as illus-

(a) Smooth straight slope (SS)

(b) Smooth slope with berm (SB)
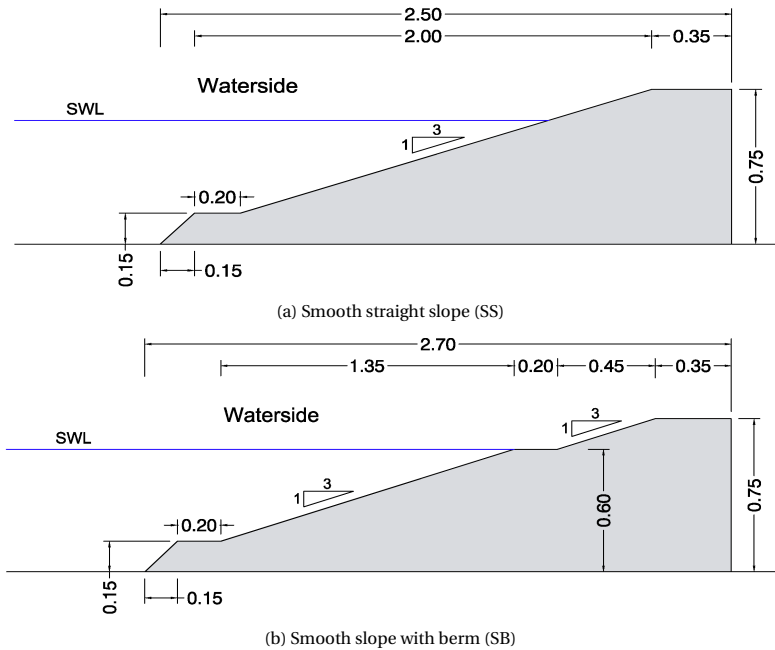
Figure 4.1: Smooth slopes with and without a berm tested in the experiments with SWL varied between 0.57 m and 0.63 m (unit in graphs: m).

trated in Figure 4.4 with a total length of 17 m and a height of 1.2 m. The dike was placed 11 m away from the inlet boundary, which is the same as the distance between the dike and waveboard in the experiments of Chen, Van Gent, et al. (2020). Three wave gauges used for incident wave analysis were defined at the same locations as those in the laboratory experiments. The modelled impermeable structures and bottom were set as non-slip conditions. A constant pressure was enforced at the atmosphere boundary which allowed the air to flow in and out while the water could only flow out. Relaxation zones were applied at the inlet and outlet boundaries to generate and absorb waves, which is described in more detail in Section 4.2.2.2.

4.2.2.1. MESH

FOR smooth slopes, including SS and SB, the numerical mesh was created by using block-Mesh and snappyHexMesh. Both blockMesh and snappyHexMesh are mesh-generation tools implemented in the OpenFOAM® package. The base mesh was created using blockMesh taking the structure into account. The mesh from the inlet boundary to the toe of the dike was orthogonal and conformal with the cell size of 0.02 m both in X direction (horizontal) and in Y direction (vertical). The overtopping discharge is closely related to the wave run-up and Wroniszewski et al. (2014) suggested that the quadrilateral grids parallel with the
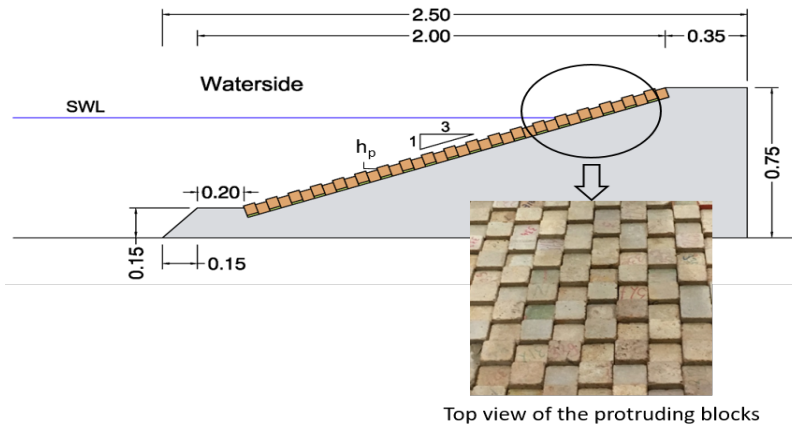
(a) Straight slope covered by protruding blocks (PbS) with protrusion height $h_p - 0.01$ m
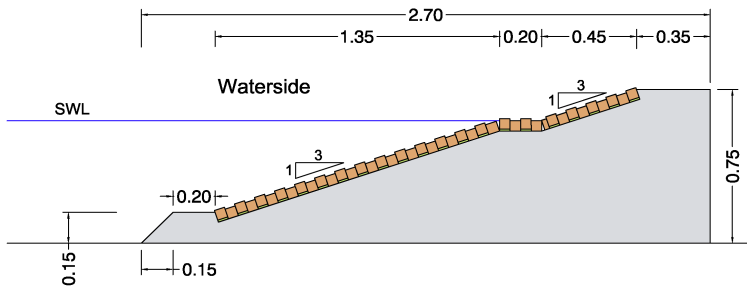
(b) Bermed slope covered by protruding blocks (PbB) with protrusion height $h_p - 0.01$ m
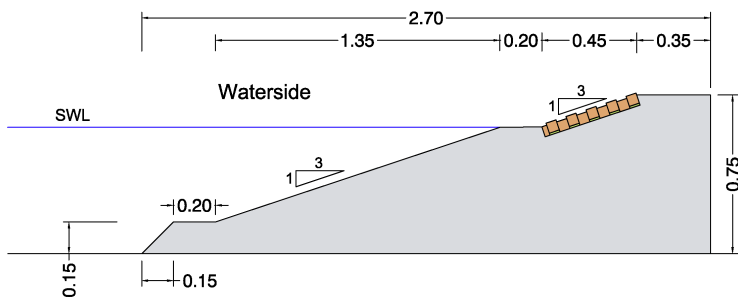
(c) Bermed slope with only the upper slope covered by protruding blocks (PbB_up) with protrusion height $h_p - 0.01$ m

Figure 4.2: Rough slopes (partially) covered by protruding blocks with SWL varied between 0.57 m and 0.63 m (unit in graphs: m).

slope surface could improve the accuracy of the simulation of the wave run-up on a slope. Thus, this type of mesh near the slope surface was used in this study as shown in Figure 4.5a. snappyHexMesh was then applied to refine the mesh around the free surface in front of the modelled structure with one refinement level, resulting in the cell size of 0.01 m in X and Y. There are nearly 12 cells to resolve per wave height, which is sufficient for modelling

Figure 4.3: Chessboard pattern of Basalton® block revetment (from Capel, 2015).
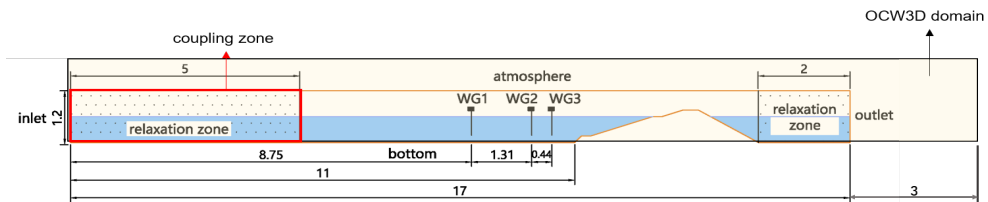
Figure 4.4: Layout of the 2D numerical wave flume (unit in graphs: m) which is inside the domain (colored in light yellow) of OCW3D model and the OCW3D model is coupled with the OpenFOAM model through the inlet relaxation zone referred to as coupling zone.

the wave propagation (Larsen et al., 2019).

The protruding blocks installed on the waterside slope were in chessboard pattern as shown in Figure 4.2c which is impossible to model in a 2DV numerical model. Therefore, the protruding blocks were simplified by only modelling the protrusions shown in Figure 4.5b. The mesh for the slopes covered by protruding blocks was created by using GMSH and snappyHexMesh. GMSH is a third-party software that is capable of generating smooth boundary conforming mesh near the wall with geometric transitions. Protrusions of block revetment were modelled explicitly by creating fine grid cells around the protrusions. GMSH was applied to create a base mesh similar to the mesh for smooth structures taking the dike and protrusions into account. The mesh around protrusions was refined based on the base mesh using snappyHexMesh (see Figure 4.5b) with the refined grid cell size of 0.0025 m in the direction perpendicular to the slope and 0.0031 m in the direction parallel with the slope. The influence of the grid size around the protrusions has been analysed for the overtopping discharge as presented in Appendix 4.A. Further refining the grid did not result in more accurate model results of average overtopping discharge. Refinement was also applied around the free surface by using snappyHexMesh with one refinement level. The aspect ratio of the computational cells in all simulations was close to 1 as suggested by Jacobsen et al. (2012) for the simulation of wave propagation and wave breaking. Table 4.1

presents the mesh resolution in different regions of the numerical domain.

(a) Mesh for smooth straight slope

(b) Refined mesh near the protruding blocks
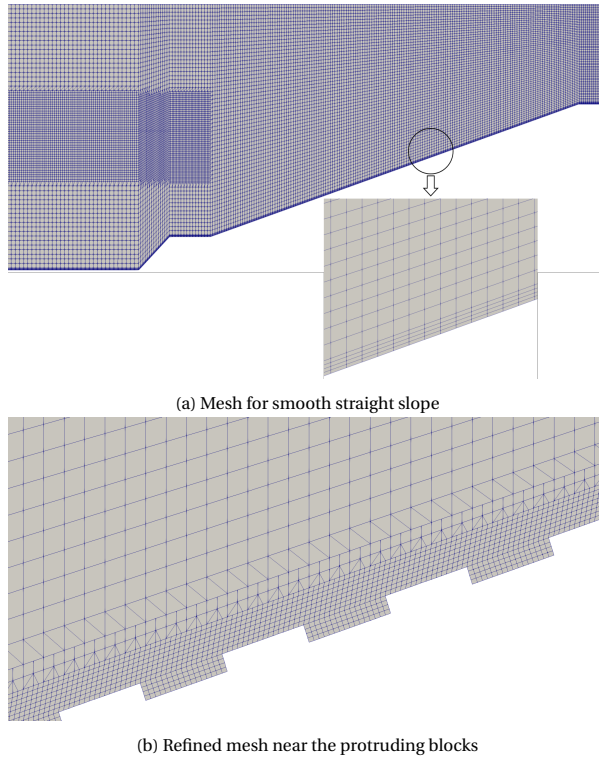
Figure 4.5: Mesh used in the OpenFOAM® numerical model.

Table 4.1: Mesh resolution for different regions

Mesh region	Grid size $\Delta x \times \Delta y$ (cm × cm)
base mesh	2×2
mesh near the water surface	1×1
mesh near the slope surface	1.4×0.22
mesh around protrusions	0.31×0.25

4.2.2.2. WAVE GENERATION

OCEANWAVE3D and waves2Foam were used in order to generate the consistent time series of irregular waves with experiments. OceanWave3D is a robust and efficient flexible-order finite difference model based on a fully nonlinear and dispersive potential flow model (Engsig-Karup et al., 2009). OceanWave3D has already been coupled into Open-FOAM/waves2Foam through the interface described in Paulsen et al. (2014). The one-way coupling makes use of the relaxation zones provided by the waves2Foam utility. The potential flow solver provides the target solution ψ_{target} in the relaxation zones also named

coupling zones where the velocity field u and the water volume fraction α are updated at each time step according to

$$\psi = (1 - \chi)\psi_{target} + \chi\psi_{computed} \qquad (4.1)$$

where ψ_{target} is the target solution in time and space given by the potential flow solver; $\psi_{computed}$ are the computed quantities by the OpenFOAM model; $\chi \in [0, 1]$ is a weighting factor. The coupling aimed to provide a fully nonlinear kinematics in the numerical model thereby improving the accuracy of modelled hydraulic loading on coastal structures (Jacobsen et al., 2018).

In this study, waves were first generated with the application of OceanWave3D by inputting the wave paddle signal files that were used in the experiments. Then, OceanWave3D provided target solution for waves2Foam from the starting time defined in the OpenFOAM model through the inlet relaxation zone which is referred to as coupling zone (shown in Figure 4.4) and then the two solvers ran side-by-side. In this way the consistent time series of water surface variation with those in the physical model tests were simulated in the numerical model. The relaxation zone implemented at the inlet also absorbed reflected waves from structures. Another relaxation zone was applied at the outlet to avoid waves reflected. The length of the inlet relaxation zone was 5 m which was about one wave length in this study. Since the wave motion behind the structure was not the focus of this study, the length of the outlet relaxation zone was only 2 m to save computational time.

4.2.2.3. TURBULENCE MODELLING

B REAKING waves at dikes will induce turbulence which has an effect on the flow velocity along the waterside slope surface, thereby influencing wave overtopping discharge at dikes. The turbulence was modelled by applying the stabilised k-ω turbulence model developed by Larsen and Fuhrman (2018). The conventional k-ω turbulence model (Wilcox, 2006) results in an exponential flow with finite strain, which gives rise to severe over-estimation of turbulence levels. Therefore, Larsen and Fuhrman (2018) proposed a solution to fix this problem by introducing a new stress limiter λ_2 in the calculation of eddy viscosity ν_t without alteration of any fundamental closure coefficients. Herein, λ_2 defines the effective potential flow threshold. The added limiter will become active only in a region of nearly potential flow. Larsen and Fuhrman (2018) mentioned that λ_2 should be small, but also large enough to work for practical applications. $\lambda_2 = 0.05$ as suggested by Larsen and Fuhrman (2018) was used in all simulations in this study. Wall functions were applied in the boundary layer instead of resolving the boundary, which saves computational time. Application of the wall functions required that the first grid near the wall should be located in the log layer. Therefore, the mesh near the wall was refined as shown in Figure 4.5a, resulting in the grid size near the wall of $\Delta y \approx 0.0022$ m. A Nikuradse's roughness height of

0.001 m was adopted to represent the smooth concrete surface used in the experiments. All simulations were solved by using waveIsoFoam which is a solver implemented with the isoAdvection scheme in waves2Foam.

4.2.2.4. TURBULENCE MODELLING

OVERTOPPING discharge was obtained by utilising the *overtopping* function in waves-2Foam. A set of cell faces at the inner edge of the crest were selected to calculate the volume of overtopped water. The volume flux over the selected faces S (Jacobsen, 2017) is calculated by

$$q = \sum_{f \in S} \phi_{F,f} \frac{\mathbf{S}_f}{\|\mathbf{S}_f\|_2}, \phi_F = \frac{\phi_\rho - \rho_{F=0}\phi}{\rho_{F=1} - \rho_{F=0}} \tag{4.2}$$

in which q is the volume flux [m³/s] and $\mathbf{S}_f$ is the non-unit normal vector to the face. ϕ_F [m³/s] is the flux of fluid across a face multiplied with the indicator function; ϕ_ρ [m³/s] is the flux of fluid across a face multiplied with the density of the fluid; ϕ [m³/s] is the flux of fluid across a face. The cumulative overtopping volume V [m³] can be obtained based on the overtopping volume flux by using the equation:

$$V_{tot} = \sum_{t=t_{start}}^{t_{end}} q \Delta t \tag{4.3}$$

where t_{start} and t_{end} are the starting time and end time of the calculation of the total overtopping volume V_{tot} [m³]; Δt [s] is the time step.

4.3. VALIDATION OF THE MODEL

IN this section, the validation of the OpenFOAM® model for reproducing the incident irregular waves and predicting the overtopping discharges at impermeable dikes is presented. 28 cases in total were simulated using the numerical model. The experimental wave conditions of these 28 cases are given in Table 4.A.1 in Appendix 4.A. The simulation time of the numerical model was set as 500 s for all simulated cases, corresponding to between 250 and 350 waves depending on the wave period. This duration of the simulation is determined by comparing the measured overtopping using partial time series with that using the whole overtopping time series. It was found that 500 s of time series gives a factor of 1 to 1.15 of the overtopping rates based on the entire time series. Thus, 500 s was adopted to comprise between the computational effort and the accuracy of the results. Model results are compared with the data from the physical model tests of Chen, Van Gent, et al. (2020). The simulated wave height time series, wave energy spectra and wave properties are first compared to the measured results obtained based on the initial 500 s from laboratory experiments to show the ability of the numerical model to reproduce the incident irregular waves. The model

results of wave overtopping discharges are then compared to the measured discharges to evaluate the performance of the model for predicting overtopping discharges at dikes with different types of configurations.

4.3.1. VALIDATION OF INCIDENT IRREGULAR WAVES

WAVE conditions for all 28 tests were validated by comparing the time series of wave height of OpenFOAM® to those of the experiments. Only two wave conditions, i.e. case SS1 and case SS7 were selected for sake of brevity to show the ability of the OpenFOAM® model in reproducing irregular waves with different wave steepnesses. Figure 4.6 presents the comparison of incident wave height time series given by the OpenFOAM® model and the experiments for cases SS1 and SS7. The incident wave height time series were obtained based on the time series of free surface elevation at WG1, WG2 and WG3 using the method proposed by Mansard and Funke (1980). The agreement between numerical and physical model results for both cases is generally good with a root mean square error (RMSE) of 0.0184m for case SS1 and a RMSE of 0.015 m for case SS7. Similar good agreement is found for all other simulated cases, which demonstrates that the numerical model can well reproduce the wave propagation.

(a) Case SS1 ($H_{m0} = 0.129$ m, $T_{m-1,0} = 1.69$ s, $s_{m-1,0} = 0.029$, $h = 0.6$ m)

(b) Case SS7 ($H_{m0} = 0.116$ m, $T_{m-1,0} = 1.23$ s, $s_{m-1,0} = 0.049$, $h = 0.6$ m)
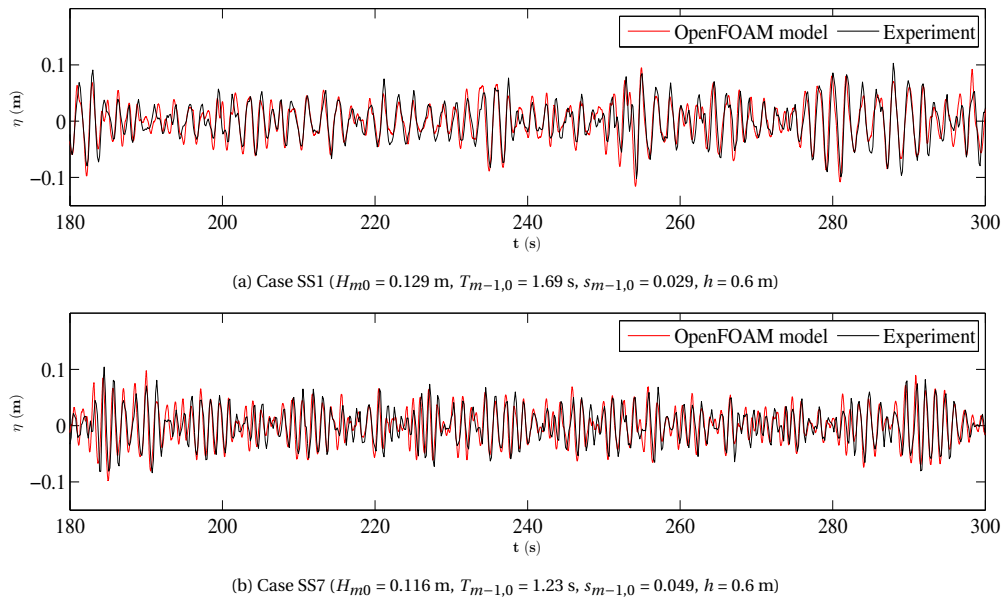
Figure 4.6: Comparisons of time series of free surface elevation (η) given by the numerical model and experiments for the cases SS1 and SS7.

An accurate reproduction of the wave energy spectra of incident waves in front of the

structure is essential for an accurate prediction of the overtopping discharge at dikes. Figure 4.7 shows the comparisons between modelled and experimental wave energy spectra of incident waves for case SS1 and case SS7. The experimental wave spectra are obtained based on the measured time series of incident wave surface elevation of 0 - 500 s corresponding to the simulation time in the numerical model. The shape of the wave energy spectra of measured incident waves from physical model is generally well predicted using the numerical model. Based on the wave energy spectra, the significant wave height H_{m0} and spectral wave period $T_{m-1,0}$ are calculated. Figure 4.8 presents the ratio of $\frac{H_{m0-OpenFOAM}}{H_{m0-experiment}}$ and the ratio of $\frac{T_{m-1,0-OpenFOAM}}{T_{m-1,0-experiment}}$ for all 28 simulated cases. Scattered data points closely around line of y=1 in Figure 4.8a demonstrate that the significant wave height H_{m0} can be well reproduced by the OpenFOAM® model. The comparison of the spectral wave period in Figure 4.8b shows that the wave period $T_{m-1,0}$ is slightly overestimated by the OpenFOAM® model. This might be caused by the slight overestimation of wave period produced by OceanWave3D which provides input of wave signal for waves2Foam. In the OceanWave3D model, the reflected waves are not totally absorbed by the sponge layer and therefore interact with the incident waves resulting in larger wave period. Nevertheless, the mean absolute percentage error ($MAPE$) for $T_{m-1,0}$ is only 5.3%, which has limited influence on the average overtopping discharge. Thus, the difference is regarded as being acceptable. The measured and modelled incident wave height H_{m0} and wave period $T_{m-1,0}$ for all simulated cases can be found in Table 4.A.1.
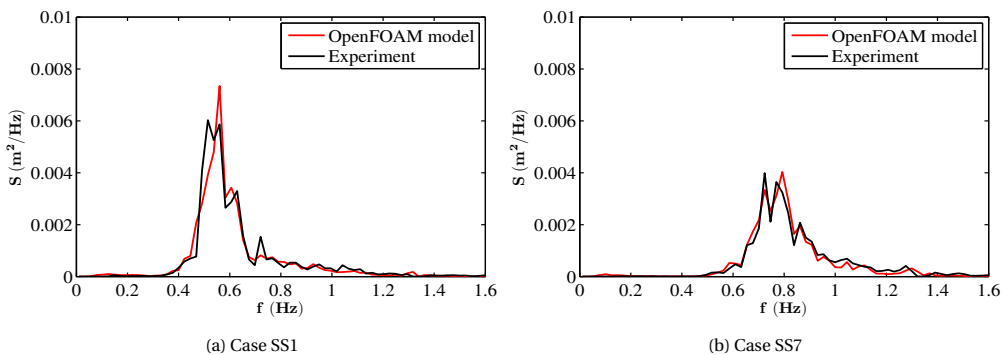
(a) Case SS1 (b) Case SS7

Figure 4.7: Wave energy spectra of incident waves for a) case SS1: $H_{m0} = 0.116$ m, $T_{m-1,0} = 1.23$ s, $s_{m-1,0} = 0.049$, $h = 0.6$ m and b) case SS7: $H_{m0} = 0.116$ m, $T_{m-1,0} = 1.23$ s, $s_{m-1,0} = 0.049$, $h = 0.6$ m.

Overall, the results presented in this section indicate that the OpenFOAM® model is capable of accurately reproducing the incident irregular waves in terms of wave propagation and wave properties including the significant wave height H_{m0} and the spectral wave period $T_{m-1,0}$.
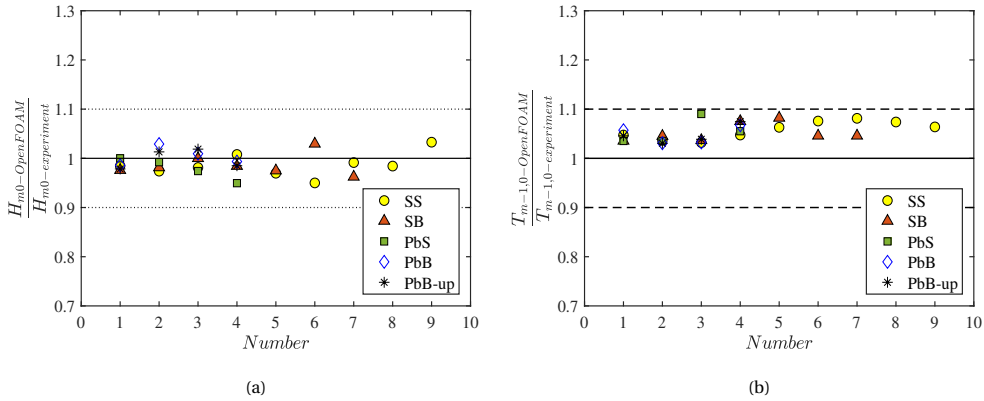
Figure 4.8: Ratios of modelled and experimental a) significant wave height H_{m0} with MAPE = 2.0% and b) spectral wave period $T_{m-1,0}$ with MAPE = 5.3%.

4.3.2. VALIDATION OF WAVE OVERTOPPING DISCHARGE

THE capability of OpenFOAM® model to predict overtopping discharge at dikes is evaluated by comparing the computed cumulative overtopping discharge by the numerical model to the measured cumulative overtopping discharge from the experiments. The overtopping volume in the physical model tests was measured using a wave gauge installed in the overtopping box to detect the variation of the water surface, which gives the opportunity to compare the time history of the accumulated overtopping volume between the numerical model and experiments.

Figure 4.9 shows the experimental and numerical time history of the accumulated overtopping volume from three cases, i.e. a) case SS7 (smooth straight slope), b) case SB5 (smooth bermed slope) and c) case PbB2 (bermed slope covered by protruding blocks). It can be seen that the numerical time series of cumulative overtopping volume shows a good agreement with the experimental result for the smooth straight slope (SS7). Figure 4.9b shows an overestimation of around 30% for a smooth bermed slope (SB5). For the bermed slope covered by protruding blocks (PbB2), the cumulative overtopping volume given by the model is about twice of the measured result as shown in Figure 4.9c. The time series of cumulative overtopping volume given by numerical model show a similar trend with the experimental results for SB5 and PbB2, which reveals that the OpenFOAM® is generally capable of capturing individual overtopping events.

The values of dimensionless average overtopping discharges q^* ($= \frac{q}{\sqrt{gH_{m0}^3}}$) predicted by the OpenFOAM® model versus experimental results for all 28 cases in total are shown in Figure 4.10. The performance of the OpenFOAM® model for predicting the overtopping discharges at dikes is quantitatively evaluated using the accuracy metrics of Bias and Nash-
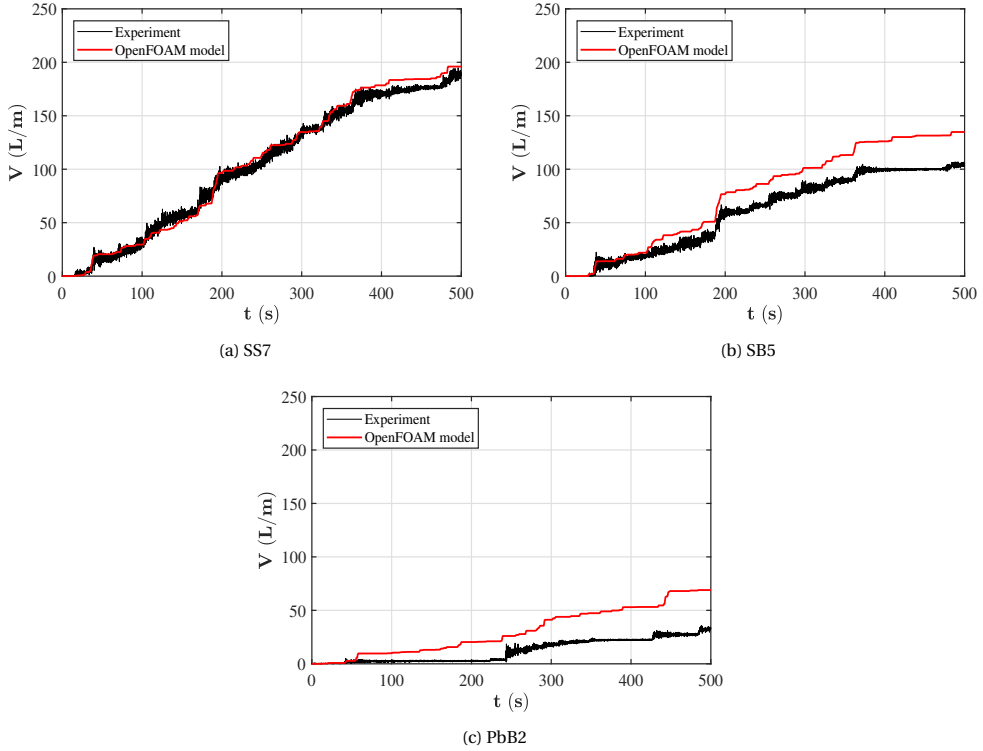
Figure 4.9: Measured and computed time series of cumulative overtopping volume per meter width V [L/m] with a) SS7 (H_{m0} = 0.115 m, $T_{m-1,0}$ = 1.33 s, $s_{m-1,0}$ = 0.049, h = 0.6 m), b) SB5 (H_{m0} = 0.117 m, $T_{m-1,0}$ = 1.45 s, $s_{m-1,0}$ = 0.04, h = 0.6 m) and c) PbB2 (H_{m0} = 0.117 m, $T_{m-1,0}$ = 1.68 s, $s_{m-1,0}$ = 0.027, h = 0.6 m).

Sutcliffe model efficiency coefficient (NSE) defined as follows:

$$Bias = \frac{1}{N} \sum_{i=1}^{N} [\log(q^*_{OpenFOAM}) - \log(q^*_{experiment})] \tag{4.4}$$

$$NSE = 1 - \frac{\sum_{i=1}^{N} [\log(q^*_{experiment}) - \log(q^*_{OpenFOAM})]^2}{\sum_{i=1}^{N} [\log(q^*_{experiment}) - \overline{\log(q^*_{experiment})}]^2} \tag{4.5}$$

where N is the total number of simulated cases; $\overline{\log(q^*_{experiment})}$ is the mean value of $\log(q^*_{experiment})$. $Bias$ indicates the tendency of the numerical model to overestimate or underestimate the average overtopping discharge. NSE measures the correlation between the experimental and numerical overtopping discharges and it varies between $-\infty$ and 1. NSE = 1 represents a perfect agreement of numerical data to the experimental data and NSE = 0 means that the numerical values are as accurate as the mean of the experimental data. NSE < 0 indicates that the experimental mean value is a better predictor than the

numerical model. Therefore, the closer the NSE is to 1, the more accurate the numerical model is.
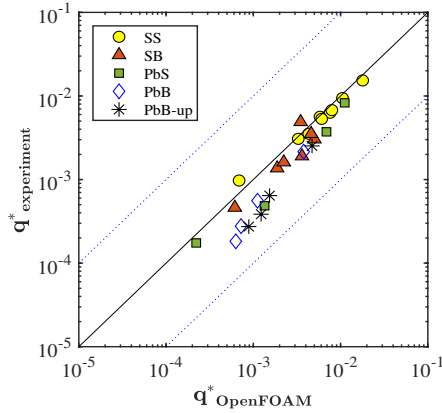
Figure 4.10: Comparisons of numerical and experimental dimensionless average overtopping discharges q^* at smooth straight slope (SS), smooth slope with berm (SB), straight slope covered by protruding blocks (PbS), bermed slope covered by protruding blocks (PbB) and bermed slope with only upper slope covered by protruding blocks (PbB_up).

Figure 4.10 shows a good agreement between the computed and measured dimensionless average overtopping discharges at smooth straight slopes within a wide range of (0.0001, 0.04). An overall slight overestimation for smooth bermed slopes might be because the air entrainment produced by the berm in experiments cannot be accounted for by the numerical model leading to less energy dissipation. For the slopes (partly) covered by protruding blocks, the average overtopping discharges are slightly overestimated by the OpenFOAM® model, resulting in the overall Bias of 0.19. One of the causes for this overestimation might be that the turbulence generated by the protrusions is underestimated in the 2D model as the blocks are in chessboard pattern in the experiments, which cannot be modelled in a 2D model. The NSE value of 0.78 shows an overall good match of the numerical average discharge with the experimental results. It can be concluded that the OpenFOAM® model is capable of predicting the overtopping discharges at dikes with simple and complex configurations with the accuracy within a factor of 1 to 3 of the experimental overtopping discharges. EurOtop (2018) stated that overtopping rates estimated by empirically derived equations are within, at best, a factor of 1 to 3 of the actual overtopping rates. Besides, Figure 15 in Chen, Van Gent, et al. (2020) showed that the empirical equations provided by TAW (2002) and EurOtop (2018) gave a factor of 1 to 8 of the measured overtopping rates from the experiments. Therefore, the accuracy of the numerical model in this study is equivalent to, or even better, than that of empirical equations.

4.4. BERM INFLUENCE

CHEN, Van Gent, et al. (2020) developed an empirical equation (4.A.7) as shown in Appendix 4.A to account for the berm influence on the average overtopping discharge based on the berm equation (4.A.2) provided by TAW (2002) by means of small-scale physical model tests. However, in those experiments, the width of the berm (B) was fixed at 0.2 m and the berm level relative to SWL (d_h) was varied in a very limited range of (-0.03 m, 0.03 m), which may limit the applicability of the empirical berm equation. Therefore, the validated OpenFOAM® model is applied to generate a numerical dataset by varying the berm width and berm level in a larger range. The numerical dataset is then analysed to investigate the influence of berm width and berm level on the average overtopping discharge at dikes.

4.4.1. NUMERICAL EXPERIMENTS

THE same configuration as shown in Figure 4.2b was considered in the numerical model, except that the berm width and berm level were varied. The berm width was varied in the range of 0.0 m to 0.6 m (on the scale of the small-scale experiments) combined with different values of the wave steepness in the numerical model. The berm level was varied between -0.15 m and 0.125 m by changing the position of the berm with the still water level (SWL) fixed at 0.6 m. The berm width was chosen as 0.2 m and 0.4 m. 28 cases (Table 4.A.2) were simulated in total. Each case was simulated for around 500 s.

4.4.2. MODEL RESULTS

MODEL results of average overtopping discharges are presented in Table 4.A.2. Figure 4.11 shows the relationship between the relative berm width (B/H_{m0}) and the ratio of the modelled dimensionless average overtopping discharge (q^*) and the modelled discharge without a berm ($q^*_{no\ berm}$). There is a clear trend of the dimensionless mean overtopping discharge decreasing with increasing relative berm width, which is in line with the results from previous studies (e.g. Figure 1 in Van Gent, 2013). It is worth noting that the application of a berm at a dike can significantly reduce the average overtopping discharge. Applying a berm with $B/H_{m0} \approx 2$ can lead to 40% less than the average overtopping discharge over smooth straight slope according to the model results. For the relative berm width $B/H_{m0} > 4$, further extension of berm width may not lead to a significant reduction of the average overtopping discharge. The berm influence factor γ_b is usually used to represent the reductive influence of a berm on overtopping discharge (e.g. TAW, 2002; EurOtop, 2018 and Chen, Van Gent, et al., 2020). Values of the berm factor γ_b can be obtained by solving the overtopping equation (4.A.1) with the overtopping discharge q substituted by the modelled average overtopping discharges. Figure 4.12 shows that the berm influence

factor γ_b decreases as the relative berm width B/L_{berm} (where L_{berm} is the characteristic berm length) increases. Here, B/L_{berm} is used since this makes it easier to compare with the empirical equations. Open markers in Figure 4.12 represent some of the experimental data on which the empirical berm equation was derived. A good agreement between the experimental results and empirical equations can be seen. Note that the B/L_{berm} from the experimental data varied due to variation in the wave height but not due to variations in the berm width since the berm width in the experiments was fixed as 0.2 m. The empirical equations show a similar trend with the model results while some differences between the model results and empirical equations can be noticed.
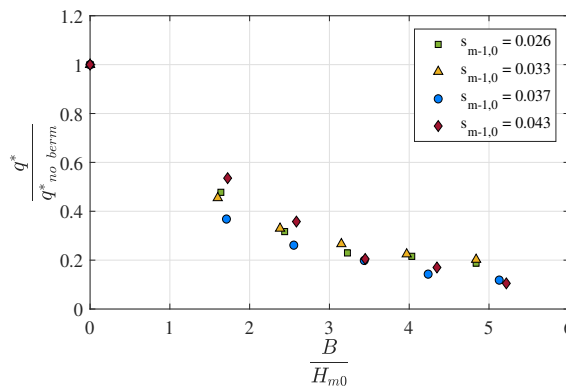
Figure 4.11: Reductive influence of berm width on the average overtopping discharge.
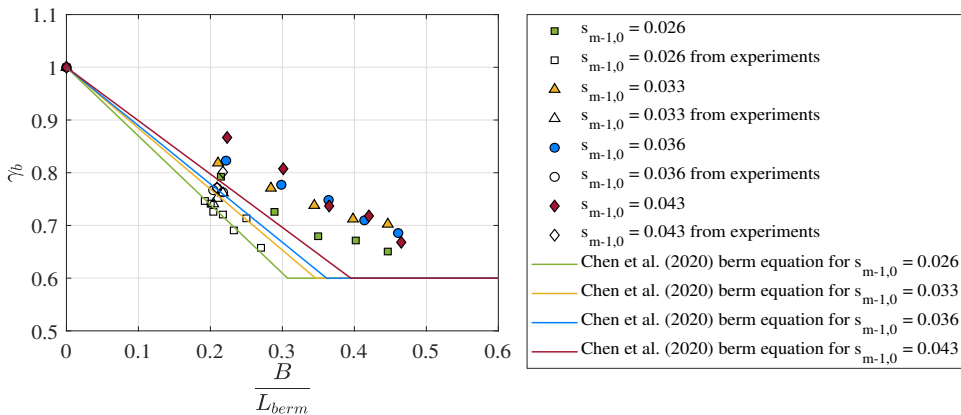
Figure 4.12: Effect of berm width on the berm influence factor given by OpenFOAM® model in comparison with empirical equations.

The numerical modelled relationship between the berm influence factor γ_b and relative berm level is shown in Figure 4.13 in which $R_{u2\%}$ is the wave run-up height that is exceeded

by 2% of the number of incoming waves at the toe of the structure. $R_{u2\%}$ can be calculated using equations (4.A.5) and (4.A.6). The empirical equation matches well with the experimental data points marked with open squares. It can be seen from the model results that the berm has the most reductive influence on the average overtopping discharge when the berm is located near the still water level while the reductive influence decreases as the distance between the berm and SWL increases. This is in accordance with the expressions for the influence of the berm as described in Chen, Van Gent, et al. (2020). For the berm width of 0.2 m (corresponding to $B/H_{m0} = 1.6$) used in the experiments, the berm equation works reasonably. Nevertheless, there are still some discrepancies between the numerical model results and the empirical equations, especially for the comparison between the computed berm factors and the berm equation for larger berm width ($B/H_{m0} = 3.2$ with B = 0.4 m), which is outside of the experimental ranges.
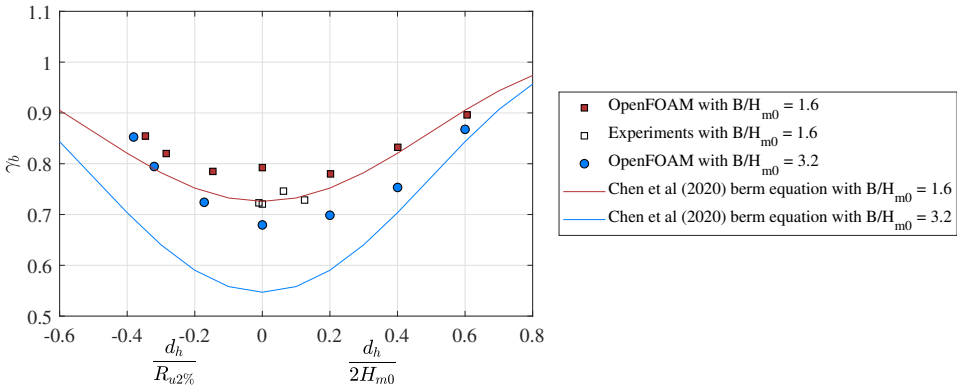
Figure 4.13: Numerical modelled results of effect of berm level on the berm influence factor in comparison with empirical equations.

Figure 4.12 and Figure 4.13 demonstrate that the numerical model is capable of simulating the behaviour of berm influence on the average overtopping discharge at dikes to a reasonable extent. Additionally, differences between the modelled results and the empirical equations show a potential modification of Chen, Van Gent, et al. (2020) berm equation for a wider range of berm width and berm level. The berm equation (4.A.7) indicates a linear relationship between γ_b and $\frac{r_B(1-r_{dh})}{\sqrt{s_{m-1,0}}}$.

Therefore, we plotted $\frac{r_B(1-r_{dh})}{\sqrt{s_{m-1,0}}}$ on the horizontal axis, where r_B is a parameter taking the berm width into account and r_{dh} is a parameter that represents the effect of the berm level on the berm influence factor, and the berm influence factor based on model results on the vertical axis (Figure 4.14). This shows a linear relationship between γ_b and $\frac{r_B(1-r_{dh})}{\sqrt{s_{m-1,0}}}$ but with a different value of the empirical coefficient b_0. By applying the least square method, the empirical coefficient b_0 was recalibrated as 0.14 based on the numerical data for wider
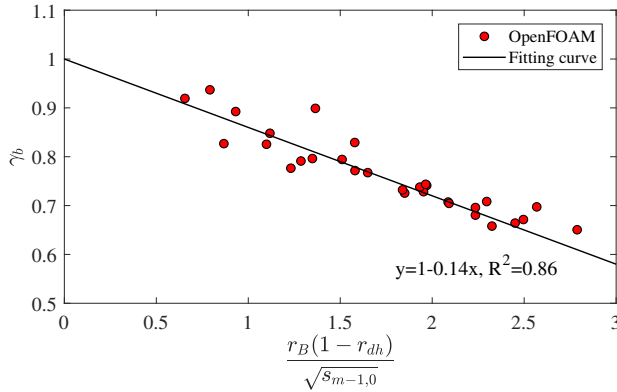
Figure 4.14: Berm influence factor γ_b as a function of $\frac{r_B(1-r_{dh})}{\sqrt{s_{m-1,0}}}$ which takes the berm width, berm level and wave steepness into account.

berms and larger berm levels that are outside of the ranges of experimental data. The best-fit formula based on the model results is defined as follows.

$$\gamma_b = 1 - \frac{0.14 r_B(1-r_{dh})}{\sqrt{s_{m-1,0}}} \tag{4.6}$$

where r_B can be calculated using Eq. (4.A.3) and r_{dh} is calculated using Eq. (4.A.4). The values of R^2 and $RMSE$ for the fitting equation (4.6) are 0.86 and 0.03 respectively. Even though Eq. (4.6) is not recommended for applications without further validation, it indicates that the empirical berm equation may require recalibration of the empirical coefficient b_0 when applying to cases outside of the experimental range.

4.5. ROUGHNESS INFLUENCE

I T is time-consuming to change the applied locations of roughness elements in the physical model tests. Therefore, in our earlier physical model tests (Chen, Van Gent, et al., 2020), we only considered the reductive influence of protruding blocks on the upper slope, blocks on the upper slope and berm, as well as blocks on the entire waterside slope surface. Chen, Van Gent, et al. (2020) concluded that the protruding blocks on the upper slope contribute the most to the total roughness influence factor. However, it remains unclear how much influence the protruding blocks have if only applied on a part of the upper slope. The numerical simulations are performed aiming to study the influence of coverage length of the protruding blocks on the partial upper slope on the total roughness factor of the waterside slope.

4.5.1. Numerical experiments

THREE configurations, including one protrusion, two protrusions and three protrusions on the upper slope, are modelled in the OpenFOAM® model. Figure 4.15 shows the meshes around protrusions for these three configurations. The water depth was kept at 0.6 m, which also means that the freeboard and berm level remained constant in all simulations. The berm width was fixed at 0.2 m. Four wave conditions which are given in Table 4.2 were considered. Combining the wave condition and dike configuration results in 12 simulations. Thus, for each dike configuration, four wave conditions were applied.
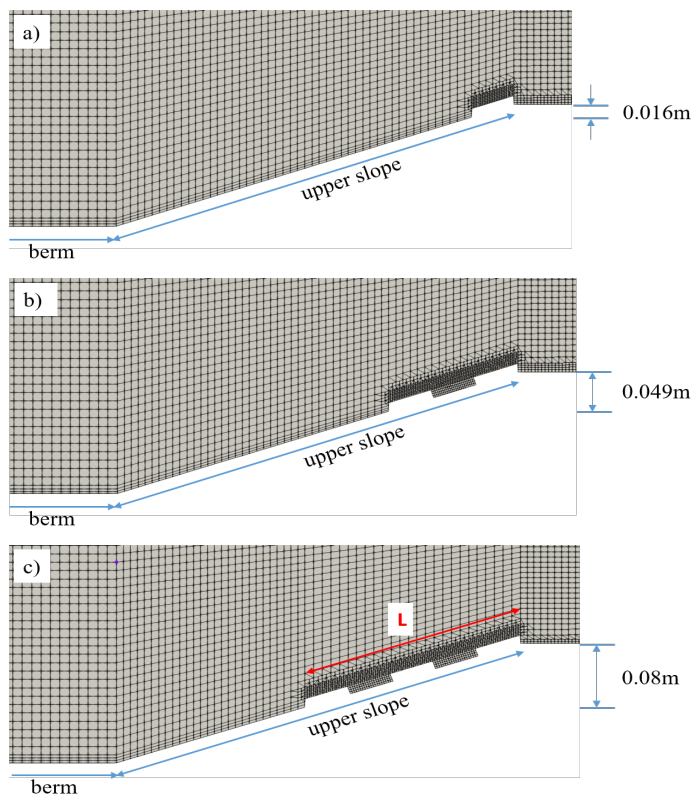
Figure 4.15: Mesh for a) one protrusion on the upper slope, b) two protrusions on the upper slope and c) three protrusions on the upper slope about half of the upper slope).

4.5.2. Model results

MODEL results of four series of simulations are reported in Table 4.A.3. As mentioned in the Section 4.3.2, the average overtopping discharges are overestimated by the OpenFOAM® model for the configurations with protruding blocks. Figure 4.16 shows the

Table 4.2: Wave conditions simulated in the OpenFOAM® model.

Wave condition	H_{m0} [m]	$T_{m-1,0}$ [s]	$s_{m-1,0}$ [-]
W1	0.139	1.75	0.029
W2	0.115	1.63	0.028
W3	0.107	1.55	0.028
W4	0.120	1.34	0.043

comparison between the measured and modelled dimensionless average overtopping discharges at slopes with upper slope covered by blocks (PbB_up) and slopes entirely covered by blocks (PbB). The OpenFOAM® model tends to give a larger overestimation for smaller overtopping discharge. A relationship between numerical and experimental results is found as shown in Figure 4.16 by fitting the data using the least square method. To analyse the trend of the computational results of the roughness influence factor of protruding blocks, the average overtopping discharge predicted by the numerical model were modified by using the following equation

$$q^*_{OpenFOAM\_Mod} = \left(\frac{q^*_{OpenFOAM}}{0.53} \right)^{1.25}$$
(4.7)

where $q^*_{OpenFOAM\_Mod}$ is the modified dimensionless average overtopping discharge and $q^*_{OpenFOAM\_Mod}$ represents the original overtopping discharge given by the OpenFOAM® model.
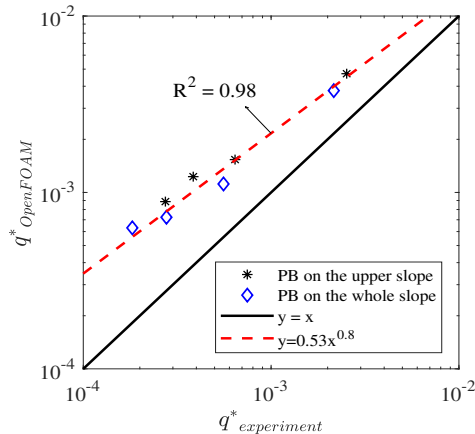
Figure 4.16: Comparison between experimental and numerical dimensionless average overtopping discharges over slopes with the upper slope covered by protruding blocks and slopes entirely covered by protruding blocks.

Table 4.3 lists the values of the roughness influence factors for all simulations includ-

ing the simulations for the bermed slope covered by protruding blocks (PbB) and for the bermed slope with the upper slope covered by protruding blocks (PbB_up). In the table, L_1 represents one protrusion on the upper slope, L_2 represents two protrusions on the upper slope, L_3 corresponds to three protrusions on the upper slope, L_4 represents the protruding blocks on the upper slope and L_5 means the protruding blocks applied on the entire slope surface. The calculated roughness influence factors for all simulations are also shown in Figure 4.17 with the relative coverage length of protruding blocks 'L/L_5' on the horizontal axis and the roughness factor on the vertical axis. The coverage length, L, is the effective length of applied protruding blocks along the slope as shown in Figure 4.15c. The roughness elements located below $0.25R_{u2\%,smooth}$ under the still water level have little or no effect on the total roughness factor according to TAW (2002). Thus, for the protruding blocks on the down slope, only the blocks lying above $0.25R_{u2\%,smooth}$ under the still water level are taken into account to calculate the coverage length. $0.25R_{u2\%,smooth}$ is the wave run-up level on a smooth slope which can be calculated using Eqs. (4.A.5 & 4.A.6). Six points from left to right in each scattered diagram in Figure 4.17 represent the roughness factors based on the model results of smooth bermed slope, one protrusion, two protrusions, three protrusions, slopes with upper slope covered by blocks and slopes entirely covered by blocks. In general, the roughness influence factor decreases, which means that the reductive influence of roughness increases, as the coverage length of protruding blocks increases. The average contribution of protruding blocks for four wave conditions to the total roughness factor is estimated using Eq. (4.8).

$$\overline{C_{pb}} = \frac{\sum_{i=1}^{M}(1-\gamma_{f-total_i})/(1-\gamma_{f-pb_i})}{M} \tag{4.8}$$

where M is the number of wave conditions ($M = 4$); $\gamma_{f-total_i}$ [-] is the calculated overall roughness factor of the waterside slope based on the model results; γ_{f-pb_i} [-] is the roughness factor of the bermed slope entirely covered by protruding blocks. The application of only one protrusion can contribute 44% to the total roughness influence. It is also worth noting that the roughness factors for three protrusions are almost the same as those for the protruding blocks on the entire upper slope (four protrusions). On average, the blocks on the half upper slope (three protrusions) contribute 76% to the total roughness influence, while five additional protrusions (blocks on the entire upper slope) also lead to a contribution of 76% to the total roughness influence (Table 4.4). This indicates that the protruding blocks on the lower part of the upper slope do not play a role in reducing the average overtopping discharge.

Table 4.3: Roughness factors based on model results for all simulations, where W represents the different wave conditions and L the different protrusion lengths with L_1 for one protrusion, L_2 for two protrusions, L_3 for three protrusions, L_4 for protruding blocks on the entire upper slope and L_5 for protruding blocks on the whole water-side slope.

	Length (m)	W1	W2	W3	W3
0	0.00	1	1	1	1
L_1	0.05	0.92	0.85	0.85	0.90
L_2	0.15	0.87	0.81	0.82	0.87
L_3	0.25	0.83	0.78	0.76	0.84
L_4	0.45	0.84	0.78	0.76	0.82
L_5	0.86	0.77	0.72	0.72	0.73
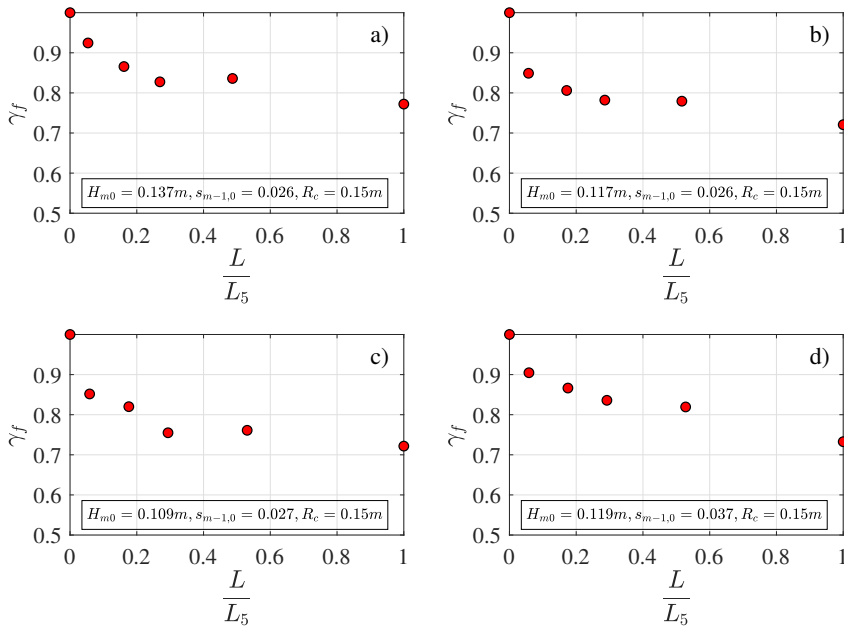
Figure 4.17: Comparison of roughness factors for from left to right the smooth bermed slope, one protrusion on the upper slope, two protrusions on the upper slope, three protrusions on the upper slope, protruding blocks on the entire upper slope and protruding blocks on the whole waterside slope under four wave conditions (W1, W2, W3 and W4).

4.6. DISCUSSION

4.6.1. APPLICABILITY AND LIMITATIONS OF THE MODEL

THIS study provides a systematic validation of the OpenFOAM® model for predicting the wave overtopping discharge resulting from irregular waves at dikes with simple and complex configurations. The model validation shows that the model is capable of predict-

Table 4.4: Average contributions of protruding blocks for four wave conditions to the total roughness influence.

	Average Contribution
L_1	44%
L_2	61%
L_3	76%
L_4	76%
L_5	100%

ing the overtopping at smooth straight and smooth bermed slope accurately. However, it overestimates the average overtopping discharges at slopes (partly) covered by protruding blocks about twice of the measured discharge from the experiments. This overestimation might be partly caused by the underestimation of the turbulence produced by protrusions in the 2D model considering the protruding blocks were placed in a chessboard pattern in the experiments. The width of the model in the experiments was 1 m. Since the slope surface in a 2DV numerical model was assumed uniform in z direction, the protrusions would act as parallel ribs across the model width instead of as protruding blocks in chessboard pattern imagining that the protrusions in the 2D numerical model were extended by 1 m along z direction. The estimated roughness influence factor of ribs (optimal) is about 0.86 using the equation (5.24) in EurOtop (2018) while the mean roughness influence factor is around 0.72 from Chen, Van Gent, et al. (2020). This indicates that the ribs might lead to less reductive influence on the overtopping and therefore larger overtopping discharge than protruding blocks in chessboard pattern. Besides, the numerical model cannot take the aeration caused by protrusions into account, which could also lead to overestimation of overtopping rate.

We applied the validated OpenFOAM® model to investigate the berm and roughness influence. Results of the berm influence show that the OpenFOAM® model is capable of computing the reductive influence of a berm on the average overtopping discharges at dikes reasonably. Comparison between numerical results and the empirical berm equation indicates similar trends of the berm factor changing with the berm width and the berm level. However, there is still some difference between the model results and the empirical berm equation derived in Chen, Van Gent, et al. (2020), which indicates that the empirical equation might require modification for applications outside of the experimental ranges. To extend the range of application, a modified berm equation was developed based on the model results by recalibrating the empirical coefficient b_0 in the empirical berm equation. We emphasize that this new berm equation needs further validation before it can be recommended for application in practice. Nevertheless, the numerical model extended the insights into the dependencies of parameters and insights into the applicability of empirical equations.

The influence of the coverage length of protruding blocks on part of the upper slope on the total roughness factor was investigated with the OpenFOAM® model. The numerical results are in line with the findings in Chen, Van Gent, et al. (2020) that the roughness elements on the higher part of the waterside slope play a major role in reducing the wave overtopping (see also Capel, 2015). Model results also show that the total roughness factor is sensitive to the location of the protruding blocks applied on the half upper slope. Applying one row of protruding blocks on the top of the upper slope can effectively increase the reductive roughness influence on the overtopping discharge. Protruding blocks on the upper half of the upper slope lead to almost the same total roughness factor as those on the entire upper slope.

The model results for berm and roughness influence demonstrate the added value of the OpenFOAM® model for predicting the average overtopping discharges at dikes with complex configurations. The numerical model can be used in combination with empirical equations to predict the overtopping discharge during a functional design of a dike, since the numerical model can deal with a wider range of wave conditions and dike configurations than that in the experimental setup. Besides, when applying berm and/or roughness elements at a dike is necessary, this numerical model can provide insights into the optimal berm width and the optimal locations and coverage length of roughness elements along the waterside slope for reducing the wave overtopping discharge. For example, model results for the roughness influence presented in Section 4.5.2 show that the roughness elements applied on the upper half of the upper slope can lead to approximately the same reductive influence of those applied on the entire upper slope, which suggests a possibility of reducing the costs related to dike construction. Although the numerical model is capable of predicting the discharge with a good accuracy, it still has some limitations. One limitation of the 2DV numerical model developed in this study is that it assumes the coastal structures and waves are alongshore-homogeneous and therefore the directional and directional spreading effects on wave overtopping and wave transformation cannot be taken into account in a 2DV approach. The numerical model was developed for impermeable structures considering dikes are often impermeable in the practical engineering. Therefore, this OpenFOAM® model requires adaptation for the cases that permeable armour units or permeable core material are applied at the coastal structures.

4.6.2. Computational efficiency of the model

In the present study, one simulation for wave overtopping at a smooth straight slope for 500 s took about 5 days parallelizing the case into 3 processors (3.6 GHz) which is quite a small number of processors. For the wave overtopping at slopes covered by protruding blocks, it took 10 days to finish one simulation of 500 s with 3 processors (3.6GHz). The

OpenFOAM® model is not the most computationally efficient model. Models based on NLSW are more computationally efficient but less accurate than the models based on RANS equations. The computational time of the numerical model developed in this study is acceptable considering the good accuracy in reproducing the incident waves and in predicting the overtopping discharge. For example, during the functional design or reinforcement of a dike, an accurate prediction of average overtopping discharge is essential. In this case, it is beneficial to have a model like this 2DV OpenFOAM® model with good accuracy and reasonable computational cost.

4.7. CONCLUSIONS

IN this paper, an investigation of the capability of the 2DV OpenFOAM® model in predicting wave overtopping for impermeable structures as well as the applicability of the numerical model in simulating the berm and roughness influence is presented.

Twenty-eight tests for five configurations from the experiments in Chen, Van Gent, et al. (2020) have been used to validate the 2DV OpenFOAM® in order to estimate the wave overtopping. Model results show that the incident waves that are used in the experiments can be well reproduced in the numerical model with the specific settings in this study in terms of wave propagation and wave properties. The comparison between the numerical and experimental overtopping discharges demonstrates that the numerical model is capable to predict the average overtopping discharge at simple and complex configurations within a factor of 1 to 3 of the experimental discharges and with a *NSE* of 0.78. Besides, similar trends of modelled and experimental time series of cumulative overtopping volume indicate that the OpenFOAM® model can also capture the individual overtopping events.

The validated OpenFOAM® model was then applied to study the berm and roughness influence on the average overtopping discharge. The numerical model showed reasonable behaviour of the variation of average overtopping discharge when taking the berm and roughness elements into account. The model results indicate a potential improvement of the empirical berm equation developed by Chen, Van Gent, et al. (2020) for the cases outside the experimental conditions. Results for roughness influence show that the roughness influence factor is very sensitive to the coverage length of roughness elements along the upper half of the upper slope. We found that protruding blocks on the upper half of the upper slope resulted in similar roughness factor with those applied on the entire upper slope.

We recommend to analyse the influence of the berm and roughness also in combination with oblique waves, with and without directional spreading.

The results of model validation and numerical experiments show potential applications of the 2DV OpenFOAM® with the specific settings used in this study in the dike design and safety assessment.

4.A. An Appendix to Chapter 4

4.A.1. Sensitivity of the overtopping discharge to grid size around protrusions

The influence of the grid size on the modeled overtopping volume at straight slope covered by protruding blocks was analyzed based on case PbS1 (H_{m0} = 0.129 m, $T_{m-1,0}$ = 1.76 s, $s_{m-1,0}$ = 0.027, h = 0.6 m). The grid sizes around protrusions considered have been 0.005 × 0.005 m for the coarse grid, 0.0025 × 0.0025 m for the medium grid size and 0.00125 × 0.00125 m for the fine grid respectively as shown in Figure 4.A.1.
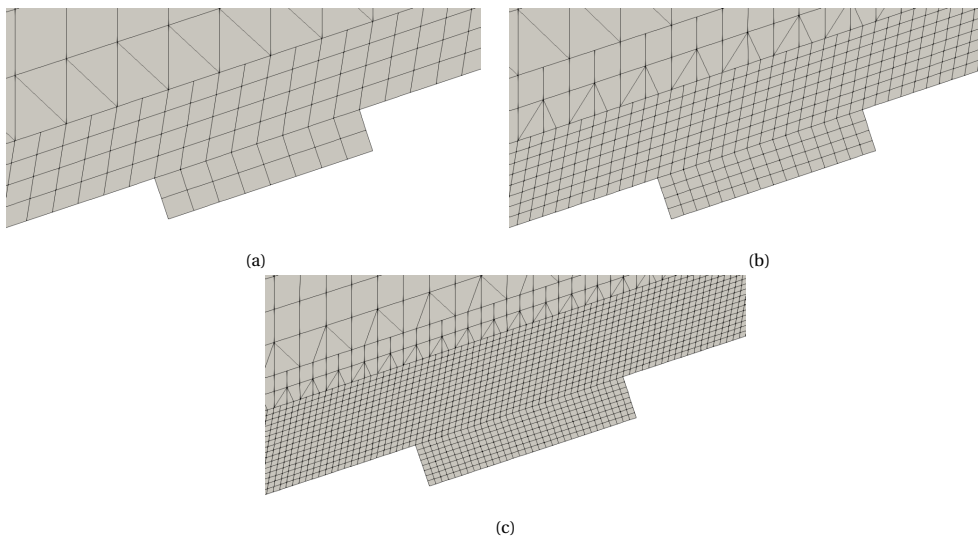
Figure 4.A.1: Mesh around protrusions with a) coarse grid size, b) medium grid size and c) fine grid size.

The influence of the grid size on the modeled overtopping volume is shown in Figure 4.A.2. It can be seen that the coarse grid results in slightly more overtopping than medium and fine grid. Besides, the medium grid and fine grid produce almost the same overtopping volume. The average overtopping discharges for the coarse grid, medium grid and fine grid

are 0.0011 m^3/s/m, 0.001 m^3/s/m and 0.001 m^3/s/m, respectively. Therefore, the model result of the cumulative overtopping volume is not very sensitive to the grid size and further refining the mesh around the protrusions did not lead to significant improvement of the model result. The medium grid size is used in this study considering it did not increase much more computation time than the coarse time and it gave a closer result of overtopping volume to the experimental overtopping volume.
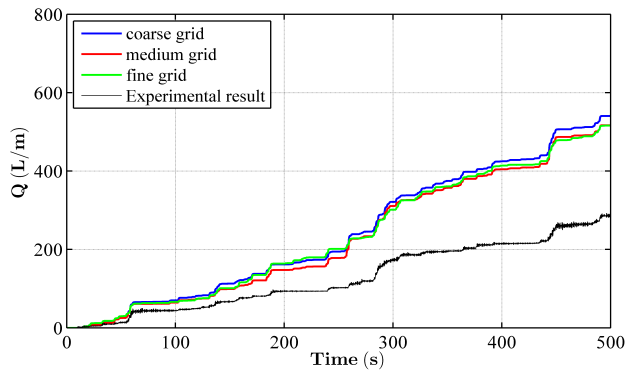
Figure 4.A.2: Influence of grid size on the accumulative overtopping volume.

4.A.2. RESULTS OF MODEL VALIDATION AND APPLICATIONS

Table 4.A.1: Experimental and numerical results of wave conditions and average overtopping discharge used for the model validation, where H_{m0_exp}, $T_{m-1,0\_exp}$ and q_{exp} represent the experimental significant wave height, spectral wave period and average overtopping discharge respectively; H_{m0_model}, $T_{m-1,0\_model}$ and q_{model} represent the numerical results.

Case name	H_{m0_exp} [m]	H_{m0_model} [m]	$T_{m-1,0\_exp}$ [s]	$T_{m-1,0\_model}$ [s]	h [m]	q_{exp} [l/s/m]	q_{model} [l/s/m]
SS1	0.129	0.127	1.69	1.77	0.6	1.37	1.49
SS2	0.115	0.112	1.64	1.7	0.6	0.77	0.89
SS3	0.107	0.105	1.56	1.61	0.6	0.618	0.619
SS4	0.128	0.129	1.69	1.77	0.63	2.2	2.6
SS5	0.099	0.096	1.27	1.35	0.57	0.095	0.064
SS6	0.12	0.114	1.32	1.42	0.6	0.46	0.52
SS7	0.116	0.115	1.23	1.33	0.6	0.38	0.4
SS8	0.127	0.125	1.49	1.6	0.6	0.96	1.1
SB1	0.125	0.122	1.69	1.75	0.6	0.42	0.67
SB2	0.107	0.105	1.55	1.62	0.6	0.15	0.2
SB3	0.114	0.114	1.64	1.7	0.6	0.59	0.42
SB4	0.127	0.125	1.46	1.57	0.6	0.27	0.5
SB5	0.12	0.117	1.34	1.45	0.6	0.21	0.28
SB6	0.102	0.105	1.53	1.6	0.63	0.36	0.49
SB7	0.106	0.102	1.53	1.6	0.57	0.05	0.0626
PbS1	0.129	0.129	1.7	1.76	0.6	0.54	1
PbS2	0.116	0.113	1.22	1.33	0.6	0.06	0.16
PbS3	0.099	0.094	1.27	1.34	0.585	0.017	0.02
PbS4	0.129	0.128	1.7	1.76	0.63	1.2	1.6
PbB1	0.139	0.137	1.75	1.85	0.6	0.35	0.6
PbB2	0.1137	0.117	1.63	1.68	0.6	0.067	0.14
PbB3	0.107	0.108	1.55	1.6	0.6	0.02	0.07
PbB4	0.1198	0.119	1.34	1.43	0.6	0.036	0.093
PbB_up1	0.139	0.136	1.75	1.83	0.6	0.41	0.74
PbB_up2	0.1145	0.116	1.63	1.68	0.6	0.078	0.19
PbB_up3	0.107	0.109	1.55	1.61	0.6	0.03	0.1
PbB_up4	0.1198	0.118	1.34	1.44	0.6	0.05	0.156

4.A.3. Empirical equations for estimating the average overtopping discharge at dikes

Chen, Van Gent, et al. (2020) recalibrated the TAW (2002) overtopping equation for breaking wave condition by recalibrating one empirical coefficient in the TAW (2002) overtopping equation. The recalibrated overtopping equation (4.A.1) was then used as a reference formula to investigate the influence of a berm and roughness on wave overtopping discharges at dikes.

$$\frac{q}{\sqrt{gH_{m0}^3}} = \frac{0.067}{\sqrt{\tan\alpha}}\gamma_b\xi_{m-1,0}\exp\left[-4.9\frac{R_c}{H_{m0}\xi_{m-1,0}\gamma_b\gamma_f\gamma_\beta\gamma_v}\right] \qquad (4.A.1)$$

in which q [m^3/s/m] is the average overtopping discharge; α is the angle of waterside slope; $\xi_{m-1,0}$ ($\xi_{m-1,0} = \tan\alpha/\sqrt{2\pi H_{m0}/(gT_{m-1,0}^2)}$) is the breaker parameter; R_c [m] is the crest level relative to the still water level; γ_b [-] is the influence factor for berms; γ_f [-] is the influence factor for roughness; γ_β [-] is the influence factor for oblique waves; γ_v [-] is the influence factor for vertical walls. TAW (2002) and EurOtop (2018) provide equations for

Table 4.A.2: Simulated cases for investigating the effects of berm width, B, and berm level on average overtopping discharges, q_{model}, at dikes. Where H_{m0} is the significant wave height; $T_{m-1,0}$ is the spectral wave period; $s_{m-1,0}$ is the wave steepness.

Case name	B [m]	H_{m0} [m]	$T_{m-1,0}$ [s]	$s_{m-1,0}$ [-]	h [m]	Berm level [m]	q_{exp} [l/s/m]	q_{model} [l/s/m]
SS1	0	0.127	1.77	0.026	0.6	0	1.37	1.49
SB1	0.2	0.122	1.75	0.026	0.6	0	0.42	0.67
SBW301	0.3	0.123	1.75	0.026	0.6	0		0.45
SBW401	0.4	0.124	1.75	0.026	0.6	0		0.33
SBW501	0.5	0.124	1.75	0.026	0.6	0		0.31
SBW601	0.6	0.124	1.76	0.026	0.6	0		0.27
SS8	0	0.125	1.6	0.031	0.6	0	0.96	1.1
SB4	0.2	0.125	1.57	0.033	0.6	0	0.27	0.5
SBW302	0.3	0.126	1.56	0.033	0.6	0		0.367
SBW402	0.4	0.127	1.56	0.033	0.6	0		0.3
SBW502	0.5	0.126	1.57	0.033	0.6	0		0.25
SBW602	0.6	0.124	1.57	0.032	0.6	0		0.22
SS9	0	0.126	1.5	0.036	0.6	0	0.71	0.85
SB5	0.2	0.117	1.45	0.036	0.6	0	0.21	0.28
SBW303	0.3	0.1175	1.44	0.036	0.6	0		0.2
SBW403	0.4	0.1164	1.43	0.036	0.6	0		0.15
SBW503	0.5	0.118	1.42	0.037	0.6	0		0.11
SBW603	0.6	0.117	1.43	0.037	0.6	0		0.09
SS7	0	0.115	1.33	0.042	0.6	0	0.38	0.4
SBW204	0.2	0.116	1.32	0.043	0.6	0		0.217
SBW304	0.3	0.116	1.32	0.043	0.6	0		0.145
SBW404	0.4	0.116	1.32	0.043	0.6	0		0.083
SBW504	0.5	0.115	1.32	0.042	0.6	0		0.068
SBD201	0.2	0.124	1.75	0.026	0.6	0.05		0.65
SBD202	0.2	0.125	1.75	0.026	0.6	0.1		0.89
SBD203	0.2	0.125	1.76	0.026	0.6	-0.05		0.7
SBD204	0.2	0.123	1.76	0.026	0.6	-0.1		0.83
SBD205	0.2	0.124	1.75	0.026	0.6	0.15		1.2
SBD206	0.2	0.124	1.75	0.028	0.6	-0.125		1
SBD401	0.4	0.125	1.75	0.028	0.6	0.05		0.39
SBD402	0.4	0.125	1.76	0.028	0.6	0.1		0.58
SBD403	0.4	0.125	1.76	0.028	0.6	0.15		1.1
SBD404	0.4	0.125	1.76	0.028	0.6	-0.05		0.48
SBD405	0.4	0.124	1.75	0.028	0.6	-0.1		0.71
SBD406	0.4	0.124	1.76	0.028	0.6	-0.125		0.99

Table 4.A.3: Simulated cases and model results of average overtopping discharge (q) for roughness influence for the four wave conditions ($W1W4$) and varying coverage length of the protruding blocks on the upper slope ($L1L5$).

W1:

Case name	H_{m0_exp} [m]	H_{m0_model} [m]	$T_{m-1,0\_exp}$ [s]	$T_{m-1,0\_model}$ [s]	$s_{m-1,0\_exp}$ [-]	$s_{m-1,0\_model}$ [-]	q_{exp} [l/s/m]	q_{model} [l/s/m]
W1L1	0.139	0.138	1.75	1.84	0.029	0.026	—	0.11
W1L2	0.139	0.136	1.75	1.83	0.029	0.026	—	0.83
W1L3	0.139	0.137	1.75	1.83	0.029	0.026	—	0.74
W1L4	0.139	0.136	1.75	1.83	0.029	0.026	0.41	0.74
W1L5	0.139	0.142	1.75	1.85	0.029	0.027	0.35	0.69

estimating the berm influence factor γ_b.

$$\gamma_b = 1 - r_B(1 - r_{dh}) \qquad \text{if} \quad 0.6 \le \gamma_b \le 1.0 \qquad (4.A.2)$$

W2:

Case name	H_{m0_exp} [m]	H_{m0_model} [m]	$T_{m-1,0\_exp}$ [s]	$T_{m-1,0\_model}$ [s]	$s_{m-1,0\_exp}$ [-]	$s_{m-1,0\_model}$ [-]	q_{exp} [l/s/m]	q_{model} [l/s/m]
W2L1	0.115	0.115	1.63	1.68	0.028	0.026	—	0.26
W2L2	0.115	0.116	1.63	1.68	0.028	0.026	—	0.22
W2L3	0.115	0.117	1.63	1.68	0.028	0.026	—	0.2
W2L4	0.115	0.116	1.63	1.68	0.028	0.026	0.078	0.19
W2L5	0.115	0.117	1.63	1.68	0.028	0.027	0.067	014

W3:

Case name	H_{m0_exp} [m]	H_{m0_model} [m]	$T_{m-1,0\_exp}$ [s]	$T_{m-1,0\_model}$ [s]	$s_{m-1,0\_exp}$ [-]	$s_{m-1,0\_model}$ [-]	q_{exp} [l/s/m]	q_{model} [l/s/m]
W3L1	0.107	0.108	1.55	1.61	0.029	0.027	—	0.16
W3L2	0.107	0.109	1.55	1.6	0.029	0.027	—	0.14
W3L3	0.107	0.11	1.55	1.6	0.029	0.028	—	0.1
W3L4	0.107	0.109	1.55	1.61	0.029	0.027	0.03	0.1
W3L5	0.107	0.108	1.55	1.6	0.029	0.027	0.02	0.07

W4:

Case name	H_{m0_exp} [m]	H_{m0_model} [m]	$T_{m-1,0\_exp}$ [s]	$T_{m-1,0\_model}$ [s]	$s_{m-1,0\_exp}$ [-]	$s_{m-1,0\_model}$ [-]	q_{exp} [l/s/m]	q_{model} [l/s/m]
W4L1	0.12	0.118	1.34	1.44	0.043	0.036	—	0.24
W4L2	0.12	0.118	1.34	1.43	0.043	0.036	—	0.2
W4L3	0.12	0.119	1.34	1.42	0.043	0.038	—	0.17
W4L4	0.12	0.118	1.34	1.44	0.043	0.036	0.05	0.156
W4L5	0.12	0.119	1.34	1.43	0.043	0.037	0.036	0.093

$$r_B = \frac{B}{L_{berm}} \tag{4.A.3}$$

$$r_{dh} = 0.5 - 0.5\cos\left(\pi\frac{d_h}{R_{u2\%}}\right) \quad \text{for a berm above still water line}$$
$$r_{dh} = 0.5 - 0.5\cos\left(\pi\frac{d_h}{2H_{m0}}\right) \quad \text{for a berm below still water line} \tag{4.A.4}$$

where L_{berm} [m] is the characteristic berm length; d_h [m] is the berm level relative to the SWL; $R_{u2\%}$ [m] is the wave run-up height that is exceeded by 2% of the number of incoming waves at the toe of the structure which can be calculated by using the following equations (TAW, 2002):

$$\frac{R_{u2\%}}{H_{m0}} = 1.65\gamma_b\gamma_f\gamma_\beta\xi_{m-1,0} \tag{4.A.5}$$

with a maximum of

$$\frac{R_{u2\%}}{H_{m0}} = \gamma_f\gamma_\beta\left(4 - \frac{1.5}{\sqrt{\xi_{m-1,0}}}\right) \tag{4.A.6}$$

Chen, Van Gent, et al. (2020) improved the TAW (2002) berm equation (4.A.2) by taking the wave steepness into account based on the analysis of experimental data.

$$\gamma_b = 1 - \frac{b_0}{\sqrt{s_{m-1,0}}}r_B(1 - r_{dh}) \tag{4.A.7}$$

in which b_0 is an empirical coefficient and b_0=0.21 for an impermeable berm; r_B and r_{dh} are calculated using Eqs. (4.A.3) & (4.A.4).

5

NUMERICAL INVESTIGATION OF THE EFFECTS OF ROUGHNESS, A BERM AND OBLIQUE WAVES ON WAVE OVERTOPPING PROCESSES AT DIKES

ABSTRACT The mean overtopping discharge and the overtopping flow parameters related to individual overtopping events are often used to characterize the wave overtopping processes at dikes. Roughness, berms and oblique waves have significant effects on the wave overtopping processes at dikes while these effects are still not fully understood. A 2DV OpenFOAM® model is validated using experimental data for predicting flow velocity and layer thickness at the waterside edge of the crest. The validated numerical model is then applied to investigate the effects of roughness and a berm on the flow velocity and layer thickness. The roughness is modelled by creating protrusions along the waterside slope. Numerical model outcomes indicate that existing empirical formulas underestimate wave overtopping quantities. Introducing a roughness factor to existing empirical formulas leads to better estimates of the flow characteristics. We found that the flow characteristics are more sensitive to the variation of the berm width than to the berm level. Model results demonstrate that existing formulas for predicting the flow characteristics, as derived based on smooth straight slopes, also work well for slopes with a berm. Rayleigh and Weibull distribution functions are derived to estimate the flow velocity and layer thickness with exceedance probabilities below 10%. In order to take oblique waves into account, the 2D numerical model is extended into the 3D model domain. This 3D OpenFOAM® model is validated using measured mean overtopping discharges. The influence of oblique waves on the mean overtopping discharge in combination with a berm is analysed. The numerical model computations confirm that the reductive influence factor of oblique waves is dependent on the berm width.

5.1. INTRODUCTION

W AVE overtopping is one of the main causes of dike breaching. Therefore, wave over-
topping has to be taken into account for the design and safety assessment of dikes.
Wave overtopping at dikes is usually characterized by the mean overtopping discharge and
by the overtopping flow parameters such as flow velocity and layer thickness related to
individual overtopping events. Previous failure analyses demonstrated that dike failures
at the landside slope are mainly caused by individual overtopping events, particularly by
the related overtopping flow velocities and layer thicknesses (Schüttrumpf, 2001; Van Gent,
2002a, 2002b; Schüttrumpf and Van Gent, 2003; Schüttrumpf and Oumeraci, 2005). Thus,
for flooding events initiated by dike breaching due to wave overtopping, overtopping flow
velocities and layer thicknesses are more important than average overtopping discharges
since the average overtopping discharge does not account for the effects of extreme individ-
ual overtopping events. However, the average overtopping discharge is still important as it
is often used to determine the crest height of coastal structures. Nowadays, risks of coastal
flood disasters are increasing as a result of climate change, sea level-rise and land subsi-
dence (Temmerman et al., 2013). Against this background, some existing dikes may require
reinforcement and adaption (Van Gent, 2019). Berms and roughness elements at the sea-
side slopes of dikes are widely applied to reduce wave overtopping quantities. In practice,
the direction of incoming waves in many circumstances is not perpendicular to the struc-
ture (Van Gent, 2021). Existing guidelines show that berms, roughness and oblique waves at
the waterside of the dike have significant effects on wave overtopping processes. Therefore,
the reductive effects of berms, roughness and oblique waves should be taken into account
when predicting the wave overtopping quantities at dikes.

Extreme conditions, i.e. flow velocity and layer thickness with a low probability of ex-
ceedance during a storm event, are usually used to characterize the wave overtopping flow.
The overtopping flow velocity and layer thickness at the waterside edge of a dike crest also
provide important boundary conditions for the estimation of wave loading parameters along
the crest and at the landward slope. For example, the analytical and numerical models
(Van Bergeijk et al. 2019, 2020) for predicting the flow parameters along the crest and land-
ward slope both require estimates of the flow velocity and layer thickness at the waterside
crest as the model input. Several predictors are available to estimate the extreme overtop-
ping flow characteristics at the seaward edge of a dike crest. Schüttrumpf (2001) and Van
Gent (2002a, 2002b) used theoretical and experimental investigations to develop empirical
formulas for extreme overtopping flow velocity and layer thickness exceeded by 2% of the
incoming waves. The results were later combined in Schüttrumpf and Van Gent (2003). Eu-
rOtop (2018) also provide empirical equations for estimating the 2%-values of flow velocity
and flow thickness. Formentin et al. (2019) performed numerical model computations and

proposed formulas based on those by Schüttrumpf (2001) and Van Gent (2002b) for esti-
mating flow characteristics at the waterside edge of the dike. Mares-Nasarre et al. (2019,
2021) extended the formulas given in Schüttrumpf and Van Gent (2003) for estimating the
overtopping flow velocity and layer thickness for applications on rubble mound breakwater
crests.

Most of the empirical equations for the extreme flow velocity and layer thickness at the
seaward edge of the dike crest are estimated using the following shape:

$$u_{2\%} = c_{v2\%} \left[\sqrt{g(R_{u2\%} - R_c)/\gamma_f{}^a} \right]^b \tag{5.1}$$

$$h_{2\%} = c_{h2\%} \left[g(R_{u2\%} - R_c)/\gamma_f{}^a \right]^b \tag{5.2}$$

where $c_{v2\%}$, $c_{h2\%}$ and b are empirical coefficients; R_c [m] is the freeboard which represents
the crest level relative to the still water level (SWL); $R_{u2\%}$ [m] is the wave run-up height ex-
ceeded by 2% of the incoming waves, which can be estimated using Eq. (5.A.1) proposed
by Van Gent (2001) or Eqs. (5.A.2) & (5.A.3) as given in EurOtop (2018). Herein, γ_f [-] is the
influence factor of slope roughness. The roughness influence factor γ_f is only included in
the Van Gent (2002b) equations corresponding to $a = 1$; γ_f is not included (which means a
is equal to 0) in other existing empirical formulas. Values of the empirical coefficients $c_{v2\%}$
and $c_{h2\%}$ provided in previous research are not consistent (see Table 5.1). The differences
could be explained by different dike configurations, experimental instruments and proce-
dures of determining the 2% values of flow parameters. Even though there is extensive liter-
ature on the overtopping flow characteristics at dikes, previous research mainly considered
the dike configurations with smooth straight waterside slopes. It still remains unclear if the
existing formulas are also applicable for predicting the flow characteristics over dikes that
have a rough waterside slope with or without a berm.

Table 5.1: Empirical coefficients for calculating the 2%-values of flow velocity and layer thickness at the waterside
edge of the dike crest, in which α [°] is the angle of the waterside slope of a dike.

	Waterside slope	$c_{v2\%}$	$c_{h2\%}$	a	b
Van Gent (2002b)	1/4	1.3	0.15	1	1
Schüttrumpf (2001)	1/6	1.37	0.33	0	1
EurOtop (2018)	1/3-1/5	1.4-1.5	0.2 for slopes of 1/3 and 1/4; 0.25 for a slope of 1/5; 0.3 for a slope of 1/6	0	1
Formentin et al. (2019)	1/4, 1/2	$0.12\cot(\alpha) + 0.41$	$0.085\cot(\alpha)$	0	1.35

Apart from the overtopping flow velocity and layer thickness, estimates of the mean
overtopping discharge still play an important role in the design and safety assessment of
coastal structures. TAW (2002) and EurOtop (2018) provide overtopping equations which
are widely used around the world, taking several influence factors (i.e. berms, roughness,

oblique waves, vertical wall) into account. A lot of research (e.g. De Waal and Van der Meer, 1992; Capel, 2015; Van der Werf and Van Gent, 2018; Schoonees et al., 2021) has been conducted on each of these influence factors. Chen, Van Gent, et al. (2020) and Chen, Marconi, et al. (2020) studied the effects of the roughness in combination with a berm on overtopping discharges and proposed empirical equations based on the analysis of experimental results. Van Gent (2020) studied the effects of roughness and a berm in combination with oblique waves by means of physical model tests. An empirical equation to account for effects of oblique waves was proposed, in which an assumption was made that the influence factor of oblique waves was dependent on the berm width. However, this assumption has not been verified for various berm widths. Verification of this assumption is important for accurately predicting the mean overtopping discharge when oblique waves and a berm are present at the same time.

Above all, the applicability of the existing formulas for estimating the overtopping flow characteristics at the waterside edge of the dike crest to dikes that have a bermed or rough waterside slope still remains unknown. Additionally, the dependency of the oblique wave influence on the berm width requires verification, which is important for accurately predicting the average overtopping discharge at dikes when the oblique waves and a berm play a role at the same time. Therefore, the objective of this study is the investigation of the effects of a berm, roughness and oblique waves on wave overtopping processes at dikes.

For that purpose, the 2DV OpenFOAM® model by Chen et al. (2021), which has been validated for predicting the overtopping discharge at dikes, is applied in this study. Physical model tests presented in Van Gent (2002b) were used to validate this 2DV OpenFOAM model for flow velocities and layer thicknesses at the waterside edge of the dike crest. Following that, the validated numerical model is applied to investigate the effects of roughness and a berm on the overtopping flow characteristics. A verification of the existing empirical formulas will be provided. Then, the 2DV numerical model is further extended into a 3D numerical model to take the oblique waves into account which is first validated using the experiments from Van Gent (2020). The berm width is varied with the wave direction fixed at 30° in the 3D numerical tank. Herein, the incident wave angle is defined as the angle between the direction of incident waves and the perpendicular to the long axis of the dike. The influence of oblique waves on the mean overtopping discharge for different berm widths is analysed to check the dependency of the influence factor of oblique waves on the berm width.

The paper is organized as follows. The methodology is described in Section 5.2. In Section 5.3, the validation of the 2D and 3D numerical models is presented. Section 5.4 is focused on the applications of the numerical models to study the effects of roughness, a berm and oblique waves on flow characteristics and overtopping discharges. In Section 5.5, the numerical model results are further discussed followed by the conclusions in Section 5.6.

5.2. METHODOLOGY

I N this section, the applied method for the 2D numerical modelling is first introduced, including a brief description of the 2D experiments that are used to validate the 2D numerical model. Then, the numerical model set-ups are introduced followed by the numerical experiments for studying the effects of roughness and a berm on overtopping flow parameters. Hereafter, the method for the 3D numerical model is introduced in a similar way.

5.2.1. 2D NUMERICAL MODELLING

5.2.1.1. DESCRIPTION OF 2D PHYSICAL TESTS

T HE small-scale physical model tests in Van Gent (2002b) were performed in the Scheldt Flume at Deltares in the Netherlands. The flume has a length of 55 m and a height of 1.2m. A foreshore with a slope of 1:100 over a length of about 30 m was applied as shown in Figure 5.1. A step with a 1:10 slope was constructed between the wave board and the start of the foreshore to obtain a sufficient depth at the wave board. The distance between the toe of the structure and the wave board was 40 m. The dike configuration with a slope of 1:4 is shown in 5.1. The slopes were smooth. The bottom elevation at the toe was 0.4 m and the crest elevation was 0.6 m above the bottom at the toe.

Three wave gauges were installed near the toe to measure the surface elevation. The incident waves at the toe were determined by repeating the tests with the foreshore but without the structure in position using the method by Mansard and Funke (1980). The position at the waterside edge of the crest was measured. The overtopping flow velocity was measured using a velocity meter which was a propeller with a diameter of approximately 10 mm. It was capable of measuring velocities in the range of 0.5 m/s to 4 m/s for waterlayers with a thickness larger than 2 mm. The devices for measuring the layer thickness were accurate with the error smaller than 0.2 mm between 1 and 100 mm.
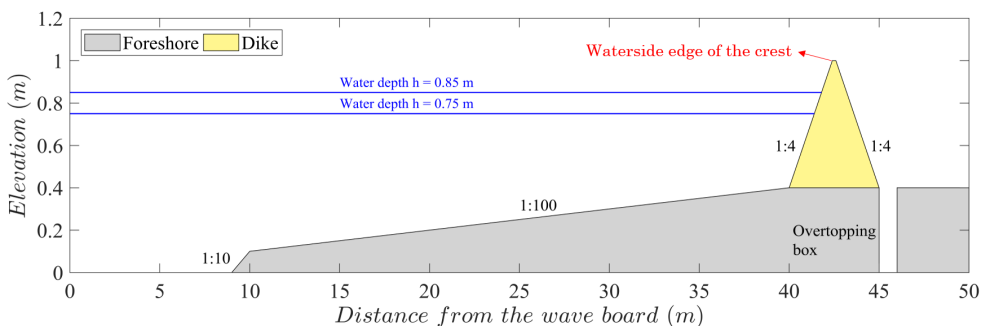
Figure 5.1: Set-up of the physical model (adapted from Van Gent, 2002b).

Ten tests were selected to validate the 2DV OpenFOAM® model as presented in Table 5.2. The water depth at the toe varied between 0.35 m and 0.45 m. The irregular waves in tests T101-T104 were generated based on the TMA-spectra (Bouws et al., 1985). Tests T201-T206 were performed with double-peaked wave energy spectra which were obtained by superposition of two single-peaked TMA spectra.

Table 5.2: Selected cases with wave conditions and measured results at the waterside edge of the dike crest from Van Gent (2002b).

Test	h_deep	h_toe	H_{m0} [m]	$T_{m-1,0}$ [s]	$h_{2\%}$ [m]	$u_{2\%}$ [m/s]
T101	0.75	0.35	0.149	2.16	0.0143	1.53
T102	0.75	0.35	0.142	1.84	0.0058	0.99
T103	0.8	0.4	0.153	2.14	0.0212	1.74
T104	0.85	0.45	0.147	1.78	0.0204	1.64
T201	0.8	0.4	0.152	2.03	0.016	1.55
T202	0.8	0.4	0.148	1.92	0.014	1.53
T203	0.8	0.4	0.139	1.84	0.0117	1.44
T204	0.8	0.4	0.13	1.86	0.0101	1.29
T205	0.8	0.4	0.142	1.69	0.0076	1.09
T206	0.8	0.4	0.138	1.62	0.0076	1.08

5.2.1.2. 2D NUMERICAL MODEL SET-UP

THE 2DV OpenFOAM® model by Chen et al. (2021) was applied in this study with the layout of the model adapted according to the physical tests in Van Gent (2002b). The length of the domain of the 2D physical tests was about 45 m. Simulating the entire domain in an OpenFOAM® model would be computationally expensive. In order to save computational time, a part of the domain between 0 m and 28 m from the wave board was simulated in the OceanWave3D which is a computationally cheaper solver. The rest of the domain was simulated in the OpenFOAM® model as shown in Figure 5.2. Since the flow characteristics are closely related to the wave run-up height according to previous literature, the wave run-up height was also simulated using the numerical model. In order to obtain wave run-up heights, a different dike configuration was modelled, in which the seaward slope was extended until the crest elevation reached 1.35 m such that no waves could overtop the crest. A constant pressure was applied at the atmosphere boundary which allowed the air to flow in and out and allowed the water to only flow out. The boundaries of the modelled impermeable structures and flume bottom were set as non-slip conditions. The turbulence was accounted for by applying a stabilized $k - \omega$ turbulence model developed by Larsen and Fuhrman (2018). Each simulation was made lasting about 600 s, resulting in 280-350 waves depending on the wave period. This time duration was adopted to compromise the computational effort and the accuracy of the model results (Chen et al., 2021).

(a) MESH
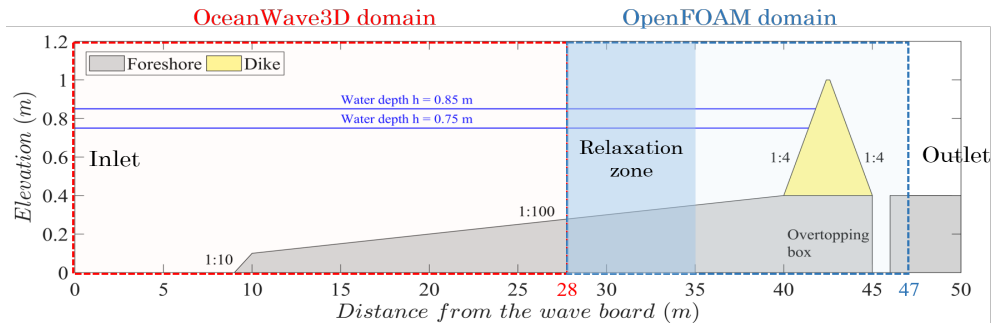
Figure 5.2: Numerical domains for OceanWave3D model and OpenFOAM® model.

The numerical mesh was created by using blockMesh which is a mesh-generation tool implemented in the OpenFOAM®. The base mesh from the inlet boundary to the toe of the dike was orthogonal and conformal with grid size of 0.026 m × 0.026 m. The grids near the free water surface were refined to 0.013 m × 0.013 m, which yielded about 12 cells in vertical to resolve per wave height and was sufficient for modelling the wave propagation as shown in Chen et al. (2021). Quadrilateral grids parallel with the slope surface were created in the area where the structure located as shown in Figure 5.3. The mesh near the structure was refined by applying ten layers of cells resulting in the grid size of 0.005 m in y direction.
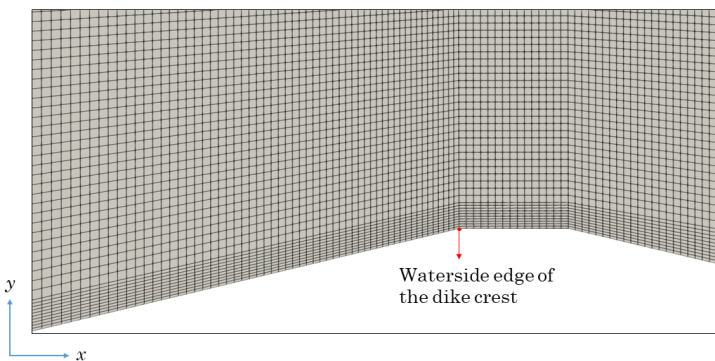
Figure 5.3: Mesh around the structure in the 2D OpenFOAM® model with the grid size Δy=0.005 m near the crest.

(b) WAVE GENERATION

The waves2Foam toolbox developed by Jacobsen et al. (2012) was applied to generate

and absorb waves using relaxation zones within the OpenFOAM® model. The relaxation technique is an extension to Mayer et al. (1998) and a relaxation function is applied inside the relaxation zone

$$\alpha_R(\chi_R) = 1 - \frac{\exp\left(\chi_R^{3.5}\right) - 1}{\exp\left(1\right) - 1} \quad \text{for} \quad \chi_R \in [0;1] \tag{5.3}$$

in the following way

$$\phi = \alpha_R \phi_{computed} + (1 - \alpha_R)\phi_{target} \tag{5.4}$$

where ϕ represents the velocity field **u** or the water volume fraction α. α_R is always 1 at the interface (χ_R) between the relaxation zone and the non-relaxed part of the numerical domain and the relaxation function is illustrated in Figure 5.4. Steering files of wave board motion based on the single-peaked or double-peaked TMA spectrum were first input to the OceanWave3D. The generated irregular waves in OceanWave3D provide the target solution ϕ_{target} for the inlet relaxation zone (also named coupling zone) of waves2Foam (for detailed information about the coupling method, reference is made to Paulsen et al., 2014). The length of the inlet relaxation zone was about one wave length as suggested by Jacobsen et al. (2012). Since the steering files were not the original files of the experiments, the generated time series of free surface elevation were not consistent with the experimental ones but the input wave properties including spectral significant wave height and spectral wave period were the same as those in the physical model tests.
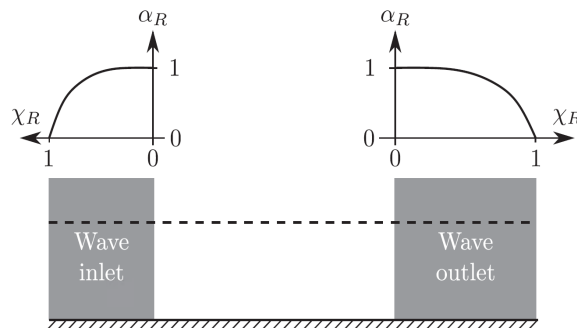
Figure 5.4: Variation of $\alpha_R(\phi_R)$ in relaxation zones (from Jacobsen et al., 2012).

(c) DATA POSTPROCESSING

The wave properties were determined using the results from three wave gauges defined near the position, where the toe of the structure was located. 30 probes were defined uniformly between 1.0 m and 1.05 m in vertical direction at the waterside edge of the crest in the OpenFOAM® model to detect the overtopping flow velocity and layer thickness. The water velocity at 5 mm above the crest (which corresponded to the centre of the velocity

propeller) was extracted to represent the overtopping flow velocity. The layer thickness was determined based on the fraction indicator α [-]. $\alpha = 1$ means that a grid cell was totally filled with water. For the first cell with $\alpha < 1$ from the bottom up, the water thickness in this cell was calculated as $\Delta y * \alpha$ where Δy was the grid size in the vertical direction. The total water-layer thickness could then be determined by adding the thickness of all cells with $\alpha = 1$ and the thickness $\Delta y * \alpha$ in the first cell with $\alpha < 1$. In order to obtain the wave run-up height, 100 probes were defined uniformly along the extended waterside slope between y = 0.55 m and y = 1.35 m. The wave run-up heights were determined using the similar approach as that for layer thickness.

The tests listed in Table 5.2 were simulated and the numerically modelled wave properties and flow characteristics were compared with the experimental results for model validation. The Nash-Sutcliff model efficiency coefficient (NSE) is used to assess the predictive power of the OpenFOAM® model as is defined as follows:

$$NSE = 1 - \frac{\sum_{i=1}^{N}(x_i - y_i)^2}{\sum_{i=1}^{N}(x_i - \overline{x})^2} \tag{5.5}$$

where N is the number of measurements; x_i is the measured value and $\overline{x}$ is the mean value of the measurement data; y_i is the predicted value. $NSE = 1$ represents a perfect match of predicted values to the measured results. $NSE = 0$ means that the predicted results are as accurate as the mean of the measured results. $NSE < 0$ indicates that the mean value of the measured data is a better predictor than the numerical model.

5.2.1.3. 2D NUMERICAL EXPERIMENTS

THE wave run-up height present in equations (5.1) & (5.2) is the fictitious 2% wave run-up height. If the fictitious 2% wave run-up level is higher than the crest level, the roughness of the seaward slope is only effective up to the crest level and not up to the fictitious wave run-up level. However, the roughness reduction factor included in the formula for wave run-up (Eq. (5.A.1) or (5.A.2)) represented the roughness of the seaward slope effective up to the fictitious wave run-up level, the roughness factor was therefore included in equations (5.1) & (5.2) suggested by Van Gent (2002b) to correct for the effect of roughness between fictitious wave run-up level and the crest level. In contrast, other research assumed that the roughness influence was completely accounted by the wave run-up height and therefore it is not necessary to include the roughness influence factor in equations (5.1) & (5.2). In order to check whether the roughness influence factor should or should not be included in equations (5.1) & (5.2), the roughness was modelled by creating protrusions at the seaward slope as shown in Figure 5.5. The protrusion height was 0.5 cm. For modelling the wave run-up height at the rough slope, the roughness was applied at the entire extended waterside slope which was often the case for determining the roughness factor in

the physical experiments. Different wave conditions were simulated. The roughness factor was determined by comparing the wave run-up heights at a rough slope with those at a smooth slope ($\gamma_f = R_{u2\%-rough}/R_{u2\%-smooth}$). Simulated cases can be found in Table 5.A.1.
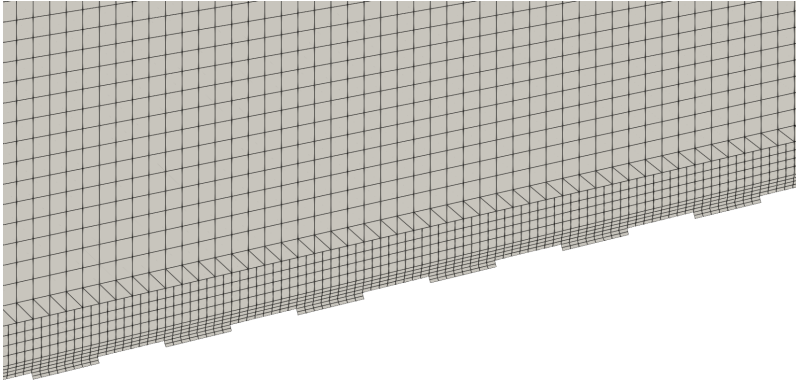
Figure 5.5: Refined mesh around protrusions along the waterside slope.

The effect of a berm on the flow velocity and layer thickness was investigated by changing the berm width and the berm level relative to SWL. The berm width was changed in the range of 0 to 0.5 m (0 m, 0.1 m, 0.2 m, 0.3 m, 0.4 m, 0.5 m) and the berm level was varied in the range of 0.7 0.9 m (0.7 m, 0.75 m, 0.8 m, 0.85 m, 0.9 m) by changing the berm position with the water level fixed at 0.8 m. The two wave conditions W103 based on single-peaked TMA spectrum and W201 based on double-peaked TMA spectrum used in the validation cases T103 and T201 were applied here. The berm influence factor was determined by comparing the wave run-up heights at smooth slope with a berm to the run-up heights at a smooth straight slope ($\gamma_b = R_{u2\%-berm}/R_{u2\%-straight}$). Table 5.A.2 presents the simulated cases for the investigation of the berm influence.

5.2.2. 3D NUMERICAL MODELLING

5.2.2.1. DESCRIPTION OF 3D PHYSICAL TESTS

THE experiments from Van Gent (2020), which were used to validate the 3D numerical model, were performed in the Delta Basin (50 m × 50 m) at Deltares. The layout of the model and tested cross-section are shown in Figure 5.6. The angle between the long axis of the structure and the wave generator was 30°. The berm width was fixed at 0.3 m through the experiments. The overtopping measurements with smooth slopes were used in the present paper.

The irregular waves were generated based on a JONSWAP wave spectrum with a peak enhancement factor of 3.3. Waves were measured at 4 m distance from the toe of the structure. The overtopping water was collected using a chute guiding into the overtopping box.

(a)

(b)
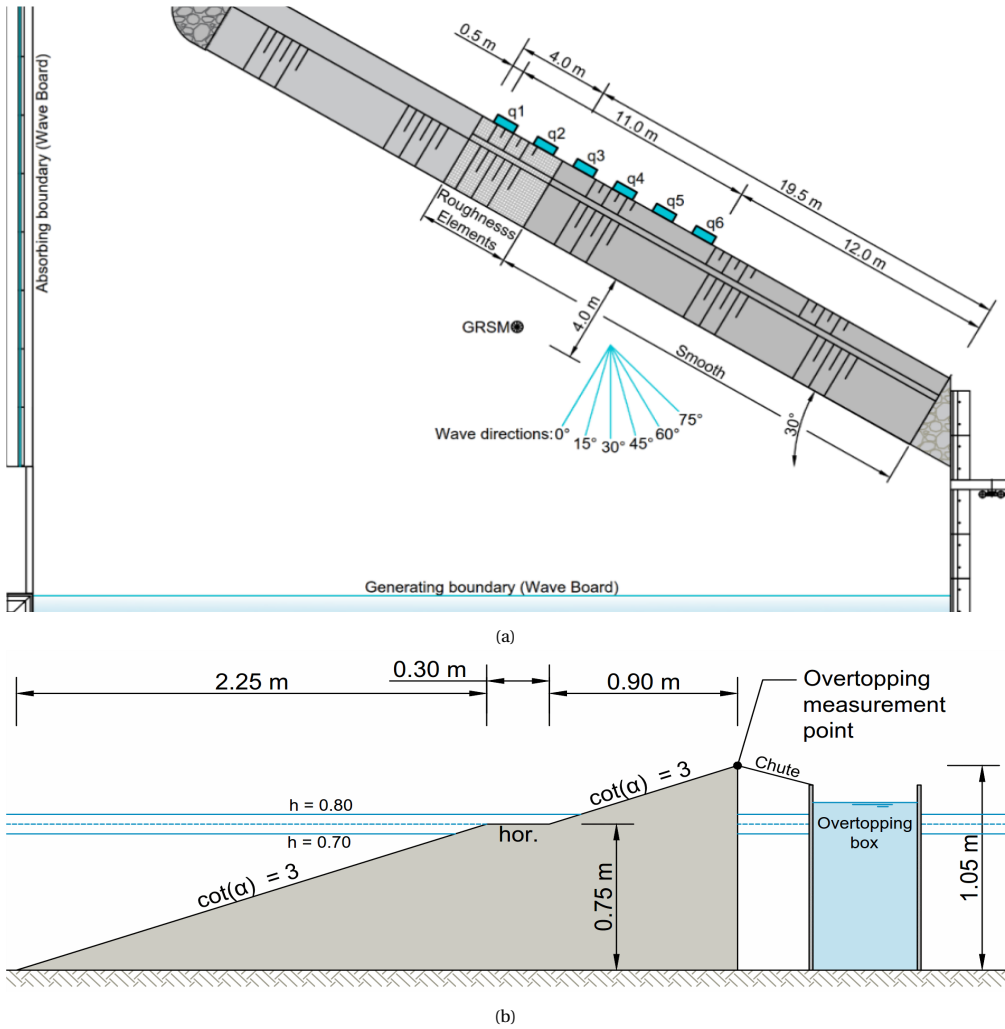
Figure 5.6: Three-dimensional physical model set-up with a) layout of the model in the wave basin and b) tested cross-section (from Van Gent, 2020).

One wave gauge was installed in the overtopping box to measure the water surface elevation, based on which the volume of the overtopping water can be determined. The overtopping discharges were measured at four positions (q3 to q6) for the smooth slope as shown in Figure 5.6a. The final average overtopping discharge were obtained using the mean values of the discharges at q3 to q6.

5.2.2.2. 3D NUMERICAL MODEL SET-UP

IN order to take the oblique waves into account, the 2DV OpenFOAM® model was extended with the second horizontal domain towards a 3D numerical model. Considering

we are more interested in the trend of the oblique wave influence changing with the varia-
tion of the berm width than the accuracy of the absolute values of the numerically modelled
average overtopping discharge, the 3D numerical model is used in a qualitative way. Addi-
tionally, the whole Delta Basin was too large to model in three dimension and therefore the
size of the wave basin was reduced in the numerical model to compromise between the
computational time and the model accuracy. The relaxation zone at the inlet was used to
generate waves. Two relaxation zones were added at the side walls to absorb reflected waves
from the structure. Figure 5.7a presents an empty numerical basin which was used to cali-
brate the wave conditions in order to ensure the simulated wave conditions are close to the
experimentally measured results. Figure 5.7b shows the layout of the three-dimensional
numerical model with the structure in position. The structure was rotated by an angle of
30° corresponding to $\beta = 30°$. The slopes were smooth.
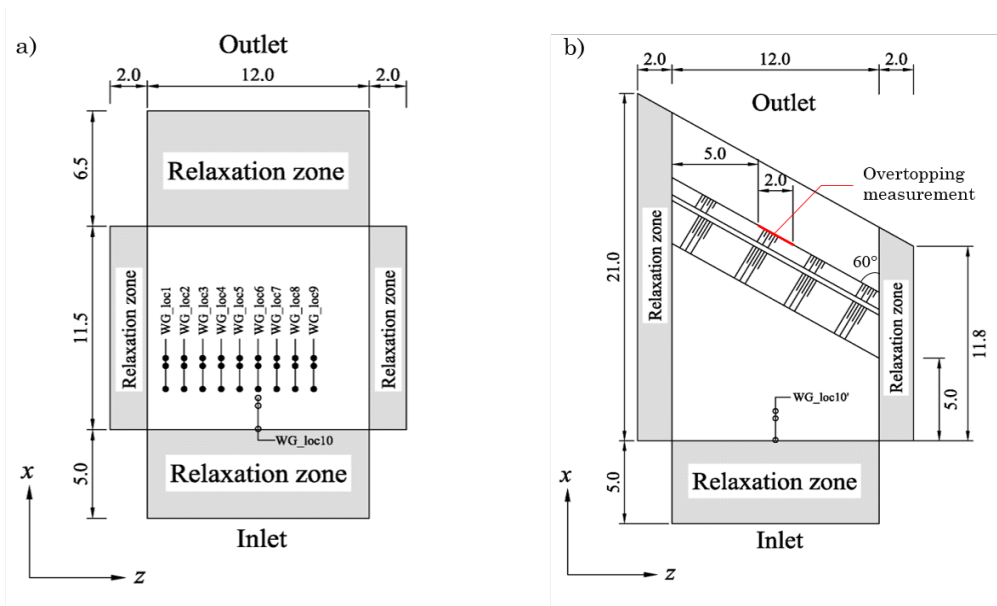
Figure 5.7: Layout of a) the numerical wave basin without the structure in position and b) the numerical wave
basin with the structure in position.

(a) MESH

For the empty 3D numerical wave basin, the mesh was orthogonal and conformal. It
presents 3 zones in x direction with variable cell size. On the first zone from x = 0 m to x =
9 m, the grid size Δx decreased linearly from 0.07 m to 0.046 m. On the second zone (x = 9
m to 16.5 m), the grid size Δx was constant and equalled to 0.046 m. On the third zone (x =
16.5 m to 23 m), the grid size Δx grew linearly to 0.06 m. The grid size Δy in y direction near
the initial free surface level was constant at 0.037m and gradually increased to 0.046 m near

the bottom and near the atmosphere boundary. In z direction, the grid size Δz was constant which was equal to 0.1m. The mesh of the numerical basin with a structure was somewhat different from the mesh of the empty numerical basin. The base mesh without the structure was not strictly orthogonal. Instead, it gradually became oblique from the inlet boundary to the structure such that the grids near the structure were parallel with the slope surface of the dikes. The grid size Δx was constant and equal to 0.046 m in the region where the dike was located. The grid size in y direction was the same as that of the empty numerical wave basin. In z direction, the grid size Δz in the range of z = 7 m to 9 m is constant and equalled to 0.05 m and increased linearly up to 0.12 m at the side walls. The reason for the finer mesh in the range of z = 7 m to 9 m is explained later in Section 5.2.2.2b. The structure was removed using snappyHexMesh with one level of refinement around the structure. The mesh generated in this way was more regular and more computationally efficient than the mesh created by removing the structure from the orthogonal and conformal base mesh. Overall, the 3D mesh was relatively coarse compared with the above 2D numerical mesh.

(b) WAVE GENERATION

The irregular waves were generated using the relaxation zone technique implemented in waves2Foam (as introduced in Section 5.2.1.2b) based on the JONSWAP spectrum using the first-order irregular wave theory that is a simple linear superposition of first order Stokes waves. The generated wave signal was not the same as that from the experiments since the original steering file from the experiments could not be used as the input of the wave generation, but had similar wave properties as the experiments. Two relaxation zones were applied at the side walls to absorb reflected waves from the structure. The width of each side wall relaxation zone was 2 m. The simulated wave condition was first calibrated in an empty numerical wave basin without the structure in position as shown in Figure 5.7a to ensure the numerically generated wave properties were close to the experimental ones. The calibrated wave condition was applied later to the numerical model with the structure in position. One set of wave gauges (WG_loc10 and WG_loc10') were defined at the start of the basin in both empty numerical model and the model including the structure, in order to check the efficiency of the side wall relaxation zone in absorbing the reflected waves from the structure by comparing the incident waves predicted by the models with and without the structure.

The 3D simulation period was set at 200 s, which took three weeks to compute paralleliz-ing the case into 22 processors (2.7 GHz). Therefore, considering the 3D numerical mod-elling was extremely time-consuming, only one 200 s numerical simulation ($H_{m0} = 0.199$ m, $T_{m-1,0} = 2.57$ s, $h = 0.8$ m and $\beta = 30°$) was performed for the validation of the 3D numerical model. Since the application of side wall relaxation zones would affect the incident waves along the z direction especially near the side relaxation zones, the waves along the z direc-

tion were not entirely uniform. The range (z = 7m to 9 m) in which the wave properties were nearly uniform was determined using nine sets of wave gauges (WG_loc1 to WG_loc9 in Figure 5.7a) defined along the z direction (See Table 5.3). A set of faces along the crest edge were selected in the range of z = 7 m to 9 m to extract the overtopping flux using the approach given by Jacobsen (2017) based on which the mean overtopping discharge could be obtained. Thus, the grid size along the width of the basin between z = 7 m and 9 m was finer than the remaining region. Then, the numerically modelled overtopping discharge can be compared with the physically measured discharge to validate the 3D numerical model.

Table 5.3: Modelled wave properties H_{m0} and $T_{m-1,0}$ in an empty 3D numerical basin (the experimental wave properties are: $H_{m0} = 0.199$ m, $T_{m-1,0} = 2.57$ s and $s_{m-1,0} = 0.019$).

	z [m]	H_{m0} [m]	$T_{m-1,0}$ [s]	$s_{m-1,0}$ [-]
WG_loc1	3	0.127	2.43	0.014
WG_loc2	4	0.158	2.46	0.017
WG_loc3	5	0.180	2.51	0.018
WG_loc4	6	0.192	2.57	0.019
WG_loc5	7	0.198	2.65	0.018
WG_loc6	8	0.199	2.67	0.018
WG_loc7	9	0.198	2.65	0.018
WG_loc8	10	0.192	2.57	0.019
WG_loc9	11	0.180	2.51	0.018

5.2.2.3. 3D NUMERICAL EXPERIMENTS

Van Gent (2020) proposed an empirical formula for estimating the influence of oblique waves on the mean overtopping discharge as follows:

$$\gamma_\beta = \cos^2\beta + 0.35(1 - \cos^2\beta)\left(1 + \frac{B}{H_{m0}}\right)^{-1} \tag{5.6}$$

Where γ_β [-] is the influence factor of oblique waves. β [°] is the angle between the direction of the waves and the perpendicular to the long axis of the dike. B [m] is the berm width. However, the berm width was fixed through the experiments, so the ratio B/H_{m0} was varied in the physical tests by varying the wave height but not by varying the berm width. Therefore, the dependency of the influence factor of oblique waves on B/H_{m0} in Eq. (5.6) is partly an assumption. In order to check the dependency of the oblique wave factor on berm width, 3D numerical experiments were performed on five berm widths (0 m, 0.1 m, 0.3 m, 0.4 m, 0.6 m). The TAW (2002) overtopping Eq. (5.7) for breaking waves was used to obtain the oblique wave factors:

$$\frac{q}{\sqrt{gH_{m0}^3}} = \frac{0.067}{\sqrt{\alpha}}\gamma_b\xi_{m-1,0}\exp\left(C_b\frac{R_c}{H_{m0}\xi_{m-1,0}\gamma_b\gamma_f\gamma_\beta}\right) \tag{5.7}$$

In order to determine the values of the oblique wave factor, the berm influence factor γ_b should be determined first. One reference case with a smooth straight waterside slope and with a perpendicular incident wave direction relative to the structure was simulated in the 2DV OpenFOAM® model, which saved a lot of computational time. Overtopping discharges over different berm widths with perpendicular incident waves direction were also simulated using the 2D numerical model. A mesh resolution similar to the 3D model at z = 6 m (Figure 5.7b) was applied in the 2D numerical model. In both 2D and 3D numerical models, the same wave condition with H_{m0} = 0.199 m, $T_{m-1,0}$ = 2.57 s and h = 0.8 m was imposed. The coefficient C_b in Eq. (5.7) was first calibrated using the 2D model results of the reference case. The berm influence factors can then be calculated by solving the Eq. (5.7) with γ_β = 1 and γ_f = 1 based on the 2D numerical data. With the coefficient C_b and berm factor γ_b known, the values of influence factor of the oblique waves can be determined using the 3D model results.

5.3. Model validation

5.3.1. Validation of the 2D numerical model

5.3.1.1. Wave characteristics

SINCE the original measured wave spectrum and wave height distribution were not available for comparison with numerically modelled results, the theoretical results (i.e. a Rayleigh wave height distribution and a TMA wave energy spectrum) were used here. Figure 5.8 shows a detailed comparison between the numerically modelled and theoretical TMA wave spectrum (Figure 5.8a) and wave height distribution (Figure 5.8b) for test T104. The numerical wave spectrum was determined near the toe of the dike. The input for the wave generation in the numerical model was based on the theoretical wave spectrum. Although the peak wave period is very close to the theoretical peak, the modelled incident wave spectrum shifts slightly to the left compared to the theoretical spectrum as shown in Figure 5.8a. This can be caused by nonlinear wave interactions that cause some energy transfer to lower frequencies in the relatively shallow water near the toe of the structure. Figure 5.8b shows that the modelled wave height distribution follows the Rayleigh distribution in general with some deviation for large wave heights. This deviation can arise from the wave breaking due to the small water depth at the toe of the structure. Overall, the modelled wave spectrum and wave height distribution match the theoretical results reasonably. Although not presented in this paper for sake of brevity, similar results were found for other cases. Numerically modelled and measured wave characteristics were compared as shown in Figure 5.9. The numerical data for the model validation are presented in Table 5.A.3. A good agreement can be observed from Figure 5.9a between the numerical and experimen-

tal significant wave height with a mean absolute percentage error ($MAPE$) of 1%. However, Figure 5.9b shows that the spectral wave period was overestimated by the numerical model with MAPE = 16%. Although the total amount of wave energy is computed accurately, it seems as if the wave energy is distributed too much to the lower frequencies. The overestimation of the wave period might be caused by some wave reflection in the OceanWave3D since the porous zone at the outlet could not completely absorb the low-frequency waves. The partly reflected waves might interact with the incident waves and then the generated waves which include incident waves and some reflected waves were input to waves2Foam, potentially leading to overestimation of the wave period. Another possible cause could be related to the wave breaking. The wave breaking could happen due to the relatively shallow water and it cannot be dealt with very well by the OceanWave3D, which could also lead to inaccuracies of the wave period. A third potential explanation of the difference may be related to the shorter computations (about 300 waves) compared to the experiments (1000 waves). Consequently, the overestimation of the wave period could cause an overestimation of the flow velocity and the layer thickness, which will be explained later in Section 5.3.1.2.

In order to find a better solution for the overestimation of wave period, sensitivity analysis of the wave period $T_{m-1,0}$ of one test T104 with the grid size and length of the inlet relaxation zone was performed as presented in Figure 5.10. It shows that refining the mesh or increasing the length of the inlet relaxation zone did not lead to significant improvement of the estimates of $T_{m-1,0}$. The overestimation of the wave period might be related to the wave breaking. The wave breaking could happen due to the presence of foreshore and it cannot be dealt with very well by the OceanWave3D as the wave breaking is taken into account by using a parameterization method, which led to inaccuracies of the wave period. The spectral wave period $T_{m-1,0}$ given by OceanWave3D was 1.93 s. This overestimation of the wave period in OceanWave3D further caused the overestimation ($T_{m-1,0}$ = 1.98 s) in the OpenFOAM model.

5.3.1.2. FLOW VELOCITY AND LAYER THICKNESS

THE calculated flow velocities and layer thicknesses using Van Gent (2002b) equations (5.1) & (5.2) were first compared with the experimental results. The wave run-up height presented in equations (5.1) & (5.2) was calculated using Eq. (5.A.1). The green squares in Figure 5.11 represent the comparison between the measured results from experiments and calculated ones in which the experimental wave height and wave period were applied. Since the empirical equations were derived based on the extensive experimental data presented in Van Gent (2002b) and the experimental data for the model validation were just a part of the entire dataset, slight deviations between the calculated and measured results can be seen in Figure 5.11. Nevertheless, there is an overall good agreement for both flow velocity and layer thickness. It is worth noting that applying the wave properties given by the nu-
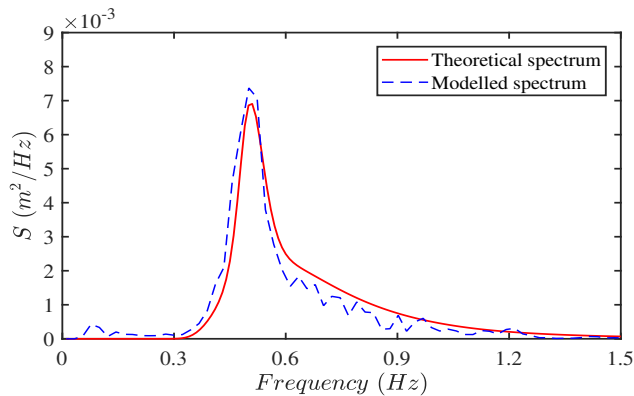
(a)
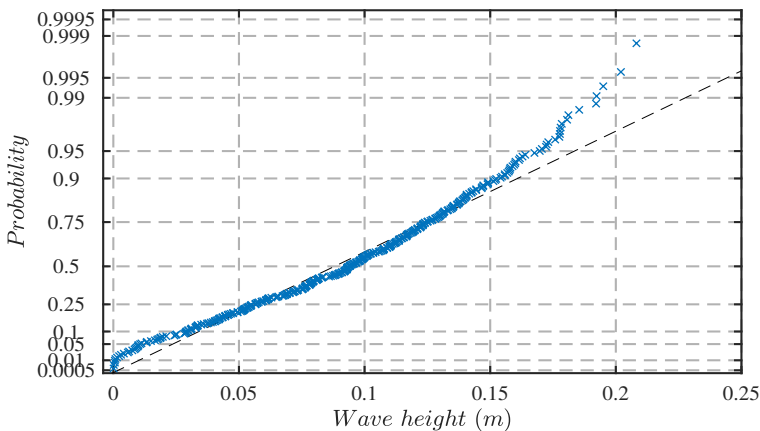
(b)

Figure 5.8: Comparison between the numerically modelled (at the toe of the dike) and theoretical (a) wave spectrum of incident waves and (b) wave height distribution for test T104 (input for the theoretical wave spectrum: H_{m0} = 0.15 m, T_p = 2.0 s, h = 0.85 m). The black dash line in (b) represents the Rayleigh distribution.

merical model to calculate the flow characteristics resulted in larger flow velocities and layer thickness (see yellow triangles). The numerical and experimental significant wave heights were almost the same as shown in Figure 5.9a while the numerical wave periods were obviously larger than the experimental ones, so Figure 5.11 indicates that larger wave periods led to larger values of flow characteristics.

Therefore, before directly comparing the numerically modelled flow velocities and layer thicknesses with the experimental ones, the modelled flow characteristics for each case were first modified by taking the overestimation of the spectral wave period into account

(a) Significant wave height H_{m0}

(b) Spectral wave period $T_{m-1,0}$
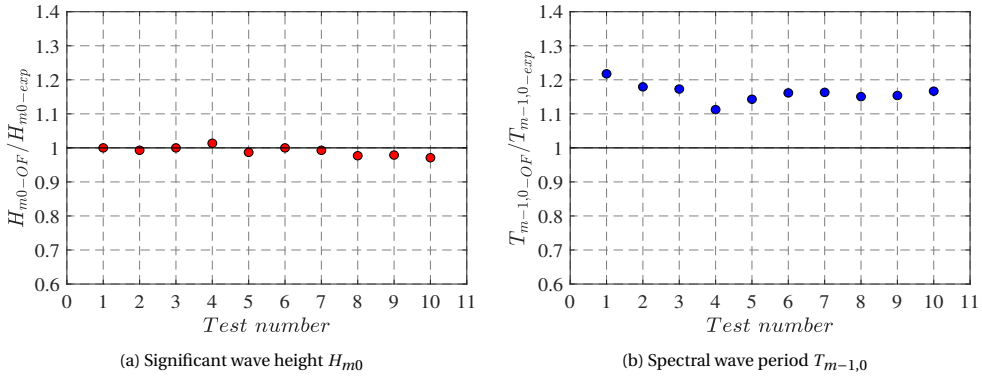
Figure 5.9: Comparison between modelled and measured wave characteristics with (a) Significant wave height H_{m0} and (b) Spectral wave period $T_{m-1,0}$.

(a)

(b)
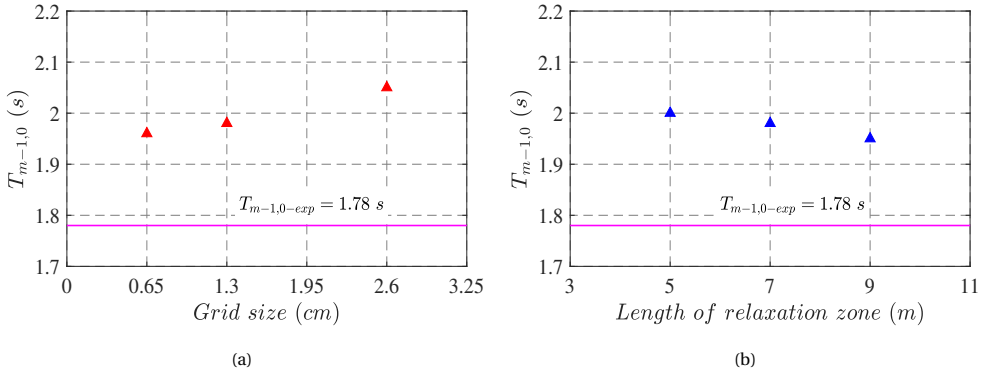
Figure 5.10: Sensitivity of the numerically modelled spectral wave period $T_{m-1,0}$ (a) with the grid size: 0.65 cm × 0.65 cm, 1.3 cm × 1.3 cm, 2.6 cm × 2.6 cm (from left to right) and (b) with the length of the inlet relaxation zone: 5 m, 7 m, 9 m (from left to right). The experimentally measured $T_{m-1,0-exp}$ is 1.78s.

using the following equation:

$$x_{2\%OFmod} = \frac{x_{2\%OF}}{x_{2\%cal-OF}/x_{2\%cal-exp}} \tag{5.8}$$

where $x_{2\%OFmod}$ [m/s] is the modified modelled flow velocity or layer thickness; $x_{2\%OF}$ is the original modelled flow parameter; $x_{2\%cal-OF}$ [m/s] is the calculated flow parameter using the empirical equations (Van Gent, 2002b) in which the numerically modelled wave characteristics were used; $x_{2\%cal-exp}$ is the calculated flow parameter using the empirical equations (Van Gent, 2002b) in which the experimental wave characteristics were applied.

The comparisons between the modified modelled and the measured flow characteristics are shown in Figure 5.12. The modified modelled flow velocity matches well with the measured results with a *NSE* of 0.75. In contrast, the *NSE* for the layer thickness is 0.03. The
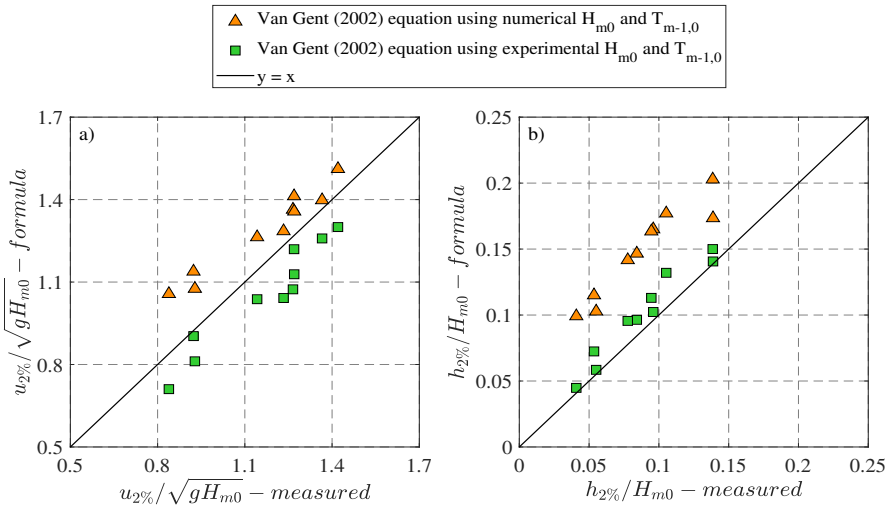
Figure 5.11: Comparison between measured and estimated flow parameters with a) flow velocity and b) layer thickness exceeded by 2% of the incident waves given by empirical equations using the experimental and numerical wave characteristics.

low value of NSE was mainly caused by the overestimation of the layer thickness given by the OpenFOAM® model. On average, the numerical model overestimated the layer thickness with a factor of 1.3 and dividing the modified modelled results of the layer thickness by 1.3 can increase the NSE from 0.03 to 0.83, illustrating that the trend in the layer thickness is well captured by the numerical model. This overestimation can be related to different time series of waves used in the OpenFOAM model and the experiments. Another possible cause might be the quality of free surface capture. The interface between water and air was not very sharp and could smear out over two layers of grid cells in the numerical model, which can further result in an overestimation of the layer thickness. Similar overestimation of layer thickness by OpenFOAM® models can also be found in Van Bergeijk et al. (2020). Refining the mesh near the waterside slope and crest can to some extent reduce the overestimation. Nevertheless, a fine mesh would significantly increase the computational time especially for the slope covered by protruding blocks. Therefore, the grid size of 0.005 m in vertical direction is adopted to comprise between the computational efficiency and the model accuracy of layer thicknesses. Despite of a low value of NSE (0.03), the overestimation with a factor of 1.3 is considered as being acceptable given the spreading that is normally observed when dealing with measurements of wave overtopping parameters (see for instance Figure 9 in Mares-Nasarre et al., 2019).

Considering the wave run-up height is a key parameter for estimating the flow velocity and layer thickness (see Eqs. (5.1) & (5.2)), the modelled wave run-up heights were compared to the empirical equations (5.A.1 and 5.A.2) as the wave run-up height was not mea-

(a) Flow velocity

(b) Layer thickness
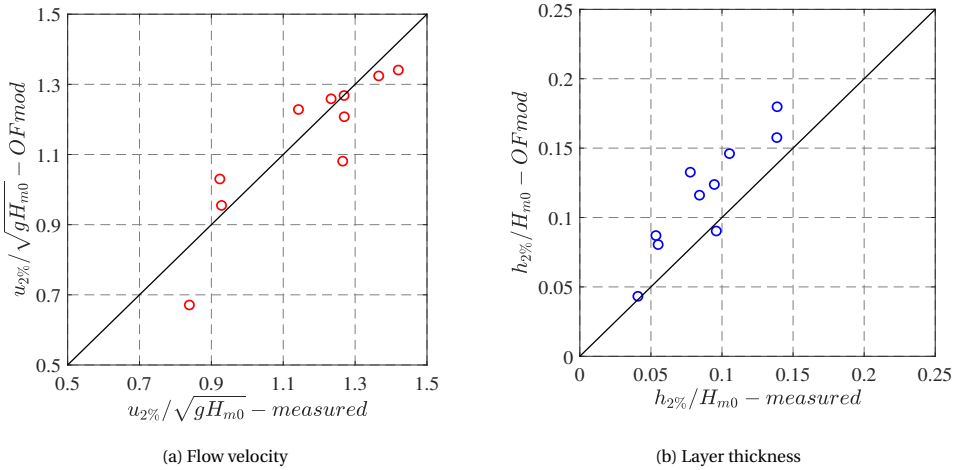
Figure 5.12: Comparison between the measured flow parameters and the modified flow parameters given by OpenFOAM® model taking the overestimation of the wave period into account.

sured in the experiments from Van Gent (2001). Figure 5.13 shows that the model results match well with the Van Gent (2001) run-up equation (5.A.1) with a *NSE* of 0.56 while the EurOtop (2018) equations (5.A.2 & 5.A.3) overestimate the wave run-up height with a factor of 1.2 and with a NSE of -3.9. The difference between Van Gent (2001) and EurOtop (2018) run-up equations mainly lies around the transition between breaking and non-breaking wave conditions; most of the data in this study are close to this transition between breaking and non-breaking waves. A smooth transition at a certain value of the Iribarren parameter $\xi_{m-1,0}$ was proposed by Van Gent (2001) considering the derivative with respect to $\xi_{m-1,0}$ of Eq. (5.A.1) should be continuous in a physical sense. EurOtop (2018) proposed an abrupt transition near the transition between breaking and non-breaking wave conditions based on the analysis of extensive datasets. Figure 5.13 indicates that the model results match better with Van Gent (2001) run-up equation (5.A.1) than with the EurOtop (2018) equations (5.A.2, 5.A.3).

Since this study focuses on the predictions of flow parameters and the influence of berms and roughness on these flow parameters (instead of on the accuracy of the incident wave characteristics), the numerical model is regarded as being capable of predicting the flow velocities and layer thickness sufficiently accurate.

5.3.2. VALIDATION OF THE 3D NUMERICAL MODEL

5.3.2.1. WAVE CHARACTERISTICS

THE incident waves at the start (WG_loc10 and WG_loc10') of the 3D numerical wave basin with and without the structure were compared as shown in Figure 5.14. A good
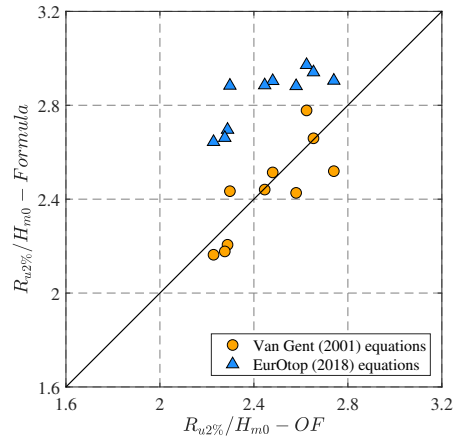
Figure 5.13: Modelled and calculated wave run-up heights using Van Gent (2001) run-up equation (5.A.1) and EurOtop (2018) run-up equations (5.A.2, 5.A.3).

agreement on both the time series of incident waves and the wave energy spectrum between the model with structure and the model without structure can be seen in Figure 5.14, which indicates that there was little wave reflection at the side walls interfering the incident waves. Table 5.4 presents the wave properties measured by the wave gauges near the inlet in the numerical basins with and without the structure. The incident wave height at the inlet of the basin is slightly larger compared with the wave height in an empty wave basin. Nevertheless, the difference is small, which is acceptable.

Table 5.4: Wave properties near the inlet in the numerical wave basins with and without structure.

	H_{m0} [m]	$T_{m-1,0}$ [s]	$s_{m-1,0}$ [-]
With structure	0.19	2.65	0.017
Without structure	0.187	2.65	0.017

5.3.2.2. MEAN OVERTOPPING DISCHARGE

The overtopping flux was extracted in the range of z = 7 m to 9 m where the waves were nearly uniform along the z axis. The measured and modelled wave conditions and overtopping discharges are given in Table 5.5. The modelled average overtopping discharge is 1.9 l/s/m which is about three times of the measured overtopping rate (q_{exp}=0.65 l/s/m). One of the causes for this overestimation might be the short simulation time (200 s) which could lead to more uncertainties than a long simulation time (e.g. 1000 waves) of the estimation of overtopping rates. However, the focus of this study is to verify the dependency on the berm width. Therefore, the trend of the overtopping discharge due to oblique waves changing with the berm width is more of interest in this study than the absolute values of the

(a) Time series of incident free surface elevation

(b) Wave energy spectrum of incident waves
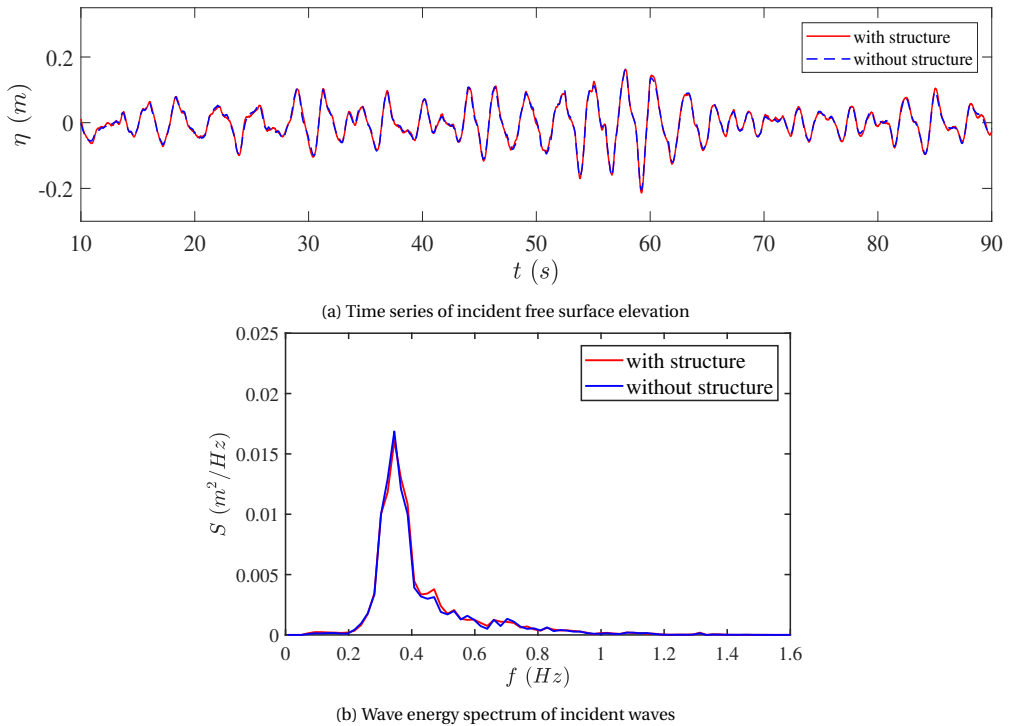
Figure 5.14: Comparison of incident waves between the numerical wave basins with and without the structure.

overtopping discharge themselves. Besides, EurOtop (2018) stated that empirical equations estimated overtopping discharges at best within a factor of 1 to 3 of the actual overtopping discharges. Therefore, this overestimation with a factor of 3 is regarded as being reasonable (see for instance Suzuki et al., 2017). The trend of the overtopping discharge due to oblique waves changing with the berm width is more of interest in this study than the absolute values of the overtopping discharge themselves. This means that the 3D numerical model is used in a qualitative way. Hence, although only one test condition was simulated for the 3D model validation, this model validation is regarded as being acceptable in this study. The wave conditions and numerical model settings for this validation test are later enforced for other 3D simulations in which only the berm width is different to find the trend of the influence factor of oblique waves varying with the berm width.

Table 5.5: Measured and modelled wave characteristics and average overtopping rates.

	Experiment	OpenFOAM®
H_{m0} [m]	0.199	0.198
$T_{m-1,0}$ [s]	2.57	2.66
$s_{m-1,0}$ [-]	0.019	0.018
q [l/s/m]	0.65	1.9

5.4. EFFECTS OF ROUGHNESS, A BERM AND OBLIQUE WAVES ON OVERTOPPING PARAMETERS

THE validated OpenFOAM® models were then applied to investigate the effects of roughness, berm and oblique waves on flow parameters and overtopping discharges. In this section, the results of both 2D and 3D numerical experiments were analysed.

5.4.1. THE INFLUENCE OF ROUGHNESS ON FLOW PARAMETERS

ACCORDING to the literature review, it still remains unclear whether to include the roughness reduction factor in Eqs. (5.1) & (5.2). To figure this out, the roughness was modelled in the 2DV numerical model by creating protrusions along the waterside slope. The modelled flow characteristics were compared with the calculated ones using empirical equations with and without the roughness influence factor. The values of roughness factor were obtained by comparing the wave run-up height at the rough slopes with that at the smooth slope. Since the 2DV numerical model was validated based on the experimental results in Van Gent (2002b), only the Van Gent (2002b) equations for flow characteristics including and excluding the roughness factor were considered here.

Figure 5.15 shows the comparison between modelled and calculated flow characteristics using the Van Gent (2002b) equations with and without the roughness influence factor. For calculations of flow velocities and layer thicknesses, the modelled wave run-up heights at the rough slope were used instead of using the empirical equation (5.A.1) for the wave run-up height. It can be observed in Figure 5.15 that excluding the roughness factor in Eqs. (5.1) & (5.2) leads to underestimation of flow characteristics. Including the roughness factor leads to better estimates of flow velocities improving the NSE from -0.5 to 0.35. However, including the roughness factor still underestimates the layer thicknesses with a factor of 0.84 of the numerically modelled layer thickness. Nevertheless, it can reduce the underestimation to some extent, considering that excluding the roughness factor results in a factor of 0.77. This underestimation of the layer thickness could partly be caused by the slight overestimation of layer thicknesses given by the OpenFOAM® model as shown in Figure 2.10b. For the smooth straight slope, the numerically modelled layer thicknesses are about 1.16 times of the estimated ones using the empirical equations. Dividing the OpenFOAM® modelled layer thicknesses by 1.16 and including the roughness factor in Eq. (5.2) finally lead to estimates of layer thicknesses with a factor of 0.97 of the numerically modelled ones and a NSE of 0.85. These results indicate that it is indeed better to include the roughness factor in Eqs. (5.1) & (5.2) as proposed. The roughness factor in this study only varied in the narrow range of 0.88 to 0.95. Therefore, the difference between including and excluding the roughness factor in Eqs. (5.1) & (5.2) for smaller values of the roughness factor can be

larger. Empirical equations similar to Eqs. (5.1) & (5.2) but excluding the roughness factor could lead to estimates of flow characteristics that are too low and thus unsafe.
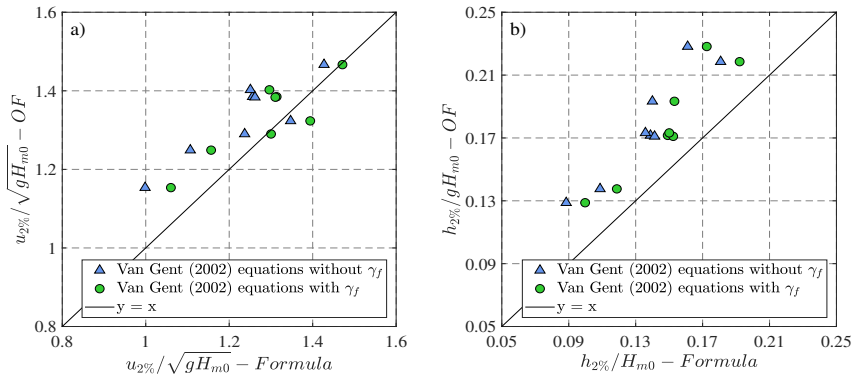
Figure 5.15: Comparison between numerically modelled a) flow velocities as well as b) layer thickness and the calculated ones over the rough slope using the Van Gent (2002b) equations (5.1) & (5.2) with and without including the roughness factor γ_f.

5.4.2. THE INFLUENCE OF A BERM ON FLOW PARAMETERS AT THE WATERSIDE EDGE OF THE CREST

I N order to study the berm influence, the berm width was varied in the range of 0 m to 0.5 m and berm level relative to SWL was changed in the range of -0.1 m to 0.1 m by changing the berm position. Figure 5.16 shows the influence of berm width and berm level on the flow velocity and layer thickness. It can be seen that the flow parameters are sensitive to the variations in the berm width. The flow velocity and the layer thickness could be reduced by nearly 30% and 40% respectively due to the application of a berm. In contrast, the berm level did not have a significant reductive effect on the flow characteristics.

The modelled flow characteristics at smooth slopes with a berm were first compared to the Van Gent (2002b) empirical formulas (Eqs. (5.1) & (5.2)). In order to calculate the flow parameters using Eqs. (5.1) & (5.2), the wave run-up height needs to be known. It is worth mentioning that the flow parameters on the horizontal axis in Figure 5.17 were calculated using the numerically modelled wave run-up heights instead of using the empirical run-up equation (5.A.1). Figure 5.17 shows that the calculated flow velocities match well with the OpenFOAM® model results with a NSE of 0.79. The calculated values of the layer thickness are generally smaller than the modelled results leading to $NSE = 0.24$. This is caused by the slight overestimation of the layer thickness given by the OpenFOAM® model as presented in Figure 5.12b. Overall, the numerical results demonstrate that the relationships between the flow parameters and the wave run-up height as given in Van Gent (2002b) equations ((5.1)
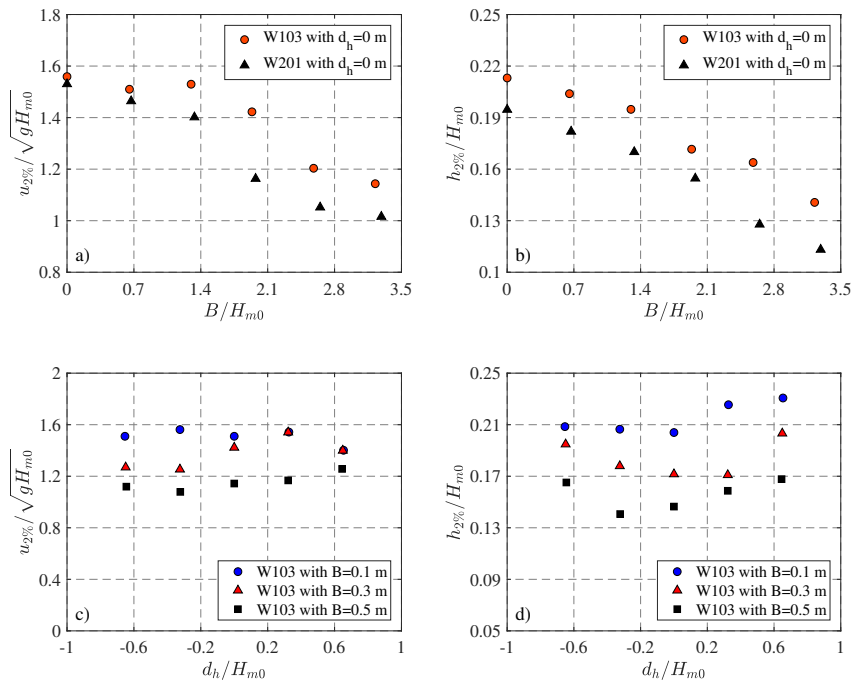
Figure 5.16: The influence of berm width (B) and berm level (d_h) on the extreme overtopping flow velocity $u_{2\%}$ and layer thickness $h_{2\%}$ with W103 representing the wave condition based on single-peaked TMA spectrum: H_{m0} = 0.152 m, $T_{m-1,0}$ = 2.51 s, h = 0.8 m and W201 representing the wave condition based on double-peaked TMA spectrum: H_{m0} = 0.149 m, $T_{m-1,0}$ = 2.32 s, h = 0.8 m.

& (5.2)) are also valid for smooth slopes with a berm, which implies that the berm influence is accounted for by the wave run-up height. Thus, the investigation of the berm effect on flow characteristics comes down to the investigation of the influence of a berm on the wave run-up height.

Figure 5.18a shows the comparison between the modelled run-up heights at straight slope as well as slopes with a berm and the calculated ones using Van Gent (2001) equation (5.A.1) and EurOtop (2018) equations (5.A.2) & (5.A.3). The berm factor γ_b, which represents the reductive influence of a berm on overtopping discharge or run-up height, in EurOtop (2018) equations (5.A.2) & (5.A.3) was determined using the empirical equation (5.A.4). In the Van Gent (2001) equation, the berm effect was taken into account by adopting a characteristic slope to be used in the breaker parameter. Thus, no additional reduction factor for berms is required. The characteristic slope was defined as $\tan\phi = c_{BERM} H_{m0}/L$ where c_{BERM} was set at 2. Figure 5.18a shows that the calculated wave run-up heights using Van Gent (2001) equation (5.A.1) match very well with the modelled values while EurOtop (2018)
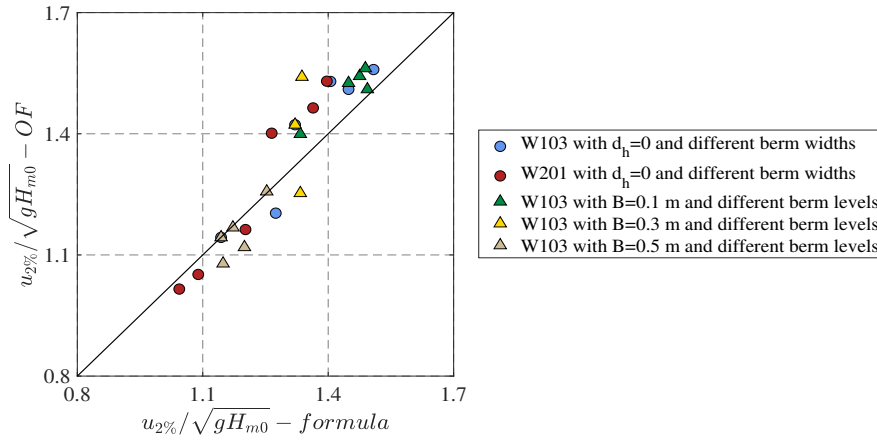
(a) Flow velocity
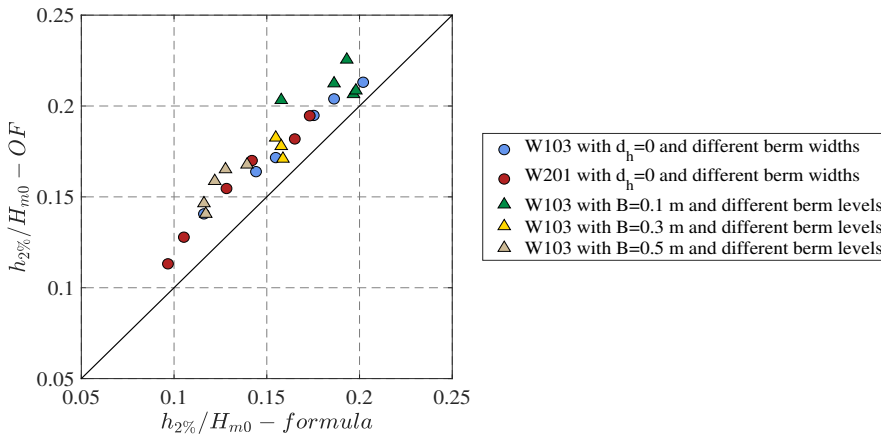
(b) Layer thickness

Figure 5.17: Comparison between the modelled flow parameters and the calculated values using modelled wave run-up heights by empirical equations with the berm width varying in the range of 0 m to 0.5 m and the berm level in the range of -0.1~0.1 m. W103 represents the wave condition based on single-peaked TMA spectrum: $H_{m0} = 0.152$ m, $T_{m-1,0} = 2.51$ s, $h = 0.8$ m and W201 represents the wave condition based on double-peaked TMA spectrum: $H_{m0} = 0.149$ m, $T_{m-1,0} = 2.32$ s, $h = 0.8$ m.

equations (5.A.2), (5.A.3) & (5.A.4) overestimate the wave run-up heights. Solid marks in Figure 5.18a denote the data of cases for model validation. Figure 5.18b shows the comparison between the berm factors obtained based on the OpenFOAM® model results and those determined using empirical equations. EurOtop (2018) berm equation (5.A.4) underestimate the berm factors, which means that the equations overestimate the reductive influence of a berm on wave run-up heights. Since no berm factor was used in Van Gent (2001) run-up equation (5.A.1), the berm effects were determined by comparing the calcu-

lated run-up heights taking the berm into account to those without considering the berm
using the equation (5.A.4). There is a good agreement between the calculated berm factors
applying Van Gent (2001) approach and the numerically modelled ones with NSE = 0.94.
Therefore, it could be concluded based on the model results that the existing empirical for-
mulas proposed by Van Gent (2001, 2002b) for flow characteristics and run-up heights are
also applicable for slopes with a berm.
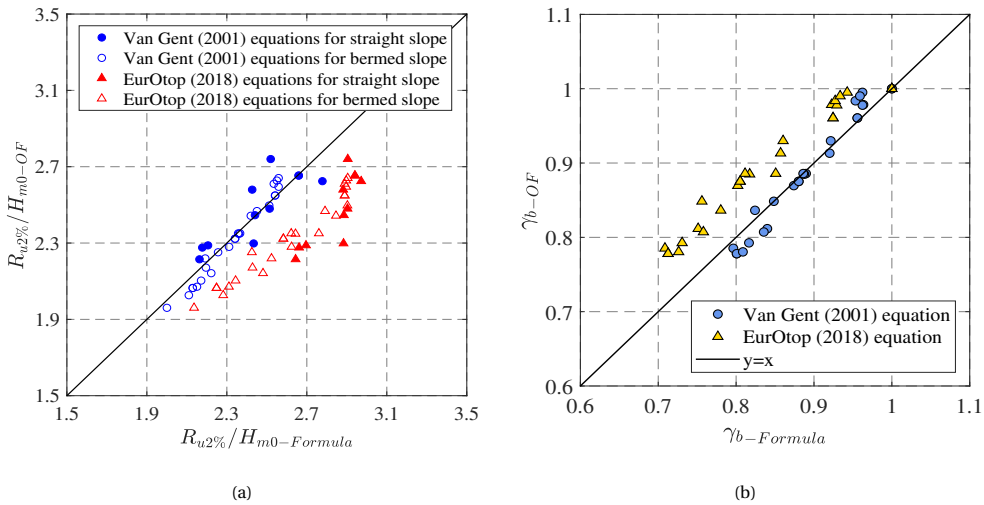
Figure 5.18: Comparisons between a) modelled and calculated wave run-up heights over straight and bermed
slopes using Van Gent (2001) equations and EurOtop (2018) equations; b) modelled and calculated berm influence
factors using empirical equations proposed by Van Gent (2001) and EurOtop (2018).

5.4.3. THE INFLUENCE OF OBLIQUE WAVES ON THE OVERTOPPING DISCHARGE

THE above 2DV numerical model was extended into the 3D model domain, consider-
ing the oblique waves in combination with the berm influence. The berm influence
was determined by comparing the overtopping discharge at slopes with a berm to that
at a straight slope using a 2DV numerical model. Based on that, the oblique wave fac-
tors could be determined using the method described in Section 5.2.2.2. Results of the 3D
OpenFOAM® models are given in Table 5.6. Figure 5.19 shows that the influence factor of
oblique waves overall decreases as the relative berm width increases, which indicates the
influence of oblique waves on the overtopping discharge is dependent on the berm width.
The blue dash line in Figure 5.19 represents the fitting curve of the numerical data. Even
though the absolute values of the oblique wave factor based on the OpenFOAM® model
results somewhat deviate from the empirical formula (Eq. (5.6)) with a vertical shift of
0.023, the trend is in accordance with the trend of the relationship between the influence of

oblique waves and berm width as indicated by Eq. (5.6). The 3D numerical model results verified the dependency of the effect of oblique waves on the berm width.

Table 5.6: Numerical results of 3D OpenFOAM® model for different berm widths with the wave direction relative to the structure $\beta = 30°$.

case	B [m]	H_{m0} [m]	$T_{m-1,0}$ [s]	$s_{m-1,0}$ [-]	q [l/s/m]
B00	0	0.198	2.66	0.018	3.1
B10	0.1	0.198	2.66	0.018	2.5
B30	0.3	0.198	2.66	0.018	1.9
B40	0.4	0.198	2.66	0.018	1.6
B60	0.6	0.198	2.66	0.018	1.2
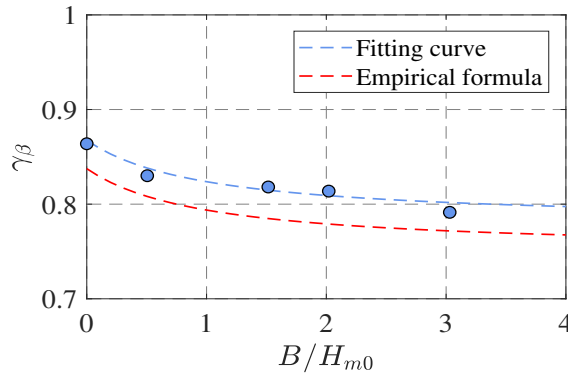
Figure 5.19: Relationship between the influence factor of oblique waves with $\beta = 30°$ and the relative berm width with the red dash line denoting the empirical formula (Eq. (5.6)) proposed by Van Gent (2020).

5.5. DISCUSSION

5.5.1. DISTRIBUTION FUNCTIONS FOR FLOW PARAMETERS

EXTREME overtopping events are important to assess the safety of dikes. The distributions of extreme overtopping parameters also provide valuable information, apart from 2%-values of the flow parameters for predicting the cover erosion, which are discussed in this section. Hughes et al. (2012) suggested Rayleigh distributions for the upper 10% of the values of flow velocity and flow thickness. The 10% of the values was used since the extreme values were more relevant to the stability of coastal structures and the entire rank-ordered values led to more scatter. However, Mares-Nasarre et al. (2019) proposed an exponential distribution function for values of the flow layer thickness associated with exceedance probabilities under 2% and a Rayleigh distribution function for flow velocities with exceedance probabilities under 2%. Hence, we also analysed the distribution func-

tions of the extreme flow parameters with exceedance probabilities below 10% based on the 2D numerical model results as suggested by Hughes et al. (2012). Flow parameters from each numerical test were rank-ordered and the Weibull distribution suggested by Hughes et al. (2012) were fit to the upper 10% of the values to determine the distribution functions for the overtopping flow velocity and layer thickness.

The Weibull distribution functions for flow velocity and layer thickness are given as below:

$$F\left(\frac{u}{u_{2\%}}\right) = 1 - \exp\left[-\left(a_1 \frac{u}{u_{2\%}}\right)^{b_1}\right] \tag{5.9}$$

$$F\left(\frac{h}{h_{2\%}}\right) = 1 - \exp\left[-\left(a_2 \frac{h}{h_{2\%}}\right)^{b_2}\right] \tag{5.10}$$

in which F represents the probability that an incident wave will lead to a flow parameter smaller than a specified flow parameter. u and h are the flow velocity and layer thickness respectively, with an exceedance probability under 10%; $u_{2\%}$ and $h_{2\%}$ were used to make u and h dimensionless as recommended by Mares-Nasarre et al. (2019); a_1 and a_2 are empirical coefficients to be calibrated; b_1 and b_2 are shape factors to be calibrated. The shape factor equal to 1 corresponds to an exponential distribution and equal to 2 corresponds to a Rayleigh distribution. The peak values of flow velocity and layer thickness were ranked in descending order for each numerical test, based on which the upper 10% (about 300 × 10%) values were selected. The a_1 and b_1 were calibrated based on the selected values for each numerical test applying the least square method. Eqs. (5.9) & (5.10) are applied on the number of incident waves in a storm. Thus, the exceedance probability corresponding to each value of the flow velocity was calculated as k/N where k is the rank of the flow velocity value and N is the number of incoming waves. 41 cases in total were simulated using the 2D numerical model, which yielded 41 sets of a_1 and b_1. The optimal values of a_1 and b_1 were determined as the median of the 41 values. The same method was applied to layer thickness and the optimal values of a_2 and b_2 can also be obtained.

Figure 5.20 shows the fitted cumulative distribution functions with $R^2 = 0.97$ for the flow velocity and $R^2 = 0.96$ for the layer thickness. The calibrated distribution functions for flow velocity and layer thickness with exceedance probabilities under 10% are presented as:

$$F\left(\frac{u}{u_{2\%}}\right) = 1 - \exp\left[-\left(2\frac{u}{u_{2\%}}\right)^{2}\right] \tag{5.11}$$

$$F\left(\frac{h}{h_{2\%}}\right) = 1 - \exp\left[-\left(2.6\frac{h}{h_{2\%}}\right)^{1.5}\right] \tag{5.12}$$

The distribution of the flow velocity with $b_1 = 2$ implies a Rayleigh distribution function, which is in accordance with previous research (Hughes et al., 2012; Mares-Nasarre et al.,

2019). However, the distribution of layer thickness with $b_2 = 1.5$ does not correspond to a Rayleigh distribution suggested by Hughes et al. (2012) nor an exponential distribution proposed by Mares-Nasarre et al. (2019). Only seven cases were considered in Hughes et al. (2012), which could lead to many uncertainties about the results. Mares-Nasarre et al. (2019) suggested that if the flow velocity followed a Rayleigh distribution function, the layer thickness would be expected to follow an exponential distribution considering the 1/2-power relationship between the flow velocity and layer thickness exceeded by 2% of the incoming waves as shown in Eq. (5.13). However, the empirical coefficient C in Eq. (5.13) can be different for a different exceedance percentage than 2%. Thus, the layer thickness does not necessarily follow an exponential distribution function. Figure 11 in Mares-Nasarre et al. (2019) also indicates that the layer thickness did not follow the exponential distribution function perfectly. The difference between the distribution functions of the layer thickness in this study and in Mares-Nasarre et al. (2019) could also be caused by different exceedance probabilities (10% in this study and 2% in Mares-Nasarre et al., 2019) being used for deriving the cumulative distribution functions.

$$u_{2\%} = C\sqrt{gh_{2\%}} \qquad (5.13)$$

5.5.2. APPLICATION AND LIMITATION OF THE 2D AND 3D NUMERICAL MODELS

THE 2DV OpenFOAM® model showed a reasonable agreement with the measured flow velocities and layer thickness. The validated 2D numerical model was then applied to investigate the influence of roughness and a berm on flow velocity and layer thickness. The roughness was modelled by creating protrusions along the waterside slope. Model results indicate that the roughness reduction factor should be included in empirical equations (5.1) & (5.2) even though the wave run-up height already takes the roughness influence into account. The existing formulas excluding the roughness factor could underestimate the flow characteristics over rough slopes. Since the flow velocity is a key input parameter in some erosion models (e.g., Dean et al., 2010), underestimation of the flow velocity might lead to underestimation of the cover erosion. This would be dangerous for reliability evaluation of coastal structures. Only one type of roughness element was modelled since this study aims to determine whether the roughness reduction factor should, or should not, be included in Eqs. (5.1) & (5.2). It is recommended to investigate the effects of different types of roughness elements with a wider range of roughness factor on the flow characteristics through physical or numerical experiments.

For the berm influence on the flow characteristics, model results demonstrate that the
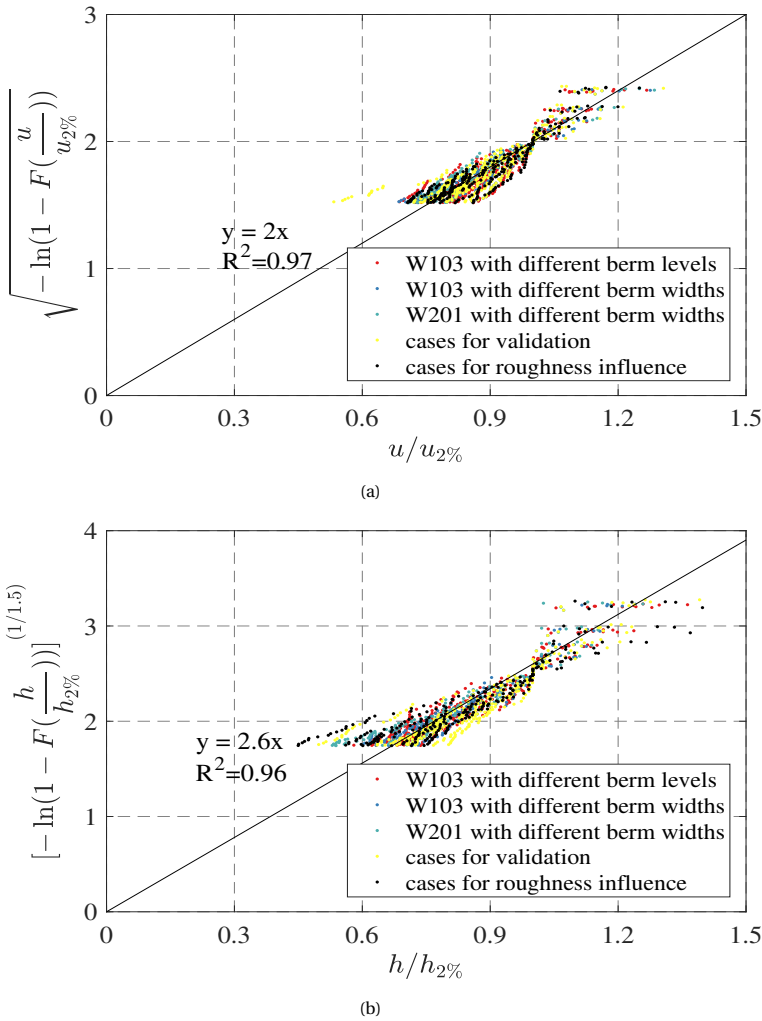
Figure 5.20: Fitted cumulative distribution function of (a) flow velocity and (b) layer thickness in equivalent probability plot. W103 represents the wave condition based on single-peaked TMA spectrum: H_{m0} = 0.152 m, $T_{m-1,0}$ = 2.51 s, h = 0.8 m and W201 represents the wave condition based on double-peaked TMA spectrum: H_{m0} = 0.149 m, $T_{m-1,0}$ = 2.32 s, h = 0.8 m.

existing empirical equations (5.1) & (5.2) proposed by Van Gent (2002b) were also applicable for the bermed slope. The berm influence on the flow characteristics was accounted for by the wave run-up height, which is different from the roughness influence that needed to be included in Eqs. (5.1) & (5.2) even though the wave run-up height had included the roughness effect. Model results of the berm influence factor showed a good agreement with the exiting empirical equation (5.1). The effect of a berm was further analyzed in combination with the oblique waves for the average overtopping discharge. The 2D numerical model

was extended into a 3D model in order to include the oblique waves. Model results verified the assumption made in Van Gent (2002b) that the influence of oblique waves on the mean overtopping discharge depends on the berm width. The 3D numerical simulations are extremely computationally expensive. A single simulation for 200 s took three weeks to compute using 22 processors (2.7 GHz) in parallel. Thus, only one test was modelled for validation and one wave direction relative to the structure was simulated. Considering the 3D numerical model was used in a qualitative way, the model validation was regarded as being acceptable. Then, the same wave conditions and numerical settings for the validation test were enforced for other 3D simulations except that the berm was varied. Although the incident waves at the position of the wave gauge at loc10 are not or hardly affected by the side relaxation zones, the wave interaction at the structure in the sections between z = 7 m to 9 m could be affected by the side relaxation zones in the numerical wave basin with the reduced size. However, if this interference would be present, it existed for all the simulated cases and it is expected that the interference of incident waves has limited influence on the trend. However, for more accurate predictions of the average overtopping discharge resulted from oblique waves, it is recommended to model the entire physical wave basin and to validate the 3D numerical model with more experimental data if the computational efficiency improves in the future. Additionally, the performance of the 3D numerical model should be further improved by for instance using finer mesh. The sensitivity of mean overtopping discharges caused by perpendicular waves with the grid size was performed by Chen, Warmink, et al. (2020) which showed that finer mesh would lead to smaller mean overtopping discharges.

In the 3D numerical model, the flow characteristics were not analyzed as no experimental data were available for validating the flow characteristics in three dimensions. It remains unknown how the oblique waves affect the flow velocity and layer thickness, which is recommended for future investigation.

5.6. CONCLUSIONS

WAVE overtopping must be considered for the design and evaluation of coastal structures. The accurate estimates of overtopping flow parameters at the crest related to individual overtopping events are important for assessing the stability of the landward slope of dikes. The mean overtopping discharge is a key parameter in determining the crest level of dikes. Berms, roughness and oblique waves have significant effects on wave overtopping. Thus, their effects should be taken into account when predicting the wave overtopping process at dikes. This paper presents a numerical investigation of the effects of roughness, berm and oblique waves on wave overtopping processes at dikes. Both overtopping flow characteristics and the mean overtopping discharge were studied.

Ten tests selected from Van Gent (2002b) were used to validate the 2D OpenFOAM®
model for predicting the overtopping flow velocity and layer thickness at the waterside edge
of the dike crest. The spectral wave period was overestimated by the numerical model,
which might be caused by the limitations of the OceanWave3D in dealing with the wave
breaking and by the shorter simulation time of the numerical model. Further research on
solving this problem is recommended. The model was shown to perform reasonably for
simulating the flow characteristics. The validated model was then applied to investigate the
effects of roughness and a berm on flow characteristics at the waterside edge of the crest.
Model results show that if the roughness factor was excluded from the existing empirical
equations (5.1) & (5.1), the flow characteristics would be underestimated. Including the
roughness factor as shown in Eqs. (5.1) & (5.1) leads to better estimates of flow velocities
and layer thicknesses.

Thirty numerical tests were performed to study the berm influence on the flow veloc-
ity and layer thickness. Model results show that the flow parameters are sensitive to the
berm width while they are not significantly influenced by the berm level. Existing empir-
ical equations (5.1) & (5.1) with coefficients by Van Gent (2002b) work well for estimating
the flow parameters over the slopes with a berm. The berm influence was accounted for by
the wave run-up height. It is recommended to use Eq. (5.A.1) to calculate the wave run-up
height over slopes with a berm.

Distribution functions were derived based on the numerical model results for the flow
velocity and layer thickness with exceedance probabilities below 10%. The extreme flow
velocities follow a Rayleigh distribution function while the layer thickness follows a Weibull
distribution function. A 3D OpenFOAM® model was also developed to take the oblique
waves into account by extending the 2D OpenFOAM® model into the 3D domain. Model
results show that the influence of the oblique waves on the mean overtopping discharge was
dependent on the berm width. It is recommended to investigate the effect of oblique waves
in combination with a berm and/or roughness on the flow velocity and layer thickness.

ACKNOWLEDGEMENT

5.A. An Appendix to Chapter 5

5.A.1. Empirical formulas for wave run-up height

Van Gent (2001) developed empirical equations (5.A.1) for estimating $R_{u2\%}$.

$$\frac{R_{u2\%}}{\gamma H_{m0}} = c_0 \xi_{m-1,0} \qquad \text{for } \xi_{m-1,0} \leq p$$

$$\frac{R_{u2\%}}{\gamma H_{m0}} = c_1 - c_2/\xi_{m-1,0} \quad \text{for } \xi_{m-1,0} \geq p \tag{5.A.1}$$

where $c_0 = 1.35$, $c_1 = 4.7$, $c_2 = 0.25 c_1^2/c_0$ and $p = 0.5 c_1/c_0$. H_{m0} [m] is the spectral significant wave height. γ [-] ($\gamma = \gamma_f \gamma_\beta$) is the reduction factor taking the influence of roughness (γ_f) and oblique wave attack (γ_β) into account. $\xi_{m-1,0}$ [-] ($\xi_{m-1,0} = \frac{\tan \alpha}{\sqrt{2\pi H_{m0}/(g T_{m-1,0}^2)}}$) is the Iribarren number. EurOtop (2018) also provides a method to estimate $R_{u2\%}$ as follows.

$$\frac{R_{u2\%}}{H_{m0}} = 1.65 \gamma_b \gamma_f \gamma_\beta \xi_{m-1,0} \tag{5.A.2}$$

with a maximum of

$$\frac{R_{u2\%}}{H_{m0}} = \gamma_f \gamma_\beta \left(4 - \frac{1.5}{\sqrt{\gamma_b \xi_{m-1,0}}} \right) \tag{5.A.3}$$

where γ_b [-] is the influence factor of berms, which can be calculated using the following equations.

$$\gamma_b = 1 - r_B (1 - r_{dh}) \qquad \text{if} \quad 0.6 \leq \gamma_b \leq 1.0 \tag{5.A.4}$$

where r_B and r_{dh} are calculated using the following equations.

$$r_B = \frac{B}{L_{berm}} \tag{5.A.5}$$

$$r_{dh} = 0.5 - 0.5 \cos\left(\pi \frac{d_h}{R_{u2\%}} \right) \quad \text{for a berm above still water line}$$

$$r_{dh} = 0.5 - 0.5 \cos\left(\pi \frac{d_h}{2 H_{m0}} \right) \quad \text{for a berm below still water line} \tag{5.A.6}$$

where L_{berm} [m] is the characteristic berm length; d_h [m] is the berm level relative to the SWL;

5.A.2. Numerical data

Table 5.A.1: Numerical (2DV) data of the roughness influence with protrusion height = 0.5 cm.

Test	h_toe	B [m]	H_{m0_OF} [m]	$T_{m-1,0\_OF}$ [s]	$h_{2\%\_OF}$ [m]	$u_{2\%\_OF}$ [m/s]	$R_{u2\%\_OF}$ [m]
R101	0.35	0	0.149	2.63	0.0205	1.51	0.358
R103	0.4	0	0.153	2.51	0.033	1.785	0.382
R104	0.45	0	0.149	1.98	0.034	1.6	0.31
R201	0.4	0	0.15	2.32	0.029	1.68	0.34
R202	0.4	0	0.148	2.23	0.0254	1.69	0.337
R203	0.4	0	0.138	2.14	0.0236	1.61	0.33
R204	0.4	0	0.127	2.14	0.022	1.44	0.315
R205	0.4	0	0.139	1.95	0.0179	1.35	0.282

Table 5.A.2: Numerical (2DV) data of the berm influence.

Test	h_toe	B [m]	d_h [m]	H_{m0_OF} [m]	$T_{m-1,0\_OF}$ [s]	$h_{2\%\_OF}$ [m]	$u_{2\%\_OF}$ [m/s]	$R_{u2\%\_OF}$ [m]
T103	0.4	0	0	0.153	2.51	0.0326	1.91	0.406
W103b1	0.4	0.1	0	0.153	2.51	0.0312	1.85	0.39
W103b2	0.4	0.2	0	0.153	2.51	0.03	1.88	0.38
W103b3	0.4	0.3	0	0.153	2.51	0.0266	1.754	0.36
W103b4	0.4	0.4	0	0.153	2.51	0.0254	1.484	0.349
W103b5	0.4	0.5	0	0.153	2.51	0.0218	1.41	0.32
W103b6	0.4	0.1	0.1	0.153	2.51	0.0353	1.717	0.404
W103b7	0.4	0.1	0.05	0.153	2.51	0.0345	1.89	0.397
W103b8	0.4	0.1	-0.05	0.153	2.51	0.0318	1.92	0.402
W103b9	0.4	0.1	-0.1	0.153	2.51	0.0319	1.85	0.402
W103b10	0.4	0.3	0.1	0.153	2.51	0.0313	1.72	0.362
W103b11	0.4	0.3	0.05	0.153	2.51	0.0265	1.9	0.364
W103b12	0.4	0.3	-0.05	0.153	2.51	0.0274	1.54	0.362
W103b13	0.4	0.5	0.1	0.153	2.51	0.026	1.55	0.344
W103b14	0.4	0.5	0.05	0.153	2.51	0.0246	1.44	0.326
W103b15	0.4	0.5	-0.05	0.153	2.51	0.0218	1.33	0.321
W103b16	0.4	0.5	-0.1	0.153	2.51	0.0256	1.38	0.332
W201	0.4	0	0	0.15	2.32	0.029	1.85	0.372
W201b1	0.4	0.1	0	0.15	2.32	0.0271	1.77	0.364
W201b2	0.4	0.2	0	0.15	2.32	0.0255	1.7	0.342
W201b3	0.4	0.3	0	0.15	2.32	0.0235	1.42	0.33
W201b4	0.4	0.4	0	0.15	2.32	0.0193	1.28	0.306
W201b5	0.4	0.5	0	0.15	2.32	0.0172	1.24	0.298

Table 5.A.3: Data for validation of the 2DV OpenFOAM® model.

Test	h_toe	H_{m0_exp} [m]	H_{m0_OF} [m]	$T_{m-1,0\_exp}$ [s]	$T_{m-1,0\_OF}$ [s]	$h_{2\%\_exp}$ [m]	$h_{2\%\_OF}$ [m]	$u_{2\%\_exp}$ [m/s]	$u_{2\%\_OF}$ [m/s]	$R_{u2\%\_OF}$ [m]
T101	0.35	0.149	0.149	2.16	2.63	0.0143	0.0217	1.53	1.66	0.391
T102	0.35	0.142	0.141	1.84	2.17	0.0058	0.0134	0.99	1.17	0.324
T103	0.4	0.153	0.153	2.14	2.51	0.0212	0.0326	1.74	1.91	0.406
T104	0.45	0.147	0.149	1.78	1.98	0.0204	0.0335	1.64	1.79	0.33
T201	0.4	0.152	0.15	2.03	2.32	0.016	0.029	1.55	1.77	0.372
T202	0.4	0.148	0.148	1.92	2.23	0.014	0.0265	1.53	1.75	0.362
T203	0.4	0.139	0.138	1.84	2.14	0.0117	0.0242	1.44	1.8	0.356
T204	0.4	0.13	0.127	1.86	2.14	0.0101	0.0244	1.29	1.65	0.348
T205	0.4	0.142	0.139	1.69	1.95	0.0076	0.0188	1.09	1.5	0.318
T206	0.4	0.138	0.134	1.62	1.89	0.0076	0.0184	1.08	1.43	0.305

6

DISCUSSION

6.1. THE APPLICATIONS AND LIMITATIONS OF EMPIRICAL FOR-MULAS

6.1.1. THE EFFECTIVENESS OF A BERM AND ROUGHNESS IN REDUCING CREST LEVELS

I N this thesis, empirical formulas for estimating the influence of a berm and roughness on the average overtopping discharge were derived (based on the experimental data described in Chapter 2). Due to climate change and sea level rise, some existing dikes may not satisfy the safety criterion and therefore require reinforcement. Reducing or limiting dike crest levels without reducing safety is often a preferred measure over raising dike crest levels, which will lead to much higher cost, social drawbacks or a negative influence on the landscape (Capel, 2015).

Figure 6.1 shows the relationship between the combined reductive influence $\gamma_b\gamma_f$ considering three types of roughness elements investigated in this thesis and the ratio of the R_c and R_{c-ss} on the left y axis. R_c represents the crest freeboard with a berm and roughness elements at the waterside slope and the crest freeboard R_{c-ss} denotes the freeboard with a smooth straight waterside slope, both of which result in the same average overtopping discharge under the same wave conditions. The influence factors γ_b and γ_f are calculated using the newly derived empirical equations (2.5) and (2.3) considering different wave conditions. It can be seen that there is nearly a linear relationship between the combined influence $\gamma_b\gamma_f$ of a berm and roughness and the crest freeboard ratio R_c/R_{c-ss}. Applying a berm and roughness elements at the waterside slope can effectively reduce the crest freeboard with R_c/R_{c-ss} varying between 0.4 and 0.6. For example, for a certain dimensionless mean overtopping discharge of 10^{-4}, using a berm and rock armour will only require a crest freeboard of $0.37R_{c-ss}$ (Figure 6.1).

Therefore, applying a berm and roughness elements at the waterside slope of dikes can be an effective solution to reduce the overtopping discharge below the acceptable limits without raising crest levels.

6.1.2. EXTENSION TO OTHER TYPES OF ROUGHNESS ELEMENTS AND BERMS

I N this thesis, the roughness equation (2.3) was first derived for protruding blocks and open blocks. Then the empirical coefficient c_0 in this equation was calibrated for rock armour. This indicates that the value of c_0 can be adapted for different types of roughness elements. The value of the coefficient c_0 is related to properties such as permeability and geometry of roughness elements. It is feasible to calibrate c_0 for other types of roughness elements based on existing or new experimental data. Similarly, the empirical coefficient b_0
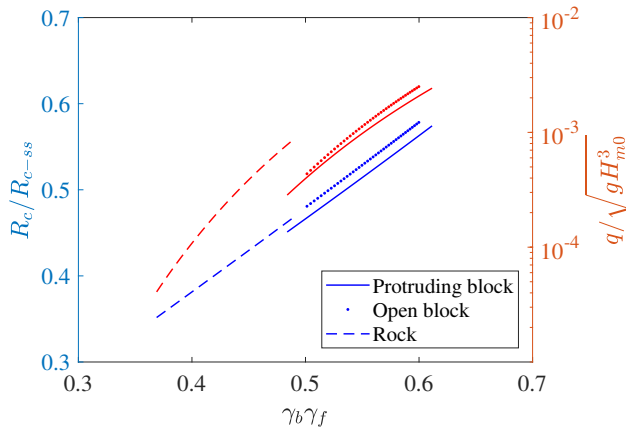
Figure 6.1: The estimated effectiveness of a berm and roughness in reducing the required crest freeboard. The significant wave height H_{m0} varies between 2.5 m and 3.5 m and the spectral wave period $T_{m-1,0}$ is fixed at 9 s (in prototype scale). The roughness influence factor γ_f is calculated by using Eq. (2.3) with $c_0 = 0.36$ for protruding blocks, $c_0 = 0.55$ for open blocks and $c_0 = 0.7$ for rock armour. The berm influence factor γ_b is calculated by using Eq. (2.5) with $b_0 = 0.21$ for protruding blocks, $b_0 = 0.13$ for open blocks and $b_0 = 0.19$ for rock armour. The dimensionless overtopping discharge $q/\sqrt{gH_{m0}^3}$ is calculated using Eqs. (2.2) and (2.A.2) taking the roughness and a berm into account and then this dimensionless overtopping discharge is used to calculate the crest freeboard R_{c-ss} without applying a berm and roughness at the waterside slope. R_c on the left y axis is fixed at 3.75 m (in prototype scale).

in the new berm equation (2.5) also depends on the properties of the roughness elements applied at the berm. The value of b_0 is constant, i.e. $b_0 = 0.21$, for an impermeable berm based on the analysis of experimental data obtained in this thesis. However, the coefficient b_0 is variable for a permeable berm. For example, the value of b_0 is different for a berm covered by open blocks and a rock-armoured berm. Therefore, b_0 requires calibration for a berm covered by the permeable revetment that is outside the tested range. The combined influence of a berm and roughness can be estimated by multiplying the roughness factor γ_f by the berm factor γ_b, i.e. $\gamma_f\gamma_b$.

There are some limitations of the new empirical formulas derived in this thesis. The improvement of the new berm equation (2.5) on the estimates of reductive influence of common berms is clear but for wide berms the improvement is limited compared to the TAW berm equation (1.2). It is recommended to investigate the effect of wide berms that may lead to berm influence factors even smaller than 0.6 on the average overtopping discharge. The applicable condition of the new roughness equation (2.3) is limited to $R_c/H_{m0} > 1.1$. For smaller crest freeboard ($R_c/H_{m0} < 1.1$), the equation (2.3) tends to underestimate the reductive influence of the roughness, which thereby can lead to conservative estimates of the average overtopping discharge. The new equation (2.6) for varying roughness along

the waterside slope is derived for roughness elements applied on the entire upper slope, the berm or the entire down slope. It still remains unknown whether the Eq. (2.6) is also applicable for the roughness elements only on a part of the upper slope. Thus, more experimental data of various roughness elements combined along the waterside slopes are needed to verify the applicability of the equation (2.6) to a wider range of conditions.

6.1.3. SCALE AND MODEL EFFECTS

Inertia and gravity forces are considered to be dominant forces for most flows related to waves. Therefore, the Froude's law is the most important criterion for the design of a coastal scale model. Gravity forces are properly scaled while other forces such as viscosity forces are overestimated in the model when applying Froude scaling to prototype conditions, because dynamic similarity cannot be fulfilled simultaneously in the same model for the other forces. Scale effects refer to all effects and errors resulting from ignoring these forces.

Schüttrumpf (2001) showed that the effect of viscosity on wave overtopping increases as the overtopping discharges decrease. Results of model are less affected by scale effects for relatively larger overtopping discharges (De Rouck et al., 2005). When the dimensionless average overtopping discharges are smaller than 10^{-6}, results of model tests can be unreliable due to scale effects (Christensen et al., 2014). In the data analyzed and measured in this study, dimensionless overtopping discharges smaller than 10^{-6} are not considered. Thus, the validity of the proposed expressions from the present research remains unknown for small dimensionless average overtopping discharges ($< 10^{-6}$), which requires further investigation although such very small discharges are normally not relevant for practical applications. It is also recommended to study the potential scale effects on the wave overtopping to obtain more reliable results.

6.2. NUMERICAL MODELLING TECHNIQUES

6.2.1. 2DV NUMERICAL MODEL

A 2DV OpenFOAM® model has been developed and validated for predicting the average overtopping discharge in Chapter 4. In this numerical model, the RANS equations are solved together with a VOF approach for tracking the free surface. The turbulence influence is modelled by applying the $k-\omega$ turbulence model. When waves impact the waterside slope, waves can break and thereby produce turbulence. The turbulence generated inside the water leads to wave energy dissipation, which results in lower overtopping discharges. Figure 6.2 shows that the simulated cumulative overtopping volume without a turbulence model is over twice the experimental result under the wave condition of $H_{m0} = 0.123$ m, $T_{m-1,0} = 1.72$ s and $h = 0.8$ m. Applying the turbulence model obviously improves the pre-

diction of the overtopping discharge. Therefore, turbulence plays an important role in modelling wave overtopping processes when wave breaking occurs and should not be ignored in the numerical model.

It is worth mentioning that the roughness of the waterside surface which was made of concrete is accounted for by using a roughness constant C_s and the roughness height K_s included in the turbulence model. The roughness constant C_s accounts for the uniformity of the roughness elements on the surface and Nikuradse (1950) determined the value of C_s as 0.5, which was adopted in this thesis, for the uniform and closely packed sand grains. The roughness height K_s represents the equivalent grain roughness which is calibrated as 0.001 m for concrete surface in this study. Figure 6.2 shows that as the roughness height increases the modelled overtopping volume decreases and $K_s = 0.001 m$ leads to a good agreement between the numerical and experimental time series of cumulative overtopping volume. It is not recommended to further increase this value too much. The grid size near the impermeable boundary should be larger than twice the roughness height because physically the flow cannot be solved below the roughness height value. Mathematically this condition does not need to be satisfied since the roughness height K_s is not modelled explicitly. However, the shear stress near the slope surface will be incorrectly modified by using the wall function, which possibly leads to inaccurate results of flow velocities near the slope surface. Therefore, increasing the roughness height would lead to coarser mesh near the wall surface which can reduce the model accuracy. This is also why the protruding blocks are modelled explicitly in Chapter 4 by refining the mesh near the protrusions (with a height of 1 cm) instead of using a roughness height K_s.
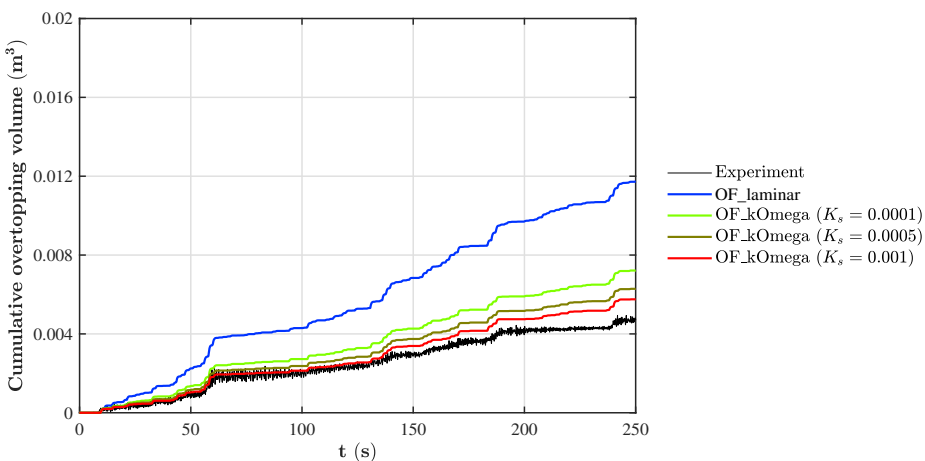
Figure 6.2: Comparison of time series of simulated cumulative overtopping volume per meter width with different settings of turbulence model under the wave condition of $H_{m0} = 0.123$ m, $T_{m-1,0} = 1.72$ s and $h = 0.8$ m.

The 2DV OpenFOAM® model is further validated for predicting the overtopping flow velocity and layer thickness at the waterside edge of the dike crest in Chapter 5. The numerical model is capable of predicting the flow velocity accurately while it gives an overestimation of the layer thickness with a factor of 1.3. This overestimation can be related to the quality of free surface capture. The interface between water and air could smear out over two or three layers of grids in the numerical model, which can further result in an overestimation of the layer thickness. Refining the mesh near the waterside slope and crest can to some extent reduce the overestimation. Nevertheless, a fine mesh would significantly increase the computational time especially for the slope covered by protruding blocks. Therefore, the grid size of 0.005 m in vertical direction is adopted to comprise between the computational efficiency and the model accuracy of layer thicknesses.

To study the roughness influence on the flow parameters, the roughness is implemented in the numerical model by applying protrusions with a height of 0.5 cm along the waterside slope. This resulted in the roughness factor varying in a limited range of 0.88 to 0.95. Since the slope with protrusions is impermeable in the 2D numerical model, the water is trapped between the protrusions and cannot flow out immediately which makes the slope surface less rough. Therefore, increasing the protrusion height in the numerical model will not increase the roughness significantly. In order to study the influence of the roughness varying in a wider range using the 2D numerical model, it might be a solution to apply permeable roughness revetments, which will be discussed in more detail in Section 6.2.3.

6.2.2. 3D NUMERICAL MODEL

IN Chapter 5, the 2DV OpenFOAM® model is extended into a 3D domain to take the oblique waves into account. The oblique waves are simulated by rotating the structure such that the direction of incident waves relative to the rotated structure is oblique. Consequently, the reflected waves at the structure propagate towards the side wall of the numerical wave basin. In order to prevent the reflected waves from re-reflecting at the side wall, relaxation zones are applied at the side walls to absorb the reflected waves. The application of the side relaxation zones results in the wave height near the central axis of the wave basin being higher and gradually decreasing towards the side walls. Therefore, the range in which the wave properties are almost uniform along the width of the numerical wave basin is selected to measure the average overtopping discharge. This requires that the wave basin should be wide enough such that the range of uniform wave properties of the incident waves can be found, which leads to significantly longer computational time. Therefore, it is recommended to develop an absorption boundary at the side walls that is capable of effectively absorbing the reflected waves without interfering the wave field in the interested area.

Only one direction of incident waves is simulated in this study since the 3D numerical model only aims to verify the dependency of the influence of oblique waves on the berm width. To take more wave directions into account, it is feasible to rotate the structure with different angles. However, to simulate very oblique waves with the incident angle relative to the structure larger than 60°, the structure needs to be rotated with a larger angle accordingly. The resulted mesh near the structure will be highly skewed which can easily cause computational divergence. It might be an option to apply the wave generation boundary for irregular directional waves which has been implemented in IHFOAM (Higuera et al., 2013). This boundary can generate directional waves directly without rotating the structure. Additionally, this wave generation approach imposes the velocity field directly at the boundary with a Dirichlet type boundary condition and does not require relaxation zones, which provides a possibility of saving computing time. However, the implemented wave paddle absorption boundary can only deal with the perpendicular incoming waves to the boundary. Further research on the improvement of wave generation and absorption boundaries is needed for simulating oblique waves in 3D numerical models.

6.2.3. Extension to permeable revetments

I n both the 2D and 3D numerical models presented in this thesis, only impermeable structures with impermeable revetments are considered since the focus of this study was on the effects of berms, roughness and oblique waves on the wave overtopping instead of developing a numerical model that is applicable for a wide range of coastal structures. Nevertheless, it is feasible to incorporate the permeable revetments in the framework of OpenFOAM® to extend the applicability of the numerical models developed in this thesis to a wider range of dike configurations.

There are some solvers available in the framework of OpenFOAM® that can solve two-phase flow within porous media based on Volume-averaged Reynolds-Averaged Navier-Stokes (VRANS) equations, such as porousWaveFoam implemented in waves2Foam (Jacobsen, 2017). Volume averaging NS equations avoid the need of a detailed description of the geometry of porous media including the individual (3D) pores (Higuera et al., 2014a) and provide the so-called filter velocities to describe the mean characteristics of the porous medium (Van Gent, 1995). The flow resistance in the porous media is described by the added mass coefficient and the linear and quadratic resistances (e.g. Van Gent, 1995; Jensen et al., 2014). The added mass coefficient accounts for the inertial effects of the porous skeleton and the linear and nonlinear drag resistances are approximated by the Darcy-Forchheimer flow resistance (e.g. Jacobsen et al., 2015). The Darcy-Forchheimer formulation includes two resistance coefficients, α and β, which require calibration from physical tests to obtain accurate model results. These two closure coefficients depend on the flow

characteristics and the shape and grading of the porous material (Losada et al., 2008). A turbulence model should be applied when the turbulence level is of interest inside the porous media and the turbulence model also needs to be volume-averaged (del Jesus et al., 2012). The only available turbulence model that has a closure for porous media for now is $k-\epsilon$ turbulence model presented in Nakayama and Kuwahara (1999). Jensen et al. (2014) suggested that when the actual turbulence levels are of minor interest the turbulence influence can be considered through the resistance coefficients α and β in the Darcy-Forchheimer equation.

Barendse (2021) extended the 2D OpenFOAM® model presented in this thesis to take a permeable placed-block revetment into account. The permeable placed-block revetment was implemented in the numerical model by defining a porous layer of which the properties were represented by the resistance coefficients α and β, the porosity n and the stone diameter d_{50}. Large-scale physical experiments performed in the Delta Flume at Deltares were used to calibrate and validate the numerical model. Comparison between the measured and numerically modelled peak pressures and peak flow velocities of individual overtopping events showed that applying the resistance coefficients $\alpha = 500$ and $\beta = 2$ as recommended by Jensen et al. (2014) for natural rock also provides a good agreement for a placed-block revetment of interlocking concrete blocks. This demonstrates the feasibility and flexibility of extending the applications of the OpenFOAM® model for dike configurations with permeable revetments.

6.2.4. COMPUTATIONAL EFFICIENCY

IN this present study, both 2DV and 3D CFD simulations are performed. For the 2D OpenFOAM® model, it takes about 5 days to compute one simulation for about 300 waves in which a smooth straight is modelled using 3 processors (3.6 GHz). The computational time can double for simulating the wave overtopping processes at slopes covered by protruding blocks since the protrusions need to be resolved using a finer mesh. The computational cost of 2D simulations is acceptable considering the good model accuracy on predicting the average overtopping discharge and overtopping flow characteristics. Nevertheless, the computational efficiency of the 2D model still requires improvement to be competitive with NSWE models in terms of computation. The 3D simulations are computationally more demanding. One 3D simulation of wave overtopping under oblique waves for about 100 waves takes nearly 21 days to compute parallelizing the numerical domain into 22 processors (2.7 GHz). Ideally, for a more reliable prediction of the average overtopping discharge, longer simulations with many more waves should be carried out which will take much more computational time.

In order to improve the computational efficiency of the numerical models, the wave generation and absorption boundary conditions implemented in IHFOAM, which elimi-

nate the need of relaxation zones, can be applied to reduce the size of the domain and thereby reduce the computational time. Recently, a new boundary condition adapted based on the classical Sommerfeld condition is proposed by Borsboom and Jacobsen (2021) using a depth-varying coefficient to improve absorption efficiency over a range of wave numbers. This boundary condition also does not need the use of relaxation zones and has been implemented in waves2Foam. Additionally, the boundary conditions in IHFOAM have been coupled with waves2Foam (Jacobsen, 2021), which allows the users to use the IH-FOAM wave definitions with pre- and run-time tools such as overtopping function available in waves2FOAM. It is also an option to couple a computationally cheap model with the OpenFOAM® model. For example, Vandebeek et al. (2018) coupled the SWASH model based on non-hydrostatic NLSW equations and OpenFOAM® and validated the coupling for the wave propagation on a flat bottom. Di Paolo et al. (2021a) proposed one-way and two-way 2D-3D multi-domain couplings for Navier-Stokes models. The computational domain was subdivided into far and near field zones. In the near field zone where three-dimensional flows in the interaction between wave and structure are often dominant, the 3D subdomain was applied while the 2D subdomain was used in the far field where three-dimensional flows are less important. The 2D-3D coupling method can significantly reduce the computational time without decreasing the accuracy of the full solution (Di Paolo et al., 2021b). Other solutions can be related to improvements of solving algorithms.

6.3. PRACTICAL IMPLICATIONS AND APPLICABILITY FOR HWBP

DIKES are important coastal structures to protect hinterland from wave attack. Due to climate change and sea-level rise, many countries are facing increasing flood risk (Temmerman et al., 2013). To reduce the flood risk, some existing dikes may require reinforcement. To prevent flooding in the Netherlands, the Flood Protection Program (HWBP) will strengthen over 1,300 kilometers of dikes in the Netherlands over the next thirty years. Reduction of overtopping risk is important for the design, management and adaption of coastal structures (EurOtop, 2018).

The crest levels of coastal structures are often determined by ensuring the average overtopping discharges are below the allowable values. EurOtop (2018) provides the allowable overtopping discharges for different situations, for example, when persons can walk on the crest or vehicles are moving behind the structure. The new empirical formulas derived in this thesis for estimating the reductive effects of a berm and roughness on the overtopping discharges can be used to predict the average overtopping discharge for the conceptual design of dikes and evaluation of existing dikes. In practice, a berm and roughness elements at the waterside slope of dikes are often applied to reduce the wave overtopping. The experimental results presented in this thesis also demonstrate that the berm and roughness

elements can effectively reduce the average overtopping discharge. New empirical formulas developed in Chapter 2 and Chapter 3 can be applied in combination with the overtopping equations given by TAW (2002) or EurOtop (2018) to estimate the average overtopping discharge taking the reductive influence of a berm and roughness into account. A more accurate prediction of the average overtopping discharge can make the design or reinforcement of a dike safer and more cost-effective.

The reductive influence of roughness at the waterside slope of a dike depends on the wave conditions, crest freeboard and properties of roughness elements (see Eq.(2.3)). The value of the roughness factor for one certain type of roughness elements can vary in a wide range under different wave conditions. For example, the roughness factor of protruding blocks varies between 0.6 and 0.8 in the tested ranges in this study. Therefore, using a constant value of the roughness factor as suggested by TAW (2002) and EurOtop (2018) can lead to an overestimation or underestimation of the average overtopping discharge with an order of magnitude. Thus, the wave conditions should be taken into account when estimating the roughness influence. Additionally, the experimental results show that the roughness elements at the upper part of the waterside slope are more effective in reducing the overtopping discharges while the roughness elements at the down slope under the still water level have limited reductive influence. From the perspective of reducing the wave overtopping, it is recommended to install roughness elements at the upper part of the waterside slope especially when it is hardly possible to raise the crest height. Whether applying roughness on the upper part actually saves construction costs depends on many other local characteristics (e.g. aesthetic requirements) as well while this will provide an additional option for dike designers to optimize the design. For the berm influence, a berm located near the still water level leads to larger reductive influence on the average overtopping discharge than a berm located below or above the still water level (EurOtop, 2018). Thus, the optimal berm level is at the reference water level that is determined based on the reference flood or reference flow over a chosen return period (Pavlin and Kuspilić, 2018). Additionally, experimental results show that a permeable berm covered by open blocks or rock armour tends to give less reduction of the average overtopping discharge compared to an impermeable berm. However, we recommend to further validate this finding using a more extensive data set of permeable berms before applying it in practice. The combined effects of berms and roughness can explicitly be taken into account by using the product of the berm factor γ_b and the roughness factor γ_f. The 3D numerical model results in Chapter 5 verified the dependency of oblique wave influence on the berm width. Therefore, the empirical formula for the influence of oblique waves proposed by Van Gent (2020), which takes this dependency into account, is recommended for the estimation of the average overtopping discharge when the berm and oblique waves are present at the same time.

However, the empirical formulas derived based on physical model tests have their ranges

of validity based on the (limited) ranges of the tested conditions as discussed in Section 6.1.2. The 2D numerical model developed in Chapter 4 can be applied as a complementary tool to predict the average overtopping discharge. It is flexible to change the dike configurations and wave conditions in the numerical model. For example, it is relatively easy to change the applied location of roughness along the waterside slope which can be used to determine the optimal applied location and coverage length of the roughness for reducing the average overtopping discharge during dike design. Additionally, the numerical model can be used to extend the database obtained from purely physical experiments, which can then be applied for the development or improvement of machine learning methods. For example, Den Bieman et al. (2021) recently developed a prediction tool named XGB-overtopping model based on extensive experimental data sets using the Gradient Boosting Decision Trees (GBDT), which is a machine learning method. This is a generic model to predict the average overtopping discharges for a wide range of wave conditions and structure configurations. However, Den Bieman et al. (2021) also pointed out that there are still many white points in the training data set. The numerical model which has been validated for the average overtopping discharge in this thesis provides a possibility of addressing some of the white spots by for instance including a wider range of dike configurations and wave conditions. For permeable structures, the numerical model requires adaption and validation before being applied to generate database for machine learning models. Additionally, the 2D numerical model was mainly validated using the experimental data in which the dimensionless average overtopping discharges (q^*) were larger than 10^{-4}. For smaller overtopping discharges, it is expected that finer mesh near the structure might be needed to resolve the thinner overtopping flow on the slope surface. Thus, it is recommended to further calibrate and validate the numerical model for small overtopping discharges ($q^* < 10^{-5}$).

The 2D OpenFOAM® model has also been validated for the overtopping flow velocities and layer thicknesses in Chapter 5.The numerical model is also capable of producing time series of flow velocities and layer thicknesses. The flow characteristics are key parameters to assess the pedestrian safety when standing on the coastal structures during the overtopping events (Mares-Nasarre et al., 2019). Suzuki et al. (2020) suggested that the overtopping risk was better characterised by time dependent flow velocity and layer thickness than maximum flow parameters. Sandoval and Bruce (2018) provided different criterion for human stability on coastal structures. For example, the criteria for a tall adult can be expressed as a stability line by the combination of U and h. By comparing the modelled flow velocities and layer thicknesses to the stability line, it is possible to estimate the stability of an adult on the crest of coastal structures under different wave conditions. This could provide some insight into the necessity of reinforcement of dikes for the accessibility criteria.

The flow parameters are also closely related to dike cover erosion. Earthen dikes covered by grass are vulnerable to overtopping (Van Bergeijk et al., 2020). The high flow velocities

during the wave run-up at the waterside slope, overtopping at the crest and landward slope can result in grass cover erosion. Several erosion models (e.g. Van der Meer, 2010; Hoffmans, 2012) are available to estimate the cover erosion which require the hydraulic load as input. The distribution functions of flow characteristics derived in Chapter 5 can be used as input to estimate the cumulative erosion damage or depth on the crest and the landward slope of a storm event using the cumulative overload method proposed by Van der Meer (2010) or analytical grass-erosion model as described in Van Bergeijk et al. (2021). Furthermore, it is easy to extract the hydraulic load such as flow velocity, shear stress and pressure at any location along the waterside slope and crest from the numerical model. In addition, previous research (e.g. Steendam et al., 2014) has shown that the presence of obstacles like stairs or piles on dikes can reduce the stability of grass covers. A 3D numerical model such as applied in this thesis can be used to analyse the flow patterns and wave forces influenced by the obstacles. The distribution of the hydraulic load along the dike profile or near the obstacles in combination of erosion models can provide insight into which location at the dike is more vulnerable to the wave run-up or overtopping loads and thereby require reinforcement.

The predictions given by the empirical formulas and numerical models developed in this thesis can be used in the conceptual design or reinforcement of dikes. However, when the consequences of wave overtopping are important, these predictions should be verified by physical model tests. Nevertheless, the numerical model is much cheaper than the physical experiments and it can be used before starting physical tests to determine the cases to be tested in physical experiments which can significantly reduce the cost of physical model tests. Additionally, the numerical model can help to find the most suitable locations where the measuring instruments should be installed in the experiments. The numerical model can be regarded as a complementary tool with physical model tests for investigating the overtopping processes at coastal structures.

With sea level continuing to rise, more regions around the world are projected to become exposed to coastal overtopping (Almar et al., 2021). The empirical formulas as proposed in this thesis have the potential to be applied in combination of a hydrodynamic model and a spectral wave model (which can provide the hydraulic boundary conditions taking the sea level rise into account for estimating overtopping) to predict the future flood risk (see for instance Ke et al., 2021). Accurate predictions of flood risks due to dike failure caused by wave overtopping can provide some insight into the necessity of protective countermeasures such as beach nourishment or dike reinforcement for low-lying coastal regions.

7

CONCLUSIONS AND RECOMMENDATIONS

7.1. Conclusions

T HE aim of the research described in this thesis is to determine the influence of rough-
ness, a berm and oblique waves on wave overtopping processes at dikes by performing
physical model tests and numerical simulations. To achieve this aim, we first developed
the empirical formulas for the roughness and berm influence factors by means of perform-
ing small-scale physical model tests. Following that, we set up a 2DV numerical based on
the OpenFOAM® framework and validated this model for predicting the average overtop-
ping discharge using the experimental data. The validated model was later applied to get
more insight into the influence of a berm and roughness on the overtopping discharges.
Then, this 2DV OpenFOAM® model was further validated for overtopping flow velocities
and layer thicknesses on the dike crest. The effects of a berm and roughness on the flow
parameters were studied using the numerical model. Finally, the 2DV numerical model was
extended into a 3D model in order to study the influence of oblique waves. We verified that
the reductive effect of oblique waves on the average overtopping discharge is dependent
on the berm width as assumed by Van Gent (2020). In this section, we answer the research
questions formulated in Section 1.5.

Q1 What are the effects of berms and roughness of block revetments on the average over-
topping discharge at dikes?

In Chapter 2, we investigated the effects of a berm and roughness on the average over-
topping discharge by performing small-scale physical model tests. In the experiments,
we tested different types of roughness elements (i.e. smooth, protruding blocks and open
blocks) applied at different locations along the waterside slope to study the roughness influ-
ence. Both straight slopes and slopes with a berm were considered to investigate the berm
influence. New empirical equations (2.3, 2.5 & 2.6) for estimating the roughness and berm
influence factors were developed based on the experimental data.

It was found that the roughness influence factor of one certain type of roughness ele-
ment was not constant as suggested by TAW (2002) and EurOtop (2018). Instead, the rough-
ness influence factor depends on wave properties, crest freeboard and properties of rough-
ness elements. Additionally, the roughness elements applied at the upper slope were more
effective in reducing the average overtopping discharge than those applied at the berm or
at the down slope. Location-weighting coefficients were introduced to describe the influ-
ence of the locations of roughness elements at the slope on the overall roughness influence
factors. Also, it was found that the upper elements on the upper slope contribute signifi-
cantly more to the reduction of overtopping than elements applied further down the upper
slope. As to the berm influence, the experimental results showed that the berm influence
decreases as the wave steepness increases. The TAW equation for the impermeable berm

influence was modified by including the wave steepness. The permeable berm covered by open blocks showed smaller reductions on the overtopping discharges than an impermeable berm. Thus, the value of the empirical coefficient b_0 in the new berm equation (2.5) was different for impermeable and permeable berms.

The newly derived empirical formulas matched well with the experimental results with a *NSE* of 0.97 and showed significantly better performance in predicting the average overtopping discharge compared to existing empirical formulas within the tested ranges.

Q2   How do the newly derived empirical equations in Q1 perform for predicting the influence factors of a berm and roughness at a rock-armoured dike?

In Chapter 3, we extended the empirical formulas developed in Chapter 2 for rock armour as it is widely used as the revetment at coastal structures. Small-scale physical model tests were performed to study the effects of a berm and roughness of rock armour on the average overtopping discharge. Test results showed that the application of a berm and rock armour can significantly reduce the average overtopping discharge compared to a smooth straight slope. Empirical equations for estimating the berm and roughness factors of rock armour were derived using part of the experimental data by recalibrating the empirical coefficients b_0 and c_0 in equations (2.5 & 2.3). The performance of the new equations was validated by using the remaining experimental data with a wider range of test conditions compared with the calibration data set. The new equations lead to a significant improvement on estimates of the average overtopping discharge at the structure with rock armour applied on the upper slope, even though the wave conditions were outside the ranges of the calibration data set. The location-weighting coefficients as proposed in Chapter 2 appeared to be valid for rock-armour as well.

The new berm equations performed comparably with the TAW berm equation for very wide berms, although very wide berms are not common for dikes. The validity of the new roughness equation is applicable for rock-armoured structures that have a larger relative freeboard ($\frac{R_c}{H_{m0}} > 1.1$). For very low relative freeboards which are not common for dikes, the roughness equation still requires improvement. Overall, the roughness and berm equations with recalibrated values of the empirical coefficients b_0 and c_0 for rock armour significantly improved the predictions of the average overtopping discharges at rock-armoured dikes with $NSE = 0.8$ within the experimental ranges.

Q3   What is the influence of berms and roughness varied outside of the tested ranges in Q1 on the average overtopping discharge by using numerical modelling?

Chapter 4 presents an investigation of the capability of the 2DV numerical model in predicting average overtopping discharges at impermeable structures as well as the applicability of the numerical model in simulating the berm and roughness influence. We developed

7

this 2D numerical model based on the framework of OpenFOAM®. Data from the physical model tests as presented in Chapter 2 were used to validate the OpenFOAM® model. The roughness of protruding blocks was modelled by creating protrusions along the waterside slope. The mesh around the protrusions was refined in order to accurately simulate the flow motion near protrusions.

The incident waves that were applied in the experiments were reproduced well in terms of wave propagation and wave properties in the numerical model. The comparison between the numerically modelled and experimental overtopping discharges showed that the OpenFOAM® model is capable of predicting the average overtopping discharge at simple and complex configurations within a factor of 1 to 3 of the measured discharges from experiments and with a NSE of 0.78. For overtopping discharges (exponential behaviour), these factors are acceptable. Moreover, the numerical model produced the time series of cumulative overtopping volume that had similar trends with those given by the experiments, which indicated that the OpenFOAM® model can also capture the individual overtopping events.

The validated numerical model was then applied to study the berm and roughness influence on the average overtopping discharge. The berm width and berm level were varied in a wider range in the numerical model than the experimental range presented in Chapter 2. Numerical model results showed that for the relative berm width $B/H_{m0} > 5$ further extension of the berm width might not significantly increase the reductive influence of a berm on the average overtopping discharge. Additionally, the berm equation developed in Chapter 2 may require improvement for the cases outside the experimental conditions as indicated by the numerical results. The roughness influence was investigated by changing the coverage length of protruding blocks on the upper part of the upper slope using the numerical model. Model results showed that the roughness elements on the higher part of the waterside slope played a major role in reducing the wave overtopping which is in line with the findings in Chapter 2. Applying one row of protruding blocks on the top of the upper slope could effectively increase the roughness influence (from smooth to 44% of the roughness of the slope entirely covered by roughness elements) on reducing the overtopping discharge. Protruding blocks on the upper half of the upper slope resulted in almost the same roughness influence as those applied on the entire upper slope.

Q4 By using numerical models, to what extent do roughness, berms and oblique waves affect the average overtopping discharge and the overtopping flow parameters including flow velocity and layer thickness?

In Chapter 5, we studied the effects of a berm and roughness on the flow velocity and layer thickness as well as the influence of a berm and oblique waves on the average overtopping discharge using both 2DV and 3D OpenFOAM® models. The 2DV OpenFOAM® model developed in Chapter 4 was further validated using the existing empirical data from literature

for predicting the overtopping flow velocity and layer thickness at the waterside edge of the dike crest. There was a good agreement between the numerically modelled and experimental flow velocities and layer thicknesses.

The protrusions were applied along the waterside slope creating the roughness in the 2DV numerical model in order to study the roughness influence on the flow velocities and layer thicknesses. Model results indicated that existing empirical formulas for flow parameters (e.g. EurOtop, 2018) excluding the roughness influence factor could lead to underestimation of the flow parameters at rough slopes. Therefore, the roughness factor should be included in the empirical equations to correctly account for the roughness influence on flow parameters as suggested by Van Gent (2002b).

The simulated flow parameters were sensitive to the variation of the berm width while the berm level had limited influence on the flow parameters. Model results of the flow velocities and layer thicknesses over slopes with a berm matched well the estimated values given the existing empirical equations proposed by Van Gent (2002b), which showed that the empirical equations derived for smooth straight slopes could also be applicable for slopes with a berm.

The 2DV numerical model was extended into a 3D model to take the oblique waves into account. This 3D numerical model was used to simulate the average overtopping discharge at the dike with a berm under oblique wave attack. It was found that, as the berm width increases the reductive influence of oblique waves on the average overtopping discharge also increases. This verifies the assumption made by Van Gent (2020) that the influence factor of oblique waves depends on the berm width. This is important for accurately predicting the average overtopping discharge at dikes when oblique waves and a berm are present at the same time.

Reflection on the main aim of this research

In this research, we investigated the influence of berms, roughness and oblique waves on the wave overtopping at dikes. New empirical formulas (Eqs. (2.3, 2.3 & 2.6)) are developed for the berm and roughness influence factors by performing small-scale physical model tests, which significantly improve the accuracy of predicted average overtopping discharges compared to existing empirical formulas within the tested range. To complement with the proposed empirical formulas which are valid for limited conditions, a 2DV OpenFOAM® model is developed and validated. The 2DV numerical model is capable of simulating average overtopping discharges accurately at dikes that have berms and/or roughness elements. The influence of berms and roughness on overtopping flow velocities and layer thicknesses was studied by using a 2DV numerical model. 2D model results show that the existing empirical formulas derived for smooth straight slopes also work well for estimating flow parameters over slopes with berms or roughness. Finally, a 3D numerical model is developed to study the influence of oblique waves on the average overtopping

discharge. Model results confirm that the reductive influence of oblique waves on the over-topping discharge is affected by the berm width. The outcomes of this research can improve the design and safety assessment of dikes.

7.2. RECOMMENDATIONS

THIS chapter is concluded with recommendations for further research on the effects of a berm, roughness and oblique waves on overtopping discharges and overtopping flow parameters, and on the numerical model related to wave overtopping processes. We also provide some recommendations for dike designers.

7.2.1. EXTEND THE APPLICABILITY OF EMPIRICAL FORMULAS

THE new empirical roughness equations as presented in Chapter 2 were developed for three types of roughness elements, i.e. protruding blocks, blocks with open space and rock armour. To apply this empirical equation to other types of roughness elements, the empirical coefficient c_0 in Eq. (2.3) should be validated, and possibly calibrated, based on existing data or new physical model tests. Furthermore, the empirical equation (2.6) for varying roughness along the waterside slope was derived based on the roughness elements applied on the entire upper slope, the entire berm or the whole down slope. It still remains unknown whether Eq. (2.6) is applicable for roughness elements applied on part of the upper slope, the berm or the down slope. Therefore, it is recommended to validate and extend the applicability of the new equation (2.6) for any certain coverage length of roughness elements along the waterside slope.

The new berm equation (2.5) was developed for both impermeable and permeable berms. The empirical coefficient b_0 in Eq. (2.5) was constant for an impermeable berm while the value of b_0 varied depending on the properties of a permeable berm. Thus, For a permeable berm covered by different types of armour units, the value of b_0 can be different. We recommend to calibrate b_0 for a wider range of permeable berms to extend the applicability of the new berm equation (2.5).

The new empirical formulas for roughness and berm influence factors were proposed based on the experimental data obtained from the physical model tests in which only limited wave conditions and dike configurations could be tested. These empirical formulas still require improvement outside of the tested ranges, e.g. for relatively small crest freeboard or very wide berms as discussed in Section 6.1.2.

7.2.2. FURTHER INVESTIGATE THE COMBINED EFFECTS OF ROUGHNESS, A BERM AND OBLIQUE WAVES ON FLOW PARAMETERS

THE influence of roughness on the flow velocity and layer thickness was investigated by using the 2D numerical model. The model results indicated that the existing empirical formulas for flow parameters can give an underestimation if the roughness factor is excluded. In the numerical model, the roughness factor was varied in a limited range which is close to 1. For a much smaller roughness factor, the underestimation of flow parameters can be larger. Therefore, it is recommended to further investigate the roughness influence on the flow velocity and layer thickness for a wider range of roughness factors.

In this thesis, we only investigated the effects of roughness and a berm on the flow velocity and layer thickness. In addition to a berm and roughness, the oblique waves can also affect the flow parameters considering the oblique waves can significantly influence the overtopping discharges. Additionally, the influence of oblique waves might be affected by the berm width. Therefore, investigation on the combined influence of roughness, a berm and obliqueness of the waves on the flow velocity and layer thickness is recommended.

7.2.3. IMPROVE THE NUMERICAL MODELS

IN the numerical model, only impermeable structures were considered. It is feasible to extend the numerical model developed in this thesis for permeable revetments. The 2D numerical model overestimated the average overtopping discharge at the slope covered by protruding blocks as shown in Chapter 4 since the chessboard pattern of the blocks could not be modelled in a 2DV model. Therefore, it is necessary to extend the 2D numerical model into a 3D domain in order to more accurately model the 3D effects of roughness elements.

It is recommended to developed an absorption boundary that can be applied at the side walls of numerical wave basin to absorb the reflected waves from the structures without disturbing the incident wave field. Finally, the mesh used in the 3D numerical model should be refined and longer simulations should be carried out to obtain a more accurate prediction of the average overtopping discharge. Thus, the computational efficiency of the 3D numerical model in Chapter 5 still requires improvement by for example using a wave generation and absorption boundary condition (e.g. Higuera et al., 2013) eliminating the need of relaxation zones.

7.2.4. RECOMMENDATIONS FOR DIKE DESIGNERS

THE application of a berm and roughness elements at the waterside slope of a dike can significantly reduce the wave overtopping. Our research showed that the roughness in-

fluence is also dependent on the wave conditions and crest freeboard apart from the properties of roughness elements. Using a constant roughness factor for one certain type of roughness element can lead to underestimation or overestimation of the average overtopping discharge. Therefore, we recommend to take the dependency of roughness factor on the wave properties and crest freeboard into account when predicting the average overtopping discharge at coastal structures. Additionally, we found that the roughness elements applied at the upper part of the waterside slope are more effective in reducing the average overtopping discharge. It is recommended to consider applying roughness elements at the higher part of the waterside slopes.

The numerical model results presented in Chapter 5 showed that the influence of oblique waves on the average overtopping discharge is affected by the berm width. Additionally, the results in Chapter 2 showed that the roughness of a straight slope might be different from a slope with a berm. It is recommended to take the interactive effects among different influence factors into account for a more reliable estimation of the wave overtopping discharges. This can be done by using the new empirical equations within their range of validity or by executing laboratory or numerical tests for which models have been developed in this thesis. It is worth mentioning that 3D numerical simulations are restricted to long-crested waves. Since the short-crested and directional spreading of waves also have a significant impact on wave run-up and wave overtopping, the influence factor for long-crested and short-crested oblique waves can also differ significantly. Further investigation on the influence of short-crested oblique waves is recommended. It is also recommended to study whether the influence factors of berms and roughness derived for overtopping discharges can be applied for overtopping velocities and water layer thicknesses as well.

Finally, we recommend to use empirical formulas in combination with the numerical models developed in this thesis to extend the range of wave conditions and structure geometries considered in the physical experiments for predicting the wave overtopping at dikes.

LIST OF REFERENCES

Ahrens, J. (1981). Irregular wave runup on smooth slopes. *U.S. Army, Corps of Engineers*, *81-17*, 26. http://repository.tudelft.nl/assets/uuid:36b36bce-a88b-4bd3-a597-047749b9161c/CETA81-17-Ahrens-runup.pdf

Akbari, H. (2017). Simulation of wave overtopping using an improved SPH method. *Coastal Engineering, 126*, 51–68.

Almar, R., Ranasinghe, R., Bergsma, E. W., Diaz, H., Melet, A., Papa, F., Vousdoukas, M., Athanasiou, P., Dada, O., Almeida, L. P., & Kestenare, E. (2021). A global analysis of extreme coastal water levels with implications for potential coastal overtopping. *Nature Communications, 12*(1), 1–9. https://doi.org/10.1038/s41467-021-24008-9

Altomare, C., Laucelli, D. B., Mase, H., & Gironella, X. (2020). Determination of semi-empirical models for mean wave overtopping using an evolutionary polynomial paradigm. *Journal of Marine Science and Engineering, 8*(8), 570.

Andre, S., Boillat, J. L., Schleiss, A. J., & Matos, J. (2004). Energy dissipation and hydrodynamic forces of aerated flow over macro-roughness linings for overtopped embankment dams. *Proc., Int. Conf. on Hydraulics of Dams and River Structures*, 189–196.

Argente, G., Gómez-Martín, M. E., & Medina, J. R. (2018). Hydraulic stability of the armor layer of overtopped breakwaters. *Journal of Marine Science and Engineering, 6*(4), 143.

Bae, H. U., Yun, K. M., Yoon, J. Y., & Lim, N. H. (2016). Human Stability with respect to overtopping flow on the breakwater. *Int. J. Appl. Eng. Res, 11*, 111–119.

Barendse, L. (2021). *Hydrodynamic modelling of wave overtopping over a block-covered dike*, Master Thesis, University of Twente.

Besley, P. (1998). *Wave overtopping of seawalls, design and assessment manual* (tech. rep.). HR Wallingford.

Bomers, A. (2015). *Road impact on erosion development during overtopping flood events*, Master Thesis, University of Twente.

Bomers, A., Aguilar-López, J. P., Warmink, J. J., & Hulscher, S. J. M. H. (2018). Modelling effects of an asphalt road at a dike crest on dike cover erosion onset during wave overtopping. *Natural hazards, 93(1),* 1–30.

Bonakdar, L., & Etemad-Shahidi, A. (2011). Predicting wave run-up on rubble-mound structures using M5 model tree. *Ocean Engineering, 38*(1), 111–118.

Borsboom, M., & Jacobsen, N. G. (2021). A generating-absorbing boundary condition for dispersive waves. *International Journal for Numerical Methods in Fluids, 93*(8), 2443–2467.

Borsje, B. W., van Wesenbeeck, B. K., Dekker, F., Paalvast, P., Bouma, T. J., van Katwijk, M. M., & de Vries, M. B. (2011). How ecological engineering can serve in coastal protection. *Ecological Engineering, 37*(2), 113–122.

Bosman, G., Van Der Meer, J., Hoffmans, G., Schüttrumpf, H., & Verhagen, H. J. (2009). Individual overtopping events at dikes. *Coastal engineering 2008: (in 5 volumes)* (pp. 2944–2956). World Scientific.

Bouws, E., Günther, H., Rosenthal, W., & Vincent, C. L. (1985). Similarity of the wind wave spectrum in finite depth water: 1. Spectral form. *Journal of Geophysical Research: Oceans, 90*(C1), 975–986.

Bruce, T., Van der Meer, J. W., Franco, L., & Pearson, J. M. (2009). Overtopping performance of different armour units for rubble mound breakwaters. *Coastal Engineering, 56*(2), 166–179.

Burcharth, H. F., & Hughes, S. A. (2002). *Fundamentals of design. In: S. Hughes (Ed.), Coastal Engineering Manual, Part VI, Design of Coastal Project Elements, Chapter VI-5, Engineer Manual 1110-2-1100.* (tech. rep.).

Capel, A. (2015). Wave run-up and overtopping reduction by block revetments with enhanced roughness. *Coastal Engineering, 104*, 76–92. https://doi.org/10.1016/j.coastaleng.2015.06.007

Chen, T., & Guestrin, C. (2016). Xgboost: A scalable tree boosting system. *Proceedings of the 22nd acm sigkdd international conference on knowledge discovery and data mining*, 785–794.

Chen, W., Marconi, A., Van Gent, M. R., Warmink, J. J., & Hulscher, S. J. (2020). Experimental study on the influence of berms and roughness on wave overtopping at rock-armoured dikes. *Journal of Marine Science and Engineering, 8*(6), 1–21. https://doi.org/10.3390/jmse8060446

Chen, W., Warmink, J. J., Van Gent, M. R. A., & Hulscher, S. J. M. H. (2021). Numerical modelling of wave overtopping at dikes using OpenFOAM®. *Coastal Engineering*, 103890.

Chen, W., Van Gent, M. R. A., Warmink, J. J., & Hulscher, S. J. M. H. (2020). The influence of a berm and roughness on the wave overtopping at dikes. *Coastal engineering, 156*, 103613. https://doi.org/https://doi.org/10.1016/j.coastaleng.2019.103613

Chen, W., Warmink, J. J., Van Gent, M. R. A., & Hulscher, S. J. M. H. (2020). Modelling of Wave Overtopping At Dikes Using Openfoam. *Coastal Engineering Proceedings, 166*(36v), 27. https://doi.org/10.9753/icce.v36v.papers.27

Christensen, N. F., Røge, M. S., Thomsen, J. B., Andersen, T. L., Burcharth, H. F., & Nørgaard, J. Q. H. (2014). Overtopping on Rubble Mound Breakwaters for Low Steep-

ness Waves in Deep and Depth Limited Conditions. *Coastal Engineering Proceedings*, *1*(34), 6. https://doi.org/10.9753/icce.v34.structures.6

CIRIA, CUR, & CETMEF. (2007). *The Rock Manual. The use of rock in hydraulic engineering (2nd edition)*. Ciria. http://www.lavoisier.fr/livre/notice.asp?ouvrage=1706922

Dan, S., Altomare, C., Suzuki, T., Spiesschaert, T., & Verwaest, T. (2020). Reduction of Wave Overtopping and Force Impact at Harbor Quays Due to Very Oblique Waves. *Journal of Marine Science and Engineering*, *8*(8), 598.

Danka, J., & Zhang, L. M. (2015). Dike failure mechanisms and breaching parameters. *Journal of Geotechnical and Geoenvironmental Engineering*, *141*(9), 4015039.

Davidson, J., Cathelain, M., Guillement, L., Huec, T. L., & V.Ringwood, J. (2015). Implementation of an OpenFOAM Numerical Wave Tank for Wave Energy Experiments. *Proceedings of the 11th European Wave and Tidal Energy Conference*, 1–10.

Dawson, R., Hall, J., Sayers, P., Bates, P., & Rosu, C. (2005). Sampling-based flood risk analysis for fluvial dike systems. *Stochastic Environmental Research and Risk Assessment*, *19*(6), 388–402.

De Rouck, J., Geeraerts, J., Troch, P., Kortenhaus, A., Pullen, T., & Franco, L. (2005). New Results on Scale Effects for Wave Overtopping at Coastal Structures. *Proceedings of the International Conference on Coastalines, Structures and Breakwaters*, 1–14.

De Waal, J. P., Tonjes, P., & van der Meer, J. W. (1996). Overtopping of sea defences. *Proc. 25th Int. Conf. on Coastal Engng. Orlando*, 2216–2229.

De Waal, J. P., & van der Meer, J. W. (1992). Wave runup and overtopping on coastal structures. *Proc. ICCE 1992*, (2), 1758–1771. https://doi.org/10.1016/B978-1-4160-5583-9.00134-9

Dean, R. G., Rosati, J. D., Walton, T. L., & Edge, B. L. (2010). Erosional equivalences of levees: Steady and intermittent wave overtopping. *Ocean Engineering*, *37*(1), 104–113. https://doi.org/10.1016/j.oceaneng.2009.07.016

Deilami-Tarifi, M., Behdarvandi-Askar, M. E., Chegini, V., & Haghighi-Pour, S. A. (2015). Effect of Slope, Size, and Arrangement of Roughness of Sea Wall on Overtopping of Random Waves. *International Journal of Biology, Pharmacy and Applied Sciences*, *4*, 1026–1034.

del Jesus, M., Lara, J. L., & Losada, I. J. (2012). Three-dimensional interaction of waves and porous coastal structures. Part I: Numerical model formulation. *Coastal Engineering*, *64*, 57–72. https://doi.org/10.1016/j.coastaleng.2012.01.008

Den Bieman, J. P., De Ridder, M. P., & Van Gent, M. R. A. (2020). Deep learning video analysis as measurement technique in physical models. *Coastal Engineering*, *158*, 103689.

Den Bieman, J. P., Van Gent, M. R. A., & Van den Boogaard, H. F. P. (2021). Wave overtopping predictions using an advanced machine learning technique. *Coastal Engineering*, *166*, 103830.

Di Paolo, B., Lara, J. L., Barajas, G., & Losada, Í. J. (2021a). Wave and structure interaction using multi-domain couplings for Navier-Stokes solvers in OpenFOAM®. Part I: Implementation and validation. *Coastal Engineering, 164*, 103799.

Di Paolo, B., Lara, J. L., Barajas, G., & Losada, Í. J. (2021b). Waves and structure interaction using multi-domain couplings for Navier-Stokes solvers in OpenFOAM®. Part II: Validation and application to complex cases. *Coastal Engineering, 164*, 103818.

Didier, E., & Neves, M. (2009). Coastal flow simulation using SPH: Wave overtopping on an impermeable coastal structure. *4th International SPHERIC Workshop.*

Eldrup, M. R., & Lykke Andersen, T. (2018). Recalibration of Overtopping Roughness Factors of Different Armour Types. *Coasts, marine structures and breakwaters 2017: Realising the potential* (pp. 1011–1020). ICE Publishing.

Endoh, K., & Takahashi, S. (1995). Numerically modeling personnel danger on a promenade breakwater due to overtopping waves. *Coastal engineering 1994* (pp. 1016–1029).

Engsig-Karup, A. P., Bingham, H. B., & Lindberg, O. (2009). An efficient flexible-order model for 3D nonlinear water waves. *Journal of computational physics, 228*(6), 2100–2118.

Esteban, M., Roubos, J. J., Iimura, K., Salet, J. T., Hofland, B., Bricker, J., Ishii, H., Hamano, G., Takabatake, T., & Shibayama, T. (2020). Effect of bed roughness on tsunami bore propagation and overtopping. *Coastal Engineering, 157*, 103539.

EurOtop. (2007). Wave Overtopping of Sea Defences and Related Structures–Assessment Manual. *UK: NWH Allsop, T. Pullen, T. Bruce. NL: JW van der Meer. DE: H. Schüttrumpf, A. Kortenhaus. www. overtopping-manual. com.*

EurOtop. (2018). *Manual on wave overtopping of sea defences and related structures.*

Fairley, I., Davidson, M., & Kingston, K. (2009). Video monitoring of overtopping of detached breakwaters in a mesotidal environment. *Coastal structures 2007: (in 2 volumes)* (pp. 1923–1932). World Scientific.

Fang, Z., Cheng, L., & Zhang, N. (2010). Development of 3-D numerical wave tank and applications on comb-type breakwater. *ASME 2010 29th International Conference on Ocean, Offshore and Arctic Engineering*, 589–596.

Formentin, S. M., Gaeta, M. G., Palma, G., Zanuttigh, B., & Guerrero, M. (2019). Flow depths and velocities across a smooth dike crest. *Water, 11*(10), 2197.

Franco, L., De Gerloni, M., & Van der Meer, J. W. (1995). Wave overtopping on vertical and composite breakwaters. *Coastal engineering 1994* (pp. 1030–1045).

Frostick, L. E., McLelland, S. J., & Mercer, T. G. (2011). *Users guide to physical modelling and experimentation: Experience of the HYDRALAB network.* CRC Press.

Fukunari, K. (2008). The Tone River Case and others. Safety of River Levee. *Japan Conference, Power Point presentation, Tokyo, Japan.*

Gallach-Sánchez, D., Troch, P., & Kortenhaus, A. (2018). A critical analysis and validation of the accuracy of wave overtopping prediction formulae for OWECs. *Energies, 11*(1), 1–20. https://doi.org/10.3390/en11010133

Galland, J.-C. (1995). Rubble mound breakwater stability under oblique waves: an experimental study. *Coastal engineering 1994* (pp. 1061–1074).

Goda, Y. (2009). Derivation of unified wave overtopping formulas for seawalls with smooth, impermeable surfaces based on selected CLASH datasets. *Coastal Engineering, 56*(4), 385–399. https://doi.org/10.1016/j.coastaleng.2008.09.007

Goda, Y., Kishara, Y., & Kamiyama, Y. (1975). Laboratory investigation on the overtopping rate of seawalls by irregular waves. *Report of the Port and Harbour Research Institute, vol 14, nr. 4.*

González-Escrivá, J. A. (2007). The role of wind in wave runup and overtopping of coastal structures. *Coastal engineering 2006: (in 5 volumes)* (pp. 4766–4778). World Scientific.

Hebsgaard, M., Sloth, P., & Juhl, J. (1998). Wave Overtopping of Rubble Mound Breakwaters. *Coastal Engineering*, 2235–2248.

Higuera, P., Lara, J. L., & Losada, I. J. (2013). Realistic wave generation and active wave absorption for Navier–Stokes models: Application to OpenFOAM®. *Coastal Engineering, 71*, 102–118.

Higuera, P., Lara, J. L., & Losada, I. J. (2014a). Three-dimensional interaction of waves and porous coastal structures using OpenFOAM®. Part I: Formulation and validation. *Coastal Engineering, 83*, 243–258. https://doi.org/10.1016/j.coastaleng.2013.08.010

Higuera, P., Lara, J. L., & Losada, I. J. (2014b). Three-dimensional interaction of waves and porous coastal structures using OpenFOAM®. Part II: Application. *Coastal Engineering, 83*, 259–270. https://doi.org/10.1016/j.coastaleng.2013.09.002

Hirabayashi, Y., Mahendran, R., Koirala, S., Konoshima, L., Yamazaki, D., Watanabe, S., Kim, H., & Kanae, S. (2013). Global flood risk under climate change. *Nature Climate Change, 3*(9), 816–821.

Hoffmans, G. J. C. M. (2012). *The influence of turbulence on soil erosion* (Vol. 10). Eburon Uitgeverij BV.

Huang, C. J., Chang, Y. C., Tai, S. C., Lin, C. Y., Lin, Y. P., Fan, Y. M., Chiu, C. M., & Wu, L. C. (2020). Operational monitoring and forecasting of wave run-up on seawalls. *Coastal Engineering, 161*, 103750.

Hughes, S., Scholl, B., & Thornton, C. (2012). Wave overtopping hydraulic parameters on protected-side slopes. *Proceedings of the 32nd USSD Annual Conference, New Orleans, Louisiana*, 1453–1466.

Hunt-Raby, A., Othman, I. K., Jayaratne, R., Bullock, G., & Bredmose, H. (2010). Effect of protruding roughness elements on wave overtopping. *Coasts, marine structures and breakwaters: Adapting to change: Proceedings of the 9th international conference organised by the Institution of Civil Engineers and held in Edinburgh on 16 to 18 September 2009*, 2–574.

Jacobsen, N. G. (2017). waves2Foam Manual. (August).

Jacobsen, N. G. (2021). *Theoretical model of an absorbing wave boundary condition* (tech. rep.). Tech. Rep. DOI: 10.13140/RG. 2.2. 22360.62726, Private work.

Jacobsen, N. G., Fuhrman, D. R., & Fredsøe, J. (2012). A wave generation toolbox for the open-source CFD library: OpenFoam®. *International Journal for Numerical Methods in Fluids, 70*(9), 1073–1088.

Jacobsen, N. G., Van Gent, M. R. A., Capel, A., & Borsboom, M. (2018). Numerical prediction of integrated wave loads on crest walls on top of rubble mound structures. *Coastal Engineering, 142*, 110–124.

Jacobsen, N. G., Van Gent, M. R. A., & Wolters, G. (2015). Numerical analysis of the interaction of irregular waves with two dimensional permeable coastal structures. *Coastal Engineering, 102*, 13–29. https://doi.org/10.1016/j.coastaleng.2015.05.004

Jafari, E., & Etemad-Shahidi, A. (2011). Derivation of a new model for prediction of wave overtopping at rubble mound structures. *Journal of Waterway, Port, Coastal, and Ocean Engineering, 138*(1), 42–52.

Jensen, B., Jacobsen, N. G., & Christensen, E. D. (2014). Investigations on the porous media equations and resistance coefficients for coastal structures. *Coastal Engineering, 84*, 56–72.

Jiménez Moreno, A. (2017). *Experimental study on the wave overtopping performance of Xbloc+ armour unit*, Master Thesis, TU Delft. https://doi.org/http://resolver.tudelft.nl/uuid:b4bbc14f-12db-4858-b9d8-2c1b12dd76c7

Jonkman, S. N., Kok, M., & Vrijling, J. K. (2008). Flood risk assessment in the Netherlands: A case study for dike ring South Holland. *Risk Analysis: An International Journal, 28*(5), 1357–1374.

Juhl, J., & Sloth, P. (1995). Wave overtopping of breakwaters under oblique waves. *Coastal engineering 1994* (pp. 1182–1196).

Kajima, R., & Sakakiyama, T. (1994). Review of works using CRIEPI flume and present work. *Coastal Dynamics94*, 614–627.

Ke, Q., Yin, J., Bricker, J. D., Savage, N., Buonomo, E., Ye, Q., Visser, P., Dong, G., Wang, S., Tian, Z., Sun, L., Toumi, R., & Jonkman, S. N. (2021). *An integrated framework of coastal flood modelling under the failures of sea dikes: a case study in Shanghai.* Springer Netherlands. https://doi.org/10.1007/s11069-021-04853-z

Kellens, W., Neutens, T., Deckers, P., Reyns, J., & De Maeyer, P. (2012). Coastal flood risks and seasonal tourism: analysing the effects of tourism dynamics on casualty calculations. *Natural hazards*, *60*(3), 1211–1229.

Kerpen, N. B., Schoonees, T., & Schlurmann, T. (2019). Wave overtopping of stepped revetments. *Water*, *11*(5), 1035.

Klapp, J., Sigalotti, L. D. G., Medina, A., López, A., & Ruiz-Chavarría, G. (2016). *Recent Advances in Fluid Dynamics with Environmental Applications*. Springer.

Knutson, T. R., McBride, J. L., Chan, J., Emanuel, K., Holland, G., Landsea, C., Held, I., Kossin, J. P., Srivastava, A. K., & Sugi, M. (2010). Tropical cyclones and climate change. *Nature geoscience*, *3*(3), 157–163.

Kobayashi, B. N., & Wurjanto, A. (1989). Wave overtopping on coastal structures. *Journal of Waterway, Port, Coastal, and Ocean Engineering*, *115*(2), 235–251.

Koosheh, A., Etemad-Shahidi, A., Cartwright, N., Tomlinson, R., & Van Gent, M. R. A. (2021). Individual wave overtopping at coastal structures: A critical review and the existing challenges. *Applied Ocean Research*, *106*, 102476.

Kortenhaus, A., Pearson, J., Bruce, T., Allsop, N. W. H., & Van der Meer, J. W. (2004). Influence of parapets and recurves on wave overtopping and wave loading of complex vertical walls. *Coastal structures 2003* (pp. 369–381).

Krom, J. (2012). *Wave overtopping at rubble mound breakwaters with a non-reshaping berm*. http://repository.tudelft.nl/assets/uuid:984bc5e5-8c04-4d35-b34a-2b871f636fa1/Thesis_J.C.Krom.pdf

Lan, Y. M., & Guo, W. H. (2013). Investigation on Wave Runup and Overtopping over a Seawall in a Numerical Flume. *Applied Mechanics and Materials*, *394*, 69–74.

Larsen, B. E., & Fuhrman, D. R. (2018). On the over-production of turbulence beneath surface waves in Reynolds-averaged Navier–Stokes models. *Journal of Fluid Mechanics*, *853*, 419–460.

Larsen, B. E., Fuhrman, D. R., & Roenby, J. (2019). Performance of interFoam on the simulation of progressive waves. *Coastal Engineering Journal*, *61*(3), 380–400.

Li, T., Troch, P., & De Rouck, J. (2004). Wave overtopping over a sea dike. *Journal of Computational Physics*, *198*(2), 686–726.

Lin, N., Emanuel, K., Oppenheimer, M., & Vanmarcke, E. (2012). Physically based assessment of hurricane surge threat under climate change. *Nature Climate Change*, *2*(6), 462–467.

Liu, S., Ju, Q., Huang, W., Hu, X., Qi, D., & Zhong, G. (2018). Effects of Crown Wall and Berm on Wave-Overtopping Discharge over a Seawall. *Journal of Coastal Research*, *34*(4), 968–978.

Lorke, S., Bornschein, A., Schüttrumpf, H., & Pohl, R. (2012). Influence of wind and current on wave-run up and wave overtopping. *Hydralab IV report for KfKI*.

Losada, I. J., Lara, J. L., Guanche, R., & Gonzalez-Ondina, J. M. (2008). Numerical analysis of wave overtopping of rubble mound breakwaters. *Coastal Engineering, 55*(1), 47–62. https://doi.org/10.1016/j.coastaleng.2007.06.003

Lykke Andersen, T., & Burcharth, H. F. (2009). Three-dimensional investigations of wave overtopping on rubble mound structures. *Coastal Engineering, 56*(2), 180–189.

Ma, G., Shi, F., & Kirby, J. T. (2012). Shock-capturing non-hydrostatic model for fully dispersive surface wave processes. *Ocean Modelling, 43*, 22–35.

Mansard, E. P. D., & Funke, E. R. (1980). The measurement of incident and reflected spectra using a least squares method. *Coastal engineering 1980* (pp. 154–172).

Mares-Nasarre, P., Argente, G., Gómez-Martín, M. E., & Medina, J. R. (2019). Overtopping layer thickness and overtopping flow velocity on mound breakwaters. *Coastal Engineering, 154*, 103561.

Mares-Nasarre, P., Molines, J., Gómez-Martín, M. E., & Medina, J. R. (2021). Explicit Neural Network-derived formula for overtopping flow on mound breakwaters in depth-limited breaking wave conditions. *Coastal Engineering, 164*, 103810.

Martínez Pés, V. (2013). *Applicability and Limitations of the SWASH model to predict Wave Overtopping* (Doctoral dissertation). Universitat Politècnica de Catalunya. https://doi.org/http://hdl.handle.net/2099.1/20373

Mase, H., Tamada, T., Yasuda, T., Hedges, T. S., & Reis, M. T. (2013). Wave runup and overtopping at seawalls built on land and in very shallow water. *Journal of waterway, port, coastal, and ocean engineering, 139*(5), 346–357.

Mayer, S., Garapon, A., & Sørensen, L. S. (1998). A fractional step method for unsteady free-surface flow with applications to non-linear wave dynamics. *International Journal for Numerical Methods in Fluids, 28*(2), 293–315.

Moghim, M. N., Boroujeni, R. F., & Tabari, M. M. R. (2015). Wave overtopping on reshaping berm breakwaters based on wave momentum flux. *Applied Ocean Research, 53*, 23–30.

Molines, J., Perez, T. J., Zarranz, G., & Medina, J. R. (2012). Influence of cube and cubipod armor porosities on overtopping. *Coastal Engineering Proceedings*, 1–8.

Nagy, L. (2012). Statistical evaluation of historical dike failure mechanism. *Riscuri si Catastrofe, 11*(2), 7–20.

Nakayama, A., & Kuwahara, F. (1999). A macroscopic turbulence model for flow in a porous medium.

Nikuradse, J. (1950). *Laws of Flow in Rough Pipes* (tech. rep.). National Advisory Committee for Aeronautics. https://doi.org/doi:10.1016/s0016-0032(40)90670-6

Owen, M. W. (1980). Design of seawalls allowing for wave overtopping. *Report Ex, 924*, 39.

Patil, A. (2019). *Numerical investigation of nearshore wave transformation and surf zone hydrodynamics*, Master Thesis, TU Delft.

Paulsen, B. T., Bredmose, H., & Bingham, H. B. (2014). An efficient domain decomposition strategy for wave loads on surface piercing circular cylinders. *Coastal Engineering, 86*, 57–76.

Pavlin, Ž., & Kuspilić, N. (2018). Reference water levels for the design of dykes and earthfill dams. *Građevinar, 70*(03.), 225–233.

Pearson, J., Bruce, T., Allsop, W., Kortenhaus, A., & van der Meer, J. (2005). Effectiveness of recurve walls in reducing wave overtopping on seawalls and breakwaters. *Coastal engineering 2004: (in 4 volumes)* (pp. 4404–4416). World Scientific.

PILECHI, A., BAKER, S., & CORNETT, A. (2018). Evaluation of a numerical wave modelling tool for studying the overtopping of rubble mound breakwaters. *Proceedings of VII International Conference on the Application of Physical Modelling in Coastal and Port Engineering and Science (Coastlab18), Santander (S).*

Pillai, K., Etemad-Shahidi, A., & Lemckert, C. (2017a). Wave overtopping at berm breakwaters: Experimental study and development of prediction formula. *Coastal Engineering, 130*(October), 85–102. https://doi.org/10.1016/j.coastaleng.2017.10.004

Pillai, K., Etemad-Shahidi, A., & Lemckert, C. (2017b). Wave overtopping at berm breakwaters: Review and sensitivity analysis of prediction models. *Coastal Engineering, 120*(October 2016), 1–21. https://doi.org/10.1016/j.coastaleng.2016.11.003

Pillai, K., Etemad-Shahidi, A., & Lemckert, C. (2019). Wave run-up on bermed coastal structures. *Applied Ocean Research, 86*, 188–194.

Pillai, K., Lemckert, C., Etemad-Shahidi, A., Cappietti, L., & Sigurdarson, S. (2019). Effect of Sea Level Rise on the Wave Overtopping Rate at Berm Breakwater. *Journal of Waterway, Port, Coastal, and Ocean Engineering, 145*(5), 4019019.

Raby, A., Jayaratne, R., Bredmose, H., & Bullock, G. (2019). Individual violent wave-overtopping events: behaviour and estimation. *Journal of Hydraulic Research.*

Regeling, H. J., van der Meer, J. W., & Bruce, T. (2005). Overtopping on rock berm with smooth upper slope. *Infram, 25*, 1–13.

Roenby, J., Bredmose, H., & Jasak, H. (2016). A computational method for sharp interface advection. *Royal Society open science, 3*(11), 160405.

Sandoval, C., & Bruce, T. (2018). Wave overtopping hazard to pedestrians: Video evidence from real accidents. *Coasts, marine structures and breakwaters 2017: Realising the potential* (pp. 501–512). ICE Publishing.

Saville, T. (1956). Wave run-up on shore structures. *Journal of the Waterways and Harbors Division, 82*(2), 921–925.

Schmocker, L., & Hager, W. H. (2009). Modelling dike breaching due to overtopping. *Journal of Hydraulic Research, 47*(5), 585–597.

Schoonees, T., Kerpen, N. B., & Schlurmann, T. (2021). Full-scale experimental study on wave overtopping at stepped revetments. *Coastal Engineering, 167*, 103887.

Schüttrumpf, H. (2001). *Wellenüberlaufströmung an Seedeichen: Experimentelle und theoretische Untersuchungen* (Doctoral dissertation). Braunschweig University.

Schüttrumpf, H., & Oumeraci, H. (2005). Layer thicknesses and velocities of wave overtopping flow at seadikes. *Coastal Engineering, 52*(6), 473–495. https://doi.org/10.1016/j.coastaleng.2005.02.002

Schüttrumpf, H., & Van Gent, M. R. A. (2003). Wave overtopping at seadikes. *Coastal Structures 2003*, 431–443.

Shankar, N. J., & Jayaratne, M. P. R. (2003). Wave run-up and overtopping on smooth and rough slopes of coastal structures. *Ocean Engineering, 30*(2), 221–238.

Siegel, F. R. (2020). Structures That Protect Coastal Populations, Assets, and GDPs: Sea Dikes, Breakwaters, Seawalls. *Adaptations of coastal cities to global warming, sea level rise, climate change and endemic hazards* (pp. 11–25). Springer.

Sigurdarson, S., & Van Der Meer, J. W. (2012). Wave overtopping at berm breakwaters in line with EurOtop. *Coastal Engineering Proceedings, 1*(33), 12.

Steendam, G. J. A. N., Van der Meer, J. W., Verhaeghe, H., BESLEY, P., FRANCO, L., & VAN GENT, M. R. A. (2005). The international database on wave overtopping. *Coastal engineering 2004: (in 4 volumes)* (pp. 4301–4313). World Scientific.

Steendam, G. J., Van Hoven, A., Van der Meer, J., & Hoffmans, G. (2014). Wave overtopping simulator tests on transitions and obstacles at grass covered slopes of dikes. *Coastal Engineering Proceedings, 1*(34), 79.

Suzuki, T., Altomare, C., Veale, W., Verwaest, T., Trouw, K., Troch, P., & Zijlema, M. (2017). Efficient and robust wave overtopping estimation for impermeable coastal structures in shallow foreshores using SWASH. *Coastal Engineering, 122*, 108–123.

Suzuki, T., Altomare, C., Yasuda, T., & Verwaest, T. (2020). Characterization of overtopping waves on sea dikes with gentle and shallow foreshores. *Journal of Marine Science and Engineering, 8*(10), 1–16. https://doi.org/10.3390/jmse8100752

Tautenhain, E., Kohlhase, S., & Partenscky, H. W. (1982). Wave run-up at sea dikes under oblique wave approach. *Coastal engineering 1982* (pp. 804–810).

TAW. (2002). *Technical report wave run-up and wave overtopping at dikes* (tech. rep.).

Temmerman, S., Meire, P., Bouma, T. J., Herman, P. M. J., Ysebaert, T., & De Vriend, H. J. (2013). Ecosystem-based coastal defence in the face of global change. *Nature, 504*(7478), 79.

Tuan, T. Q. (2013). Influence of low sea-dike crown-walls on wave overtopping discharge. *Coastal Engineering Journal, 55*(4), 1350011–1350013.

Van Baars, S., & Van Kempen, I. M. (2009). The causes and mechanisms of historical dike failures in the Netherlands. *E-WAter journal, 2009*.

Van Bergeijk, V. M., Verdonk, V. A., Warmink, J. J., & Hulscher, S. J. (2021). The cross-dike failure probability by wave overtopping over grass-covered and damaged dikes. *Water, 13*(5), 1–22. https://doi.org/10.3390/w13050690

Van Bergeijk, V. M., Warmink, J. J., & Hulscher, S. J. (2020). Modelling the wave overtopping flow over the crest and the landward slope of grass-covered flood defences. *Journal of Marine Science and Engineering, 8*(7). https://doi.org/10.3390/JMSE8070489

Van Bergeijk, V. M., Warmink, J. J., van Gent, M. R. A., & Hulscher, S. J. M. H. (2019). An analytical model for wave overtopping flow velocities on dike crests and landward slopes. *Coastal Engineering, 149*, 28–38.

Van der Meer, J. W., & De Waal, J. (1990). *Invloed van scheve inval en richtingspreiding op golfoploop en overslag* (tech. rep.). Waterloopkundig Laboratorium,Verslag modelonderzoek H638 (in Dutch).

Van der Meer, J. W., & De Waal, J. (1993). *Waterbeweging op taluds, Invloed van berm, ruwheid, ondiep voorland en scheve lang- en kortkammige golfaanval* (tech. rep.). Waterloopkundig Laboratorium, Verslag H1256 (in Dutch).

Van der Meer, J., & Bruce, T. (2014). New Physical Insights and Design Formulas on Wave Overtopping at Sloping and Vertical Structures. *Journal of Waterway, Port, Coastal, and Ocean Engineering, 140*(6), 04014025. https://doi.org/10.1061/(ASCE)WW.1943-5460.0000221

Van der Meer, J. W. (2004). *Overtopping on rock berm with smooth upper slope. Validation tests at University of Edinburgh* (tech. rep.). Infram report 04i080.

Van der Meer, J. W. (2017). Wave run-up and overtopping. *Dikes aimd revetments* (pp. 145–160). Routledge.

Van der Meer, J. W., Hardeman, B., Steendam, G.-J., Schüttrumpf, H., & Verheij, H. (2010). Flow depths and velocities at crest and landward slope of a dike, in theory and with the wave overtopping simulator. *Coastal Engineering Proceedings, 1*(32), 10.

Van der Werf, I. M., & Van Gent, M. R. A. (2018). Wave overtopping over dikes with oblique wind and swell. *Coastlab*, (3), 1–8.

Van Doorslaer, K., De Rouck, J., Audenaert, S., & Duquet, V. (2015). Crest modifications to reduce wave overtopping of non-breaking waves over a smooth dike slope. *Coastal Engineering, 101*, 69–88.

Van Doorslaer, K., De Rouck, J., Boderé, T., Vanhouwe, G., & Troch, P. (2010). The influence of a berm and a vertical wall above SWL on the reduction of wave overtopping. *Proc. Coastlab 2010*.

Van Gent, M. R. A. (1999). Physical model investigations on coastal structures with shallow foreshores: 2D model tests on the Petten sea-defence. *Delft Hydraulics Report H3129, Delft*.

Van Gent, M. R. A. (2002a). Wave overtopping events at dikes. *World Scientific, ICCE 2002, 2,* 2203–2215. https://doi.org/10.1142/9789812791306

Van Gent, M. R. A., Plate, S. E., Berendsen, E., Spaan, G. B. H., Van Der Meer, J. W., & d'Angremond, K. (1999). Single-layer rubble mound breakwaters. *Proc. Coastal Structures, 99.*

Van Gent, M. R. A. (1995). *Wave interaction with permeable coastal structures* (Doctoral dissertation). TU Delft.

Van Gent, M. R. A. (2000). *Wave runup on dikes with berms* (tech. rep.). WL | Delft Hydraulics. Delft, Report H3205. WL | Delft Hydraulics.

Van Gent, M. R. A. (2001). Wave Runup on Dikes with Shallow Foreshores. *Journal of Waterway, Port, Coastal, and Ocean Engineering, 127,* 254–262. https://doi.org/10.1061/(ASCE)0733-950X(2001)127:5(254)

Van Gent, M. R. A. (2002b). Low-exceedance wave overtopping events: Measurements of velocities and the thickness of water-layers on the crest and inner slope of dikes. *Delft cluster DC1-322-3.*

Van Gent, M. R. A. (2013). Rock stability of rubble mound breakwaters with a berm. *Coastal Engineering, 78,* 35–45.

Van Gent, M. R. A. (2019). Climate adaptation of coastal structures. *Keynote in proc. applied coastal research (scacr 2019).*

Van Gent, M. R. A. (2020). Influence of oblique wave attack on wave overtopping at smooth and rough dikes with a berm. *Coastal Engineering, 160,* 103734.

Van Gent, M. R. A. (2021). Influence of oblique wave attack on wave overtopping at caisson breakwaters with sea and swell conditions. *Coastal Engineering, 164,* 103834.

Van Gent, M. R. A., & Luis, L. (2013). Application of Cubes in a single layer. *Proceedings of the 6th International Short Course/Conference on Applied Coastal Research (SCACR).*

Van Gent, M. R. A., Van den Boogaard, H. F. P., Pozueta, B., & Medina, J. R. (2007). Neural network modelling of wave overtopping at coastal structures. *Coastal Engineering, 54*(8), 586–593.

Van Gent, M. R. A., & Van der Werf, I. M. (2019). Influence of oblique wave attack on wave overtopping and forces on rubble mound breakwater crest walls. *Coastal Engineering, 151,* 78–96.

Van Loon-Steensma, J. M., & Schelfhout, H. A. (2017). Wide Green Dikes: A sustainable adaptation option with benefits for both nature and landscape values? *Land Use Policy, 63,* 528–538.

Van Steeg, P., Joosten, R. A., & Steendam, G. J. (2018). Physical model tests to determine the roughness of stair shaped revetments. *3th International Conference on Protection against Overtopping, UK,* (June), 1–8.

Van Steeg, P., Breteler, M. K., & Provoost, Y. V. O. (2016). Large-scale physical model tests to determine influence factor of roughness for wave run-up of channel shaped blocks revetments. *Coastlab*, 10–13.

Van Steeg, P., De Ridder, M., Capel, A., & Bottema, M. (2021). Influence of water depth on wave overtopping. *FLOODrisk 2020-4th European Conference on Flood Risk Management*.

Vandebeek, I., Gruwez, V., Altomare, C., Suzuki, T., Vanneste, D., De Roo, S., Toorman, E., & Troch, P. (2018). Towards an efficient and highly accurate coupled numerical modelling approach for wave interactions with a dike on a very shallow foreshore. *Coastlab 2018*, 1–10.

Verhaeghe, H., De Rouck, J., & van der Meer, J. (2008). Combined classifier–quantifier model: a 2-phases neural model for prediction of wave overtopping at coastal structures. *Coastal Engineering, 55*(5), 357–374.

Vieira, F., Taveira-Pinto, F., & Rosa-Santos, P. (2021). New developments in assessment of wave overtopping on single-layer cube armoured breakwaters based on laboratory experiments. *Coastal Engineering, 166*, 103883.

Ward, D. L., & Ahrens, J. P. (1992). *Overtopping rates for seawalls* (tech. rep.). COASTAL ENGINEERING RESEARCH CENTER VICKSBURG MS.

Wilcox, D. C. (2006). Turbulence modeling for CFD, 3rd. *DCW Industries: La Canada, California, U.S.A.*

Williams, H. E., Briganti, R., Romano, A., & Dodd, N. (2019). Experimental analysis of wave overtopping: A new small scale laboratory dataset for the assessment of uncertainty for smooth sloped and vertical coastal structures. *Journal of Marine Science and Engineering, 7*(7), 217.

Wolters, G., & Van Gent, M. R. A. (2007). Maximum wind effect on wave overtopping of sloped coastal structures with crest elements. *Coastal structures 2007: (in 2 volumes)* (pp. 1263–1274). World Scientific.

Wroniszewski, P. A., Verschaeve, J. C. G., & Pedersen, G. K. (2014). Benchmarking of Navier-Stokes codes for free surface simulations by means of a solitary wave. *Coastal Engineering, 91*, 1–17.

Zanuttigh, B., Formentin, S. M., & van der Meer, J. W. (2016). Prediction of extreme and tolerable wave overtopping discharges through an advanced neural network. *Ocean Engineering, 127*, 7–22.

Zijlema, M., Stelling, G., & Smit, P. (2011). SWASH: An operational public domain code for simulating wave fields and rapidly varied flows in coastal waters. *Coastal Engineering, 58*(10), 992–1012. https://doi.org/10.1016/j.coastaleng.2011.05.015

ABOUT ME

Weiqiu Chen was born on 6th of July 1991 in a small village in Xuzhou, Jiang Province of China. In 2010, she started her BSc in Harbor, Waterway and Coastal Engineering at Hohai University. After obtaining her Bachelor degree in 2014, she was recommended to continue her MSc in Harbor, Coastal and Nearshore Engineering at the same university. In 2015, she went to Nanjing Hydraulic Research Institute for internship. During the internship, she gained valuable experience in designing and performing physical model tests. In June of 2017, she obtained a Master degree of Harbor, Coastal and Nearshore Engineering. At the same year, she moved to the Netherlands and started working as a PhD student in Marine and Fluvial Systems at University of Twente and in Coastal Structures and Waves at Deltares following the guidance of Prof. Suzanne Hulscher, Prof. Marcel van Gent and Dr. Jord Warmink. During her PhD study, she mainly focused on the coastal hydrodynamics and wave overtopping at dikes. After finishing her PhD thesis in September 2021, she started working as a PostDoc in Shaping the Beach project, focusing on the sand transport in swash zone.

LIST OF PUBLICATIONS

PEER-REVIEWED JOURNAL PAPERS

1. **Chen, W.**, Warmink, J. J., van Gent, M. R. A. and Hulscher, S. J. M. H (2021). Numerical investigation of the effects of roughness, a berm and oblique waves on wave overtopping processes at dikes. Applied Ocean Research. https://doi.org/10.1016/j.apor.2021.102971.

2. **Chen, W.**, Warmink, J. J., van Gent, M. R. A. and Hulscher, S. J. M. H. (2021). Numerical modelling of wave overtopping at dikes using OpenFOAM®. *Coastal Engineering*, 166, 103890. https://doi.org/10.1016/j.coastaleng.2021.103890.

3. **Chen, W.**, Marconi, A., van Gent, M. R. A., Warmink, J. J., and Hulscher, S. J. M. H. (2020). Experimental study on the influence of berms and roughness on wave overtopping at rock-armoured dikes. *Journal of Marine, Science and Engineering*, 8(6), 446. https://doi.org/10.3390/jmse8060446.

4. **Chen, W.**, van Gent, M. R. A., Warmink, J. J., and Hulscher, S. J. M. H. (2020). The influence of a berm and roughness on the wave overtopping at dikes. *Coastal Engineering*, 156, 103613. https://doi.org/10.1016/j.coastaleng.2019.103613.

5. Wang D., Ju, L., Zhu, J., Wang, Z., Sun, T., and **Chen, W.** (2017). Experimental study on mean overtopping of sloping seawall under oblique irregular waves. *China Ocean Engineering*, 31(3), 350-356.

6. Wang D., Sun T., **Chen, W.**, Zhu, J. (2016). Model test research of breakwater core material influence on wave propagation. *China Ocean Engineering*, 30(5), 786-793.
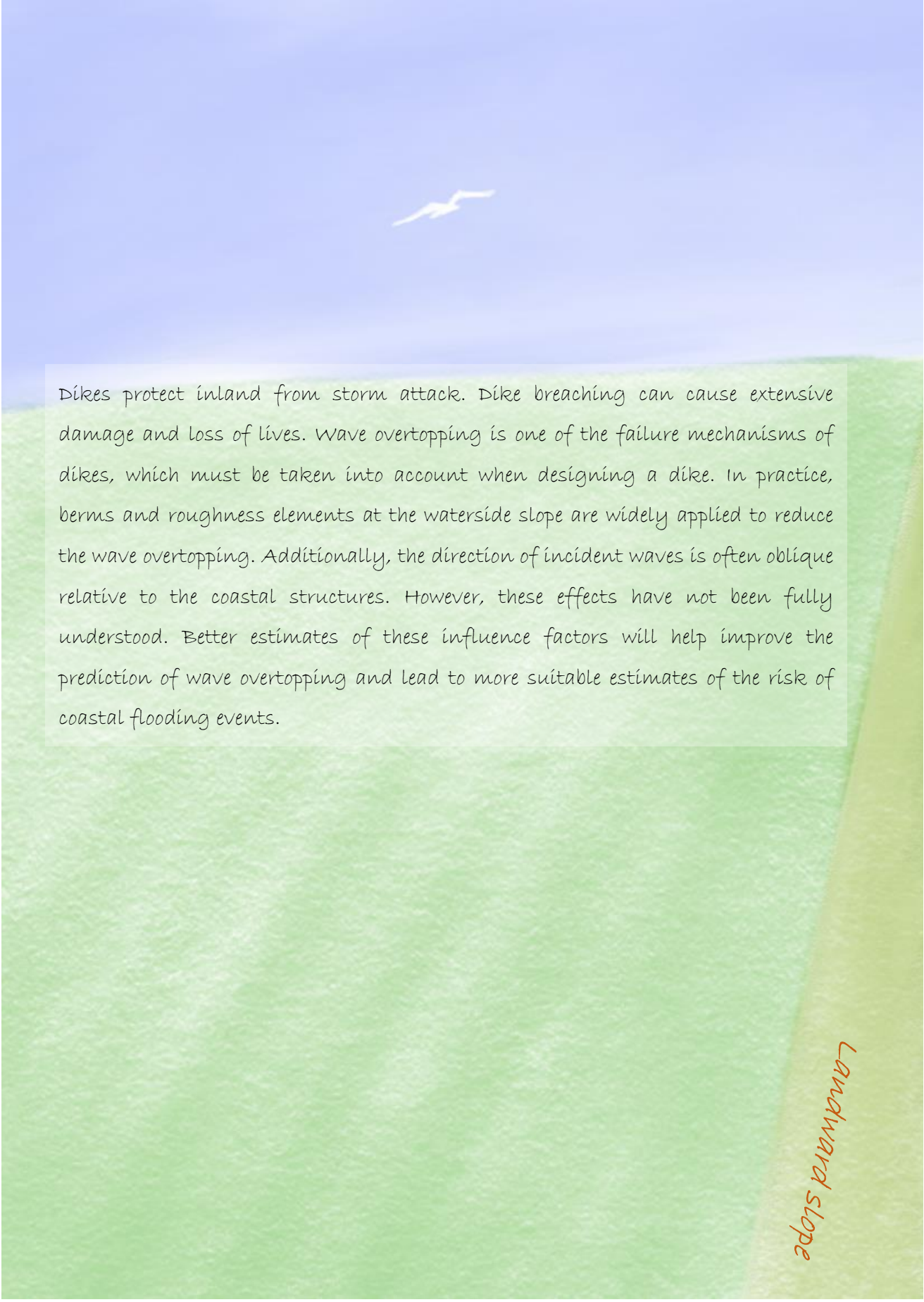
CONFERENCE PAPERS AND ABSTRACTS

1. **Chen, W.**, Warmink, J. J., van Gent, M. R. A. and Hulscher, S. J. M. H. Modelling of overtopping flow parameters at the seaward side of the dike crest. 14. *Abstract from NCK Days 2021*, Online Event, Netherlands.

2. Barendse, L., van Bergeijk, V. M., **Chen, W.**, Warmink, J. J., van Gent, M. R. A., Hulscher, S. J. M. H., Mughal, A. and Hill, D. (2021). Hydrodynamic modelling of wave overtopping over a block-covered dike. 5. *Abstract from NCK Days 2021*, Online Event, Netherlands.

3. Marconi, A., **Chen, W.**, van Gent, M. R. A., Warmink, J. J., and Hulscher, S. J. M. H. (2020). The influence of berms and roughness on wave overtopping at rock-armoured dikes. *Proceedings of the 1st IAHR Young Professionals Congress.*

4. **Chen, W.**, Warmink, J. J., van Gent, M. R. A. and Hulscher, S. J. M. H. (2020). Modelling of wave overtopping at dikes using OpenFOAM. *Coastal Engineering Proceedings*, (36v), 27-27.

5. **Chen, W.**, Warmink, J. J., van Gent, M. R. A. and Hulscher, S. J. M. H. (2019). Experimental study on the influence of berms and roughness on wave overtopping over dikes. Coastal Structures 2019, 1086-1096.

6. **Chen, W.**, Warmink, J. J., van Gent, M. R. A. and Hulscher, S. J. M. H. (2018). Experimental study on the influence of transitions on wave overtopping. Abstract from NCK-Days 2018, Haarlem, Netherlands.

7. Warmink, J. J., van Bergeijk, V. M., **Chen, W.** and Hulscher, S. J. M. H. (2018). Modelling wave overtopping for flood defence reliability, the outline of a research project. *e-Proc. ICCE 2018*, Baltimore, USA, 709745.

8. Warmink, J.J, van Bergeijk, V. M., **Chen, W.**, Aguilar-Lopez, J., Bomers, A. and Hulscher, S. J. M. H. (2018). Modelling wave overtopping for flood defense reliability. *3rd International Conference on Protection against Overtopping*, 6-8 June 2018, Grange-over-Sands, UK.

9. **Chen, W.**, Wang, D., Sun, T. and Kuai, Y. (2017). Experimental study on stable thickness of concrete slab revetment on inner slope of dikes. Proceedings of the 37th IAHR World Congress. Kuala Lumpur, Malaysia.

OTHER CONTRIBUTIONS

1. **Chen, W.**, Warmink, J. J., van Gent, M. R. A. and Hulscher, S. J. M. H. (2019). Influence of a berm and roughness on wave overtopping at dikes. Burgers Symposium 2019, Lunteren, Netherlands.

2. **Chen, W.** (2019). Study on wave overtopping of flood defenses, literature report (CE&M Research Report; No. 2019R-002/WEM-002). University of Twente.

3. Van Bergeijk, V. M., **Chen, W.**, Warmink, J. J., van Gent, M. R. A. and Hulscher, S. J. M. H. (2018). Wave overtopping on dikes: The effect of transitions on the flow and dike cover erosion. *ConcepTueel*, 27(3), 32-35.

Dikes protect inland from storm attack. Dike breaching can cause extensive damage and loss of lives. Wave overtopping is one of the failure mechanisms of dikes, which must be taken into account when designing a dike. In practice, berms and roughness elements at the waterside slope are widely applied to reduce the wave overtopping. Additionally, the direction of incident waves is often oblique relative to the coastal structures. However, these effects have not been fully understood. Better estimates of these influence factors will help improve the prediction of wave overtopping and lead to more suitable estimates of the risk of coastal flooding events.

Landward slope